Study of Decay Properties of Heavy Flavor and Exotic Hadrons

A thesis submitted to

The Maharaja Sayajirao University of Baroda

For the Degree of

Doctor of Philosophy

in

Applied Physics

by

Soni Nakul Rajendrakumar

Reg. No.: FOTE/873, Reg. Date: March 06, 2015

Under Supervision of

Dr. Jignesh N Pandya

Applied Physics Department
Faculty of Technology and Engineering
The Maharaja Sayajirao University of Baroda
Vadodara 390 001, Gujarat, INDIA.

February 2019

APPLIED PHYSICS DEPARTMENT
FACULTY OF TECHNOLOGY AND ENGINEERING
THE MAHARAJA SAYAJIRAO UNIVERSITY OF BARODA
VADODARA – 390 001. GUJARAT, INDIA.
DST-FIST & UGC-DRS Sponsored Department

Date: 23/02/2019

Certificate

This is to certify that the work presented in the thesis entitled **"Study of Decay Properties of Heavy Flavor and Exotic Hadrons"** which is being submitted by **Soni Nakul Rajendrakumar** (Ph.D. Reg. No. FOTE/873, Date: 06/03/2015), Applied Physics Department, Faculty of Technology and Engineering, The Maharaja Sayajirao University of Baroda for the award of degree of **Doctor of Philosophy** in **Applied Physics** has been carried out by him under my supervision and guidance. The matter presented in this thesis is original and has not been submitted for the award of any other degree or diploma.

23/2/19

Supervisor
Dr. J. N. Pandya
Applied Physics Department
Faculty of Technology and Engineering
The M. S. University of Baroda.

Head
Dr. B. S. Chakrabarty
Applied Physics Department,
Faculty of Technology and Engineering
The M. S. University of Baroda.

Head
Applied Physics Department
Faculty of Technology & Engineering
The Maharaja Sayajirao University of Baroda.
Vadodara - 390 001.

Dean
Prof. Arun Pratap
Faculty of Technology and Engineering
The M. S. University of Baroda.

Dean
Faculty of Tech. & Engg.
The M. S. University of Baroda.
Vadodara.

Declaration

I, hereby declare that the research work presented in thesis entitled "**Study of Decay Properties of Heavy Flavor and Exotic Hadrons**" has been carried out by me in the Applied Physics Department, Faculty of Technology and Engineering, The Maharaja Sayajirao University of Baroda, Vadodara, *INDIA* under the supervision of Dr. J. N. Pandya. I declare that the results embodied in this thesis have not been submitted for the award of any Degree or Diploma to this University or any other University or Institute.

Date: 23/02/2019

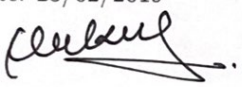

Nakul R Soni
Research Scholar

Dedicated
to
My Family

Acknowledgement

First I would like to thank my supervisor Dr. J. N. Pandya for his valuable guidance, continuous encouragement and admirable patience during this research work. His eagerness and enthusiasm to take up challenging tasks inspired me a lot in exploring the subject in more detail. He gave me complete freedom and support to do the things in the way I wanted. I feel blessed to have a mentor like him. I would also like to thank Prof. P. C. Vinodkumar, Sardar Patel University for his help and suggestions in the initial stage of this work.

I would like to thank Prof. Mikhail A. Ivanov, BLTP, JINR, Dubna, Russia in collaboration with whom the numerical work was done for D and D_s mesons. He carefully explained the Covariant Confined Quark Model calculations in minute details during my visit to JINR for Helmhotz International Summer School. I feel highly privileged to have guidance and support from him throughout these calculations. I also thank our collaborator Chien-Thang Tran from Naples University for helping in computations for D and D_s decays. The support from Prof. Jürgen G. Körner from Mainz University and Prof. P. Santorelli from Naples University are highly appreciated. My special thanks to my friend Shesha with whom I started learning the Quantum Field Theory. She helped me in understanding and solving Feynman diagrams.

I would also like to thank Dr. Arun Anand and Dr. Kirit Lad whose continuous motivation, clear guidance and support were a great work force for me. I am thankful to Dr. B. S. Chakrabarty, Head of the Department and Prof. Arun Pratap, Dean, Faculty of Technology and Engineering for providing me research facilities. I thank our M.Sc. dissertation students Foram, Kanan, Dhruvit, Akshay, Brijal, Radhika and Hemangi for providing lot of inputs for this thesis. I also express my thanks to the colleagues and very good friends Harshal, Sohan, Sonal, Supriya, Laxmi, Nimit, Avani, Swapnil Prabhu, Vismay, Kevil, Rahul, Piyush, Deepak, Dhavalbhai, Margi, Priyanka, Janki, Mugdha, Nirav and Parth.

I am also thankful to my friends Raghav, Chaitanya, Gargi and Preeti for being there with me in the difficult times and also handling my frustrations and anger. Also I would also like to thank Chaxu, Payal, Kajal for providing moral support and encouragement.

I would like to express my deep sense of gratitude to my parents and sister for their patience and continued encouragement, without whose cooperation and moral support it would not have been possible to carry out this work.

My acknowledgement is also due to University Grants Commission, New Delhi for providing me research fellowship through a major research project on Decay Properties of Hadrons undertaken by Dr. J N Pandya in this department.

(Nakul R Soni)

Contents

Abstract

In this thesis, we study the mass spectra and decay properties of heavy quarkonia, doubly heavy baryons, exotic states and open flavor mesons using different approaches. For heavy quarkonia, we employ Cornell potential and the ground state energy is obtained by solving the Schrödinger equation numerically. Using the potential parameters and numerical solution of wave-function, we study the decay properties of charmonia, bottomonia and B_c mesons. The computation of excited state masses and decay properties are then performed without additional parameters. For doubly heavy baryons, we employ the relativistic harmonic confinement potential and ground state energy is obtained using the non-relativistic reduction of Dirac equation. The exotic states are investigated using the modified Woods-Saxon potential by solving the Schrödinger equation numerically. We also compute the leptonic and semileptonic branching fractions of D and D_s mesons in Covariant Confined Quark Model based on the effective field theory formalism.

List of Figures

List of Tables

Chapter 1

Theoretical Developments in Particle Physics

One of the most challenging task in particle physics is to encompass the diversity and the complexity observed in the decay modes and fractional widths of particles. For example, there are twenty-two quantitative modes and total forty-nine decay modes of $K^{\pm}$, and ratio of highest to lowest of these fractions amounts to the order of 10^{11}. The spectroscopy and decay rates of various hadronic states are quite important to study due to availability of huge amount of high precession data acquired using large number of experimental facilities viz. BESIII at the Beijing Electron Positron Collider (BEPC), E835 at Fermilab and CLEO at the Cornell Electron Storage Ring (CESR), the B-meson factories, BaBar at PEP-II, Belle at KEKB, the CDF and D0 experiments at Fermilab, the Selex experiment at Fermilab, ZEUS and H1 at DESY, PHENIX and STAR at RHIC, NA60 and LHCb at CERN and new future facility $\overline{\mathsf{P}}\mathsf{ANDA}$ at FAIR, GSI. The plethora of observations from these facilities offer greater challenges and opportunities in theoretical high energy physics. The hadronic states are not only identified with their masses but also with their various decay rates. All the hadronic states along with experimentally identified decay channels are reported in Particle Data Group (PDG) [1].

1.1 Status of Experimental facilities

The study of Hadron Physics has created lot of interest because of many experimental facilities available world wide. They are collecting huge data in the heavy flavor sectors as well as open flavor sectors. These facilities are working on possible

interpretation of data within Standard Model (SM) and beyond Standard Model (BSM). The BSM includes possible exotic states that are bound states with more than three quarks namely tetra-quark, penta-quark, hexa-quark or hybrid (consisting of quarks and gluons) states. The BSM also includes the rare decays, search for supersymmetry, leptoquarks phenomenology, lepton flavor violation decays and many more.

The experimental collider facilities world wide are divided mainly into two categories: fixed target method and particle colliders. The detailed Physics objectives of the experimental facilities are given in Tab. 1.1.

1.2 Status of Theoretical approaches

The experimental facilities tabulated in Tab. 1.1 are aimed at different areas and all of them are trying to understand the structure and dynamics of the basic building blocks of nature. Presently, the analysis and interpretation of huge data coming from experiments is the most crucial and challenging task. Theoretical methods are focused towards the direction of explaining these data and providing predictions for investigation by the upcoming experimental facilities. The theoretical approaches may be divided in three categories: (i) theories based on first principles such as lattice quantum chromodynamics (LQCD), (ii) QCD sum rules and (iii) theories based on effective field theories as well as phenomenological potential models.

1.2.1 Lattice Quantum Chromodynamics

The Lattice Quantum Chromodynamics (LQCD) is based on the first principles utilizing non-perturbative approach to calculate the hadronic spectrum and matrix element for any interaction explained using Feynman diagram. It is a non-perturbative lattice gauge theory formulated on grid of Euclidian space time allowing the construction of the correlation function between the hadronic state with the help of quark and gluon degrees of freedom. Here, the potential term comes from the interaction at the lattice point and therefore LQCD is considered to be the most realistic theory among all other theories and the results from LQCD calculations have been the closest to experimental data so far.

Table 1.1: Experimental facility and their objective

Collaboration	Country	Type	Objective
CMS	CERN, Switzerland	$p\bar{p}$	Search for Higgs bosons Look for Physics BSM eg. Supersymmetry
		$Pb-Pb$	Heavy ion Collision
ATLAS	CERN, Switzerland	$p\bar{p}$	Search for Higgs bosons Search for CP violation in B and D meson decays Search for supersymmetry
ALICE	CERN, Switzerland	$Pb-Pb$ $Pb-p$	Study of Quark gluon plasma Physics of strongly interacting matter
LHCb	CERN, Switzerland	$p\bar{p}$	B Physics Search for CP violation Search for FCNC decays
BABAR	SLAC, USA	e^+e^-	Search for CP violation in B meson CKM measurement Heavy quarkonium production
Belle	KEK, Japan	e^+e^-	Search for CP violation Search for rare decays in B mesons Search for exotic states
CLEO	CESR, USA	e^+e^-	Study of B Physics including Υ resonance Quarkonium production Study of Charm Physics
BESIII	BEPC, China	e^+e^-	Charm Physics Search for CP violation in $D_{(s)}$ decays Production and decays of light hadrons Search for Physics beyond SM
$D0$	Fermilab, USA	$p\bar{p}$	Search for Higgs bosons B Physics
CDF	Fermilab, USA	$p\bar{p}$	Search for Physics beyond SM Production and decay of top and b quark
SELEX	Fermilab, USA	Fixed Target	Search for charm meson and baryons Search for exotic states
FOCUS	Fermilab, USA	Fixed Target	Spectroscopy of charmed hadrons Search for rare and forbidden decays Search for doubly charmed baryons and pentaquark
CBM	FAIR, Germany	$A-A$	Explore QCD phase diagram at high baryon density
PANDA	FAIR, Germany	Fixed Target	Study of hadron structure and exotic hadrons
NUSTAR	FAIR, Germany		Study of nuclear structure Astrophysics
STAR	BNL, USA	$Au-Au$	Characteristics of the quark-gluon plasma Properties of QGP and equation os state

With the advancement in the computation facilities, many interesting results are available, particularly in the heavy quark sector. In the heavy flavor spectrum, the LQCD have provided most accurate results with a very small standard deviation. LQCD have successfully provided the mass spectrum of charmonia and bottomonia in the papers [2–12] and also successfully predicted the leptonic decay

constants [13, 14]. However, the information regarding the excited states are yet to be reported. Also the LQCD have not yet provided the information regarding all decay properties of heavy quarkonia and mass spectra of B_c mesons. The reviews on LQCD calculations on heavy quarkonium physics is given in the Ref. [15, 16]. In the open flavor sector, the meson form factors are computed for the channel $D \to (\pi, K)\ell^+\nu_\ell$ channels [17–19]. Heavy to light meson form factors are also computed in the papers [20–22], where the authors of [22] have computed the form factors for $D_s \to \eta^{(\prime)}$ as a pilot study only. The $D_s \to \phi$ form factors are also computed for the first time by the HPQCD collaborations [21]. However, the branching fractions computation is not yet reported using LQCD. The mass spectrum for the heavy baryons is also reported by Refs. [23–28].

1.2.2 QCD sum rules

The QCD sum rules (QCDSR) also known as Shifman–Vainshtein–Zakharov sum rules [29] is the nonperturbative tool for hadronic phenomenology. In QCDSR, the hadrons are written in terms of interpolating quark currents and treated in the framework of gauge invariant operator product expansion. This calculation technique gives excellent agreement with the experimental data and also believed to the best theoretical approach after the LQCD.

1.2.3 Effective Field Theories

The computation of hadronic process from the first principles is not trivial and also requires lot of computational power. The alternative to the real scale processes is the Effective Field Theories (EFT). EFT is the fundamental framework to hadronic interaction with the quantum field theory. The EFTs are generally known as the nonrelativistic QCD (NRQCD) [30, 31] which takes into account the energy scale of the order $m_Q \gg m_Q v \gg m_Q v^2$. The remaining energy scale $m_Q \ll m_Q v$ is extracted using the potential NRQCD (pNRQCD) [32,33]. The NRQCD has been successfully employed for the spectroscopy of heavy quarkonia (charmonia, bottomonia and B_c mesons). Both pNRQCD and NRQCD have incorporated the correction in interacting potential of the order $1/m_Q^2$. It is important to note here that this potential is determined by LQCD simulations. They have successfully predicted the mass spectra of the heavy quarkonia. For computing the decay properties of the heavy

quarkonia, the relativistic corrections are also employed to match the experimental data. In the heavy quarkonium spectroscopy, these theories have played very important role in development of the heavy quarkonium physics as the LQCD and QCDSR have not provided the detailed information for the excited states as well as for the decay properties.

EFTs are also developed for understanding the hadrons containing at least one heavy quark (c and/or b) whose masses are more than the QCD scale Λ_{QCD}, e.g. The heavy quark effective theory. This theory assumes that the heavy quark in hadron moves with the constant velocity and hence is considered to be the spectator in the rest frame of heavy hadrons. This theory basically falls in the category of low energy physics which is useful for studying the $D_{(s)}$ and $B_{(s)}$ mesons and understanding the flavor dynamics in these mesons. This can be helpful in studying the weak and strong interactions in the charm and bottom sectors. Their decay properties, especially the leptonic and semileptonic decays allow the direct measurement of Cabibbo-Kobayashi-Maskawa (CKM) matrix elements via hadronic form factors. The CKM matrix is unitary matrix providing the information regarding quark mixing which basically takes place in the weak interactions. The flavor dynamics also gives the information regarding the origin of the CP violation. Currently, the CP violation is one of the main search for most of the experimental facilities.

1.2.4 Other Phenomenological Approaches

The very important problem in theoretical approaches in Particle Physics is quark confinement wherein the isolated color charged quark is not freely available and the quarks and gluons are permanently confined within the hadrons. In the theories based on first principles, the confinement evolves from the QCD computations. The confinement of quarks within hadrons is assumed in the phenomenological approaches. The earliest confinement model is the Bag model developed by Bogolioubov *et al.* that considers the quarks to be confined within the spherical volume and the force acting between the quarks to be the attractive force with strength of the attraction of the order of quark mass [34, and the references therein]. After the discovery of asymptotic freedom, the more advanced MIT Bag model was developed for the hadronic interactions.

The phenomenological approaches include both relativistic as well as nonrelativis-

tic treatment of the quarks comprising the hadrons. The oldest but still effective approach is the potential models inspired from the QCD. In potential models, the interaction is chosen from the LQCD calculations. The next task is to solve the relativistic Dirac equation or the nonrelativistic Schrödinger equation to obtain the bound state mass of the hadrons. For the heavy quarkonium, heavy baryons and the exotic states involving the heavy quarks, the Schrödinger mechanism may be adopted because of the inclusion of heavy quark (c and/or b quark). This is justified to a great extent as the heavy quarks have Significantly low momentum compared to the bound state system constituting the basis for nonrelativistic treatment for heavy hadron spectroscopy. However, for open flavor meson spectroscopy, the non-relativistic treatment is not valid because of the inclusion of light flavor quark.

In potential model calculations, the short distance behaviour is of the Coulomb type interaction and long distance coefficients are essentially confinement part and in the literature, there are various forms of potentials are available. For the hadronic interaction, relativistic as well as non relativistic potential models are reported. The oldest and still applicable potential is Cornell potential using the linear confinement. The potential equation is given by [35],

$$V(r) = Ar - \frac{4}{3}\frac{\alpha_s}{r} \tag{1.1}$$

This potential is also supported by LQCD calculations. Where A is the confinement strength analogous to the string tension and r is the inter-quark separation. For the heavy quarkonia, the Cornell potential is used for computing the mass spectra of ground state as well as excited states. This potential also takes care of the asymptotic freedom, at short distances the Coulomb term dominates where as at the large distances, the confinement term dominates. Here, α_s is the strong running coupling constant.

In Cornell potential Eq. (1.1), the confinement is the special case of the general Martin potential of the form [36]

$$V(r) = A + Br^{\nu}, \qquad n > 0 \tag{1.2}$$

with A and B to be the model constant parameters. This potential was employed for upsilon and charmonium spectra [36].

The logarithmic confinement is also used for computing the quarkonium mass spectra

by Quigg-Rosner. The potential is of the type [37]

$$V(r) = CLog\left(\frac{r}{r_0}\right) \tag{1.3}$$

where C and r_0 are the constants to be determined from the experimental data.

The harmonic confinement also has been employed to compute the mass spectra and decay properties of mesons and baryons. Here, the relativistic Dirac equation is reduced nonrelativistically and the binding energy is obtained. The potential is given by [38]

$$V(r) = \frac{1}{2}(1+\gamma_0)A^2r^2 + B \tag{1.4}$$

Where A and B are the relativistic harmonic model (RHM) parameters. Initially RHM was applied to the light flavor sector only and later extended to the heavy flavor sectors (ERHM) [38,39] with inclusion of Colour Confinement Model [40–42].

The ψ and Υ spectroscopy are also computed in Buchmuller and Tye potential given by [43]

$$V(r) = -\frac{4}{3}\frac{1}{(2\pi)^3}\int d^3q \;\; e^{iqr}\left(\frac{4\pi\alpha_s}{q^2}\right) \tag{1.5}$$

There are many other potentials available in the literature. All the potentials have their different range of applicability. The potential models should reproduce the experimental ground state masses and also predict the excited states correctly. Also the potential models should correctly predict the decay properties. The computation of decay properties depend on the wave function chosen to solve the Schrödinger equation or Dirac equation. But not all potential models successfully predict the mass spectra as well as all decay properties. Till date, not a single potential model has successfully predict the mass spectra and decay properties. As a result, attempts towards the development of potential model to computed all properties of hadrons are still in progress. For example, in calculations of decay properties, different relativistic correction factors are also incorporated to match the experimental data.

1.3 Objectives of the present study and organisation of thesis

The heavy quarkonia ($c\bar{c}$, $b\bar{b}$ and $c\bar{b}$) are the most powerful systems for understanding the heavy quark antiquark interactions in QCD. For charmonia and bottomonia,

there are more than 15 experimentally identified states for both the systems and for B_c mesons only pseudoscalar states for $1S$ and $2S$ states are available. As explained in the previous section, there are many ways in which these systems are studied. The oldest but still relevant approach is the potential model wherein the widely accepted potential for the interaction between constituent quarks is the Cornell potential given by Eq. (1.1). There are many individual studies for the spectroscopy and decay properties of the heavy quarkonia. Many of them provide good prediction for mass spectra but when it comes to predicting the decay properties such as weak decays, not all models provide successful computation of the decay properties [35, 36, 43–50]. In Chapter 2, we compute the mass spectra of charmonia, bottomonia and B_c mesons with the least number of model parameters. For computing the spectra, we employed the nonrelativistic approach for Cornell potential Eq. (1.1) and Schrödinger equation is solved numerically. For computing the masses of excited states, we add the spin dependent part of one gluon exchange potential perturbatively. With the help of model parameters and numerical wave function, we compute various decay properties such as leptonic decay constants, various annihilation widths (digamma, three gamma, digluon, three gluon, γgg, dilepton), electromagnetic transition widths. We also compute the weak decays of B_c mesons in a spectator model and also compute its life time. We compare our findings with the available experimental data, LQCD results and other theoretical and we observe that our results are in good agreement with them.

In chapter 3, we compute the spectroscopy of doubly heavy baryons in harmonic confinement scheme considering the potential of the type Lorentz scalar plus vector potential Eq. (1.4). Here, we employ the nonrelativistic reduction of the Dirac equation. For computing octet and decuplet masses, the spin dependent part of the one gluon exchange potential is employed perturbatively. Using the model parameters and spin flavor wave function, we compute the magnetic moment of the doubly heavy baryons. We also compute the radiative decay width for the transition $3/2^+ \to 1/2^+$ using the transition magnetic moments. We compare our findings with the available experimental data as well with the other theoretical approaches.

In last decade, with the advancement of the experimental facilities, lots of new and sometimes unexpected results have been reported. The first unexpected result came in 2003 when Belle collaboration reported the first new state $X(3872)$ in the channel $B \to K(\pi^+\pi^- J/\phi)$ [51]. The structure of this state was beyond the conventional

quark model. It was observed that this state has a structure of 4 quark state. Later on, this state was also confirmed by BABAR collaboration in the same channel [52, 53]. Further this state was also confirmed by other experimental facilities such as CDF [54], and LHCb [55] collaborations. After 10 years of the discovery, LHCb collaboration has determined its quantum number to be $J^{PC} = 1^{++}$ [56]. Further, many different multi-quark states – so called exotic states were also identified. In PDG 2018, more than 20 tetra-quark states are reported along with several penta-quark and hexa-quark states. There are different ways in which these states are perceived theoretically. These include four quark, di-mesonic, hadro-quarkonium or composite molecular states. In chapter 4, we study exotic states considering them as di-meson molecules. For computing the bound state masses of these states, we solve the Schrödinger equation for the generalised Woods-Saxon potential. We also compute the strong two body decay widths using the interaction Lagrangian mechanism. We compare our results for masses as well as decay widths with the experimental data and other theoretical predictions.

In chapters 2, 3 and 4, we have successfully computed the mass spectra and decay properties of heavy quarkonia, doubly heavy baryons and exotic states considering the nonrelativistic treatment for heavy hadrons. But this nonrelativistic treatment is not applicable for the spectroscopy of open flavor mesons because of inclusion of light quark. In some crude approximation there are also some papers available in the literature where open flavor mesons are considered in the nonrelativistic approximation. But since their momenta are close to the bound state mass, it can not be treated nonrelativistically.

Next in chapter 5, we compute the decay properties of open flavor mesons, particularly charmed mesons. The open flavor mesons are important tool for understanding the dynamics of weak and strong interactions in the charm sectors. The semileptonic branching fractions of these mesons are proportional to the Cabibbo-Kobayashi-Maskawa (CKM) matrix elements, therefore these channels provide the direct determinations of $c \to q$ matrix element where $q = d, s$. We compute the decay properties of charmed and charmed-strange (D and D_s) mesons in a effective quantum field theory approach. We study the weak decay properties such as leptonic and semileptonic decay decays of $D_{(s)}$ mesons in the covariant confined quark model (CCQM) with built-in ifrared confinement developed by G. V. Efimov and M. A. Ivanov [57, 58]. The interaction Lagrangian is written in terms of the constituent

quarks. In this model, the confinement of the quark can be introduced using the compositeness conditions [59,60]. One of the important key feature of the CCQM is computation of form factors in the entire physical range of momentum transfer. We study the leptonic branching fractions $D_{(s)} \to \ell^+\nu_\ell$ for $\ell = e, \mu$ and τ and semileptonic branching fractions for the channels $D_{(s)} \to (P, V)\ell^+\nu$ for $\ell = e$ and μ. Here P and V corresponds to the pseudoscalar and vector mesons. It is important to note that in semileptonic decays $D_{(s)}$ mesons the tau mode is kinematically forbidden. We also compare our findings of form factors and branching fractions with latest BESIII data along with other experimental data and other theoretical predictions.

Finally in chapter 6, we conclude the present study. We also discuss the future prospects of research in the area of weak decays using the covariant confined quark model. We also discuss the other possibilities of the application of potential models for heavy quarkonium spectroscopy.

Chapter 2

Heavy Quarkonium Spectroscopy

2.1 Introduction

Quarkonia are the flavorless mesons that have both quark and antiquark of the same type making them the best tools for understanding the dynamics of strongly interacting systems. The first quarkonium state J/ψ ($c\bar{c}$ or charmonia) was discovered experimentally and announced by Stanford Linear Accelerator Center and Brookhaven National Laboratory on November 11, 1974 [61]. The E760 collaboration at Fermilab measured the masses as well as the total widths of P states namely χ_{c1} and χ_{c2} [62]. Then, the 1^3D_2 state was discovered in B decays by BESIII collaboration [63]. The first ground state singlet charmonium η_c was also discovered in Mark-II and Crystal ball experiments. Similarly, Υ ($b\bar{b}$ or bottomonia) was first discovered by E288 at Fermilab [64, 65]. After 30 years, the first singlet state $\eta_b(1S)$ was discovered by Belle Collaboration [66] in 2008. Later, $\eta_b(2S)$ was also discovered by *BABAR* [67], CLEO [68] and Belle [69] collaborations. Also in 90's, the nonrelativistic potential models predicted not only the ground state mass of the tightly bound state of c and $\bar{b}$ in the range of 6.2–6.3 GeV [70, 71], but also predicted to have very rich spectroscopy. In 1998, CDF collaboration [72] reported B_c mesons in $p\bar{p}$ collisions at $\sqrt{s} = 1.8$ TeV and was later confirmed by D0 [73] and LHCb [74] collaborations. The LHCb collaboration has also made the most precise measurement of the lifetime of B_c mesons [75]. Its first excited state has also been reported by ATLAS Collaborations [76] in $p\bar{p}$ collisions with significance of 5.2σ. Many experimental groups such as CLEO, LEP, CDF, D0 and NA50 have provided data and *BABAR*, Belle, CLEO-III, ATLAS, CMS and LHCb are producing and expected to produce more precise data in upcoming experiments, particularly for the heavy

quarkonium physics. Comprehensive reviews on the status of experimental heavy quarkonium physics are found in literature [15, 16, 77–80].

There are many theoretical groups working on the heavy quarkonium spectroscopy as well as its decay properties. The models based on first principles and fully non-perturbative ones such as lattice quantum chromodynamics (LQCD) [2–12], QCD sum rules [45,81] with QCD [82,83], perturbative QCD [84], lattice NRQCD [85,86] and effective field theories [87] that have attempted to explain the production and decays of these states. The other approaches include phenomenological potential models such as the relativistic quark model based on quasi-potential approach [88–94], where the relativistic quasi-potential including one loop radiative corrections reproduce the mass spectrum of quarkonium states. The quasi-potential has also been employed along with leading order radiative correction to heavy quark potential [95–98], relativistic potential model [99–101] as well as semirelativistic potential model [102]. In nonrelativistic potential models, there exist several forms of quark antiquark potentials in the literature. Common element among them is the coulomb repulsive plus quark confinement interaction potential. The authors of [46–50, 103, 104] have considered the confinement of power potential Ar^{ν} with ν varying from 0.1 to 2.0 and the confinement strength A to vary with potential index ν. Confinement of the order $r^{2/3}$ have also been attempted [105]. Linear confinement of quarks has been considered by many groups [35, 37, 106–116] and they have been in good agreement with the experimental data for quarkonium spectroscopy along with decay properties. The Bethe-Salpeter approach was also employed for the mass spectroscopy of charmonia and bottomonia [110, 111, 117]. The quarkonium mass spectrum was also computed in the nonrelativistic quark model [118], screened potential model (SPM) [115,116] and constituent quark model [119]. There are also other non-linear potential models that predict the mass spectra of the heavy quarkonia successfully [36, 43, 44, 120–127].

The interaction potential for mesonic states is difficult to derive for full range of quark antiquark separation from first principles of QCD. So most forms of QCD inspired potential would result in uncertainties in the computation of spectroscopic properties particularly in the intermediate range. Different potential models may produce similar mass spectra matching with experimental observations but they may not be in mutual agreement when it comes to decay properties like decay constants, leptonic decays or radiative transitions. Moreover, the mesonic states are

identified with masses along with certain decay channels, therefore the test for any successful theoretical model is to reproduce the mass spectrum along with decay properties. Relativistic as well as nonrelativistic potential models have successfully predicted the spectroscopy but they are found to differ in computation of the decay properties [35, 36, 43–50].

In this chapter, we employ nonrelativistic potential with one gluon exchange (essentially Coulomb like) plus linear confinement (Cornell potential) as this form of the potential is also supported by LQCD [128–130]. We solve the Schrödinger equation numerically for the potential to get the spectroscopy of the quarkonia. We first compute the mass spectra of charmonia and bottomonia states to determine quark masses and confinement strengths after fitting the spin-averaged ground state masses with experimental data of respective mesons. Using the potential parameters and numerical wave functions, we compute the decay properties such as leptonic decay constants, digamma, dilepton, digluon decay width using the Van-Royen Weiskopf formula. These parameters are then used to compute the mass spectra and lifetime of B_c meson. We also compute the electromagnetic ($E1$ and $M1$) transition widths of heavy quarkonia and B_c mesons. This work was published in European Physical Journal C [131]. We have also computed the decay properties of charmonia and bottomonia in the extended harmonic confinement model (ERHM) [38, 39] as well as in nonrelativistic treatment for Coulomb plus power potential ($CPP_{\nu=1}$) using variational trial wave function [46–49, 132, 133]. This work was also published in Chinese Physics C [134].

2.2 Methodology

The bound state of two body systems in QCD is nonperturbative in nature and only LQCD can explain its properties. However, other methods are also found to exist in literature. The mesonic bound state within relativistic quantum field is described in Bethe-Salpeter formalism but the Bethe-Salpeter equation is solved only in the ladder approximations. Also, Bethe-Salpeter approach in harmonic confinement is successful in low flavor sectors [135, 136]. The alternative, old and still effective approach is the nonrelativistic potential model approach. Sufficiently small momenta of the charm and bottom quark compared to bound state mass of charmonia and bottomonia constitutes the basis of nonrelativistic treatment for heavy quarkonium

spectroscopy. Though Lattice QCD calculations in the quenched approximation suggest a linearly increasing potential in the confinement range [2–12], a specific form of interaction potential in the full range is not yet known. At short distances relativistic effects are more important as they give rise to quark-antiquark pairs from the vacuum that in turn affect the nonrelativistic Coulomb interaction in the presence of sea quarks. The mass spectra of quarkonia is not sensitive to these relativistic effects at short distances. However, the decay properties show significant difference with inclusion of relativistic corrections. So we choose to compute the charmonium mass spectra nonrelativistically in present study. The nonrelativistic Hamiltonian for the study of heavy bound state of mesons such as $c\bar{c}$, $c\bar{b}$ and $b\bar{b}$ given by

$$H = M + \frac{p^2}{2M_{cm}} + V_{\text{Cornell}}(r) + V_{SD}(r) \tag{2.1}$$

with

$$M = m_Q + m_{\bar{Q}} \quad \text{and} \quad M_{cm} = \frac{m_Q m_{\bar{Q}}}{m_Q + m_{\bar{Q}}} \tag{2.2}$$

where m_Q and $m_{\bar{Q}}$ are the masses of quark and antiquark respectively, $\vec{p}$ is the relative momentum of the each quark and $V_{\text{Cornell}}(r)$ is the quark-antiquark potential of the type coulomb plus linear confinement (Cornell potential) given by

$$V_{\text{Cornell}}(r) = -\frac{4}{3}\frac{\alpha_s}{r} + Ar. \tag{2.3}$$

Here, $1/r$ term is analogous to the Coulomb type interaction corresponding to the potential induced between quark and antiquark through one gluon exchange that dominates at small distances. The second term is the confinement part of the potential with the confinement strength A as the model parameter. The confinement term becomes dominant at the large distances. α_s is a strong running coupling constant and can be computed as

$$\alpha_s(\mu^2) = \frac{4\pi}{(11 - \frac{2}{3}n_f)\ln(\mu^2/\Lambda^2)} \tag{2.4}$$

where n_f is the number of flavors, μ is renormalization scale related to the constituent quark masses as $\mu = 2m_Q m_{\bar{Q}}/(m_Q + m_{\bar{Q}})$ and Λ is a QCD scale which is taken as 0.15 GeV by fixing $\alpha_s = 0.1185$ [1] at the Z-boson mass.

The confinement strengths with respective quark masses are fine tuned to reproduce the experimental spin averaged ground state masses of both $c\bar{c}$ and $b\bar{b}$ mesons and they are given in Table 2.1. We compute the masses of radially and orbitally excited states without any additional parameters. Similar work has been done by [49,50,104]

and they have considered different values of confinement strengths for different potential indices. The Cornell potential has been shown to be independently successful in computing the spectroscopy of ψ and Υ families. In this chapter, we compute the mass spectra of the ψ and Υ families along with B_c meson with minimum number of parameters.

Using the parameters defined in Table 2.1, we compute the spin averaged masses of quarkonia and the excited state masses are computed employing the spin dependent part of one gluon exchange potential (OGEP) $V_{SD}(r)$ perturbatively which includes spin-spin, spin-orbit and tensor terms given by [45, 83, 109, 118]

$$V_{SD}(r) = V_{SS}(r)\left[S(S+1) - \frac{3}{2}\right] + V_{LS}(r)(\vec{L}\cdot\vec{S}) + V_T(r)\left[S(S+1) - 3(S\cdot\hat{r})(S\cdot\hat{r})\right] \quad (2.5)$$

The spin-spin interaction term gives the hyper-fine splitting while spin-orbit and

Table 2.1: Parameters for quarkonium spectroscopy

m_c	m_b	A_{cc}	A_{bb}
1.317 GeV	4.584 GeV	0.18 GeV^2	0.25 GeV^2

Table 2.2: Mass spectrum of S and P-wave charmonia (in GeV)

State	Present [131]	RQM [88]	NRQM [115]	BSE [117]	SPM [126]	RPM [100]	PM [123]	NRPM [109]	NRQM [118]	PM [120]	LQCD [11]	PDG [1]
1^1S_0	2.989	2.981	2.984	2.925	2.979	2.980	2.980	2.982	3.088	2.979	2.884	2.984
1^3S_1	3.094	3.096	3.097	3.113	3.097	3.097	3.097	3.090	3.168	3.096	3.056	3.097
2^1S_0	3.602	3.635	3.637	3.684	3.623	3.597	3.633	3.630	3.669	3.600	3.535	3.639
2^3S_1	3.681	3.685	3.679	3.676	3.673	3.685	3.690	3.672	3.707	3.680	3.662	3.686
3^1S_0	4.058	3.989	4.004	–	3.991	4.014	3.992	4.043	4.067	4.011	–	–
3^3S_1	4.129	4.039	4.030	3.803	4.022	4.095	4.030	4.072	4.094	4.077	–	4.039
4^1S_0	4.448	4.401	4.264	–	4.250	4.433	4.244	4.384	4.398	4.397	–	–
4^3S_1	4.514	4.427	4.281	–	4.273	4.477	4.273	4.406	4.420	4.454	–	4.421
5^1S_0	4.799	4.811	4.459	–	4.446	–	4.440	–	–	–	–	–
5^3S_1	4.863	4.837	4.472	–	4.463	–	4.464	–	–	–	–	–
6^1S_0	5.124	5.155	–	–	4.595	–	4.601	–	–	–	–	–
6^3S_1	5.185	5.167	–	–	4.608	–	4.621	–	–	–	–	–
1^3P_0	3.428	3.413	3.415	3.323	3.433	3.416	3.392	3.424	3.448	3.488	3.412	3.415
1^3P_1	3.468	3.511	3.521	3.489	3.510	3.508	3.491	3.505	3.520	3.514	3.480	3.511
1^1P_1	3.470	3.525	3.526	3.433	3.519	3.527	3.524	3.516	3.536	3.539	3.494	3.525
1^3P_2	3.480	3.555	3.553	3.550	3.556	3.558	3.570	3.556	3.564	3.565	3.536	3.556
2^3P_0	3.897	3.870	3.848	3.833	3.842	3.844	3.845	3.852	3.870	3.947	–	3.918
2^3P_1	3.938	3.906	3.914	3.672	3.901	3.940	3.902	3.925	3.934	3.972	–	–
2^1P_1	3.943	3.926	3.916	3.747	3.908	3.960	3.922	3.934	3.950	3.996	–	–
2^3P_2	3.955	3.949	3.937	–	3.937	3.994	3.949	3.972	3.976	4.021	4.066	3.927
3^3P_0	4.296	4.301	4.146	–	4.131	–	4.192	4.202	4.214	–	–	–
3^3P_1	4.338	4.319	4.192	3.912	4.178	–	4.178	4.271	4.275	–	–	–
3^1P_1	4.344	4.337	4.193	–	4.184	–	4.137	4.279	4.291	–	–	–
3^3P_2	4.358	4.354	4.211	–	4.208	–	4.212	4.317	4.316	–	–	–
4^3P_0	4.653	4.698	–	–	–	–	–	–	–	–	–	–
4^3P_1	4.696	4.728	–	–	–	–	–	–	–	–	–	–
4^1P_1	4.704	4.744	–	–	–	–	–	–	–	–	–	–
4^3P_2	4.718	4.763	–	–	–	–	–	–	–	–	–	–
5^3P_0	4.983	–	–	–	–	–	–	–	–	–	–	–
5^3P_1	5.026	–	–	–	–	–	–	–	–	–	–	–
5^1P_1	5.034	–	–	–	–	–	–	–	–	–	–	–
5^3P_2	5.049	–	–	–	–	–	–	–	–	–	–	–

Table 2.3: Mass spectrum of D and F-wave charmonia (in GeV)

State	Present [131]	RQM [88]	NRQM [115]	BSE [117]	SPM [126]	RPM [100]	PM [123]	NRPM [109]	NRQM [118]	PM [120]
1^3D_3	3.755	3.813	3.808	3.869	3.799	3.831	3.844	3.806	3.809	3.798
1^1D_2	3.765	3.807	3.805	3.739	3.796	3.824	3.802	3.799	3.803	3.796
1^3D_2	3.772	3.795	3.807	3.550	3.798	3.824	3.788	3.800	3.804	3.794
1^3D_1	3.775	3.783	3.792	–	3.787	3.804	3.729	3.785	3.789	3.792
2^3D_3	4.176	4.220	4.112	3.806	4.103	4.202	4.132	4.167	4.167	4.425
2^1D_2	4.182	4.196	4.108	–	4.099	4.191	4.105	4.158	4.158	4.224
2^3D_2	4.188	4.190	4.109	–	4.100	4.189	4.095	4.158	4.159	4.223
2^3D_1	4.188	4.105	4.095	–	4.089	4.164	4.057	4.142	4.143	4.222
3^3D_3	4.549	4.574	4.340	–	4.331	–	4.351	–	–	–
3^1D_2	4.553	3.549	4.336	–	4.326	–	4.330	–	–	–
3^3D_2	4.557	4.544	4.337	–	4.327	–	4.322	–	–	–
3^3D_1	4.555	4.507	4.324	–	4.317	–	4.293	–	–	–
4^3D_3	4.890	4.920	–	–	–	–	4.526	–	–	–
4^1D_2	4.892	4.898	–	–	–	–	4.509	–	–	–
4^3D_2	4.896	4.896	–	–	–	–	4.504	–	–	–
4^3D_1	4.891	4.857	–	–	–	–	4.480	–	–	–
1^3F_2	3.990	4.041	–	–	–	4.068	–	4.029	–	–
1^3F_3	4.012	4.068	–	3.999	–	4.070	–	4.029	–	–
1^1F_3	4.017	4.071	–	4.037	–	4.066	–	4.026	–	–
1^3F_4	4.036	4.093	–	–	–	4.062	–	4.021	–	–
2^3F_2	4.378	4.361	–	–	–	–	–	4.351	–	–
2^3F_3	4.396	4.400	–	–	–	–	–	3.352	–	–
2^1F_3	4.400	4.406	–	–	–	–	–	4.350	–	–
2^3F_4	4.415	4.434	–	–	–	–	–	4.348	–	–
3^3F_2	4.730	–	–	–	–	–	–	–	–	–
3^3F_3	4.746	–	–	–	–	–	–	–	–	–
3^1F_3	4.749	–	–	–	–	–	–	–	–	–
3^3F_4	4.761	–	–	–	–	–	–	–	–	–

tensor terms gives the fine structure of the quarkonium states. The coefficients of spin dependent terms of the Eq. (2.5) can be written as [83],

$$V_{SS}(r) = \frac{1}{3m_Q m_{\bar{Q}}}\nabla^2 V_V(r) = \frac{16\pi\alpha_s}{9m_Q m_{\bar{Q}}}\delta^3(\vec{r}) \tag{2.6}$$

$$V_{LS}(r) = \frac{1}{2m_Q m_{\bar{Q}} r}\left(3\frac{dV_V(r)}{dr} - \frac{dV_S(r)}{dr}\right) \tag{2.7}$$

$$V_T(r) = \frac{1}{6m_Q m_{\bar{Q}}}\left(3\frac{dV_V^2(r)}{dr^2} - \frac{1}{r}\frac{dV_V(r)}{dr}\right) \tag{2.8}$$

Where $V_V(r)$ and $V_S(r)$ correspond to the vector and scalar part of the Cornell potential in Eq. (2.3) respectively. Using all the parameters defined above, the Schrödinger equation is numerically solved using *Mathematica* notebook utilizing the Runge-Kutta method [137]. It is generally believed that the charmonia need to be treated relativistically due to their lighter masses, but we note here that the computed wave functions of charmonia using relativistic as well as nonrelativistic approaches don't show significant difference [94]. The computed mass spectra of heavy quarkonia and B_c mesons are listed in Tables 2.2–2.7.

In the ERHM approach, we use the scalar plus vector potential for the quark confinement. This method was successful in predicting the low lying hadronic properties in the relativistic schemes for quark confinement [139,140] and later it was extended to

Table 2.4: Mass spectrum of S and P-wave bottomonia (in GeV)

State	Present [131]	RQM [114]	RQM [88]	NRQM [116]	BSE [117]	SPM [127]	RPM [101]	PM [123]	NRCQM [119]	PDG [1]
1^1S_0	9.428	9.402	9.398	9.390	9.414	9.389	9.393	9.392	9.455	9.398
1^3S_1	9.463	9.465	9.460	9.460	9.490	9.460	9.460	9.460	9.502	9.460
2^1S_0	9.955	9.976	9.990	9.990	9.987	9.987	9.987	9.991	9.990	9999
2^3S_1	9.979	10.003	10.023	10.015	10.089	10.016	10.023	10.024	10.015	10.023
3^1S_0	10.338	10.336	10.329	10.326	–	10.330	10.345	10.323	10.330	–
3^3S_1	10.359	10.354	10.355	10.343	10.327	10.351	10.364	10.346	10.349	10.355
4^1S_0	10.663	10.523	10.573	10.584	–	10.595	10.623	10.558	–	–
4^3S_1	10.683	10.635	10.586	10.597	–	10.611	10.643	10.575	10.607	10.579
5^1S_0	10.956	10.869	10.851	10.800	–	10.817	–	10.741	–	–
5^3S_1	10.975	10.878	10.869	10.811	–	10.831	–	10.755	10.818	10.876
6^1S_0	11.226	11.097	11.061	10.997	–	11.011	–	10.892	–	–
6^3S_1	11.243	11.102	11.088	10.988	–	11.023	–	10.904	10.995	11.019
1^3P_0	9.806	9.847	9.859	9.864	9.815	9.865	9.861	9.862	9.855	9.859
1^3P_1	9.819	9.876	9.892	9.903	9.842	9.897	9.891	9.888	9.874	9.893
1^1P_1	9.821	9.882	9.900	9.909	9.806	9.903	9.900	9.896	9.879	9.899
1^3P_2	9.825	9.897	9.912	9.921	9.906	9.918	9.912	9.908	9.886	9.912
2^3P_0	10.205	10.226	10.233	10.220	10.254	10.226	10.230	10.241	10.221	10.232
2^3P_1	10.217	10.246	10.255	10.249	10.120	10.251	10.255	10.256	10.236	10.255
2^1P_1	10.220	10.250	10.260	10.254	10.154	10.256	10.262	10.261	10.240	10.260
2^3P_2	10.224	10.261	10.268	10.264	–	10.269	10.271	10.268	10.246	10.269
3^3P_0	10.540	10.552	10.521	10.490	–	10.502	–	10.511	10.500	–
3^3P_1	10.553	10.538	10.541	10.515	10.303	10.524	–	10.507	10.513	–
3^1P_1	10.556	10.541	10.544	10.519	–	10.529	–	10.497	10.516	–
3^3P_2	10.560	10.550	10.550	10.528	–	10.540	–	10.516	10.521	–
4^3P_0	10.840	10.775	10.781	–	–	10.732	–	–	–	–
4^3P_1	10.853	10.788	10.802	–	–	10.753	–	–	–	–
4^1P_1	10.855	10.790	10.804	–	–	10.757	–	–	–	–
4^3P_2	10.860	10.798	10.812	–	–	10.767	–	–	–	–
5^3P_0	11.115	11.004	–	–	–	10.933	–	–	–	–
5^3P_1	11.127	11.014	–	–	–	10.951	–	–	–	–
5^1P_1	11.130	11.016	–	–	–	10.955	–	–	–	–
5^3P_2	11.135	11.022	–	–	–	10.965	–	–	–	–

Table 2.5: Mass spectrum of D and F-wave bottomonia (in GeV)

State	Present [131]	RQM [114]	RQM [88]	NRQM [116]	BSE [117]	SPM [127]	RPM [101]	PM [123]	NRCQM [119]	PDG [1]
1^3D_3	10.073	10.115	10.166	10.157	10.232	10.156	10.163	10.177	10.127	–
1^1D_2	10.074	10.148	10.163	10.153	10.194	10.152	10.158	10.166	10.123	–
1^3D_2	10.075	10.147	10.161	10.153	10.145	10.151	10.157	10.162	10.122	10.163
1^3D_1	10.074	10.138	10.154	10.146	–	10.145	10.149	10.147	10.117	–
2^3D_3	10.423	10.455	10.449	10.436	–	10.442	10.456	10.447	10.422	–
2^1D_2	10.424	10.450	10.445	10.432	–	10.439	10.452	10.440	10.419	–
2^3D_2	10.424	10.449	10.443	10.432	–	10.438	10.450	10.437	10.418	–
2^3D_1	10.423	10.441	10.435	10.425	–	10.432	10.443	10.428	10.414	–
3^3D_3	10.733	10.711	10.717	–	–	10.680	–	10.652	–	–
3^1D_2	10.733	10.706	10.713	–	–	10.677	–	10.646	–	–
3^3D_2	10.733	10.705	10.711	–	–	10.676	–	10.645	–	–
3^3D_1	10.731	10.698	10.704	–	–	10.670	–	10.637	–	–
4^3D_3	11.015	10.939	10.963	–	–	10.886	–	10.817	–	–
4^1D_2	11.015	10.935	10.959	–	–	10.883	–	10.813	–	–
4^3D_2	11.016	10.934	10.957	–	–	10.882	–	10.811	–	–
4^3D_1	11.013	10.928	10.949	–	–	10.877	–	10.805	–	–
1^3F_2	10.283	10.350	10.343	10.338	–	–	10.353	–	10.315	–
1^3F_3	10.287	10.355	10.346	10.340	10.302	–	10.356	–	10.321	–
1^1F_3	10.288	10.355	10.347	10.339	10.319	–	10.356	–	10.322	–
1^3F_4	10.291	10.358	10.349	10.340	–	–	10.357	–	–	–
2^3F_2	10.604	10.615	10.610	–	–	–	10.610	–	–	–
2^3F_3	10.607	10.619	10.614	–	–	–	10.613	–	–	–
2^1F_3	10.607	10.619	10.647	–	–	–	10.613	–	–	–
2^3F_4	10.609	10.622	10.617	–	–	–	10.615	–	–	–
3^3F_2	10.894	10.850	–	–	–	–	–	–	–	–
3^3F_3	10.896	10.853	–	–	–	–	–	–	–	–
3^1F_3	10.897	10.853	–	–	–	–	–	–	–	–
3^3F_4	10.898	10.856	–	–	–	–	–	–	–	–

Table 2.6: Mass spectrum of S and P-wave B_c meson (in GeV)

State	Present [131]	PM [103]	RQM [88]	RQM [113]	RQM [138]	PDG [1]
1^1S_0	6.272	6.278	6.272	6.271	6.275	6.275
1^3S_1	6.321	6.331	6.333	6.338	6.314	–
2^1S_0	6.864	6.863	6.842	6.855	6.838	6.842
2^3S_1	6.900	6.873	6.882	6.887	6.850	–
3^1S_0	7.306	7.244	7.226	7.250	–	–
3^3S_1	7.338	7.249	7.258	7.272	–	–
4^1S_0	7.684	7.564	7.585	–	–	–
4^3S_1	7.714	7.568	7.609	–	–	–
5^1S_0	8.025	7.852	7.928	–	–	–
5^3S_1	8.054	7.855	7.947	–	–	–
6^1S_0	8.340	8.120	–	–	–	–
6^3S_1	8.368	8.122	–	–	–	–
1^3P_0	6.686	6.748	6.699	6.706	6.672	–
1^3P_1	6.705	6.767	6.750	6.741	6.766	–
1^1P_1	6.706	6.769	6.743	6.750	6.828	–
1^3P_2	6.712	6.775	6.761	6.768	6.776	–
2^3P_0	7.146	7.139	7.094	7.122	6.914	–
2^3P_1	7.165	7.155	7.134	7.145	7.259	–
2^1P_1	7.168	7.156	7.094	7.150	7.322	–
2^3P_2	7.173	7.162	7.157	7.164	7.232	–
3^3P_0	7.536	7.463	7.474	–	–	–
3^3P_1	7.555	7.479	7.510	–	–	–
3^1P_1	7.559	7.479	7.500	–	–	–
3^3P_2	7.565	7.485	7.524	–	–	–
4^3P_0	7.885	–	7.817	–	–	–
4^3P_1	7.905	–	7.853	–	–	–
4^1P_1	7.908	–	7.844	–	–	–
4^3P_2	7.915	–	7.867	–	–	–
5^3P_0	8.207	–	–	–	–	
5^3P_1	8.226	–	–	–	–	
5^1P_1	8.230	–	–	–	–	
5^3P_2	8.237	–	–	–	–	

Table 2.7: Mass spectrum of D and F-wave B_c meson (in GeV)

State	Present [131]	PM [103]	RQM [88]	RQM [113]	RQM [138]
1^3D_3	6.990	7.026	7.029	7.045	6.980
1^1D_2	6.994	7.035	7.026	7.041	7.009
1^3D_2	6.997	7.025	7.025	7.036	7.154
1^3D_1	6.998	7.030	7.021	7.028	7.078
2^3D_3	7.399	7.363	7.405	–	–
2^1D_2	7.401	7.370	7.400	–	–
2^3D_2	7.403	7.361	7,399	–	–
2^3D_1	7.403	7.365	7.392	–	–
3^3D_3	7.761	–	7.750	–	–
3^1D_2	7.762	–	7.743	–	–
3^3D_2	7.764	–	7.741	–	–
3^3D_1	7.762	–	7.732	–	–
4^3D_3	8.092	–	–	–	–
4^1D_2	8.093	–	–	–	–
4^3D_2	8.094	–	–	–	–
4^3D_1	8.091	–	–	–	–
1^3F_2	7.234	–	7.273	7.269	–
1^3F_3	7.242	–	7.269	7.276	–
1^1F_3	7.241	–	7.268	7.266	–
1^3F_4	7.244	–	7.277	7.271	–
2^3F_2	7.607	–	7.618	–	–
2^3F_3	7.615	–	7.616	–	–
2^1F_3	7.614	–	7.615	–	–
2^3F_4	7.617	–	7.617	–	–
3^3F_2	7.946	–	–	–	–
3^3F_3	7.954	–	–	–	–
3^1F_3	7.953	–	–	–	–
3^3F_4	7.956	–	–	–	–

accommodate multi-quark states with unequal quark masses [38, 39]. The detailed computation technique is given in the Chapter 3. The spin average masses of the charmonia and bottomonia are obtained using the model parameters $m_c = 1.428$ GeV, $m_b = 4.637$ GeV, $A = 2166$ MeV$^{3/2}$ [134].

In CPP_ν approach also the quarks and antiquarks are treated nonrelativistically. The interacting potential is given by

$$V(r) = -\frac{\alpha_c}{r} + Ar^\nu \tag{2.9}$$

with $\alpha_c = 4/3\alpha_s$, A is the confinement strength and ν is the general power ranges from 0.5 to 2 and $\nu = 1$ corresponds to the Cornell potential. The Schrödinger equation for the potential Eq. (2.9) is solved using the hydrogenic trial wave function given by,

$$R_{nl}(r) = \sqrt{\frac{\mu^3(n-l-1)!}{2n(n+l)!}}(\mu r)^l e^{-\mu r/2} L^{2l+1}_{n-l-1}(\mu r) \tag{2.10}$$

Here, μ is the variational parameter and $L^{2l+1}_{n-l-1}(\mu r)$ is the associated Laguerre polynomial. For the given ν, the variational parameter is determined using the virial theorem

$$\langle KE \rangle = \frac{1}{2}\left\langle r\frac{dV}{dr}\right\rangle \tag{2.11}$$

The potential parameters are $m_c = 1.31$ GeV, $m_b = 4.66$ GeV, $\alpha_c = 0.4$ for charmonia and $\alpha_c = 0.3$ for bottomonia. In this chapter, we present our results for the $\nu = 1$ only.

It is important to note that Eq. (2.3) and Eq. (2.9) for $\nu = 1$ is same but in our paper Ref. [131], the Schrödinger equation was solved numerically while in our paper Ref. [134], the Schrödinger equation was solved using the variational trial wave function.

2.3 Decay Properties

In PDG [1], the quarkonium states are reported with masses along with their decay channels and in fact the mass spectra are determined from the decay channels only. Therefore it is important to validate any potential model with not only mass spectrum but also with the decay channels without using any additional parameter. In nonrelativistic limit, the decay channels are directly related to the corresponding

Table 2.8: Leptonic decay constant of charmonia (in MeV)

State	Present [131]	PM [104]	BSE [144]	NRQM [118]	LQCD [13]	QCDSR [13]	PDG [1]
J/ψ	325.876	338	411	393	418(8)(5)	401 ± 46	416 ± 6
$\eta_c(1S)$	350.314	363	378	402	387(7)(2)	309 ± 39	335 ± 75
$\psi(2S)$	257.340	254	155	293	–	–	304 ± 4
$\eta_c(2S)$	278.447	275	82	240	–	–	–
$\psi(3S)$	229.857	220	188	258	–	–	–
$\eta_c(3S)$	249.253	239	206	193	–	–	–
$\psi(4S)$	212.959	200	262	–	–	–	–
$\eta_c(4S)$	231.211	217	87	–	–	–	–
$\psi(5S)$	200.848	186	–	–	–	–	–
$\eta_c(5S)$	218.241	202	–	–	–	–	
$\psi(6S)$	191.459	175	–	–	–	–	–
$\eta_c(6S)$	208.163	197	–	–	–	–	–

wave function. In this section, we test our potential parameters and wave function to compute the weak decays, particularly decay constants, annihilation widths and electromagnetic transitions.

2.3.1 Leptonic decay constants

The leptonic decay constants are helpful in understanding the weak decays. The matrix elements for leptonic decay constants of pseudoscalar and vector mesons are given by

$$\langle 0|\bar{Q}\gamma^{\mu}\gamma_5 Q|P_{\mu}(k)\rangle = if_P k^{\mu} \tag{2.12}$$

$$\langle 0|\bar{Q}\gamma^{\mu} Q|P_{\mu}(k)\rangle = if_V M_V \epsilon^{*\mu} \tag{2.13}$$

where k is the momentum of pseudoscalar meson, $\epsilon^{*\mu}$ is the polarization vector of meson. In the nonrelativistic limit, the decay constants of pseudoscalar and vector mesons are given by Van Royen-Weiskopf formula with QCD correction factor [141–143]

$$f^2_{P/V} = \frac{3|R_{nsP/V}(0)|^2}{\pi M_{nsP/V}}\left[1-\frac{\alpha_s}{\pi}\left(\delta^{P/V}-\frac{m_Q-m_{\bar{Q}}}{m_Q+m_{\bar{Q}}}\ln\frac{m_Q}{m_{\bar{Q}}}\right)\right]. \tag{2.14}$$

With $\delta^P = 2$ and $\delta^V = 8/3$. Using the above relation, we compute the leptonic decay constants and the results are listed in Tables 2.8 – 2.11 in comparison with other models including LQCD.

Table 2.9: Leptonic decay constant of bottomonia (in MeV)

State	Present [131]	PM [104]	BSE [144]	NRQM [118]	BSE [145]	LQCD [14]	PDG [1]
$\Upsilon(1S)$	647.250	706	707	665	498±(20)	649(31)	715 ± 5
$\eta_b(1S)$	646.025	744	756	599	–	–	–
$\Upsilon(2S)$	519.436	547	393	475	366±(27)	481(39)	498 ± 8
$\eta_b(2S)$	518.803	577	285	411	–	–	–
$\Upsilon(3S)$	475.440	484	9	418	304±(27)	–	430 ± 4
$\eta_b(3S)$	474.954	511	333	354	–	–	–
$\Upsilon(4S)$	450.066	446	20	388	259±(22)	–	336 ± 18
$\eta_b(4S)$	449.654	471	40	–	–	–	–
$\Upsilon(5S)$	432.437	419	–	367	228±(16)	–	–
$\eta_b(5S)$	432.072	443	–	–	–	–	–
$\Upsilon(6S)$	418.977	399	–	351	–	–	–
$\eta_b(6S)$	418.645	422	–	–	–	–	–

Table 2.10: Pseudoscalar decay constant of B_c meson (in MeV)

State	f_P Present [131]	PM [104]	RQM [91]	QCDSR [45]	PM [71]	RQM [138]
$1S$	432.955	465	503	460±(60)	500	554.125
$2S$	355.504	361	–	–	–	
$3S$	325.659	319	–	–	–	
$4S$	307.492	293	–	–	–	
$5S$	294.434	275	–	–	–	
$6S$	284.237	261	–	–	–	

Table 2.11: Vector decay constant of B_c meson (in MeV)

State	f_V Present [131]	PM [104]	RQM [91]	QCDSR [45]	PM [71]
$1S$	434.642	435	433	460±(60)	500
$2S$	356.435	337	–	–	–
$3S$	326.374	297	–	–	–
$4S$	308.094	273	–	–	–
$5S$	294.962	256	–	–	–
$6S$	284.709	243	–	–	–

Table 2.12: Digamma decay width of S and P-wave charmonia (in keV)

State	Present [131]	ERHM [134]	CPP_ν [134]	SPM [126]	RQM [93]	NRQM [118]	BSE [158]	PDG [1]
1^1S_0	7.231	6.21	12.99	8.5	5.5	7.18	7.14±0.95	5.1±0.4
2^1S_0	5.507	4.21	5.63	2.4	1.8	1.71	4.44±0.48	2.15±1.58
3^1S_0	4.971	2.17	3.84	0.88	–	1.21	–	–
4^1S_0	4.688	1.01	3.01	–	–	–	–	–
5^1S_0	4.507	–	–	–	–	–	–	–
6^1S_0	4.377	–	–	–	–	–	–	–
1^3P_0	8.982	71.04	27.91	2.5	2.9	3.28	–	2.34±0.19
1^3P_2	1.069	75.06	5.76	0.31	0.50	–	–	0.53±0.4
2^3P_0	9.111	5.87	146.57	1.7	1.9	–	–	–
2^3P_2	1.084	5.91	30.49	0.23	0.52	–	–	–
3^3P_0	9.104	–	–	1.2	–	–	–	–
3^3P_2	1.0846	–	–	0.17	–	–	–	–
4^3P_0	9.076	–	–	–	–	–	–	–
4^3P_2	1.080	–	–	–	–	–	–	–
5^3P_0	9.047	–	–	–	–	–	–	–
5^3P_2	1.077	–	–	–	–	–	–	–

2.3.2 Annihilation widths

In this subsection we compute $\gamma\gamma$, $\gamma\gamma\gamma$, gg, ggg, γgg and $\ell^+\ell^-$ annihilation decay widths of heavy quarkonia.

Photon annihilation widths

The measurement of digamma decay widths provides the information regarding the internal structure of meson. The decays $\eta_c \to \gamma\gamma$, $\chi_{c0,2} \to \gamma\gamma$ were reported by CLEO-c [146], *BABAR* [147] and then BESIII [148] collaboration have reported high accuracy data. LQCD is found to underestimate the decay widths of $\eta_c \to \gamma\gamma$ and $\chi_{c0} \to \gamma\gamma$ when compared to experimental data [149, 150]. Other approaches to attempt computation of annihilation rates of heavy quarkonia include NRQCD [31, 151–154], relativistic quark model [92, 93], effective Lagrangian [155, 156] and next-to-next-to leading order QCD correction to $\chi_{c0,2} \to \gamma\gamma$ in the framework of nonrelativistic QCD factorization [157].

The meson decaying into two photons suggests that the spin can never be one [160, 161]. Corresponding digamma decay width of a pseudoscalar meson in nonrel-

Table 2.13: Digamma decay width of S and P-wave bottomonia (in keV)

State	Present [131]	ERHM [134]	CPP_ν [134]	SPM [127]	RQM [112]	RQM [93]	NRQM [118]	BSE [158]
1^1S_0	0.387	0.35	0.37	0.527	0.214	0.35	0.23	0.384 ± 0.047
2^1S_0	0.263	0.20	0.10	0.263	0.121	0.15	0.07	0.191 ± 0.025
3^1S_0	0.229	0.09	0.06	0.172	0.906	0.10	0.04	–
4^1S_0	0.212	0.07	0.054	0.105	0.755	–	–	–
5^1S_0	0.201	–	–	0.121	–	–	–	–
6^1S_0	0.193	–	–	0.050	–	–	–	–
1^3P_0	0.0196	1.39	0.08	0.050	0.0208	0.038	–	–
1^3P_2	0.0052	1.40	0.018	0.0066	0.0051	0.008	–	–
2^3P_0	0.0195	0.10	0.43	0.037	0.0227	0.029	–	–
2^3P_2	0.0052	0.10	0.09	0.0067	0.0062	0.006	–	–
3^3P_0	0.0194	–	–	0.037	–	–	–	–
3^3P_2	0.0051	–	–	0.0064	–	–	–	–
4^3P_0	0.0192	–	–	–	–	–	–	–
4^3P_2	0.0051	–	–	–	–	–	–	–
5^3P_0	0.0191	–	–	–	–	–	–	–
5^3P_2	0.0050	–	–	–	–	–	–	–

Table 2.14: 3γ decay widths of charmonia (in eV) and bottomonia (in 10^{-6} keV)

State	Present	PM [159]	PDG [1]	State	Present	NRCQM [119]
J/ψ	1.36	3.95	1.08 ± 0.032	$\Upsilon(1S)$	7.05	3.44
$\psi(2S)$	1.01	1.64	–	$\Upsilon(2S)$	4.79	2.00
$\psi(3S)$	0.91	1.39	–	$\Upsilon(3S)$	4.16	1.55
$\psi(4S)$	0.85	1.30	–	$\Upsilon(4S)$	3.85	1.29
$\psi(5S)$	0.81	1.25	–	$\Upsilon(5S)$	3.64	–
$\psi(6S)$	0.79	1.22	–	$\Upsilon(6S)$	3.51	–

ativistic limit is given by Van Royen-Weiskopf formula [141, 162],

$$\begin{aligned}
\Gamma_{n^1S_0\to\gamma\gamma} &= \frac{3\alpha_e^2 e_Q^4 |R_{nsP}(0)|^2}{m_Q^2}\left[1+\frac{\alpha_s}{\pi}\left(\frac{\pi^2-20}{3}\right)\right] \\
\Gamma_{n^3P_0\to\gamma\gamma} &= \frac{27\alpha_e^2 e_Q^4 |R'_{nP}(0)|^2}{m_Q^4}\left[1+\frac{\alpha_s}{\pi}\left(\frac{3\pi^2-28}{9}\right)\right] \\
\Gamma_{n^3P_2\to\gamma\gamma} &= \frac{36\alpha_e^2 e_Q^4 |R'_{nP}(0)|^2}{5m_Q^4}\left[1-\frac{16}{3}\frac{\alpha_s}{\pi}\right]
\end{aligned} \tag{2.15}$$

Also the 3γ decay width of the vector quarkonia is given by [163]

$$\Gamma_{n^3S_1\to 3\gamma} = \frac{4(\pi^2-9)e_Q^6\alpha_e^3|R_{nS}(0)|^2}{3\pi m_Q^2}\left[1-\frac{12.6\alpha_s}{\pi}\right] \tag{2.16}$$

where the bracketed quantities are QCD next-to-leading order radiative corrections [162, 164].

Annihilation widths into gluon

Digluon annihilation of quarkonia is not directly observed in detectors as digluonic state decays into various hadronic states making it a bit complex to compute digluon annihilation widths from nonrelativistic approximations derived from first principles. The digluon decay width of pseudoscalar meson along with the QCD leading order radiative correction is given by [155, 162, 164, 165],

$$\begin{aligned}
\Gamma_{n^1S_0\to gg} &= \frac{2\alpha_s^2|R_{nsP}(0)|^2}{3m_Q^2}[1+C_Q(\alpha_s/\pi)] \\
\Gamma_{n^3P_0\to gg} &= \frac{6\alpha_s^2|R'_{nP}(0)|^2}{m_Q^4}[1+C_{0Q}(\alpha_s/\pi)] \\
\Gamma_{n^3P_2\to gg} &= \frac{4\alpha_s^2|R'_{nP}(0)|^2}{5m_Q^4}[1+C_{2Q}(\alpha_s/\pi)]
\end{aligned} \tag{2.17}$$

Also the $3g$ decay width of vector quarkonia is given by

$$\Gamma_{n^3S_1\to 3g} = \frac{10(\pi^2-9)\alpha_s^3|R_{nS}(0)|^2}{81\pi m_Q^2}\left[1-\frac{3.7\alpha_s}{\pi}\right] \tag{2.18}$$

Here, the coefficients in the bracket have values of $C_Q = 4.8$, $C_{0Q} = 9.5$, $C_{2Q} = -2.2$ for the charm quark and $C_Q = 4.4$, $C_{0Q} = 10.0$, $C_{2Q} = -0.1$ for the bottom quark [162].

Also the annihilation width into γgg given by [119],

$$\Gamma_{n^3S_1\to\gamma gg} = \frac{8(\pi^2-9)e_Q^2\alpha_e\alpha_s|R_{nS(0)}|^2}{9\pi m_Q^2}\left[1-\frac{6.7\alpha_s}{\pi}\right] \tag{2.19}$$

Table 2.15: Digluon decay width of S and P-wave charmonia (in MeV)

State	Present [131]	ERHM [134]	CPP_ν [134]	PM [120]	BSE [158]	PDG [1]
1^1S_0	35.909	19.04	124.08	22.37	19.60	26.7±3.0
2^1S_0	27.345	12.91	53.77	16.74	12.1	14.7±0.7
3^1S_0	24.683	6.64	36.64	14.30	–	–
4^1S_0	23.281	3.1	28.74	–	–	–
5^1S_0	22.379	–	–	–	–	–
6^1S_0	23.736	–	–	–	–	–
1^3P_0	37.919	0.19	0.195	9.45	–	10.4±0.7
1^3P_2	3.974	0.2	6.93	2.81	–	2.03±0.12
2^3P_0	38.462	5.31	1.02	10.09	–	–
2^3P_2	4.034	5.43	36.69	7.34	–	–
3^3P_0	38.433	–	–	–	–	–
3^3P_2	4.028	–	–	–	–	–
4^3P_0	38.315	–	–	–	–	–
4^3P_2	4.016	–	–	–	–	–
5^3P_0	39.191	–	–	–	–	–
5^3P_2	4.003	–	–	–	–	–

Table 2.16: Digluon decay width of S and P-wave bottomonia (in MeV)

State	Present [131]	ERHM [134]	CPP_ν [134]	PM [50]	BSE [158]	RPM [166]
1^1S_0	5.448	9.95	23.72	17.945	6.98	12.46
2^1S_0	3.710	5.64	6.61	–	3.47	–
3^1S_0	3.229	2.61	3.86	–	–	–
4^1S_0	2.985	2.07	3.45	–	–	–
5^1S_0	2.832	–	–	–	–	–
6^1S_0	2.274	–	–	–	–	–
1^3P_0	0.276	38.17	4.90	5.250	–	2.15
1^3P_2	0.073	38.57	0.66	0.822	–	0.22
2^3P_0	0.275	1.92	25.04	–	–	–
2^3P_2	0.073	1.92	3.39	–	–	–
3^3P_0	0.273	–	–	–	–	–
3^3P_2	0.072	–	–	–	–	–
4^3P_0	0.271	–	–	–	–	–
4^3P_2	0.072	–	–	–	–	–
5^3P_0	0.269	–	–	–	–	–
5^3P_2	0.071	–	–	–	–	–

Table 2.17: $3g$ decay widths of charmonia (in keV) and bottomonia (in keV)

State	Present	PM [159]	PDG [1]	State	Present	NRCQM [119]	PDG [1]
J/ψ	264.25	269.06	59.55	$\Upsilon(1S)$	39.15	41.63	–
$\psi(2S)$	196.05	112.03	31.16	$\Upsilon(2S)$	26.59	24.25	18.80
$\psi(3S)$	175.43	94.57	–	$\Upsilon(3S)$	23.13	18.76	7.25
$\psi(4S)$	164.66	88.44	–	$\Upsilon(4S)$	21.37	15.58	–
$\psi(5S)$	157.77	85.30	–	$\Upsilon(5S)$	20.27	–	–
$\psi(6S)$	152.86	83.19	–	$\Upsilon(6S)$	19.49	–	–

Table 2.18: γgg decay widths of charmonia (in keV) and bottomonia (in keV)

State	Present	PM [159]	PDG [1]	State	Present	NRCQM [119]	PDG [1]
J/ψ	7.51	8.90	8.17	$\Upsilon(1S)$	0.85	0.79	–
$\psi(2S)$	5.57	3.75	3.03	$\Upsilon(2S)$	0.58	0.46	0.60
$\psi(3S)$	4.99	3.16	–	$\Upsilon(3S)$	0.50	0.36	1.97
$\psi(4S)$	4.68	2.96	–	$\Upsilon(4S)$	0.46	0.30	–
$\psi(5S)$	4.48	2.85	–	$\Upsilon(5S)$	0.44	–	–
$\psi(6S)$	4.35	2.78	–	$\Upsilon(6S)$	0.42	–	–

Annihilation widths into electron

The vector mesons have quantum numbers 1^{--} and can annihilate into dilepton. The dileptonic decay of vector meson along with one loop QCD radiative correction is given by [141, 162]

$$\Gamma_{n^3S_1\to\ell^+\ell^-} = \frac{4\alpha_e^2 e_Q^2 |R_{nsV}(0)|^2}{M_{nsV}^2}\left[1-\frac{16\alpha_s}{3\pi}\right] \tag{2.20}$$

Here, α_e is the electromagnetic coupling constant, α_s is the strong running coupling constant in Eq. (2.4) and e_Q is the charge of heavy quark in terms of electron charge. In above relations, $|R_{nsP/V}(0)|$ corresponds to the wave function of S-wave at origin for pseudoscalar and vector mesons while $|R'_{nP}(0)|$ is the derivative of P-wave radial

Table 2.19: Dilepton decay width of charmonia (in keV)

State	Present [131]	RPM [123]	PM [104]	RPM [100]	RQM [92]	PDG [1]
$1S$	2.925	4.95	6.99	1.89	5.4	5.547 ± 0.14
$2S$	1.533	1.69	3.38	1.04	2.4	2.359 ± 0.04
$3S$	1.091	0.96	2.31	0.77	–	0.86 ± 0.07
$4S$	0.856	0.65	1.78	0.65	–	0.58 ± 0.07
$5S$	0.707	0.49	1.46	–	–	–
$6S$	0.602	0.39	1.24	–	–	–

Table 2.20: Dilepton decay width of bottomonia (in keV)

State	Present [131]	RPM [123]	RPM [101]	PM [104]	RQM [92]	SPM [167]	PDG [1]
$1S$	1.098	1.20	1.33	1.61	1.3	0.98	1.340 ± 0.018
$2S$	0.670	0.52	0.62	0.87	0.5	0.41	0.612 ± 0.011
$3S$	0.541	0.33	0.48	0.66	–	0.27	0.443 ± 0.008
$4S$	0.470	0.24	0.40	0.53	–	0.20	0.272 ± 0.029
$5S$	0.422	0.19	–	0.44	–	0.16	–
$6S$	0.387	0.16	–	0.39	–	0.12	–

wave function at origin. The annihilation rates of heavy quarkonia are listed in Tables 2.12 - 2.20.

2.3.3 Electromagnetic transition widths

The electromagnetic transitions can be determined broadly in terms of electric and magnetic multipole expansions and their study can help in understanding the non-perturbative regime of QCD. We consider the leading order terms i.e. electric ($E1$) and magnetic ($M1$) dipoles with selection rules $\Delta L = \pm 1$ and $\Delta S = 0$ for the $E1$ transitions while $\Delta L = 0$ and $\Delta S = \pm 1$ for $M1$ transitions. We now employ the numerical wave function for computing the electromagnetic transition widths among quarkonia and B_c meson states in order to test parameters used in present work. For $M1$ transition, we restrict our calculations for transitions among S-waves only. In the nonrelativistic limit, the radiative $E1$ and $M1$ widths are given by [16, 35, 106, 168, 169]

$$\Gamma(n^{2S+1}L_{iJ_i} \to n'^{2S+1}L_{fJ_f} + \gamma) = \frac{4\alpha_e \langle e_Q \rangle^2 \omega^3}{3}(2J_f + 1)S_{if}^{E1}|M_{if}^{E1}|^2 \quad (2.21)$$

$$\Gamma(n^3S_1 \to n'^1S_0 + \gamma) = \frac{\alpha_e \mu^2 \omega^3}{3}(2J_f + 1)|M_{if}^{M1}|^2 \quad (2.22)$$

where, mean charge content $\langle e_Q \rangle$ of the $Q\bar{Q}$ system, magnetic dipole moment μ and photon energy ω are given by

$$\langle e_Q \rangle = \left| \frac{m_{\bar{Q}} e_Q - e_{\bar{Q}} m_Q}{m_Q + m_{\bar{Q}}} \right| \quad (2.23)$$

$$\mu = \frac{e_Q}{m_Q} - \frac{e_{\bar{Q}}}{m_{\bar{Q}}} \quad (2.24)$$

$$\omega = \frac{M_i^2 - M_f^2}{2M_i} \quad (2.25)$$

Table 2.21: $E1$ transition width of charmonia (in keV)

Transition	Present [131]	ERHM [134]	$CPP\nu$ [134]	RPM [100]	RQM [91]	SPM [126]	NRQM [115]	PDG [1]
$2^3S_1 \to 1^3P_0$	21.863	9.92	38.2	45.0	51.7	74	22	29.8 ± 1.5
$2^3S_1 \to 1^3P_1$	43.292	18.6	73.6	40.9	44.9	62	42	27.9 ± 1.5
$2^3S_1 \to 1^3P_2$	62.312	11.3	37.2	26.5	30.9	43	38	26 ± 1.5
$2^1S_0 \to 1^1P_1$	36.197	–	–	8.3	8.6	146	49	–
$3^3S_1 \to 2^3P_0$	31.839	16.4	51.4	87.3	–	–	–	–
$3^3S_1 \to 2^3P_1$	64.234	43.3	65.2	65.7	–	–	–	–
$3^3S_1 \to 2^3P_2$	86.472	54.2	4	31.6	–	–	–	–
$3^3S_1 \to 1^3P_0$	46.872	129.4	583.9	1.2	–	–	–	–
$3^3S_1 \to 1^3P_1$	107.088	336.4	1531	2.5	–	–	–	–
$3^3S_1 \to 1^3P_2$	163.485	410.1	4379	3.3	–	–	–	–
$3^1S_0 \to 2^1P_1$	51.917	–	–	–	–	–	–	–
$3^1S_0 \to 1^1P_1$	178.312	–	–	–	–	–	–	–
$1^3P_0 \to 1^3S_1$	112.030	325.9	209	142.2	161	167	284	119.5 ± 8
$1^3P_1 \to 1^3S_1$	146.317	426.2	269	287.0	333	354	306	295 ± 13
$1^3P_2 \to 1^3S_1$	157.225	680.7	421	390.6	448	473	172	384.2 ± 16
$1^1P_1 \to 1^1S_0$	247.971	1076	1015	610.0	723	764	361	357 ± 280
$2^3P_0 \to 2^3S_1$	70.400	231.0	190	53.6	–	61	–	–
$2^3P_1 \to 2^3S_1$	102.672	258.9	316	208.3	–	103	–	–
$2^3P_2 \to 2^3S_1$	116.325	325.3	701	358.6	–	225	–	–
$2^1P_1 \to 2^1S_0$	163.646	611.7	843	–	–	309	–	–
$2^3P_0 \to 1^3S_1$	173.324	643.5	822	20.8	–	74	–	–
$2^3P_1 \to 1^3S_1$	210.958	661.3	962	28.4	–	83	–	–
$2^3P_2 \to 1^3S_1$	227.915	700.1	1279	33.2	–	101	–	–
$2^1P_1 \to 1^1S_0$	329.384	951.6	549	–	–	134	–	–
$1^3D_1 \to 1^3P_0$	161.504	–	–	–	423	486	272	172 ± 30
$1^3D_1 \to 1^3P_1$	93.775	–	–	–	142	150	138	70 ± 17
$1^3D_1 \to 1^3P_2$	5.722	–	–	–	5.8	5.8	7.1	≤ 21
$1^3D_2 \to 1^3P_1$	165.176	–	–	317.3	297	342	285	–
$1^3D_2 \to 1^3P_2$	50.317	–	–	65.7	62	70	91	–
$1^3D_3 \to 1^3P_2$	175.212	–	–	62.7	252	284	350	–
$1^1D_2 \to 1^1P_1$	205.93	–	–	–	335	575	362	–

respectively. Also the symmetric statistical factor is given by

$$S_{if}^{E1} = \max(L_i, L_f) \left\{ \begin{array}{ccc} J_i & 1 & J_f \\ L_f & S & L_i \end{array} \right\}^2 . \tag{2.26}$$

The matrix element $|M_{if}|$ for $E1$ and $M1$ transition can be written as

$$\left|M_{if}^{E1}\right| = \frac{3}{\omega} \left\langle f \left| \frac{\omega r}{2} j_0\left(\frac{\omega r}{2}\right) - j_1\left(\frac{\omega r}{2}\right) \right| i \right\rangle \tag{2.27}$$

$$\left|M_{if}^{M1}\right| = \left\langle f \left| j_0\left(\frac{\omega r}{2}\right) \right| i \right\rangle \tag{2.28}$$

The electromagnetic transition widths are listed in Tables 2.21 - 2.26 and also compared with experimental results as well as theoretical predictions.

Table 2.22: $E1$ transition width of bottomonia (in keV)

Transition	Present [131]	ERHM [134]	$CPP\nu$ [134]	RPM [100]	RQM [91]	SPM [127]	NRQM [116]	PDG [1]
$2^3S_1 \to 1^3P_0$	2.377	0.24	0.4	1.15	1.65	1.67	1.09	1.22 ± 0.11
$2^3S_1 \to 1^3P_1$	5.689	0.40	0.74	1.87	2.57	2.54	2.17	2.21 ± 0.19
$2^3S_1 \to 1^3P_2$	8.486	0.12	0.38	1.88	2.53	2.62	2.62	2.29 ± 0.20
$2^1S_0 \to 1^1P_1$	10.181	–	–	4.17	3.25	6.10	3.41	–
$3^3S_1 \to 2^3P_0$	3.330	0.35	0.32	1.67	1.65	1.83	1.21	1.20 ± 0.12
$3^3S_1 \to 2^3P_1$	7.936	0.82	0.62	2.74	2.65	2.96	2.61	2.56 ± 0.26
$3^3S_1 \to 2^3P_2$	11.447	0.80	0.30	2.80	2.89	3.23	3.16	2.66 ± 0.27
$3^3S_1 \to 1^3P_0$	0.594	3.91	15.4	0.03	0.124	0.07	0.097	0.055 ± 0.010
$3^3S_1 \to 1^3P_1$	1.518	9.50	41.4	0.09	0.307	0.17	0.0005	0.018 ± 0.010
$3^3S_1 \to 1^3P_2$	2.354	9.86	54.7	0.13	0.445	0.15	0.14	0.20 ± 0.03
$3^1S_0 \to 1^1P_1$	3.385	–	–	0.03	0.770	1.24	0.67	–
$3^1S_0 \to 2^1P_1$	13.981	–	–	–	3.07	11.0	4.25	–
$1^3P_2 \to 1^3S_1$	57.530	61.96	26.7	31.2	29.5	38.2	31.8	–
$1^3P_1 \to 1^3S_1$	54.927	39.58	21.3	27.3	37.1	33.6	31.9	–
$1^3P_0 \to 1^3S_1$	49.530	30.72	18.7	22.1	42.7	26.6	27.5	–
$1^1P_1 \to 1^1S_0$	72.094	62.70	37.7	37.9	54.4	55.8	35.8	–
$2^3P_2 \to 2^3S_1$	28.848	14.57	23.4	16.8	18.8	18.8	15.5	15.1 ± 5.6
$2^3P_1 \to 2^3S_1$	26.672	10.65	18.2	13.7	15.9	15.9	15.3	19.4 ± 5.0
$2^3P_0 \to 2^3S_1$	23.162	8.98	15.9	9.90	11.7	11.7	14.4	–
$2^1P_1 \to 2^1S_0$	35.578	15.67	25.4	–	23.6	24.7	16.2	–
$2^3P_2 \to 1^3S_1$	29.635	45.03	33.0	7.74	8.41	13.0	12.5	9.8 ± 2.3
$2^3P_1 \to 1^3S_1$	28.552	41.71	30.2	7.31	8.01	12.4	10.8	8.9 ± 2.2
$2^3P_0 \to 1^3S_1$	26.769	40.12	28.8	6.69	7.36	11.4	5.4	–
$2^1P_1 \to 1^1S_0$	34.815	49.57	1.07	–	9.9	15.9	16.1	–
$1^3D_1 \to 1^3P_0$	9.670	–	–	–	24.2	23.6	19.8	–
$1^3D_1 \to 1^3P_1$	6.313	–	–	–	12.9	12.3	13.3	–
$1^3D_1 \to 1^3P_2$	0.394	–	–	–	0.67	0.65	1.02	–
$1^3D_2 \to 1^3P_1$	11.489	–	–	19.3	24.8	23.8	21.8	–
$1^3D_2 \to 1^3P_2$	3.583	–	–	5.07	6.45	6.29	7.23	–
$1^3D_3 \to 1^3P_2$	14.013	–	–	21.7	26.7	26.4	32.1	–
$1^1D_2 \to 1^1P_1$	14.821	–	–	–	30.2	42.3	30.3	–

Table 2.23: $E1$ transition width of B_c meson (in keV)

Transition	Present [131]	RQM [91]	RQM [113]	PM [103]
$2^3S_1 \to 1^3P_0$	4.782	5.53	2.9	0.94
$2^3S_1 \to 1^3P_1$	11.156	7.65	4.7	1.45
$2^3S_1 \to 1^3P_2$	16.823	7.59	5.7	2.28
$2^1S_0 \to 1^1P_1$	18.663	4.40	6.1	3.03
$3^3S_1 \to 2^3P_0$	7.406	–	–	–
$3^3S_1 \to 2^3P_1$	17.049	–	–	–
$3^3S_1 \to 2^3P_2$	25.112	–	–	–
$3^3S_1 \to 1^3P_0$	6.910	–	–	–
$3^3S_1 \to 1^3P_1$	17.563	–	–	–
$3^3S_1 \to 1^3P_2$	27.487	–	–	–
$3^1S_0 \to 1^1P_1$	38.755	–	–	–
$3^1S_0 \to 2^1P_1$	27.988	–	–	–
$1^3P_2 \to 1^3S_1$	55.761	122	83	64.24
$1^3P_1 \to 1^3S_1$	53.294	87.1	11	51.14
$1^3P_0 \to 1^3S_1$	46.862	75.5	55	58.55
$1^1P_1 \to 1^1S_0$	71.923	18.4	80	72.28
$2^3P_2 \to 2^3S_1$	41.259	75.3	55	64.92
$2^3P_1 \to 2^3S_1$	38.533	45.3	45	50.40
$2^3P_0 \to 2^3S_1$	38.308	34.0	42	55.05
$2^1P_1 \to 2^1S_0$	52.205	13.8	52	56.28
$2^3P_2 \to 1^3S_1$	60.195	–	14	–
$2^3P_1 \to 1^3S_1$	57.839	–	5.4	–
$2^3P_0 \to 1^3S_1$	52.508	–	1.0	–
$2^1P_1 \to 1^1S_0$	74.211	–	19	–
$1^3D_1 \to 1^3P_0$	44.783	133	55	–
$1^3D_1 \to 1^3P_1$	28.731	65.3	28	–
$1^3D_1 \to 1^3P_2$	1.786	3.82	1.8	–
$1^3D_2 \to 1^3P_1$	51.272	139	64	–
$1^3D_2 \to 1^3P_2$	16.073	23.6	15	–
$1^3D_3 \to 1^3P_2$	60.336	149	78	–
$1^1D_2 \to 1^1P_1$	66.020	143	63	–

Table 2.24: $M1$ transition width of charmonia (in keV)

Transition	Present [131]	ERHM [134]	$CPP\nu$ [134]	RPM [100]	RQM [91]	NRQM [115]	PM [125]	PDG [1]
$1^3S_1 \to 1^1S_0$	2.722	0.703	9.68	2.7	1.05	2.39	3.28	1.58 ± 0.37
$2^3S_1 \to 2^1S_0$	1.172	0.151	0.55	1.2	0.99	0.19	1.45	0.21 ± 0.15
$2^3S_1 \to 1^1S_0$	7.506	20.51	58.13	0.0	0.95	7.80	–	1.24 ± 0.29
$3^3S_1 \to 3^1S_0$	9.927	20.521	58.13	–	–	0.088	–	–

Table 2.25: $M1$ transition width of bottomonia (in eV)

Transition	Present [131]	ERHM [134]	$CPP\nu$ [134]	RPM [100]	RQM [91]	NRQM [116]	PM [125]	PDG [1]
$1^3S_1 \to 1^1S_0$	37.668	2.33	9.13	4.0	5.8	10	15.36	–
$2^3S_1 \to 2^1S_0$	5.619	0.169	0.17	0.05	1.40	0.59	1.82	–
$2^3S_1 \to 1^1S_0$	77.173	1395	799	0.0	6.4	66	–	12.5 ± 4.9
$3^3S_1 \to 3^1S_0$	2.849	0.050	0.036	–	0.8	3.9	–	–
$3^3S_1 \to 2^1S_0$	36.177	–	–	–	1.5	11	–	≤ 14
$3^3S_1 \to 1^1S_0$	76.990	–	–	–	10.5	71	–	10 ± 2

Table 2.26: $M1$ transition width of B_c meson (in eV)

Transition	Present [131]	RQM [91]	RQM [113]	PM [103]
$1^3S_1 \to 1^1S_0$	53.109	33	80	2.2
$2^3S_1 \to 2^1S_0$	21.119	17	10	0.014
$2^3S_1 \to 1^1S_0$	481.572	428	600	495
$2^1S_0 \to 1^3S_1$	568.346	488	300	1092

2.3.4 Weak decays of B_c mesons

The decay modes of B_c mesons are different from charmonia and bottomonia because of the inclusion of different flavor quarks. Their decay properties are very important probes for the weak interaction as B_c meson decays only through weak decays, therefore have relatively quite long lifetime. The pseudoscalar state can not decay via strong or electromagnetic decays because of this flavor asymmetry.

In the spectator model [170], the total decay width of B_c meson can be broadly classified into three ways: (i) Decay of b quark considering c quark as a spectator, (ii) Decay of c quark considering b quark as a spectator and (iii) Annihilation channel $B_c \to \ell^+\nu_\ell$. The total width is given by

$$\Gamma(B_c \to X) = \Gamma(b \to X) + \Gamma(c \to X) + \Gamma(Anni) \tag{2.29}$$

In the calculations of total width, we have not considered the interference among them as all these decays lead to different channel. In the spectator approximation, the inclusive decay width of b and c quark is given by

$$\Gamma(b \to X) = \frac{9G_F^2|V_{cb}|^2 m_b^5}{192\pi^3} \tag{2.30}$$

$$\Gamma(c \to X) = \frac{9G_F^2|V_{cs}|^2 m_c^5}{192\pi^3} \tag{2.31}$$

$$\Gamma(Anni) = \frac{G_F^2}{8\pi}|V_{cb}|^2 f_{B_c}^2 M_{B_c} m_q^2 \left(1 - \frac{m_q^2}{M_{B_c^2}}\right)^2 C_q \tag{2.32}$$

Where $C_q = 3|V_{cs}|$ for D_s mesons and m_q is the mass of heaviest fermions. V_{cs} and V_{cb} are the CKM matrices and we have taken the value of CKM matrices from the PDG. G_f is the Fermi coupling constant. Here we have used the model quark masses, B_c meson mass and decay constants for the computation of total width. Here we compute the decay width of B_c meson using Eq. (2.29) and corresponding lifetime. The computed lifetime comes out to be 0.539×10^{-12} s which is in very good agreement with the world averaged mean life time $(0.507 \pm 0.009) \times 10^{-12}$ s [1].

2.4 Results and Discussion

Having determined the model parameters namely confinement strength and quark masses in Tab. 2.1, we present our numerical results. We first compute the mass spectra of the heavy quarkonia and B_c mesons. In almost all the papers based on potential models, the model parameters are independently fixed for experimental ground state masses of $c\bar{c}$, $b\bar{b}$ and $c\bar{b}$ mesons. But it is observed that the confinement strength of $c\bar{b}$ meson is the arithmetic mean of those for $c\bar{c}$ and $b\bar{b}$ mesons which discards the requirement of additional independent parameter for the B_c meson. Similar approach was used long back within QCD potential model [171]. We also compute various decay properties of heavy quarkonia and B_c mesons without additional parameter.

In Tables 2.2 - 2.5, we present our result for charmonium and bottomonium mass spectra. We compare our findings with PDG data [1], lattice QCD [11] data, relativistic quark model [88], nonrelativistic quark model [115,116,118], QCD relativistic functional approach [117], relativistic potential model [100], nonrelativistic potential models [109, 120, 123, 126, 127] and covariant constituent quark model [119]. Our results are in very good agreement with the PDG data [1]. For charmonia, our results show very good agreement with the LQCD data [11] with less than 2% deviation. Our results for charmonia and bottomonia also close to the relativistic quark model (RQM) [91] with less than 1% deviation. Our results are also consistent with other theoretical approaches. In Tables 2.6 and 2.7, we also predict the B_c meson mass spectra. Experimentally only pseudoscalar state for $n = 1$ and 2 is available and our results match well with very few % error. It is worth noting that the masses

of orbitally excited states (to be specific for $n = 1$) of charmonia is systematically lower than the other models and experimental data. This tendency decreases as one moves to higher excited states. But this trend is not there in B_c and bottomonia systems suggesting that the relativistic treatment may improve the results in lower energy regime of charmonia.

Using the mass spectra of heavy quarkonia and B_c meson, we plot the Regge trajectories in (J, M^2) and (n_r, M^2) planes where $n_r = n - 1$. The following relations are utilised [88]

$$J = \alpha M^2 + \alpha_0 \tag{2.33}$$

$$n_r = \beta M^2 + \beta_0 \tag{2.34}$$

where α, β are slopes and α_0, β_0 are the intercepts that can be computed using the methods given in Ref. [88]. In Figs. 2.1, 2.2 and 2.3, we plot the Regge trajectories. Regge trajectories from present approach and relativistic quark model [88] show similar trend i.e. for charmonium spectra, the computed mass squared fits very well to a linear trajectory and is found to be almost parallel and equidistant in both the planes. Also, for bottomonia and B_c mesons, we observe the nonlinearity in the parent trajectories. The nonlinearity increases as we go from $c\bar{b}$ to $b\bar{b}$ mesons indicating increasing contribution from the inter-quark interaction over confinement.

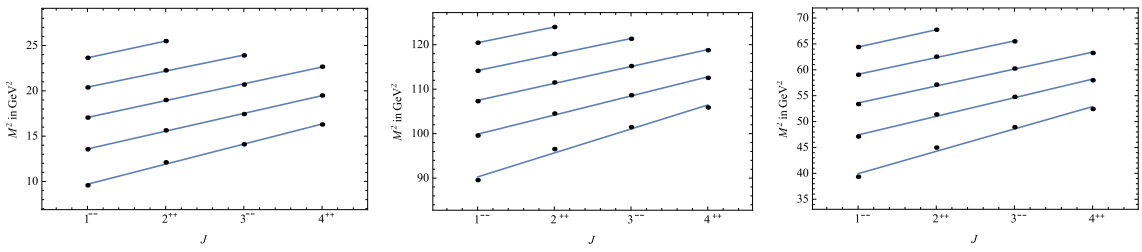

Figure 2.1: Parent and daughter Regge trajectories (J, M^2) for charmonia (left), bottomonia (middle) and B_c (right) mesons with natural parity $(P = (-1)^J)$.

Using the potential parameters and numerical wave function, we compute the various decay properties of heavy quarkonia. We first compute the leptonic decay constants of pseudoscalar and vector mesons and our numerical results are tabulated in Tables 2.8 – 2.11. For the case of charmonia, our results are higher than those using LQCD and QCDSR [13] and discrepancy removed when we include the QCD correction factors [142]. After introducing the correction factors, our results match with PDG,

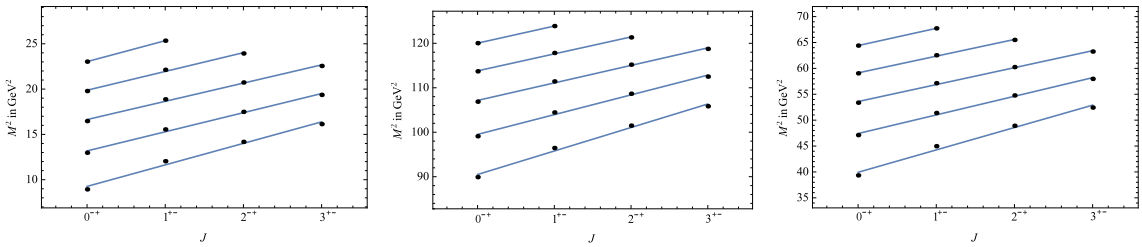

Figure 2.2: Parent and daughter Regge trajectories (J, M^2) for charmonia (left), bottomonia (middle) and B_c (right) mesons with unnatural parity $(P = (-1)^{J+1})$.

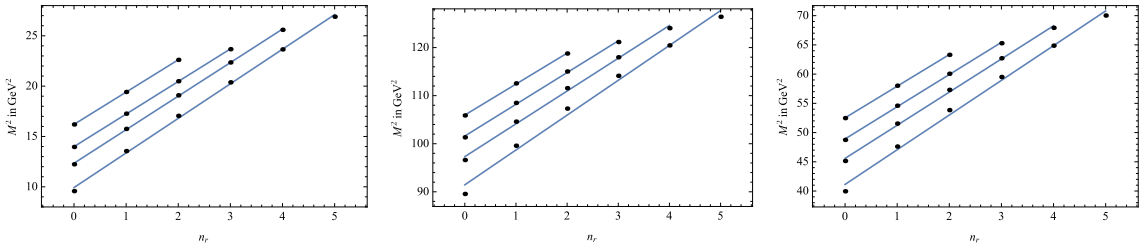

Figure 2.3: Parent and daughter Regge trajectories $(n_r \to M^2)$ for charmonia (left), bottomonia (middle) and B_c (right) mesons

LQCD and QCDSR [13] along with other theoretical models. We also compute the decay constants of bottomonia and B_c mesons. In this case, our results match with other theoretical predictions without incorporating the relativistic corrections. In the case of vector decay constants of bottomonia, our results are very close to experimental results as well as those obtained in LQCD Ref. [14]. For the decay constants of B_c mesons, we compare our results with nonrelativistic potential models [104, 138].

Then we compute the various annihilation widths of pseudoscalar and vector heavy quarkonia using the relations Eqs.(2.15)–(2.20). Where the bracketed quantities are the first order radiative corrections to the decay widths. We also compare our outcomes with the available experimental data and other theoretical results such as screened potential model (SPM) [126, 127, 167], Martin-like potential model [123], relativistic quark model (RQM) [92, 93], heavy quark spin symmetry [156], relativistic Salpeter model [158] and other theoretical models.

In Tables 2.12 and 2.13 we present our results for digamma decay widths for charmonia and bottomonia respectively. Our results for $\Gamma(\eta_c \to \gamma\gamma)$ and $\Gamma(\eta_c(2S) \to \gamma\gamma)$ are higher than the experimental data and the first order radiative correction (bracketed terms in Eq. (2.15)) was utilized to incorporate the difference and it is observed that our results along with the correction match with the data [1]. Our results for P-wave charmonia are higher than that of screened potential model [126] and rel-

ativistic quark model [93]. Our results for $\Gamma(\eta_b \to \gamma\gamma)$ match quite well with the experimental data while computed $\Gamma(\eta_b(2S) \to \gamma\gamma)$ value is overestimated when compared with the PDG data. For the excited state of S-wave bottomonia, our results fall in between those obtained in screened potential model [127] and relativistic quark model with linear confinement [114]. The scenario is similar with P-wave bottomonia and charmonia. In Tab. 2.14, we present our results for 3γ decay widths of vector quarkonia and also compared with the nonrelativistic constituent quark model [119] and potential mdoel results [159]. Our results are matching well the experimental data for the channel $J/\psi \to 3\gamma$ and other states are also inline with the others.

Digluon decay has substantial contribution to hadronic decay of quarkonia below $c\bar{c}$ and $b\bar{b}$ threshold. In Tables 2.15 and 2.16 we represent our results for digluon decay width of charmonia and bottomonia respectively. Our results for $\Gamma(\eta_c \to gg)$ match perfectly with the PDG data [1] but in the case of $\Gamma(\eta_c(2S) \to gg)$ our result is higher than the PDG data. We also compare the results obtained with that of the relativistic Salpeter method [158] and an approximate potential model [120]. It is seen from Table 2.15 that the relativistic corrections provide better results in case of P-wave charmonia where as that for bottomonia are underestimated in present calculations when compared to relativistic QCD potential model [166] and power potential model [50]. In Tab. 2.17 and 2.18 we present our results of three gluon decay and γgg decays with the comparing PDG data as well as other nonrelativistic approaches [119, 159]. It is observed that our results also in good accordance with the PDG data and theoretical models except for the channel $\psi(nS) \to 3g$.

We present the result of dilepton decay widths in the Table 2.19 and 2.20 and it is observed that our results matches with the PDG data [1] upto $n = 3$ for both charmonia and bottomonia. The contribution of the correction factor is more significant in the excited states with compared to that in the ground states of the quarkonia, indicating different dynamics in the intermediate quark-antiquark distance. Our results are also in good accordance with the other theoretical models.

Next, we present our results of $E1$ transitions in Tables 2.21 - 2.23 in comparison with theoretical attempts such as relativistic potential model [100], quark model [91], nonrelativistic screened potential model [116, 126, 127]. We also compare our results of charmonia transitions with available experimental results. We also compare our

results of ERHM and CPP_ν results [134]. Our result for $\Gamma(\psi(2S) \to \chi_{cJ}(1P) + \gamma)$ is in good agreement with the experimental result for $J = 0$ but our results for $J = 1, 2$ are higher than the PDG data. Our results also agree well for the transition $\Gamma(\chi_{c2}(1P) \to J/\psi + \gamma)$. We also satisfy the experimental constraints for the transition $\Gamma(1^3D_1 \to \chi_{cJ} + \gamma)$ for $J = 0, 1, 2$. Our results share the same range with the results computed in other theoretical models. The $E1$ transitions of bottomonia agree fairly well except for the channel $\Gamma(\Upsilon(3S) \to \chi_{bJ}(3P))$, where our results are higher than the experimental results. The comparison of our results of $E1$ transitions in B_c mesons with relativistic quark model [91, 113] and power potential model [103] are found to be in good agreement. In Tables 2.24 - 2.26, we present our results of $M1$ transitions and also compared with relativistic potential model [100], quark model [91, 114], nonrelativistic screened potential model [115, 116], power potential [103] as well as with available experimental results. Our results of $\Gamma(\mathrm{n}\psi \to \mathrm{n}'\eta_c + \gamma)$ are in very good agreement with the PDG data as well with the other theoretical predictions. Computed $M1$ transitions in B_c mesons are also within the results obtained from theoretical predictions. The computed $M1$ transition of bottomonia are found to be higher than the PDG data and also theoretical predictions. It is important to note that the experimental data of many channels are not yet available, the validity of either of the approaches can be validated only after observations in forthcoming experiments.

Chapter 3

Decay Properties of Heavy Baryons

3.1 Introduction

Baryons are strongly interacting three quark fermions. This chapter is dedicated to the study of doubly heavy baryons i.e. baryons having two heavy quarks (c and/or b) as they might prove to be important tool for testing quantum chromodynamics [172, 173]. These states were also predicted long back in the quark model [174]. After the experimental discovery of the first doubly heavy baryon, Ξ_{cc}^{+} by SELEX Collaboration [175] and later confirmed by them [176]. The next doubly heavy baryon Ξ_{cc}^{++} was discovered experimentally by LHCb collaboration in the $\Lambda_c^+ K^- \pi^+ \pi^-$ mass spectrum [177]. LHCb collaboration has also recently reported the life time of Ξ_{cc}^{++} baryon [178]. As an outcome of the LHCb upgrade, one can expect more detailed information on existing doubly heavy baryons and also the discovery of other doubly heavy baryons [177–179].

With the advancement in the detector technology and new results on the properties of doubly heavy baryons, it has created lot of interest for the theoreticians world wide. In the literature, there are two ways in which the spectroscopy and decay properties of the heavy baryons are studied theoretically: quark-diquark picture and other is three quark picture. In quark-diquark picture, the masses and radiative decay properties are studied in Bethe-Salpeter approach [180] and relativistic quark model (RQM) [181, 182]. The spectroscopy of doubly heavy baryons is also studied in the nonrelativistic framework of quark model using the potential of the type Buchmüller and Tye [183], chiral perturbation theory (χPT) [184–188] and also in Ref [189]. In three quark picture, the spectroscopy and decay properties are

studied in Bag model [190, 191], effective Lagrangian approach [192], SU(4) chiral constituent quark model (χCQM) [193], relativistic quark model (RQM) [194, 195], chromomagnetic model [196], nonrelativistic quark model (NRQM) [197–200] non-relativistic hypercentral constituent quark model (hCM) [104, 201–204]. The mass spectra are also computed on the model based on first principles such as lattice quantum chromodynamics LQCD [23–28], QCD sum rules [205–208] and NRQCD sum rules [209], light cone sum rules [210]. The mass spectra of heavy baryons are also studied using the Regge phenomenology [211, 212].

In this chapter, we employ the three quark picture of relativistic harmonic model for computing the masses of the doubly heavy baryon (ERHM). The spin dependent part of the one gluon exchange potential employed perturbatively for computing the masses of $1/2^+$ and $3/2^+$ states. The magnetic moments of the doubly heavy baryons are computed using the spin flavor wave function of the baryons. We also compute the radiative transition widths without using additional parameter.

This chapter is organised in the following way: After the brief introduction and survey on doubly heavy baryons in Sec. 3.1, we give the essential components of relativistic harmonic confinement model in Sec. 3.2 and compute the masses of doubly heavy baryons. In Sec. 3.3, we compute the magnetic moments using the spin flavor wave functions. Next, in Sec. 3.4 we compute the radiative decays using the transition magnetic moments. In Sec. 3.5 we present our results of masses, magnetic moments and radiative decay widths. We also compare our results with the available experimental results and other theoretical predictions.

3.2 Methodology

For computation of bound state masses of baryon, we use the relativistic harmonic confinement model in which the quarks are confined through the Lorentz scalar plus vector potential of the form

$$V_{conf}(r) = \frac{1}{2}(1+\gamma_0)A^2r^2 \tag{3.1}$$

Where A is the confinement strength mean field parameter and γ_0 is the Dirac matrix. The Dirac equation is solved using the method of non-relativistic reduction and the eigen energy (ϵ_{conf}) is obtained. The detailed computation technique is given in the Ref. [38, 39], here we provide only the essential components of the

model. We perturbatively add contribution due to the Coulomb potential along with state dependent colour dielectric coefficient ω given by

$$V_{coul}(r) = \frac{k\alpha_s(\mu)}{\omega r} \tag{3.2}$$

The mass of a baryon in the different $n^{2S+1}L_J$ state according to different J^{PC} can be written as [38, 39, 134]

$$M_N^J = \sum_{i=1}^{3} \epsilon_N(q_i)_{conf} + \sum_{i<j=1}^{3} \epsilon(q_i, q_j)_{coul} + \sum_{i<j=1}^{3} \epsilon_N^J(q_i, q_j)_{S.D.} \tag{3.3}$$

Table 3.1: Model parameters

A	k	m_u	m_d	m_s	m_c	m_b
2166 MeV$^{3/2}$	0.37	240 MeV	243 MeV	450 MeV	1313 MeV	4632 MeV

In above Eq. 3.3, the first term corresponds to total confinement energy of the constituent quarks inside the baryon which is computed in the relativistic harmonic confinement model [139]. In order to obtain the confinement energy, the Dirac equation is reduced to the nonrelativistic case [38]. The confinement energy is given by

$$\epsilon_N(q)_{conf} = \left((2N+3)\Omega_N(q) + m_q^2 - \frac{3m_q}{\sum_i^3 m_{q_i}}\Omega_0(q) \right)^{1/2} \tag{3.4}$$

where m_q is the quark mass, Ω_N is the energy dependent size parameter given by

$$\Omega_N = \sqrt{E_N + m_q}\ \ A \tag{3.5}$$

and the energy eigen value coming from the nonrelativistic reduation of Dirac equation given by

$$E_N^2 = m_q^2 + (2N+3)\Omega_N \quad \text{with} \quad N = 0, 1, 2, 3... \tag{3.6}$$

with the radial solution of Dirac equation

$$R_{n\ell}(r) = \sqrt{\frac{\Omega_N^{3/2}}{2\pi}\frac{n!}{\Gamma(n+\ell+3/2)}}\ \ (\Omega_N^{1/2}r)^\ell\ \ exp\left(-\frac{\Omega_N r^2}{2}\right)\ \ L_N^{\ell+3/2}(\Omega_N r^2). \tag{3.7}$$

The second term in Eq. (3.3) corresponds to the Coulomb energy which is the expectation value of the Coulomb potential Eq. (3.2). In Eq. (3.2), ω is the state

dependent color dielectric constant [38]. α_s is the strong running coupling constant. The Coulomb energy can be computed as

$$\epsilon_N(q_1, q_2)_{coul} = \langle NS|V_{coul}(r)|NS\rangle \tag{3.8}$$

The third term in Eq. (3.3) corresponds to the expectation value of spin dependent part of the confined one gluon exchange potential [213]. The single particle energy given by Eq. (3.6) which is the results of the nonrelativistic reduction of Dirac equation. This methodology also treats the quark and antiquarks on the equal basis. Also the confinement energy of the quarks and antiquarks within the baryons are computed by subtracting the contribution to the centre of mass energy from the single particle energy (last term of Eq. (3.4)). In harmonic confinement model, the residual Coulomb interaction has been introduced for the heavy flavor sector (ERHM) [38, 39]. This method is general and applicable to the hadronic state with any number of constituent quarks.

Table 3.2: Masses of doubly heavy baryons (in MeV)

State	Quark Content	Present	RQM [91]	hCM [202–204]	NRQM [197]	RQM [181]	Chromo [196]	LQCD [24]	QCDSR [207]	QCDSR [205, 206]
Ξ_{cc}^{++}	ccu	3621	3620	3511	3676	3606	3633.3 ± 9.3	3610(23)(22)	4260	3720
Ξ_{cc}^{*++}	ccu	3744	3727	3687	4029	3675	3696.1 ± 7.4	3692(28)(21)	3900	3720
Ξ_{cc}^{+}	ccd	3623	3620	3520	3676	–	–	–		–
Ξ_{cc}^{*+}	ccd	3744	3727	3695	4019	–	–	–		–
Ω_{cc}^{+}	ccs	3756	3778	3650	3815	3715	3731.8 ± 9.8	3738(20)(20)	4250	3730
Ω_{cc}^{*+}	ccd	3815	3872	3810	4180	3772	3802.4 ± 8.0	3822(20)(22)	3810	3780
Ξ_{bc}^{+}	bcu	6931	6933	6914	7011	–	6922.3 ± 6.9	6943(33)(28)	6750	6720
Ξ_{bc}^{*+}	bcu	7003	6980	6980	7047	–	6973.2 ± 5.5	6985(36)(28)	8000	7200
Ξ_{bc}^{0}	bcd	6933	6933	6920	7011	–	–	–		–
Ξ_{bc}^{*0}	bcd	7003	6980	6986	7047	–	–	–		–
Ω_{bc}^{0}	bcs	7051	7088	7136	7136	–	7010.7 ± 9.3	6998(27)(20)	7020	6750
Ω_{bc}^{*0}	bcs	7084	7130	7187	7187	–	7065.7 ± 7.5	7059(28)(21)	7540	7350
Ξ_{bb}^{0}	bbu	10205	10202	10312	10340	10138	10168.9 ± 9.2	10143(30)(23)	9780	9960
Ξ_{bb}^{*0}	bbu	10229	10237	10355	10576	10169	10188.8 ± 7.1	10178(30)(24)	10350	10300
Ξ_{bb}^{-}	bbd	10206	10202	10317	10340	–	–	–		–
Ξ_{bb}^{*-}	bbd	10229	10237	10340	10576	–	–	–		–
Ω_{bb}^{-}	bbs	10311	10359	10446	10454	10230	10259.0 ± 15.5	10273(27)(20)	9850	9970
Ω_{bb}^{*-}	bbs	10322	10389	10467	10693	10258	10267.5 ± 12.1	10308(27)(21)	10280	10400
Ω_{ccc}^{*++}	ccc	4465	–	4806	4965	–	–	–		
Ω_{ccb}^{+}	ccb	7720	–	–	8245	–	7990.3 ± 12.2	8007(9)(20)		
Ω_{ccb}^{*+}	ccb	7728	–	–	8265	–	8021.8 ± 9.0	8037(9)(20)		
Ω_{cbb}^{0}	cbb	10965	–	–	11535	–	11165.0 ± 11.8	11195(8)(20)		
Ω_{cbb}^{*0}	cbb	10967	–	–	11554	–	11196.4 ± 8.5	11229(8)(20)		
Ω_{bbb}^{*-}	bbb	14198	–	14496	14834	–	14309.7 ± 11.8	–		

3.3 Magnetic Moments

The magnetic moment can provide the information regarding the structure of the baryons. The magnetic moment of the doubly heavy baryons in terms of constituent

quarks as [201]

$$\mu_B = \sum_i \langle \phi_{sf} | \mu_i \vec{\sigma_i} | \phi_{sf} \rangle \tag{3.9}$$

with

$$\mu_i = \frac{e_i}{2m_i^{eff}} \tag{3.10}$$

Where e_i is the charge of the quark and σ_i is the spin of the quark, $|\phi_{sf}\rangle$ is the spin-flavor wave function of the respective baryons and m_i^{eff} is the effective mass of the quarks within the baryons can be computed as

$$m_i^{eff} = m_i \left(1 + \frac{E + \langle V_{spin} \rangle}{\sum_i m_i}\right). \tag{3.11}$$

Using Eqs. 3.9 –3.11 we compute the magnetic moments of doubly heavy baryons and tabulated in Tab. 3.3. We also compare our findings with the other theoretical approaches.

Table 3.3: Magnetic moment in μ_N

State	μ [104, 201]	Present	hCM [202, 203]	hCM [104, 201]	NRQM [198]	NRQM [199, 200]	exBag [191]	LCSR [210]
Ξ_{cc}^{++}	$\frac{4}{3}\mu_c - \frac{1}{3}\mu_u$	−0.185	0.031	−0.133	$-0.208^{+0.035}_{-0.086}$	–	−0.110	0.23 ± 0.05
Ξ_{cc}^{*++}	$2\mu_c + \mu_u$	2.724	2.218	2.663	$2.670^{+0.27}_{-0.25}$	2.52	2.35	–
Ξ_{cc}^{+}	$\frac{4}{3}\mu_c - \frac{1}{3}\mu_d$	0.843	0.784	0.833	$0.785^{+0.050}_{-0.030}$	–	0.719	0.43 ± 0.09
Ξ_{cc}^{*+}	$2\mu_c + \mu_d$	−0.256	0.068	−0.163	$-0.311^{+0.052}_{-0.130}$	0.035	−0.178	–
Ω_{cc}^{+}	$\frac{4}{3}\mu_c - \frac{1}{3}\mu_s$	0.710	0.692	0.756	$0.635^{+0.012}_{-0.015}$	–	0.645	0.39 ± 0.09
Ω_{cc}^{*+}	$2\mu_c + \mu_s$	0.208	0.285	0.120	$0.139^{+0.009}_{-0.017}$	0.21	0.0475	–
Ξ_{bc}^{+}	$\frac{2}{3}\mu_b + \frac{2}{3}\mu_c - \frac{1}{3}\mu_u$	−0.532	−0.204	−0.394	$-0.475^{+0.040}_{-0.088}$	−0.369		–
Ξ_{bc}^{*+}	$\mu_b + \mu_c + \mu_u$	2.663	1.562	2.017	$2.270^{+0.27}_{-0.14}$	2.022	1.88	–
Ξ_{bc}^{0}	$\frac{2}{3}\mu_b + \frac{2}{3}\mu_c - \frac{1}{3}\mu_d$	0.626	0.354	0.469	$0.518^{+0.048}_{-0.020}$	0.48		–
Ξ_{bc}^{*0}	$\mu_b + \mu_c + \mu_d$	−0.776	−0.372	−0.558	$-0.712^{+0.059}_{-0.133}$	−0.508	−0.534	–
Ω_{bc}^{0}	$\frac{2}{3}\mu_b + \frac{2}{3}\mu_c - \frac{1}{3}\mu_s$	0.457	0.439	0.389	$0.368^{+0.010}_{-0.011}$	0.407		–
Ω_{bc}^{*0}	$\mu_b + \mu_c + \mu_s$	−0.258	−0.181	−0.310	$-0.261^{+0.015}_{-0.021}$	−0.309	−0.329	–
Ξ_{bb}^{0}	$\frac{4}{3}\mu_b - \frac{1}{3}\mu_u$	−0.893	−0.663	−0.650	$-0.742^{+0.044}_{-0.091}$	−0.63	−0.581	0.51 ± 0.09
Ξ_{bb}^{*0}	$2\mu_b + \mu_u$	2.302	−1.607	1.559	$1.870^{+0.27}_{-0.13}$	1.507	1.40	–
Ξ_{bb}^{-}	$\frac{4}{3}\mu_b - \frac{1}{3}\mu_d$	0.316	0.196	0.188	$0.251^{+0.045}_{-0.021}$	0.215	0.171	0.28 ± 0.04
Ξ_{bb}^{*-}	$2\mu_b + \mu_d$	−1.324	−1.737	−0.941	$-1.110^{+0.06}_{-0.14}$	−1.029	−0.880	–
Ω_{bb}^{-}	$\frac{4}{3}\mu_b - \frac{1}{3}\mu_s$	0.133	0.108	0.107	$0.101^{+0.007}_{-0.007}$	0.138	0.112	0.42 ± 0.05
Ω_{bb}^{*-}	$2\mu_b + \mu_s$	−0.782	−1.239	−0.702	$-0.662^{+0.022}_{-0.024}$	−0.805	−0.697	–
Ω_{ccc}^{*++}	$3\mu_c$	1.261	–	1.189	–	1.16	0.989	–
Ω_{ccb}^{+}	$\frac{4}{3}\mu_c - \frac{1}{3}\mu_b$	0.618	–	0.502	–	0.522	0.455	–
Ω_{ccb}^{*+}	$\mu_b + 2\mu_c$	0.831	–	0.651	–	0.703	0.594	–
Ω_{cbb}^{0}	$\frac{4}{3}\mu_b - \frac{1}{3}\mu_c$	−0.24	–	−0.203	–	−0.2	−0.187	–
Ω_{cbb}^{*0}	$2\mu_b + \mu_c$	0.329	–	0.216	–	0.225	0.204	–
Ω_{bbb}^{*-}	$3\mu_b$	−0.198	–	−0.195	–	−0.198	−0.178	–

3.4 Radiative decays

The radiative decay width can be expressed in terms of transition magnetic moment (in nuclear magneton μ_N) as [214]

$$\Gamma_{B^* \to B\gamma} = \frac{\omega^3}{4\pi} \frac{2}{2J+1} \frac{e^2}{m_p^2} \mu^2_{B^* \to B\gamma} \tag{3.12}$$

where, m_p is the mass of proton, μ is the transition magnetic moment that can be written in terms of magnetic moment of constituent quark of final and initial state of baryons as $\mu_{B^*\to B\gamma} = \langle B|\hat{\mu}_{B^*z}|B^*\rangle$. Our results for the transition magnetic moment and radiative decay widths are tabulated in Tab. 3.4 and 3.5 in comparison with other theoretical predictions such as Bag models, chiral perturbation theory and different quark model results.

Table 3.4: Transition magnetic moment in μ_N

Transition	$\mu_{B'\to B\gamma}$ [184]	Present	χPT [184]	Bag [190]	exBag [191]	χCQM [193]	NRQM [199]
$\Xi_{cc}^{*++} \to \Xi_{cc}^{++}$	$\frac{2\sqrt{2}}{3}(\mu_u - \mu_c)$	1.563	−2.35	−0.787	−1.27	1.33	1.35
$\Xi_{cc}^{*+} \to \Xi_{cc}^{+}$	$\frac{2\sqrt{2}}{3}(\mu_d - \mu_c)$	−1.295	1.55	0.945	1.07	−1.41	1.06
$\Omega_{cc}^{*+} \to \Omega_{cc}^{+}$	$\frac{2\sqrt{2}}{3}(\mu_s - \mu_c)$	−0.897	1.54	0.789	0.869	−0.89	0.88
$\Xi_{bc}^{*+} \to \Xi_{bc}^{+}$	$\frac{\sqrt{2}}{3}(\mu_c + \mu_b - 2\mu_u)$	−2.010	−2.56	0.695	1.12	–	–
$\Xi_{bc}^{*0} \to \Xi_{bc}^{0}$	$\frac{\sqrt{2}}{3}(\mu_c + \mu_b - 2\mu_d)$	1.249	1.34	−0.747	−0.919	–	–
$\Omega_{bc}^{*0} \to \Omega_{bc}^{0}$	$\frac{\sqrt{2}}{3}(\mu_c + \mu_b - 2\mu_s)$	0.769	1.33	−0.624	−0.748	–	–
$\Xi_{bb}^{*0} \to \Xi_{bb}^{0}$	$\frac{2\sqrt{2}}{3}(\mu_b - \mu_u)$	−4.631	−2.77	−1.039	−1.45	–	–
$\Xi_{bb}^{*-} \to \Xi_{bb}^{-}$	$\frac{2\sqrt{2}}{3}(\mu_b - \mu_d)$	2.199	1.13	0.428	0.643	–	–
$\Omega_{bb}^{*-} \to \Omega_{bb}^{-}$	$\frac{2\sqrt{2}}{3}(\mu_b - \mu_s)$	1.174	1.12	−0.624	0.478	–	–

Table 3.5: Radiative decay width (in keV)

Transition	Present	χPT [184]	Bag [190]	exBag [191]	χQM [215]	RQM [181]	RQM [195]
$\Xi_{cc}^{*++} \to \Xi_{cc}^{++}$	18.545	22	1.43	2.79	16.7	7.21	23.46
$\Xi_{cc}^{*+} \to \Xi_{cc}^{+}$	12.145	9.57	2.08	2.17	14.6	3.90	28.79
$\Omega_{cc}^{*+} \to \Omega_{cc}^{+}$	0.678	9.45	0.949	1.60	6.93	0.82	2.11
$\Xi_{bc}^{*+} \to \Xi_{bc}^{+}$	6.042	26.2	0.533	1.31	–	–	0.49
$\Xi_{bc}^{*0} \to \Xi_{bc}^{0}$	2.22	7.19	0.612	0.876	–	–	0.24
$\Omega_{bc}^{*0} \to \Omega_{bc}^{0}$	0.087	7.08	0.239	0.637	–	–	0.12
$\Xi_{bb}^{*0} \to \Xi_{bb}^{0}$	1.233	31.1	0.126	0.137	1.19	0.98	0.31
$\Xi_{bb}^{*-} \to \Xi_{bb}^{-}$	0.265	5.17	0.022	0.0268	0.24	0.21	0.0587
$\Omega_{bb}^{*-} \to \Omega_{bb}^{-}$	0.008	5.08	0.011	0.0148	0.08	0.04	0.0226

3.5 Results and Discussion

After determining all the required model parameters, we present our numerical results. In Tab. 3.2, we present our results for the masses of doubly heavy baryons. It is observed that our result for Ξ_{cc}^{++} matches perfectly with the LHCb results [177].

In Tab. 3.2 we also compare our results with the other theoretical approaches such as hypercentral model [202–204], nonrelativistic quark model [197] chromomagnetic model [196] that are based on three quark picture of baryons. We also compare with the quark-diquark models such as relativistic quark model [91,181]. In NRQM [197], the authors have used the NRQM Hamilton and the wave function chosen to be on the basis of Harmonic Oscillator wave function. In hypercentral model [202–204], the authors have computed the mass spectra by solving the Schrödinger equation for the hypercentral Cornell potential. Our results are in very good agrement with the RQM [91] for Ξ_{QQ} baryons. For Ω_{QQ} baryons, our results are nearly $40 - 50$ MeV lower. This is may be because of the different methodology as the authors of Ref. [91] has used the relativistic treatment for the light quarks where as we have treated the all systems as nonrelativistically. Our results are also in good accordance with the chromagnetic model [196], in which the authors have used the effect of color interaction in chromomagnetic model. But for triply heavy baryons, our results are systematically lower than others. We also compare our results with the LQCD data [24] and we found that our results for doubly heavy baryons match well but for triply heavy baryons, our results underestimate LQCD data.

In Tab. 3.3 we present our results of magnetic moment of doubly heavy baryons using the spin flavor wave function of the respective baryons. Note that we have not introduced any additional parameter to compute the magnetic moments of spin 1/2 and 3/2 baryons. Our results are in good agreement with the hypercentral model [201] and also nonrelativistic quark models [198] and [199, 200]. For triply heavy baryons also our predictions are matching well with the NRQM [199, 200].

Next, we compute the radiative decays of doubly heavy baryons and tabulate in Tab. 3.5. We consider here the transition from spin $3/2^+ \to 1/2^+$ only. The required transition magnetic moments are presented in Tab. 3.4. Still the radiative decays of doubly heavy baryons are not reported in any experimental facility but theoretical results are available in the literature. We compare our findings with the theoretical approaches such as RQM [194] and [181]. We also compare with the results from χQM [215], χPT [184] and Bag model [190] predictions. There are wide range of results predicted in theory. Our results for the radiative decay widths of Ξ_{cc} baryon is very close to those obtained using χPT [184] and χQM [215]. For Ω_{cc} baryons, our results are near to the Bag model [190] and RQM [181]. For Ξ_{bc} and Ω_{bc} baryons, our results are higher than Bag model [190] and RQM [194] where as it is lower than

the χPT [184]. For Ξ_{bb} baryons, our results are very nearer to the χQM [215] and RQM [181]. For Ω_{bb}, our result underestimate with χQM [215] by one order. But as discussed earlier, there are a wide range of radiative decay widths available in the literature and also no experimental as well as LQCD results are available, our results might be interesting for the point of view of future experiments.

Chapter 4

Study of Exotic States as Dimesonic Molecules

4.1 Introduction

$Z_c^{\pm}(3900)$ is the charged charmonium-like state observed first time by BESIII [216] and then Belle [217] collaboration in the channel $e^+e^- \to \pi^+\pi^- J/\psi$. This state was also confirmed by CLEO collaboration [218]. BESIII have also determined parity to be $J^P = 1^+$ using the partial wave analysis [219]. Also the charged bottomonium-like states $Z_b(10610)$ and $Z_b(10650)$ observed in Belle Collaboration [220] and later also confirmed by them [221, 222]. These states are also identified with the parity to be $J^P = 1^+$. These states (Z_c and Z_b) don't fit into the conventional quark model and their minimal quark content to be $c\bar{c}d\bar{u}$ or $b\bar{b}d\bar{u}/b\bar{b}u\bar{d}$ which are beyond the conventional $q\bar{q}$ or qqq model. These states have masses nearer to threshold of two heavy flavor mesons and gained lot of attentions for both experimentalists and theoreticians world wide. There are different ways in which these states are studied theoretically based on tetraquark states [223–231], hadro-quarkonium state [232–234] in which the exotic states are considered as coupling to the light and heavy quarkonium state to intermediate open-flavor mesons. These states are also studied on the basis of hadronic composite molecular pictures [235–247]. These states are studied in the different approaches such as chiral quark model [248], relativistic quark model [249], effective field theory [250, 251], holographic QCD [252] and QCD sum rules [253]. The comprehensive reviews on the status of these exotic states are given in the literature [246, 254, 255].

In this chapter, we restrict our study to the exotic states namely Z_c^+, Z_b^+ and

Z_b' considering them as a hadronic composite molecule of $D^+\bar{D}^*$, $B\bar{B}^*$ and $B^*\bar{B}^*$ respectively as their masses are below these threshold. The bound state masses are computed by sloving the Schrödinger equation nemerically for the generalized Woods - Saxon potantial. We also compute the two body strong decays of these states using the phenomenological Lagrangian mechanism. We compare our findings with the available experimental data and other theoretical predictions. We have presented this work in the XXII DAE High energy Physics Symposium held at University of Delhi during December 12-16, 2016 and published in a conference proceeding [256].

4.2 Methodology

There are various approaches available in the literature for studying these exotic states but since their masses are nearer to the $D^*\bar{D}$, $B^*\bar{B}$ and $B^*\bar{B}^*$ threshold, these states are considered as a hadronic composite molecules of these mesons. We consider here the potential of the form modified Woods Saxon potential for the confinement of the exotic state along with the Coulomb replusive term. The potential equation is given by [257, 258],

$$V(r) = \frac{V_0}{1+e^{\frac{r-R_0}{a}}} + \frac{Ce^{\frac{r-R_0}{a}}}{\left(1+e^{\frac{r-R_0}{a}}\right)^2} - \frac{b}{r} \tag{4.1}$$

where, V_0 is the potential strength, b is the strength of Coulomb interaction. R_0 is the radius of the molecule. a is the diffuseness of the surface [257], C is the depth of the potential which range from $0 < C < 150$ MeV [258], where $C = 0$ MeV corresponds to the standard Woods-Saxon Potential. The plot of the potential is also shown in the Fig. 4.1 with the variation in the depth of the potential C.

Table 4.1: Fitted parameters for computing the masses

Potential Strength V_0	15 MeV
Radius of the molecule R_0	1.75 fm
Strength of coulomb interaction b	0.08
Diffuseness of the potential	-0.51 fm
Potential Depth Range	$0 < C < 150$ MeV [258]
Size Parameter Λ:	500 MeV

For computing the bound state masses of the exotic states the Schrödinger equation is sloved nemerically for the potential Eq. (4.1) using the *Mathematica* notebook utilizing the Runge–Kutta method [137] and the binding energy is obtained. The

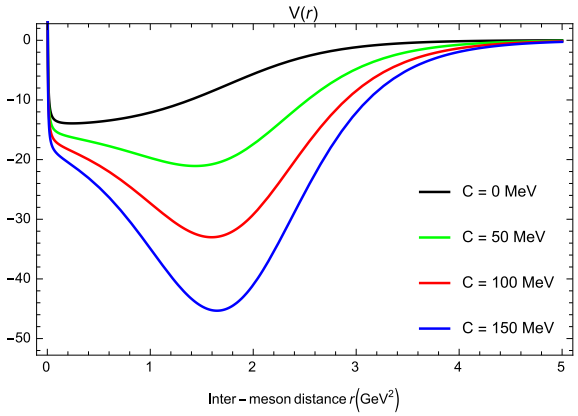

Figure 4.1: Wood-Saxon potential with variation in potential depth

masses of the dimesonic states are obtained using constituent mesons and binding energy

$$M_{12} = M_1 + M_2 - BE. \tag{4.2}$$

The model parameters are fitted to obtain the masses of the respective exotic states.

Table 4.2: Masses of $Z_c^+(D^+\bar{D}^*)$, $Z_b^+(B\bar{B}^*)$ and $Z_b'(B^*\bar{B}^*)$ molecular states (in MeV) with the variation in potential depth C (in MeV)

C	$D^+\bar{D}^*$		$B\bar{B}^*$		$B^*\bar{B}^*$	
	Binding Energy	Mass	Binding Energy	Mass	Binding Energy	Mass
0	11.82	3864.74	5.58	10598.9	5.54	10644.9
50	11.96	3864.61	7.05	10597.4	7.01	10643.4
100	12.07	3864.5	8.04	10596.4	8.02	10642.4
150	12.15	3864.42	8.72	10595.7	8.70	10641.7
PDG [1]		3883.9±4.5		10607.2±2.0		10652.2 ± 1.5

4.3 Strong decay width

The strong two body decay widths are computed using the phenomenological Lagrangian mechanism given in Ref. [235, 236]. The the Lagrangian corresponding to the coupling of Z_c and Z_b states to its constituent can be written as [235, 236],

$$\begin{aligned}
\mathcal{L}_{Z_c}(x) &= \frac{g_{Z_c}}{\sqrt{2}} M_{Z_c} Z_c^{\mu}(x) \int d^4y \Phi_{Z_c}(y^2) \left\{ D\left(x+\frac{y}{2}\right) \bar{D}_{\mu}^*\left(x-\frac{y}{2}\right) + D_{\mu}^*\left(x+\frac{y}{2}\right) \bar{D}\left(x-\frac{y}{2}\right) \right\} \\
\mathcal{L}_{Z_b'}(x) &= \frac{g_{Z_b'}}{\sqrt{2}} i\epsilon_{\mu\nu\alpha\beta} \int d^4y \Phi_{Z_b'}(y^2) B^{*\alpha}\left(x+\frac{y}{2}\right) \bar{B}^{*\beta}\left(x-\frac{y}{2}\right) \\
\mathcal{L}_{Z_b}(x) &= \frac{g_{Z_b}}{\sqrt{2}} M_{Z_b} Z_b^{\mu}(x) \int d^4y \Phi_{Z_b}(y^2) \left\{ B\left(x+\frac{y}{2}\right) \bar{B}_{\mu}^*\left(x-\frac{y}{2}\right) + B_{\mu}^*\left(x+\frac{y}{2}\right) \bar{B}\left(x-\frac{y}{2}\right) \right\}
\end{aligned} \tag{4.3}$$

where y is the relative Jacobi coordinate, g_{Z_c}, g_{Z_b} and $g_{Z_b'}$ are the dimensional coupling constants of Z_c, Z_b and Z_b' to the molecular $D^+\bar{D}^*$, $B\bar{B}^*$ and $B^*\bar{B}^*$ com-

ponents, respectively. $\Phi_{Z_c}(y^2)$, $\Phi_{Z_b'}(y^2)$ and $\Phi_{Z_b'}(y^2)$ are the correlation functions, which describes the distributions of the constituent mesons in the bound states.

The strong two body decay widths are given by [235, 236]

$$\begin{aligned}
\Gamma_{Z_c^+\to\Psi(ns)\pi^+} &\simeq \frac{g^2_{Z_c\Psi(ns)\pi}}{96\pi M^3_{Z_c}}\lambda^{3/2}(M^2_{Z_c}, M^2_{\psi(ns)}, M^2_\pi)\left(1+\frac{M^2_{\psi(ns)}}{2M^2_{Z_c}}\right)\\
\Gamma_{Z_b^+\to\Upsilon(ns)\pi} &\simeq \frac{g^2_{Z_b\Upsilon(ns)\pi}}{16\pi M_{Z_b}}\lambda^{1/2}(M^2_{Z_b}, M^2_{\Upsilon(ns)}, M^2_\pi)\\
\Gamma_{Z_b'^+\to\Upsilon(ns)\pi} &\simeq \frac{g^2_{Z_b\Upsilon(ns)\pi}}{16\pi M_{Z_b'}}\lambda^{1/2}(M^2_{Z_b'}, M^2_{\Upsilon(ns)}, M^2_\pi)
\end{aligned} \tag{4.4}$$

where $\lambda(x,y,z) = x^2+y^2+z^2-2xy-2yz-2zx$ is the Källen function, $g_{Z_c\Psi(ns)\pi}$, $g_{Z_b\Upsilon(ns)\pi}$ and $g_{Z_b'\Upsilon(ns)\pi}$ are the decay coupling constants, expressed as [235, 236]

$$\begin{aligned}
g_{Z_c\Psi(ns)\pi} &= 8g_{Z_c}\frac{g_F g_H}{F_\pi M_J}J_{Z_c}M_{Z_c}\\
g_{Z_b\Upsilon(ns)\pi} &= g_{Z_b}g_{BB^*\Upsilon(ns)\pi}J_{Z_b}\\
g_{Z_b'\Upsilon(ns)\pi} &= g_{Z_b'}g_{B^*B^*\Upsilon(ns)\pi}M_{Z_b'}J_{Z_b'}
\end{aligned} \tag{4.5}$$

with $g's$ and $J's$ are the coupling constants and loop integrals respectively given by

$$\begin{aligned}
\frac{1}{g^2_{Z_c}} &= \frac{M^2_{Z_c}}{32\pi^2\Lambda^2}\int_0^\infty \frac{d\alpha_1 d\alpha_2}{\Delta_1^3}(\alpha_{12}+2\alpha_1\alpha_2)\left(1+\frac{\Lambda^2}{2M^2_{D^*}\Delta_1}\right)\\
&\quad\times\exp\left(-\frac{M^2_{D^*}\alpha_1+M^2_D\alpha_2}{\Lambda^2}+\frac{M^2_{Z_c}}{2\Lambda^2}\frac{\alpha_{12}+2\alpha_1\alpha_2}{\Delta_1}\right)\\
\frac{1}{g^2_{Z_b}} &= \frac{M^2_{Z_b}}{32\pi^2\Lambda^2}\int_0^\infty \frac{d\alpha_1 d\alpha_2}{\Delta_1^3}(\alpha_{12}+2\alpha_1\alpha_2)\left(1+\frac{\Lambda^2}{2M^2_{B^*}\Delta_1}\right)\\
&\quad\times\exp\left(-\frac{M^2_{B^*}\alpha_1+M^2_B\alpha_2}{\Lambda^2}+\frac{M^2_{Z_b}}{2\Lambda^2}\frac{\alpha_{12}+2\alpha_1\alpha_2}{\Delta_1}\right)\\
\frac{1}{g^2_{Z_b'}} &= \frac{M^2_{Z_b}}{32\pi^2\Lambda^2}\int_0^\infty \frac{d\alpha_1 d\alpha_2}{\Delta_1^2}\left(\frac{\Lambda^2}{M^2_{Z_b'}}+\frac{\alpha_{12}+2\alpha_1\alpha_2}{2\Delta_1}\right)\left(1+\frac{\Lambda^2}{M^2_{B^*}\Delta_1}\right)\\
&\quad\times\exp\left(-\frac{M^2_{B^*}\alpha_{12}}{\Lambda^2}+\frac{M^2_{Z_b'}}{2\Lambda^2}\frac{\alpha_{12}+2\alpha_1\alpha_2}{\Delta_1}\right)
\end{aligned} \tag{4.6}$$

and

$$\begin{aligned}
J_{Z_c} &= \frac{1}{8\pi^2}\int_0^\infty \frac{d\alpha_1 d\alpha_2}{\Delta_2^2}\left(1+\frac{\Lambda^2}{2M^2_{D^*}\Delta_2}\right)\exp\left(-\frac{M^2_{D^*}\alpha_1+M^2_D\alpha_2}{\Lambda^2}+\frac{M^2_{Z_c}}{4\Lambda^2}\frac{\alpha_{12}+4\alpha_1\alpha_2}{\Delta_2}\right)\\
J_{Z_b} &= \frac{1}{8\pi^2}\int_0^\infty \frac{d\alpha_1 d\alpha_2}{\Delta_2^2}\left(1+\frac{\Lambda^2}{2M^2_{B^*}\Delta_2}\right)\exp\left(-\frac{M^2_{B^*}\alpha_1+M^2_B\alpha_2}{\Lambda^2}+\frac{M^2_{Z_b}}{4\Lambda^2}\frac{\alpha_{12}+4\alpha_1\alpha_2}{\Delta_2}\right)\\
J_{Z_b'} &= \frac{1}{8\pi^2}\int_0^\infty \frac{d\alpha_1 d\alpha_2}{\Delta_2^2}\left(1+\frac{\Lambda^2}{2M^2_{B^*}\Delta_2}\right)\exp\left(-\frac{M^2_{B^*}\alpha 12}{\Lambda^2}+\frac{M^2_{Z_b'}\alpha_{12}}{4\Lambda^2}\frac{\alpha_{12}+4\alpha_1\alpha_2}{\Delta_2}\right)
\end{aligned}$$

with $\Delta_1 = 2 + \alpha_{12}$, $\Delta_2 = 1 + \alpha_{12}$, $\alpha_{12} = \alpha_1 + \alpha_2$ and Λ is the size parameter which characterizes the effective size of the hadrons. For computation we take $\Lambda = 0.5$ GeV [235, 236].

The strong two body decay widths are computed using Eq. (4.4) and the results are tabulated in Tab. 4.3.

Table 4.3: Hadronic decay widths of Z_c^+, Z_b^+ and Z_b' molecular states (in MeV)

Decay Mode	Decay width				Exp [259]	[235, 236]	[260]	[261]	[262]
	C = 0	C = 50	C = 100	C = 50					
$Z_c \to \psi(1s) + \pi$	11.72	11.76	11.78	11.81	–	10.43 − 23.89	12.00	3.67	
$Z_c \to \psi(2s) + \pi$	2.12	2.11	2.11	2.11	–	1.28 − 2.94	0.9749	8.24	
$Z_b \to \Upsilon(1s) + \pi$	22.84	22.93	23.00	23.06	22.9±7.3	13.3 − 30.8	19.34	–	5.9 ± 0.4
$Z_b \to \Upsilon(2s) + \pi$	26.93	26.99	27.04	27.09	21.1±4.0	15.4 − 35.7	23.54	–	–
$Z_b^{'} \to \Upsilon(1s) + \pi$	23.43	23.51	23.58	23.64	12±10±3	14.0 − 31.7	19.49	–	$9.5^{+0.7}_{-0.6}$
$Z_b^{'} \to \Upsilon(2s) + \pi$	28.77	28.84	28.90	28.95	16.4±3.6	16.9 − 39.3	25.07	–	–

4.4 Results and Discussion

In this chapter we compute the masses of exotic states considering the dimeson molecules considering interaction of type modified Woods - Saxon potential. We have also analysed the nature of potential with the depth of the potential. From the potential plot Fig. 4.1, it is clear that as the depth of the potential increases, the binding energy increases. Solving Schrödinger equation numerically, we obtain the binding energy of the exotic states and the bound state masses are obtained. The bound state masses of the exotic states are in good agreement with PDG data [1]. We have also computed the two body strong decay widths of these states in interaction Lagrangian mechanism from Ref. [235, 236] and compare with the experiments. Our predictions of decay widths are in good agreement with the experimental data [1]. We also compare our findings with the other theoretical approaches such as covariant quark model [262], light front model [261] and potential model [260]. It is observed that our results are also matching well with the theoretical approaches.

Chapter 5

Weak Decays of Open Flavor Mesons

5.1 Introduction

Charm sector is a good platform to test the absolute scale of computed decay amplitudes in terms of form factors because the Cabibbo-Kobayashi-Maskawa (CKM) matrix elements can be determined independently for D decays by exploiting the CKM unitarity and numerical values of the matrix elements for B decays. Study of charm decays is also important for understanding of new physics (NP) affecting the up-type quark dynamics as it is the only up-type quark displaying flavor oscillations [263, 264]. Some hints about the dynamics of TeV scale QCD are expected from charm flavour oscillations in the same line of charm mass and dynamics predictions from experimentally observed low energy kaon oscillations [265]. These flavour oscillations are very sensitive probes for the underlying new physics interactions involving charged particles.

Semileptonic decays have reasonably large amplitudes making them more accessible in recently upgraded experimental facilities and hence are considered to be primary source to get information about CKM matrix elements. Charmed meson semileptonic decays are the easiest direct way to determine the magnitude of quark-mixing parameters i.e. direct access to $|V_{cs}|$ and $|V_{cd}|$. The study of charm semileptonic decays provides insight to $|V_{cq}|^2$ via matrix elements that describe strong interaction effects and may contribute to a precise determination of the CKM matrix element $|V_{ub}|$ via constraints provided by charm decays to reduce the model dependence in extracting $|V_{ub}|$ from exclusive charmless B semileptonic decays. For example, flavour symmetry relates the form factors of the semileptonic decays of D and B

systems. Recently, the matrix elements $|V_{cd(s)}|$ was extracted (PDG [1]) from the experimental results from the $BABAR$ [266,267], Belle [268], BESIII [269], CLEO [270] in the channel $D \to \pi(K)\ell^+\nu_\ell$.

Many lattice quantum chromodynamics (LQCD) papers are available in literature regarding the semileptonic form factors for the channel $D \to (K, \pi)\ell\nu_\ell$. However, in the light sector of daughter meson, the first successful computation of form factors for $D_s \to \phi\ell^+\nu_\ell$ from full LQCD was reported by HPQCD collaboration [21]. Later, $D_s \to \eta^{(\prime)}\ell^+\nu_\ell$ semileptonic form factors were also reported for the first time using LQCD [22]. The heavy ($D_{(s)}$) to light (π, ρ, ω, ϕ, $\eta^{(\prime)}$, K) form factors have also been computed within the QCD sum rules [271,272] and light cone QCD sum rules (LCSR) [273–276]. The LCSR along with heavy quark effective theory (HQET) has also been employed for computing the transition form factors and branching fractions [277]. Recently, computation of form factors and semileptonic branching fractions of $D \to \rho$ decays have been reported using LCSR with chiral correlator [278]. The heavy to light form factors are also computed in the heavy quark limit of the large energy effective theory [279], constituent quark model [280], chiral quark model (χQM) [281] and chiral perturbation theory [282]. The form factors and semileptonic branching fractions of $D_{(s)}$ mesons are also computed in the frame work of heavy meson chiral theory (HMχT) [283, 284] and the light front quark model (LFQM) [285–287]. The authors of Ref. [288] have computed the semileptonic branching fractions of $D_{(s)}$ mesons in the chiral unitary (χUA) approach.

In this chapter, we compute the semileptonic branching fractions of the charmed (D) and charmed-strange (D_s^+) meson to light mesons (ρ, ω, ϕ, $\eta^{(\prime)}$ and $K^{(*)0}$). The required transition form factors are computed in the frame work of Covariant Confined Quark Model (CCQM) [57,58,289]. The CCQM is the effective field theory approach with the infrared confinement for the hadronic interactions with their constituents. This allows us to compute the form factors in the complete physical range of momentum transfer. We also compute the semileptonic branching fractions for $D^+_{(s)} \to D^0 e^+\nu_e$. These are the rare class of semileptonic decays where the light quark decays weakly leaving behind the heavy quark as a spectator. Recently, BESIII collaboration has reported the upper bound on the branching fraction for the channel $D^+ \to D^0 e^+\nu_e$ at 90% confidence level to be 1.0×10^{-4} [290]. These channels were studied within the SU(3) symmetry [291] as well as heavy flavour conserving decays [292].

The next section gives detailed formulation of the model CCQM. Next, we provide the branching fractions in terms of helicity structure functions followed by the results in comparison with the experimental data and theoretical predictions. This study comprising computation of leptonic and semileptonic decays of D and $D_{(s)}$ mesons is published in Physical Review D [293,294]. In these papers, we have considered the channels $D^0 \to (K^-, \pi^-, \rho^-, K^*(892)^-)\ell^+\nu_\ell$, $D^+ \to (\bar{K}^0, \pi^0, \eta, \eta', \rho^0, \omega, \bar{K}^*(892)^0)\ell^+\nu_\ell$ and $D_s^+ \to (K^0, \eta, \eta', \phi, K^*(892)^-)\ell^+\nu_\ell$ for $\ell = e$ and μ.

5.2 Methodology

The CCQM is an effective quantum field approach [57, 58, 289] for hadronic interactions that utilizes an effective Lagrangian for hadrons interacting with the constituent quarks. In this model it is assumed that hadrons interact with the constituent quarks only. The Lagrangian describing the coupling of meson $M(q_1\bar{q}_2)$ to its constituent quarks q_1 and $\bar{q}_2$ is given by

$$\mathcal{L}_{int} = g_M M(x) \int dx_1 \int dx_2 F_M(x; x_1, x_2) \bar{q}_2(x_2) \Gamma_M q_1(x_1) + H.c. \tag{5.1}$$

where Γ_M is the Dirac matrix and projects onto the spin quantum number of relevant mesonic field $M(x)$. F_M is the vertex factor which characterizes the finite size of the meson and is invariant under translation $F_M(x + a, x_1 + a, x_2 + a) = F_M(x, x_1, x_2)$. This ensures the Lorentz invariance of the Lagrangian Eq. (5.1) for any value of four-vector a. We choose the following form of the vertex function

$$F_M(x, x_1, x_2) = \delta^{(4)}\left(x - \sum_{i=1}^{2} w_i x_i\right) \Phi_M\left((x_1 - x_2)^2\right) \tag{5.2}$$

with Φ_M is the correlation function of two constituent quarks with masses m_{q_1} and m_{q_2} and $w_{q_i} = m_{q_i}/(m_{q_1} + m_{q_2})$ such that $w_1 + w_2 = 1$.

We choose Gaussian function for vertex function as

$$\tilde{\Phi}_M(-p^2) = \exp\ (p^2/\Lambda_M^2) \tag{5.3}$$

with the parameter Λ_M characterized by the finite size of the meson. Note that any form of Φ_M is appropriate as long as it falls off sufficiently fast in the ultraviolet region of Euclidian space in order to overcome the ultraviolet divergence of the loop integral. The local fermion propagator for the constituent quarks is given by

$$S_q(k) = \frac{1}{m_q - \not{k}} \tag{5.4}$$

with an effective constituent quark mass m_q. The compositeness condition [59, 60]

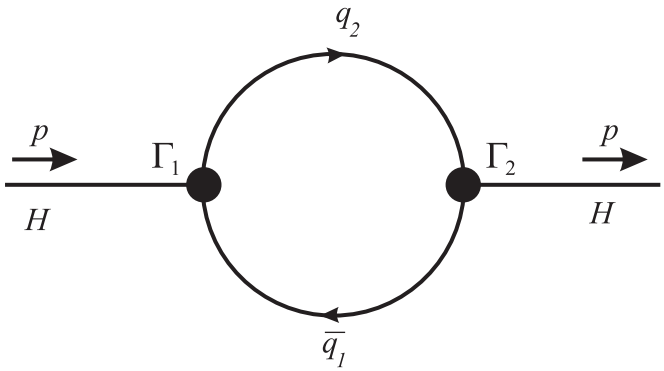

Figure 5.1: Diagram describing meson mass operator.

is used to determine the coupling constant g_M in Eq. (5.1)

$$Z_M = 1 - \frac{3g_M^2}{4\pi^2}\tilde{\Pi}'_M(m_M^2) = 0, \tag{5.5}$$

where $\tilde{\Pi}'_M(p^2)$ is the derivative of the mass operator taken on the mass-shell $p^2 = m_M^2$. By using the Fourier transformation of the vertex function in Eq. (5.3) and quark propagator in Eq. (5.4), one can write the meson mass function defined in Fig. 5.1. For pseudoscalar meson

$$\tilde{\Pi}_P(p^2) = N_c g_P^2 \int \frac{d^4k}{(2\pi)^4 i}\tilde{\Phi}_P^2(-k^2)\mathrm{tr}\Big(\gamma^5 S_1(k+w_1 p)\gamma^5 S_2(k-w_2 p)\Big), \tag{5.6}$$

and for vector meson

$$\tilde{\Pi}_V^{\mu\nu}(p^2) = N_c g_V^2 \int \frac{d^4k}{(2\pi)^4 i}\tilde{\Phi}_V^2(-k^2)\mathrm{tr}\Big(\gamma^\mu S_1(k+w_1 p)\gamma^\nu S_2(k-w_2 p)\Big) \tag{5.7}$$

where $N_c = 3$ is the number of colors. Since the vector meson is on its mass-shell, one has $\epsilon_V \cdot p = 0$ and needs only the part of the vector meson function proportional to $g_{\mu\nu}$, given by

$$\tilde{\Pi}_V(p^2) = \frac{1}{3}\left(g_{\mu\nu} - \frac{p_\mu p_\nu}{p^2}\right)\tilde{\Pi}_V^{\mu\nu}(p). \tag{5.8}$$

The loop integrations in Eqs. (5.6) and (5.7) are performed with Fock-Schwinger representation of quark propagators

$$\begin{aligned} S_q(k+p) &= \frac{1}{m_q - \not{k} - \not{p}} = \frac{m_q + \not{k} + \not{p}}{m_q^2 - (k+p)^2} \\ &= (m_q + \not{k} + \not{p})\int_0^\infty d\alpha\, e^{-\alpha[m_q^2 - (k+p)^2]}, \end{aligned} \tag{5.9}$$

allowing tensor loop integral by conversion of the loop momentum to the derivative of the exponential function. All the loop integrations are performed in Euclidean space transformed from Minkowski space using the Wick rotation

$$k_0 = e^{i\frac{\pi}{2}} k_4 = ik_4 \tag{5.10}$$

so that $k^2 = k_0^2 - \vec{k}^2 = -k_4^2 - \vec{k}^2 = -k_E^2 \leq 0$. Simultaneously one has to rotate all external momenta, i.e. $p_0 \to ip_4$ so that $p^2 = -p_E^2 \leq 0$. Then the quadratic form in Eq. (5.9) becomes positive-definite,

$$m_q^2 - (k+p)^2 = m_q^2 + (k_E + p_E)^2 > 0 \tag{5.11}$$

where the integral over α is convergent.

Collecting the representation of the vertex function Eq. (5.3) and quark propagator Eq. (5.4), we perform the Gaussian integration in the derivatives of the mass functions in Eqs. (5.6) and (5.7). The exponential function has the form $ak^2 + 2kr + z_0$, where $r = bp$. Using the following properties

$$\begin{aligned} k^\mu \, \exp(ak^2 + 2kr + z_0) &= \frac{1}{2}\frac{\partial}{\partial r_\mu} \exp(ak^2 + 2kr + z_0), \\ k^\mu k^\nu \, \exp(ak^2 + 2kr + z_0) &= \frac{1}{2}\frac{\partial}{\partial r_\mu}\frac{1}{2}\frac{\partial}{\partial r_\nu} \exp(ak^2 + 2kr + z_0), \text{ etc.} \end{aligned}$$

one can replace $\not{k}$ by $\not{\partial}_r = \gamma^\mu \frac{\partial}{\partial r_\mu}$ in order to perform the exchange of tensor integrations for differentiation of the Gaussian exponent. The r-dependent Gaussian exponent $e^{-r^2/a}$ can be moved to the left through the differential operator $\not{\partial}_r$ using

$$\begin{aligned} \frac{\partial}{\partial r_\mu} e^{-r^2/a} &= e^{-r^2/a}\left[-\frac{2r^\mu}{a} + \frac{\partial}{\partial r_\mu}\right], \\ \frac{\partial}{\partial r_\mu}\frac{\partial}{\partial r_\nu} e^{-r^2/a} &= e^{-r^2/a}\left[-\frac{2r^\mu}{a} + \frac{\partial}{\partial r_\mu}\right]\cdot\left[-\frac{2r^\nu}{a} + \frac{\partial}{\partial r_\nu}\right], \text{ etc.} \end{aligned} \tag{5.12}$$

Finally, we move the derivatives to the right by using the commutation relation

$$\left[\frac{\partial}{\partial r_\mu}, r^\nu\right] = g^{\mu\nu}. \tag{5.13}$$

The last step has been done by using a FORM code [295] which works for any numbers of loops and propagators. In the remaining integrals over the Fock-Schwinger parameters $0 \leq \alpha_i < \infty$, we introduce an additional integration which converts the set of Fock-Schwinger parameters into a simplex. Using the transformation [296]

$$\prod_{i=1}^n \int_0^\infty d\alpha_i f(\alpha_1, \ldots, \alpha_n) = \int_0^\infty dt t^{n-1} \prod_{i=1}^n \int d\alpha_i \delta\left(1 - \sum_{i=1}^n \alpha_i\right) f(t\alpha_1, \ldots, t\alpha_n) \tag{5.14}$$

Finally, we have

$$\tilde{\Pi}_M(p^2) = \frac{3g_M^2}{4\pi^2}\int_0^\infty \frac{dt\,t}{a_M^2}\int_0^1 d\alpha\, e^{-t\,z_0+z_M}\, f_M(t,\alpha), \tag{5.15}$$

$$\begin{aligned} z_0 &= \alpha m_{q_1}^2 + (1-\alpha)m_{q_2}^2 - \alpha(1-\alpha)p^2, \\ z_M &= \frac{2s_M t}{2s_M + t}(\alpha - w_2)^2 p^2, \\ a_M &= 2s_M + t, \qquad b = (\alpha - w_2)t. \end{aligned}$$

where $S_M = 1/\Lambda_M^2$ and the function $f_M(t,\alpha)$ coming from the trace evaluation in Eqs. (5.6) and (5.7).

It can be seen that the integral over t in Eq. (5.15) is well defined and convergent below the threshold $p^2 < (m_{q_1} + m_{q_2})^2$. The convergence of the integral above threshold $p^2 \geq (m_{q_1} + m_{q_2})^2$ is ensured by incrementing the quark mass by an imaginary part, i.e. $m_q \to m_q - i\epsilon,\ \epsilon > 0$, in the quark propagator Eq. (5.4). This allows transformation of the integration variable t to imaginary axis $t \to it$. As a result, the integral Eq. (5.15) becomes convergent, however it does obtain an imaginary part that accounts for quark pair production.

However, by truncating the scale of integration to the upper limit by introducing the infrared cutoff

$$\int_0^\infty dt(\ldots) \to \int_0^{1/\lambda^2} dt(\ldots), \tag{5.16}$$

all possible thresholds present in the initial quark diagram can be removed [289]. Thus the infrared cutoff parameter λ ensures the confinement. This method is quite general and can be used for diagrams with an arbitrary number of loops and propagators. In CCQM, the infrared cutoff parameter λ is taken to be universal for all physical processes.

Since the model CCQM is not based on the first principle, we need to fix the parameters such as quark masses (m_q) and meson size parameters (Λ_M) as in Tab. 5.1 and Tab. 5.2 respectively. The model parameters are determined by fitting computed leptonic and radiative decay constants to available experimental data or LQCD for pseudoscalar and vector mesons. The matrix elements of the leptonic decays are described by the Feynman diagram shown in Fig. 5.2. The leptonic decay constants

Table 5.1: Quark masses and infrared cutoff parameter in GeV

$m_{u/d}$	m_s	m_c	m_b	λ
0.241	0.428	1.672	5.05	0.181

Table 5.2: Meson size parameters in GeV

Λ_D	Λ_{D_s}	Λ_K	Λ_{K^*}	Λ_ϕ	Λ_ρ	Λ_ω	Λ_π	$\Lambda_\eta^{q\bar{q}}$	$\Lambda_\eta^{s\bar{s}}$	$\Lambda_{\eta'}^{q\bar{q}}$	$\Lambda_{\eta'}^{s\bar{s}}$
1.600	1.784	1.014	0.805	0.883	0.624	0.488	0.870	0.881	1.973	0.257	2.797

of the pseudoscalar and vector mesons are defined by

$$\begin{aligned} N_c g_P \int \frac{d^4k}{(2\pi)^4 i} \tilde{\phi}_P(-k^2) \mathrm{tr}[O^\mu S_1(k+w_1 p)\gamma^5 S_2(k-w_2 p)] &= f_p p^\mu \\ N_c g_V \int \frac{d^4k}{(2\pi)^4 i} \tilde{\phi}_V(-k^2) \mathrm{tr}[O^\mu S_1(k+w_1 p)\ \not{\epsilon}_v S_2(k-w_2 p)] &= m_V f_V \epsilon_V^\mu \end{aligned} \quad (5.17)$$

where N_c is the number of colors and $O^\mu = \gamma^\mu(1-\gamma_5)$ is the weak Dirac matrix with left chirality. Our results for the leptonic decay constants are given in the Table 5.3.

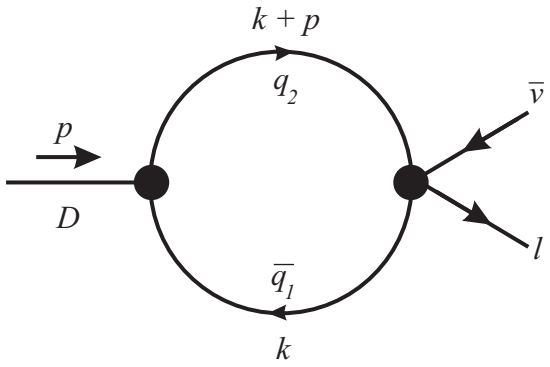

Figure 5.2: Quark model diagrams for the D-meson leptonic decay

The decay constants we use in our calculations match quite well with PDG, LQCD and QCD sum rules (QCDSR) parameters.

In the SM, pure leptonic decays $D_{(s)}^+ \to \ell\nu_\ell$ proceed by exchange of virtual W boson. The leptonic branching fraction is given by

$$B(D_{(s)}^+ \to \ell\nu_\ell) = \frac{G_F^2}{8\pi} m_{D_{(s)}} m_\ell^2 \left(1 - \frac{m_\ell^2}{m_{D_{(s)}}^2}\right)^2 f_{D_{(s)}}^2 |V_{cd}|^2 \tau_{D_{(s)}} \quad (5.18)$$

where, G_F is the fermi coupling constant, m_D and m_ℓ are the D-meson and lepton masses respectively and $\tau_{D_{(s)}}$ is the $D_{(s)}$-meson lifetime. $f_{D_{(s)}}$ is the leptonic decay constant of D-meson from Table 5.3. The resultant branching fractions for $\ell = \tau, \mu$

Table 5.3: Leptonic decay constants f_H (in MeV)

f_H	Present	Data	Reference
f_D	206.08	202.2 (2.2) (2.6)	LQCD [297]
		210 ± 11	QCDSR [298]
		211.9(1.1)	PDG [1]
f_{D_s}	257.70	258.7 (1.1) (2.9)	LQCD [297]
		259 ± 10	QCDSR [298]
		249.0(1.2)	PDG [1]
f_{D_s}/f_D	1.25	1.173(3)	PDG [1]
f_K	156.96	155.37(34)	LQCD [299]
		157.9 ± 1.5	LQCD [300]
		155.6(0.4)	PDG [1]
f_π	130.30	130.39 (20)	LQCD [299]
		132.3 ± 1.6	LQCD [300]
		130.2(1.7)	PDG [1]
f_K/f_π	1.20	1.1928(26)	PDG [1]
f_{D^*}	244.27	$278 \pm 13 \pm 10$	LQCD [301]
		263 ± 21	QCDSR [298]
$f_{D_s^*}$	272.08	311 ± 9	LQCD [301]
		308 ± 21	QCDSR [298]
f_{K^*}	226.81	222 ± 8	QCDSR [302]
f_ρ	218.28	$208.5 \pm 55 \pm 0.9$	LQCD [303]
f_ϕ	226.56	238 ± 3	LQCD [304]
		215 ± 5	QCDSR [302]
f_ω	198.38	194.60 ± 3.24	LFQM [286]

and e are given in Table 5.4. I is important to note here that the branching fractions are affected by different lepton masses through the helicity flip factor $(1-m_\ell^2/m_{D_{(s)}}^2)^2$.

Table 5.4: Leptonic $D_{(s)}^+$ branching fractions

Channel	Present	PDG Data [1]
$D^+ \to e^+\nu_e$	8.42×10^{-9}	$< 8.8 \times 10^{-6}$
$D^+ \to \mu^+\nu_\mu$	3.57×10^{-4}	$(3.74 \pm 0.17) \times 10^{-4}$
$D^+ \to \tau^+\nu_\tau$	0.95×10^{-3}	$< 1.2 \times 10^{-3}$
$D_s^+ \to e^+\nu_e$	1.40×10^{-7}	$< 8.3 \times 10^{-5}$
$D_s^+ \to \mu^+\nu_\mu$	5.97×10^{-3}	$(5.50 \pm 0.23) \times 10^{-3}$
$D_s^+ \to \tau^+\nu_\tau$	5.82 %	$(5.48 \pm 0.23)\%$

5.3 Form factors and differential decay distribution

After fixing all the model parameters, we employ CCQM to compute the semileptonic branching fractions of $D_{(s)} \to P/V$ transition where P and V corresponds to pseudoscalar and vector daughter mesons. We start with the definitions of the form factors. The invariant matrix element for this decay can be written as

$$M(D_{(s)} \to (P,V)\ell^+\nu_\ell) = \frac{G_F}{\sqrt{2}} V_{cx} \langle (P,V)|\bar{x}\gamma^\mu(1-\gamma_5)c|D_{(s)}\rangle \ell^+ O^\mu \nu_\ell \tag{5.19}$$

where $O^\mu = \gamma_\mu(1-\gamma_5)$ and $x = d, s$. The matrix elements for the above semileptonic transitions in the covariant quark model are defined by the diagram in Fig 5.3. The

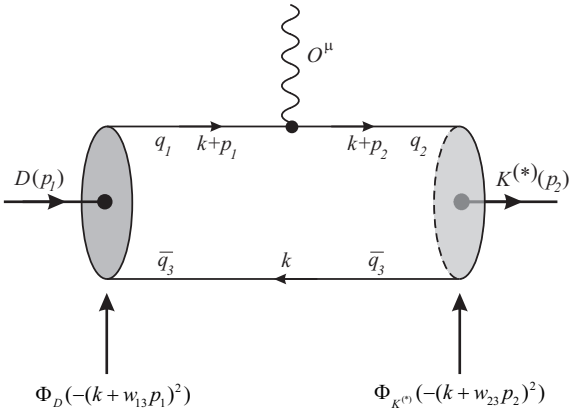

Figure 5.3: Quark model diagrams for the D-meson semileptonic decay

matrix element for the semileptonic transition can be written as

$$\begin{aligned}
\langle P(p_2)|\bar{x}O^\mu c|D_{(s)}(p_1)\rangle &= N_c g_{D_{(s)}} g_P \int \frac{d^4k}{(2\pi)^4 i} \tilde{\Phi}_{D_{(s)}}(-(k+w_{13}p_1)^2)\tilde{\Phi}_P(-(k+w_{23}p_2)^2) \\
&\quad \times \mathrm{tr}[O^\mu S_1(k+p_1)\gamma^5 S_3(k)\gamma^5 S_2(k+p_2)] \\
&= F_+(q^2)P^\mu + F_-(q^2)q^\mu
\end{aligned} \tag{5.20}$$

$$\begin{aligned}
\langle V(p_2,\epsilon_\nu)|\bar{x}O^\mu c|D_{(s)}(p_1)\rangle &= N_c g_{D_{(s)}} g_V \int \frac{d^4k}{(2\pi)^4 i} \tilde{\Phi}_{D_{(s)}}(-(k+w_{13}p_1)^2)\tilde{\Phi}_V(-(k+w_{23}p_2)^2) \\
&\quad \times \mathrm{tr}[O^\mu S_1(k+p_1)\gamma^5 S_3(k) \not{\epsilon}^\dagger_\nu S_2(k+p_2)] \\
&= \frac{\epsilon^\dagger_\nu}{m_1+m_2}\left[-g^{\mu\nu}P\cdot q A_0(q^2) + P^\mu P^\nu A_+(q^2)\right. \\
&\quad \left. + q^\mu P^\nu A_-(q^2) + i\varepsilon^{\mu\nu\alpha\beta}P_\alpha q_\beta V(q^2)\right]
\end{aligned} \tag{5.21}$$

with $P = p_1 + p_2$, $q = p_1 - p_2$ and ϵ_ν to be the polarization vector such that $\epsilon^\dagger_\nu \cdot p_2 = 0$ and on-shell conditions of particles require $p_1^2 = m_1^2 = m^2_{D_{(s)}}$ and $p_2^2 = m_2^2 = m^2_{P,V}$. Since there are three quarks involved in this transition, we use $w_{ij} = m_{q_j}/(m_{q_i} + m_{q_j})$

$(i,\ j = 1,\ 2,\ 3)$ such that $w_{ij} + w_{ji} = 1$. Performing the loop integration in Eqs (5.20) and (5.21), we obtain the semileptonic form factors within the entire range of momentum transfer $0 \leq q^2 \leq q^2_{max}$ with $q^2_{max} = (m_{D_{(s)}} - m_{P,V})^2$. The required multi-dimensional integration appeared in Eqs. (5.20) and (5.21) are computed numerically using *Mathematica* as well as FORTRAN codes with NAG library. We also represent our form factors using double pole parametrization as

$$F(q^2) = \frac{F(0)}{1 - as + bs^2}, \qquad s = \frac{q^2}{m_1^2} \tag{5.22}$$

In Tab. 5.5, we list the quark channel and the CKM matrix for the semileptonic decays of $D_{(s)}$ mesons and in Tab. 5.6, we give the numerical results of the form factors and associated double pole parameters. For the comparison of our form

Table 5.5: Quark channel and associated CKM matrix element for semileptonic decays ($\phi = 39.3\,\mathrm{deg}$)

Channel	qq_1	qq_2	V_{ckm}	Channel	qq_1	qq_2	V_{ckm}
$D^0 \to K^-$	$c\bar{u}$	$s\bar{u}$	V_{cs}	$D^+ \to K^0$	cd	sd	V_{cs}
$D^0 \to K^*(892)^-$	$c\bar{u}$	$s\bar{u}$	V_{cs}	$D^+ \to K^*(892)^0$	$c\bar{d}$	$s\bar{d}$	V_{cs}
$D_s^+ \to K^0$	$c\bar{s}$	$d\bar{s}$	V_{cd}	$D_s^+ \to K^*(892)^0$	$c\bar{s}$	$d\bar{s}$	V_{cd}
$D^0 \to \pi^-$	$c\bar{u}$	$d\bar{u}$	V_{cd}	$D^+ \to \pi^0$	$c\bar{d}$	$d\bar{d}$	$V_{cd}/\sqrt{2}$
$D^0 \to \rho^-$	$c\bar{u}$	$d\bar{u}$	V_{cd}	$D^+ \to \rho^0$	$c\bar{d}$	$d\bar{d}$	$-V_{cd}/\sqrt{2}$
$D^+ \to \omega$	$c\bar{d}$	$d\bar{d}$	$V_{cd}/\sqrt{2}$	$D_s^+ \to \phi$	$c\bar{s}$	$s\bar{s}$	V_{cs}
$D^+ \to \eta$	$c\bar{d}$	$d\bar{d}$	$V_{cd}\cos\phi/\sqrt{2}$	$D_s^+ \to \eta$	$c\bar{s}$	$s\bar{s}$	$V_{cs}\sin\phi$
$D^+ \to \eta'$	$c\bar{d}$	$d\bar{d}$	$V_{cd}\sin\phi/\sqrt{2}$	$D_s^+ \to \eta'$	$c\bar{s}$	$s\bar{s}$	$V_{cs}\cos\phi$
$D^+ \to D^0$	$c\bar{d}$	$c\bar{u}$	V_{ud}	$D_s^+ \to D^0$	$c\bar{s}$	$c\bar{u}$	V_{us}

factors with the other studies, we need to transform our form factors to the Bauer-Stech-Wirbel (BSW) form factors. The relation reads [305]

$$\begin{aligned} A_2' &= A_+, \quad V' = V \\ A_1' &= \frac{M_1 - M_2}{M_1 + M_2} A_0 \\ A_0' &= \frac{M_1 - M_2}{2M_2}\left(A_0 - A_+ - \frac{q^2}{M_1^2 - M_2^2} A_-\right) \end{aligned} \tag{5.23}$$

and

$$F_0' = F_+ + \frac{q^2}{M_1^2 - M_2^2} F_-, \quad F_+' = F_+ \tag{5.24}$$

Once the form factors are known, it is straight forward to calculate the semileptonic decay rates. The differential decay widths are written in terms of helicity amplitudes

Table 5.6: Form factors and associated double pole parameters

F	$F(0)$	a	b	F	$F(0)$	a	b
$A_+^{D\to K^*}$	0.68	0.86	0.09	$A_-^{D\to K^{*0}}$	−0.90	0.96	0.14
$A_0^{D\to K^*}$	2.08	0.40	−0.10	$V^{D\to K^{*0}}$	0.90	0.97	0.13
$A_+^{D\to \rho}$	0.57	0.96	0.15	$A_-^{D\to \rho}$	−0.74	1.11	0.22
$A_0^{D\to \rho}$	1.47	0.47	−0.10	$V^{D\to \rho}$	0.76	1.13	0.23
$A_+^{D\to \omega}$	0.55	1.01	0.17	$A_-^{D\to \omega}$	−0.69	1.17	0.26
$A_0^{D\to \omega}$	1.41	0.53	−0.10	$V^{D\to \omega}$	0.72	1.19	0.27
$A_+^{D_s\to \phi}$	0.67	1.06	0.17	$A_-^{D_s\to \phi}$	−0.95	1.20	0.26
$A_0^{D_s\to \phi}$	2.13	0.59	−0.12	$V^{D_s\to \phi}$	0.91	1.20	0.25
$A_+^{D_s\to K^*}$	0.57	1.13	0.21	$A_-^{D_s\to K^*}$	−0.82	1.32	0.34
$A_0^{D_s\to K^*}$	1.53	0.61	−0.11	$V^{D_s\to K^*}$	0.80	1.32	0.33
$F_+^{D\to K}$	0.77	0.73	0.05	$F_-^{D\to K}$	−0.39	0.78	0.07
$F_+^{D\to \pi}$	0.63	0.86	0.09	$F_-^{D\to \pi}$	−0.41	0.93	0.13
$F_+^{D\to \eta}$	0.36	0.93	0.12	$F_-^{D\to \eta}$	−0.20	1.02	0.18
$F_+^{D\to \eta'}$	0.36	1.23	0.23	$F_-^{D\to \eta'}$	−0.03	2.29	1.71
$F_+^{D\to D^0}$	0.91	5.88	4.40	$F_-^{D\to D^0}$	−0.026	6.32	8.37
$F_+^{D_s\to \eta}$	0.49	0.69	0.002	$F_-^{D_s\to \eta}$	−0.26	0.74	0.008
$F_+^{D_s\to \eta'}$	0.59	0.88	0.018	$F_s^{D_s\to \eta'}$	−0.23	0.92	0.009
$F_+^{D_s\to K}$	0.60	1.05	0.18	$F_-^{D_s\to K}$	−0.38	1.14	0.24
$F_+^{D_s\to D^0}$	0.92	5.08	2.25	$F_-^{D_s\to D^0}$	−0.34	6.79	8.91

as

$$\frac{d\Gamma(D_{(s)}\to (P,V)\ell^+\nu_\ell)}{dq^2} = \frac{G_F^2|V_{cq}|^2|\mathbf{p_2}|q^2}{96\pi^3 M_1^2}\Big(1-\frac{m_\ell^2}{q^2}\Big)^2 \times\Big[\Big(1+\frac{m_\ell^2}{2q^2}\Big)\sum|H_n|^2 + \frac{3m_\ell^2}{2q^2}|H_t|^2\Big], \quad (5.25)$$

with $|\mathbf{p_2}| = \lambda^{1/2}(M_1^2, M_2^2, q^2)/2M_1$ is the momentum of the daughter meson in the rest frame of the $D_{(s)}$ meson and the index n runs through $(+,-,0)$. The helicity amplitudes are related to the form factors in the following manner:

For $D_{(s)}\to P$ channel:

$$H_t = \frac{1}{\sqrt{q^2}}(PqF_+ + q^2F_-),$$
$$H_\pm = 0 \quad and \quad H_0 = \frac{2m_1|\mathbf{p_2}|}{\sqrt{q^2}}F_+ \quad (5.26)$$

For $D_{(s)} \to V$ channel:

$$\begin{aligned} H_t &= \frac{1}{m_1+m_2}\frac{m_1|\mathbf{p_2}|}{m_2\sqrt{q^2}}\left((m_1^2-m_2^2)(A_+-A_-)+q^2A_-\right) \\ H_\pm &= \frac{1}{m_1+m_2}(-(m_1^2-m_2^2)A_0 \pm 2m_1|\mathbf{p_2}|V) \\ H_0 &= \frac{1}{m_1+m_2}\frac{1}{2m_2\sqrt{q^2}}(-(m_1^2-m_2^2)(m_1^2-m_2^2-q^2)A_0+4m_1^2|\mathbf{p_2}|^2A_+) \end{aligned} \quad (5.27)$$

For studying the lepton-mass effect, we define the physical observables such as forward-backward asymmetry $\mathcal{A}_{FB}^{\ell}(q^2)$, the longitudinal $P_L^{\ell}(q^2)$ and transverse $P_T^{\ell}(q^2)$ polarization of the charged lepton in the final state. They are also related to the helicity amplitude via the relations

$$\mathcal{A}_{FB}^{\ell}(q^2) = -\frac{3}{4}\frac{|H_+|^2-|H_-|^2+4\delta_\ell H_0H_t}{(1+\delta_\ell)\sum|H_n|^2+3\delta_\ell|H_t|^2}, \quad (5.28)$$

$$P_L^{\ell}(q^2) = -\frac{(1-\delta_\ell)\sum|H_n|^2-3\delta_\ell|H_t|^2}{(1+\delta_\ell)\sum|H_n|^2+3\delta_\ell|H_t|^2}, \quad (5.29)$$

$$P_T^{\ell}(q^2) = -\frac{3\pi}{4\sqrt{2}}\frac{\sqrt{\delta_\ell}(|H_+|^2-|H_-|^2-2H_0H_t)}{(1+\delta_\ell)\sum|H_n|^2+3\delta_\ell|H_t|^2}, \quad (5.30)$$

where $\delta_\ell = m_\ell^2/2q^2$ is the helicity-flip factor. The detailed analytical calculations of the helicity amplitudes and differential distributions are given in our recent papers [293,294,306,307]. The averages of these observables in the q^2 range is better suited for experimental measurements with low statistics. In order to compute the averages of these observables Eqns. 5.28 – 5.30, one has to multiply and divide the numerator and denominator with the phase factor $|\mathbf{p_2}|(q^2-m_\ell^2)^2/q^2$ and integrate seperately. These observables are sensitive to contributions of physics beyond the SM and can be used to test LFU violations [308–313].

5.4 Results and Discussion

Having determined all the model parameters we are now in a position to represent our results. First we compute the leptonic branching fractions using the Eq. (5.18) and tabulated in Tab. 5.4. We compare our results with the latest PDG data [1] and it is observed that our results satisfies the experimental constraint for electron channel and for muon and tau channel also our results are in very good agreement with the PDG data.

Then we compute the form factors for the semileptonic decays of $D_{(s)}$ mesons in the entire physical range of momentum transfer. We also compare our findings with the

other theoretical approaches. For comparing our form factors with other studies, we need to transform to BSW form factors Eq. (5.24 and 5.24). We note that based on the method we used in the model-parameter fitting, as well as comparisons of our predictions with experimental data in previous studies, the estimation of the errors for the form factors in our model are of order 20% for small q^2 and 30% for large q^2 .

Table 5.7: Comparison of $F_+(0)$ for $D_{(s)} \to P$ transitions at maximum recoil.

	$D \to \pi$	$D \to K$	$D \to \eta$	$D \to \eta'$	$D_s \to \eta$	$D_s \to \eta'$	$D_s \to K^0$
Present	0.63	0.77	0.36	0.36	0.49	0.59	0.60
CQM [280]	0.69	0.78	–	–	0.50	0.60	0.72
LFQM [286]	0.66	0.79	0.39	0.32	0.48	0.59	0.66
LQCD [22]	–	–	–	–	0.564(11)	0.437(18)	–
LQCD [22]	–	–	–	–	0.542(13)	0.404(25)	–
LQCD [17]	0.612(35)	0.765(31)	–	–	–	–	–
LCSR [274]	–	–	0.552 ± 0.051	0.458 ± 0.105	0.432 ± 0.033	0.520 ± 0.080	–
LCSR [276]	–	–	$0.429^{+0.165}_{-0.141}$	$0.292^{+0.113}_{-0.104}$	$0.495^{+0.030}_{-0.029}$	$0.558^{+0.047}_{-0.045}$	–

Table 5.8: Ratios of the $D_{(s)} \to V$ transition form factors at maximum recoil.

Channel	Ratio	Present	PDG [1]	LQCD [21]	CQM [280]	LFQM [286]	HMχT [284]
$D \to \rho$	r_2	0.93	0.83 ± 0.12	–	0.83	0.78	0.51
	r_V	1.26	1.48 ± 0.16	–	1.53	1.47	1.72
$D^+ \to \omega$	r_2	0.95	1.06 ± 0.16	–	–	0.84	0.51
	r_V	1.24	1.24 ± 0.11	–	–	1.47	1.72
$D \to K^*$	r_2	0.92	0.80 ± 0.021	–	0.74	0.92	0.5
	r_V	1.22	1.49 ± 0.05	–	1.56	1.26	1.60
$D_s^+ \to \phi$	r_2	0.99	0.84 ± 0.11	0.74(12)	0.73	0.86	0.52
	r_V	1.34	1.80 ± 0.08	1.72(21)	1.72	1.42	1.80
$D_s^+ \to K^{*0}$	r_2	0.99	$0.77 \pm 0.28 \pm 0.07$ [314]	–	0.74	0.82	0.55
	r_V	1.40	$1.67 \pm 0.34 \pm 0.16$ [314]	–	1.82	1.55	1.93

In Tab. 5.7, we compare our results of the form factor F_+ at the maximum recoil for the channel $D_{(s)} \to P$ transition with the other theoretical approaches. It is observed that our results are in very good agreement with the Quark model predictions such as CQM [280] and LFQM [286]. For $D \to \pi(K)$ channels, our results are in excellent agreement with the LQCD calculations [17,18]. For $D_{(s)} \to \eta^{(\prime)}$ channels, our results are LCSR [274,276] and LQCD [22] but is is to be noted that the authors of Ref. [22] have considered the LQCD calculations as a pilot study.

For vector form factors, we compare the ratios at the maximum recoil as

$$r_2 = \frac{A_2(0)}{A_1(0)} \quad \text{and} \quad r_V = \frac{V(0)}{A_1(0)} \tag{5.31}$$

In Tab. 5.8, we compare our ratios with the PDG averages data [1] and other theoretical approaches. It is observed that our results for the ratios of the form factors agree well with the PDG data within the uncertanity except for the channel $D_s \to \phi$. It is also important to note that our result $r_V(D_s \to \phi) = 1.34$ is very close to the value 1.42 from LFQM [286].

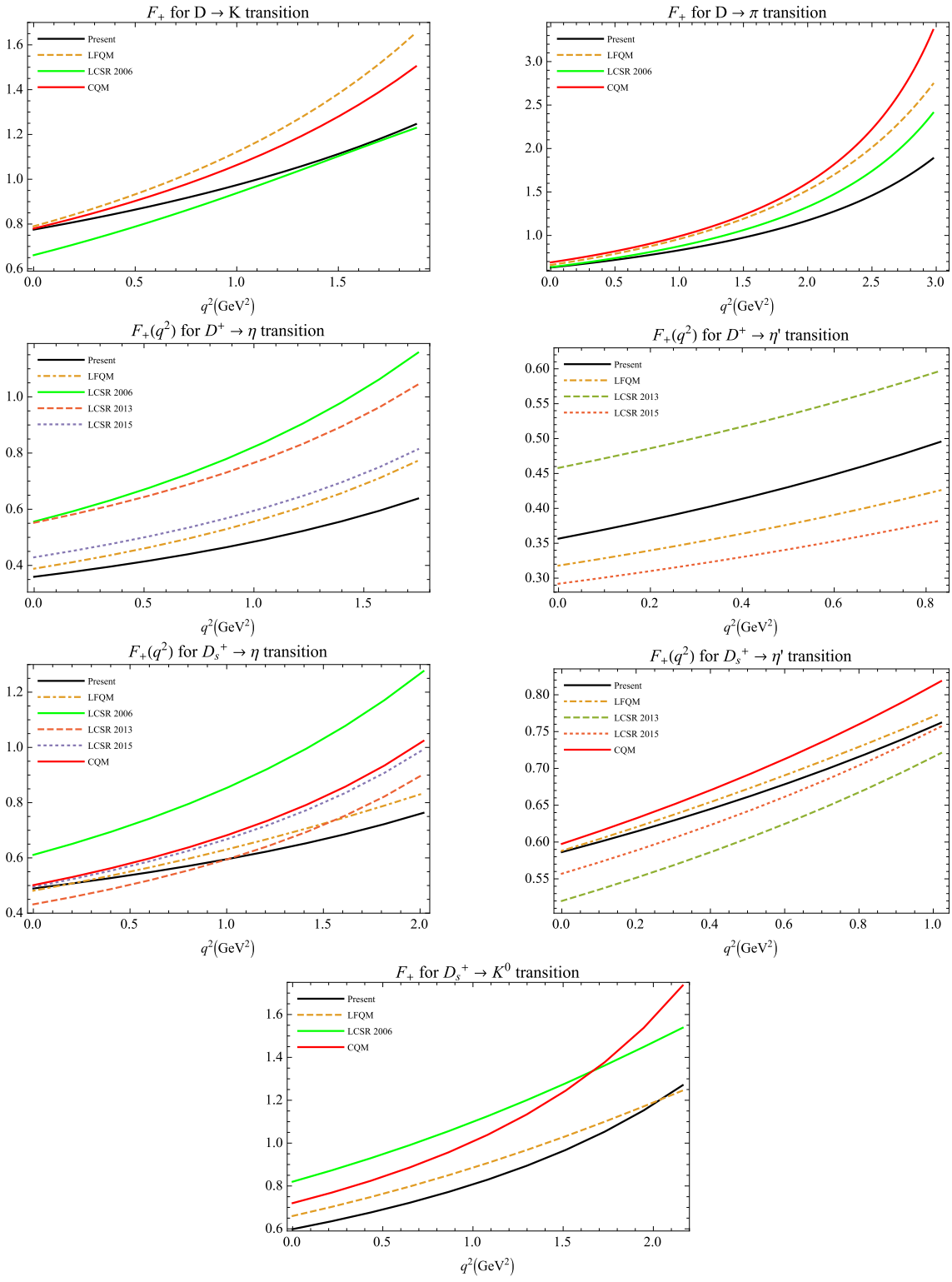

Figure 5.4: The form factors for semileptonic $D \to K, \pi$, $D^+_{(s)} \to \eta^{(\prime)}$ and $D^+_s \to K^0$ transitions with comparison to LCSR, LFQM and CQM.

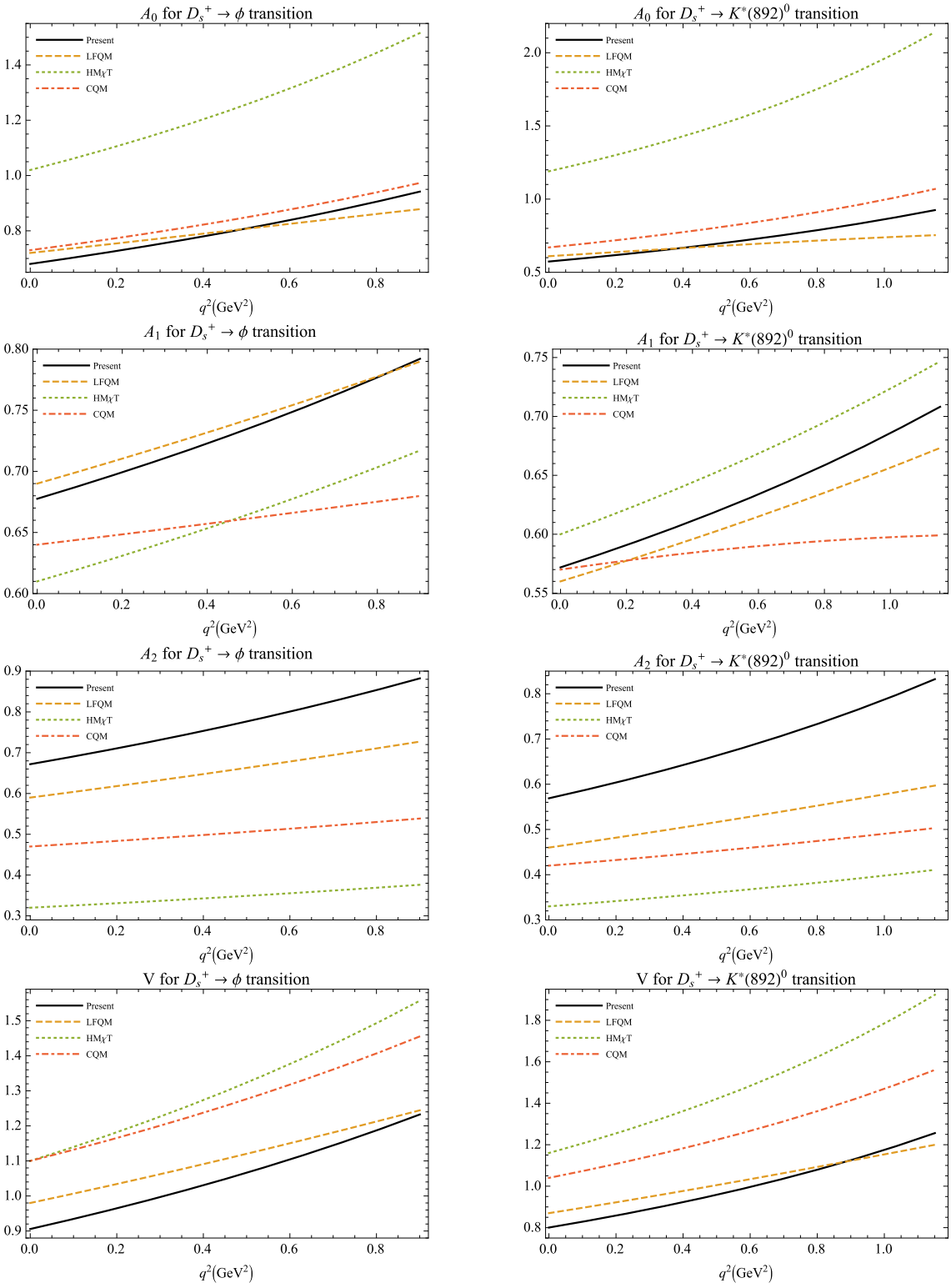

Figure 5.5: The form factors for semileptonic $D_s^+ \to \phi$ (left) and $D_s^+ \to K^*(892)^-$ (right) transitions with comparison to LFQM, HMχT and CQM.

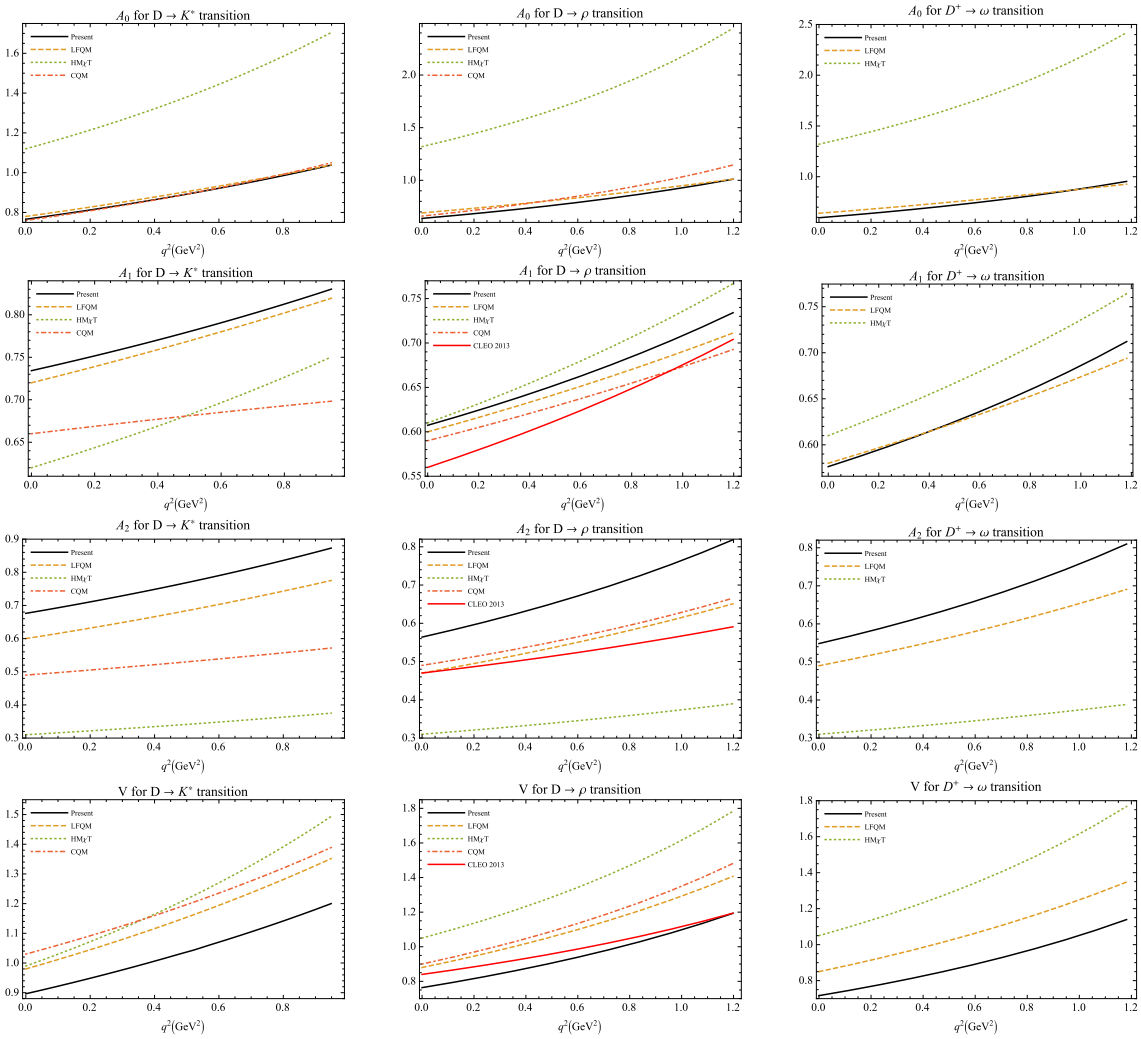

Figure 5.6: The form factors for semileptonic $D^+ \to K^*$ (left), $D \to \rho$ (middle) and $D \to \omega$ (right) transitions with comparison to LFQM, HMχT, CQM and CLEO data.

In Figs. 5.4 – 5.6 we plot the form factors in the entire q^2 range of momentum transfer i.e. $0 \leq q^2 \leq q^2_{max} = (m_{D_{(s)}} - m_{P/V})^2$. It is interesting to note that our results are in excellent agreement with the LFQM [286] for all the channels. It is also observed that the HMχT [284] predictions for the $A_0(q^2)$ is much higher than the other theoretical calculations.

It is important to note that the form factor computation to the η and η' channel is different since they are the mixture of s-quark and light quarks component. The quark content in the approximation of $m_u = m_d \equiv m_q$ can be written as [315]

$$\begin{pmatrix} \eta \\ \eta' \end{pmatrix} = - \begin{pmatrix} \sin\delta & \cos\delta \\ -\cos\delta & \sin\delta \end{pmatrix} \begin{pmatrix} q\bar{q} \\ s\bar{s} \end{pmatrix}, \qquad q\bar{q} \equiv \frac{u\bar{u} + d\bar{d}}{\sqrt{2}}. \tag{5.32}$$

The angle δ is defined by $\delta = \theta_P - \theta_I$, where $\theta_I = \arctan(1/\sqrt{2})$ is the ideal mixing

angle. We adopt the value $\theta_P = -15.4^\circ$ from Ref. [315]. Also, in computing the form factors for the channel $D \to \eta^{(\prime)}$, we take the contribution from the $q\bar{q}$ component while for the $D_s \to \eta^{(\prime)}$ channel, we take the contribution from the $s\bar{s}$ component only [285].

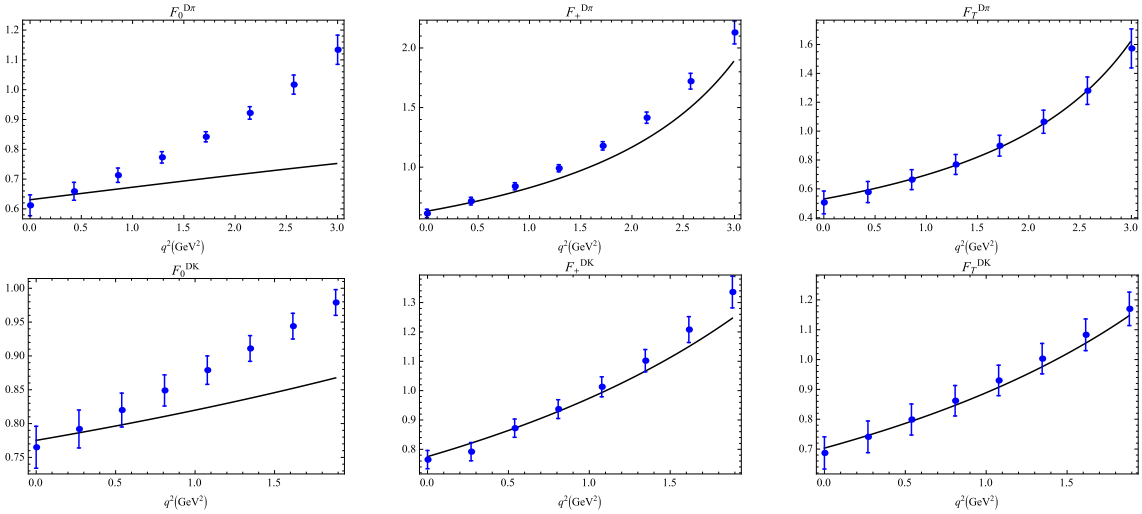

Figure 5.7: $D \to \pi(K)$ form factors obtained in our model (solid lines) and in LQCD calculations (dots with error bar) by ETM collaboration.

Table 5.9: $D \to \pi(K)\ell\nu$ form factors and their ratios at $q^2 = 0$.

	$f_+^{D\pi}$	f_+^{DK}	$f_T^{D\pi}$	f_T^{DK}	$f_T^{D\pi}/f_+^{D\pi}$	f_T^{DK}/f_+^{DK}
Present	0.63	0.78	0.53	0.70	0.84	0.90
ETM [17, 18]	0.612(35)	0.765(31)	0.506(79)	0.687(54)	0.827(114)	0.898(50)

Recently, ETM collaboration has provided the LQCD calculations [17, 18] for the full set of form factors for the channel $D \to \pi(K)\ell\nu_\ell$ and $D \to \pi(K)\ell\ell$ including tensor and scalar form factors. The tensor form factor is defined as

$$\langle P(p_2)|\bar{q}\sigma^{\mu\nu}(1-\gamma^5)c|D(p_1)\rangle = \frac{iF^T(q^2)}{M_1+M_2}\left(P^\mu q^\nu - P^\nu q^\mu + i\varepsilon^{\mu\nu Pq}\right). \tag{5.33}$$

and the scalar form factor $F_0(q^2)$ can be computed using $F_+(q^2)$ and $F_-(q^2)$ defined in Eq. (5.20)

$$F_0(q^2) = F_+(q^2) + \frac{q^2}{M_1^2 - M_2^2}F_-(q^2). \tag{5.34}$$

In Fig. 5.7, we compare our form factors for the channel $D \to \pi(K)$ with the LQCD data by ETM Collaboration. It is observed that our plot for $F_0(q^2)$ agrees well with ETM in low q^2 region. However, our plot for $F_+(q^2)$ is very close to ETM and the tensor form factors are in excellent agreement with ETM. In Tab. 5.9, we

also present our results of the form factors at the maximum recoil along with the comparison with ETM. It is worth noting that our results agree well with ETM calculations within the uncertainties.

Next we compute the semileptonic branching fractions. In Tab. 5.10 – 5.12, we summarize our outcomes with the other theoretical approaches and the recent data given by CLEO and BESIII collaborations.

Table 5.10: Semileptonic decays of D^0 mesons (in %)

Channel	Present	Other	Reference	Data	Reference
$D^0 \to K^- e^+ \nu_e$	3.63	3.4	HMχT [283]	$3.505 \pm 0.014 \pm 0.033$	BESIII [316]
				$3.50 \pm 0.03 \pm 0.04$	CLEO [270]
				$3.45 \pm 0.07 \pm 0.20$	Belle [268]
$D^0 \to K^- \mu^+ \nu_\mu$	3.53			$3.413 \pm 0.019 \pm 0.035$	BESIII [317]
$D^0 \to \pi^- e^+ \nu_e$	0.22	0.27	HMχT [283]	$0.295 \pm 0.004 \pm 0.003$	BESIII [316]
				$0.2770 \pm 0.0068 \pm 0.0092$	*BABAR* [266]
				$0.288 \pm 0.008 \pm 0.003$	CLEO [270]
				$0.255 \pm 0.019 \pm 0.016$	Belle [268]
$D^0 \to \pi^- \mu^+ \nu_\mu$	0.22			$0.272 \pm 0.008 \pm 0.006$	BESIII [318]
$D^0 \to K^*(892)^- e^+ \nu_e$	2.96	2.15	χUA [288]	$2.033 \pm 0.046 \pm 0.047$	BESIII [319]
		2.2	HMχT [284]	$2.16 \pm 0.15 \pm 0.08$	CLEO [320]
$D^0 \to K^*(892)^- \mu^+ \nu_\mu$	2.80	1.98	χUA [288]		
$D^0 \to \rho^- e^+ \nu_e$	0.16	0.197	χUA [288]	$0.1445 \pm 0.0058 \pm 0.0039$	BESIII [321]
		$0.1749^{+0.0421}_{-0.0297}$	LCSR	$0.177 \pm 0.012 \pm 0.010$	CLEO [322] [278]
		0.20	HMχT [284]		
		0.1	ISGW2 [323]		
$D^0 \to \rho^- \mu^+ \nu_\mu$	0.15	0.184	χUA [288]	–	–

In Tab. 5.10, we summarize our results for $D^0 \to (P, V)\ell^+\nu_\ell$ channel. The following are our comments:

- For $D^0 \to K^-\ell^+\nu_\ell$ channel, our results are in very good agreement with the recent BESIII data also with the CLEO and Belle data.
- For $D^0 \to K^*(892)^-$ channel, our results are higher than the CLEO data for the electrono channel and for still experimental results are still not available.
- For $D^0 \to \pi^-$ channel, our results are higher than the recent BESIII data but it is nearer to the data from Belle results.
- For $D^0 \to \rho^- e^+ \nu_e$ channel, our results are matching very well with the central values of the CLEO data [322].

In Tab. 5.11 we summarize our results on $D^+ \to (P, V)\ell^+\nu_\ell$ channels. Our results are in good agreement with the experimental data. The following are our comments:

- For $D^+ \to \bar{K}^0\ell^+\nu_\ell$ channel, our results are nearly 8 % higher than the BESIII data.

Table 5.11: Semileptonic decays of D^+ mesons

Channel	Unit	Present	Other	Reference	Data	Reference
$D^+ \to \bar{K}^0 e^+ \nu_e$	10^{-2}	9.28	8.4	HMχT [283]	$8.60 \pm 0.06 \pm 0.15$	BESIII [324]
			10.32 ± 0.93	LFQM [287]	$8.83 \pm 0.10 \pm 0.20$	CLEO [270]
$D^+ \to \bar{K}^0 \mu^+ \nu_\mu$	10^{-2}	9.02	10.07 ± 0.91	LFQM [287]	$8.72 \pm 0.07 \pm 0.18$	BESIII [325]
$D^+ \to \pi^0 e^+ \nu_e$	10^{-2}	0.29	0.33	HMχT [283]	$0.350 \pm 0.011 \pm 0.010$	BESIII [318]
			0.41 ± 0.03	LFQM [287]		
$D^+ \to \pi^0 \mu^+ \nu_\mu$	10^{-2}	0.28	0.41 ± 0.03	LFQM [287]		
$D^+ \to \bar{K}^*(892)^0 e^+ \nu_e$	10^{-2}	7.61	5.56	χUA [288]		
			5.6	HMχT [284]		
$D^+ \to \bar{K}^*(892)^0 \mu^+ \nu_\mu$	10^{-2}	7.21	5.12	χUA [288]		
$D^+ \to \rho^0 e^+ \nu_e$	10^{-3}	2.09	2.54	χUA [288]	$1.860 \pm 0.070 \pm 0.061$	BESIII [321]
			$2.217^{+0.534}_{-0.376} \pm 0.015$	LCSR [278]	$2.17 \pm 0.12^{+0.12}_{-0.22}$	CLEO [322]
			2.5	HMχT [284]		
$D^+ \to \rho^0 \mu^+ \nu_\mu$	10^{-3}	2.01	2.37	χUA [288]	2.4 ± 0.4	PDG [1]
$D^+ \to \omega e^+ \nu_e$	10^{-3}	1.85	2.46	χUA [288]	$1.63 \pm 0.11 \pm 0.08$	BESIII [316]
			2.5	HMχT [284]	$1.82 \pm 0.18 \pm 0.07$	CLEO [322]
			2.1 ± 0.2	LFQM [287]		
$D^+ \to \omega \mu^+ \nu_\mu$	10^{-3}	1.78	2.29	χUA [288]	–	–
			2.0 ± 0.2	LFQM [287]		
$D^+ \to \eta e^+ \nu_e$	10^{-4}	9.38	12 ± 1	LFQM [287]	$10.74 \pm 0.81 \pm 0.51$	BESIII [326]
			24.5 ± 5.26	LCSR [274]	$11.4 \pm 0.9 \pm 0.4$	CLEO [327]
			14.24 ± 10.98	LCSR [276]		
$D^+ \to \eta \mu^+ \nu_\mu$	10^{-4}	9.12	12 ± 1	LFQM [287]	–	–
$D^+ \to \eta' e^+ \nu_e$	10^{-4}	2.00	1.8 ± 0.2	LFQM [287]	$1.91 \pm 0.51 \pm 0.13$	BESIII [326]
			3.86 ± 1.77	LCSR [274]	$2.16 \pm 0.53 \pm 0.07$	CLEO [327]
			1.52 ± 1.17	LCSR [276]		
$D^+ \to \eta' \mu^+ \nu_\mu$	10^{-4}	1.90	1.7 ± 0.2	LFQM [287]	–	–

- For $D^+ \to \bar{K}^*(892)^0 \ell^+ \nu_\ell$ channel, still the experimental results are not available. Also our results are nearer to the other theoretical approaches.

- $D^+ \to \pi^0 \ell^+ \nu_\ell$ channel, our results are very well within the range predicted by the BESIII data.

- For $D^+ \to \omega e^+ \nu_e$ channel, our result is a bit higher than the BESIII data [316], but it is well within the range predicted by CLEO data [322].

- For $D^+ \to \eta^{(\prime)}$ channel, the branching fractions are very small and also wide range of uncertainties have been reported in the experiments. Our results remain within the range predicted by recent BESIII data [326] and also with the results on CLEO data [328]. We also compare our results with the results from LCSR data [274] and [276].

- We have compared our results with the other theoretical approaches such as LCSR [274, 276, 278], χUA [288], LFQM [287], HMχT [283] and ISGW2 [323]. Our results for $D \to \rho e^+ \nu_e$ give very good agreement with the LCSR [278] and χUA [288] results. For muon channel also, our results are very nearer to those obtained in χUA [288]. For $D^+ \to \omega \ell^+ \nu_\ell$ channel, our results are matching with the LFQM [287]. For $D^+ \to \eta^{(\prime)} \ell^+ \nu_\ell$ channel, our results are deviating from the results obtained in LCSR [274, 276], but are very close to the LFQM data [287].

In Tab 5.12, we summarize the results on $D_s \to (P, V) \ell \nu_\ell$ channels. The short

Table 5.12: Semileptonic branching fractions of D_s mesons (in %).

Channel	Present	Other	Reference	Experimental Data	Reference
$D_s^+ \to \phi e^+ \nu_e$	3.01	2.12	χUA [288]	$2.26 \pm 0.45 \pm 0.09$	BESIII [329]
		3.1 ± 0.3	LFQM [287]	$2.61 \pm 0.03 \pm 0.08 \pm 0.15$	*BABAR* [267]
		2.4	HMχT [284]	$2.14 \pm 0.17 \pm 0.08$	CLEO [328]
$D_s^+ \to \phi \mu^+ \nu_\mu$	2.85	1.94	χUA [288]	$1.94 \pm 0.53 \pm 0.09$	BESIII [329]
		2.9 ± 0.3	LFQM [287]		
$D_s^+ \to K^0 e^+ \nu_e$	0.20	0.27 ± 0.02	LFQM [287]	$0.39 \pm 0.08 \pm 0.03$	CLEO [328]
$D_s^+ \to K^0 \mu^+ \nu_\mu$	0.19	0.26 ± 0.02	LFQM [287]	–	
$D_s^+ \to K^*(892)^0 e^+ \nu_e$	0.18	0.202	χUA [288]	$0.18 \pm 0.04 \pm 0.01$	CLEO [328]
		0.19 ± 0.02	LFQM [287]		
		0.22	HMχT [284]		
$D_s^+ \to K^*(892)^0 \mu^+ \nu_\mu$	0.17	0.189	χUA [288]	–	–
		0.19 ± 0.02	LFQM [287]		
$D_s^+ \to \eta e^+ \nu_e$	2.24	2.26 ± 0.21	LFQM [287]	$2.30 \pm 0.31 \pm 0.08$	BESIII [330]
		2.0 ± 0.32	LCSR [274]	$2.28 \pm 0.14 \pm 0.19$	CLEO [328]
		2.40 ± 0.28	LCSR [276]		
$D_s^+ \to \eta \mu^+ \nu_\mu$	2.18	2.22 ± 0.20	LFQM [287]	$2.42 \pm 0.46 \pm 0.11$	BESIII [329]
$D_s^+ \to \eta' e^+ \nu_e$	0.83	0.89 ± 0.09	LFQM [287]	$0.93 \pm 0.30 \pm 0.05$	BESIII [330]
		0.75 ± 0.23	LCSR [274]	$0.68 \pm 0.15 \pm 0.06$	CLEO [328]
		0.79 ± 0.14	LCSR [276]		
$D_s^+ \to \eta' \mu^+ \nu_\mu$	0.79	0.85 ± 0.08	LFQM [287]	$1.06 \pm 0.54 \pm 0.07$	BESIII [329]

comments are:

- For $D_s^+ \to \phi \ell^+ \nu_\ell$ channel, our result is quite high compared to recent BESIII [329] and the results based on CLEO [328] data but it is observed to be within the range predicted by *BABAR* data [267].

- For $D_s^+ \to K^0 \ell^+ \nu_\ell$ channel, our result for branching fraction is almost double with compared to CLEO data [328]. For electron and muon channels, experimental results are yet to be reported. Our result for the channel $D_s^+ \to K^*(892)^0 e^+ \nu_e$ is matching perfectly with the central value of the CLEO data [328]. The discrepancy of our results with the experimental results seems obvious as there are large deviations of the form factors, particularly A_0 and A_2 in the Figs. 5.5 and f_+ in the last plot in Fig. 5.4.

- For $D_s^+ \to \eta^{(\prime)} \ell^+ \nu_\ell$, there is wide range of uncertainties reported in the experimental data and LCSR results. Our results are in excellent agreement with the BESIII [330] and CLEO [328] results for the electron channel. For muonic channel, our results give excellent agreement with the BESIII data [326] which is a first time ever experimental observation.

- Here also we compare our findings with the theoretical models such as χUA [288], LCSR [274, 276], HMχT [284] and LFQM [287]. For $D_s^+ \to \phi \ell^+ \nu_\ell$ channel, though our result is higher than BESIII and *BABAR* data, it is in good agreement with the LFQM [287] data. But for the $D_s^+ \to K^0 \ell^+ \nu_\ell$ channel, our result is lower than the LFQM predictions. For the rest of the D_s^+ semileptonic decays, our results are in good accordance with the LFQM [287] and LCSR [274, 276] predictions.

Overall, our results are in very good agreement with the experimental results along with theoretical models such as LFQM and LCSR predictions. In Tab. 5.13, we

Table 5.13: Ratios of the semileptonic decays

Ratio	SM	Value	Data	Reference
$\Gamma(D^0 \to K^- e^+ \nu_e)/\Gamma(D^+ \to \bar{K}^0 e^+ \nu_e)$	1.0	0.99	$1.08 \pm 0.22 \pm 0.07$	BESIII [331]
			$1.06 \pm 0.02 \pm 0.03$	CLEO [332]
$\Gamma(D^0 \to K^- \mu^+ \nu_\mu)/\Gamma(D^+ \to \bar{K}^0 \mu^+ \nu_\mu)$	1.0	0.99		
$\Gamma(D^+ \to \bar{K}^0 \mu^+ \nu_\mu)/\Gamma(D^+ \to \bar{K}^0 e^+ \nu_e)$	1.0	0.97		
$\Gamma(D^0 \to K^- \mu^+ \nu_\mu)/\Gamma(D^0 \to K^- e^+ \nu_e)$	1.0	0.97	$0.974 \pm 0.007 \pm 0.012$	BESIII [317]
$\mathcal{B}(D^0 \to \pi^- \mu^+ \nu_\mu)/\mathcal{B}(D^0 \to \pi^- e^+ \nu_e)$	1.0	0.98	$0.922 \pm 0.030 \pm 0.022$	BESIII [318]
$\mathcal{B}(D^+ \to \pi^0 \mu^+ \nu_\mu)/\mathcal{B}(D^+ \to \pi^0 e^+ \nu_e)$	1.0	0.98	$0.964 \pm 0.037 \pm 0.026$	BESIII [318]
$\Gamma(D^0 \to \pi^- e^+ \nu_e)/\Gamma(D^+ \to \pi^0 e^+ \nu_e)$	2.0	1.97	$2.03 \pm 0.14 \pm 0.08$	CLEO [332]
$\Gamma(D^0 \to \rho^- e^+ \nu_e)/2\Gamma(D^+ \to \rho^0 e^+ \nu_e)$	1.0	0.98	$1.03 \pm 0.09^{+0.08}_{-0.02}$	CLEO [322]
$\mathcal{B}(D^+ \to \eta' e^+ \nu_e)/\mathcal{B}(D^+ \to \eta e^+ \nu_e)$	–	0.21	0.19 ± 0.05	CLEO [327]
			0.18 ± 0.05	BESIII [326]
$\mathcal{B}(D_s^+ \to \phi \mu^+ \nu_\mu)/\mathcal{B}(D_s^+ \to \phi e^+ \nu_e)$	1.0	0.95	0.86 ± 0.29	BESIII [329]
$\mathcal{B}(D_s^+ \to \eta' e^+ \nu_e)/\mathcal{B}(D_s^+ \to \eta e^+ \nu_e)$	–	0.37	0.36 ± 0.14	CLEO [333]
			0.40 ± 0.14	BESIII [330]
$\mathcal{B}(D_s^+ \to \eta' \mu^+ \nu_\mu)/\mathcal{B}(D_s^+ \to \eta \mu^+ \nu_\mu)$	–	0.36	0.44 ± 0.23	BESIII [329]

present the ratios of different semileptonic decay widths. It is observed that our results are very well within the isospin conservation rules [334]. It is worth mentioning here that very recently, the BESIII collaboration has reported their measurement of $\mathcal{B}(D^0 \to K^- \mu^+ \nu_\mu)$ [317] with significantly improved presicion and they also approved our prediction of the model for the channel $\mathcal{B}(D^0 \to K^- \mu^+ \nu_\mu)/\mathcal{B}(D^0 \to K^- e^+ \nu_e)$ provided in our paper Ref. [293].

Table 5.14: Semileptonic branching fractions for $D^+_{(s)} \to D^0 \ell^+ \nu_\ell$

Channel	Present	Theory Data	Reference	Experimental Data	Reference
$D^+ \to D^0 e^+ \nu_e$	2.23×10^{-13}	2.78×10^{-13}	[291]	$< 1.0 \times 10^{-4}$	BESIII [290]
		2.71×10^{-13}	[292]		
$D_s^+ \to D^0 e^+ \nu_e$	2.52×10^{-8}	$(2.97 \pm 0.03) \times 10^{-8}$	[291]	–	–
		3.34×10^{-8}	[292]		

In Tab. 5.14, we present our results on the rare semileptonic branching fractions of $D^+_{(s)} \to D^0 e^+ \nu_e$. Our results for branching fraction for the channel $D^+ \to D^0 e^+ \nu_e$ satisfies the experimental constraints predicted by the recent BESIII [290] collaboration. Our results also satisfies the theoretical predictions using SU(3) symmetry [291] and also heavy flavour conserving decays [292].

Finally, in Table 5.15 we list our predictions for the forward-backward asymmetry $\langle \mathcal{A}^\ell_{FB} \rangle$, the longitudinal polarization $\langle P^\ell_L \rangle$, and the transverse polarization $\langle P^\ell_T \rangle$ of the charged lepton in the final state. It is seen that for the $P \to V$ transitions, the

Table 5.15: Forward-backward asymmetry and longitudinal polarization.

Channel	$\langle \mathcal{A}_{FB}^{e} \rangle$	$\langle \mathcal{A}_{FB}^{\mu} \rangle$	$\langle P_L^e \rangle$	$\langle P_L^\mu \rangle$
$D^0 \to K^- \ell^+ \nu_\ell$	-6.14×10^{-6}	-0.06	-1.00	-0.87
$D^0 \to K^*(892)^- \ell^+ \nu_\ell$	0.18	0.14	-1.00	-0.92
$D^0 \to \pi^- \ell^+ \nu_\ell$	-3.84×10^{-6}	-0.04	-1.00	-0.90
$D^0 \to \rho^- \ell^+ \nu_\ell$	0.21	0.18	-1.00	-0.92
$D^+ \to K^0 \ell^+ \nu_\ell$	-6.11×10^{-6}	-0.06	-1.00	-0.87
$D^+ \to \bar{K}^*(892)^- \ell^+ \nu_\ell$	0.18	0.14	-1.00	-0.92
$D^+ \to \pi^0 \ell^+ \nu_\ell$	-3.80×10^{-6}	-0.04	-1.00	-0.91
$D^+ \to \rho^0 \ell^+ \nu_\ell$	0.22	0.19	-1.00	-0.93
$D^+ \to \omega \ell^+ \nu_\ell$	0.21	0.18	-1.00	-0.93
$D^+ \to \eta \ell^+ \nu_\ell$	-6.18×10^{-6}	-0.06	-1.00	-0.87
$D^+ \to \eta' \ell^+ \nu_\ell$	-13.23×10^{-6}	-0.10	-1.00	-0.82
$D^+ \to D^0 \ell^+ \nu_\ell$	-0.094	–	-0.73	–
$D_s^+ \to \phi \ell^+ \nu_\ell$	0.18	0.14	-1.00	-0.92
$D_s^+ \to K^{*0} \ell^+ \nu_\ell$	0.22	0.19	-1.00	-0.93
$D_s^+ \to K^0 \ell^+ \nu_\ell$	-4.75×10^{-6}	-0.05	-1.00	-0.89
$D_s^+ \to \eta \ell^+ \nu_\ell$	-5.75×10^{-6}	-0.06	-1.00	-0.87
$D_s^+ \to \eta' \ell^+ \nu_\ell$	11.20×10^{-6}	-0.09	-1.00	-0.83
$D_s^+ \to D^0 \ell^+ \nu_\ell$	-5.33×10^{-4}	–	-1.00	–

lepton-mass effect in $\langle \mathcal{A}_{FB}^{\ell} \rangle$ is small, resulting in a difference of only $10\% - 15\%$ between the corresponding electron and muon modes. For the $P \to P'$ transitions, $\langle \mathcal{A}_{FB}^{\mu} \rangle$ are about 10^4 times larger than $\langle \mathcal{A}_{FB}^{e} \rangle$. This is readily seen from Eq. (5.28): for $P \to P'$ transitions the two helicity amplitudes $H_\pm$ vanish and the forward-backward asymmetry is proportional to the lepton mass squared. Regarding the longitudinal polarization, the difference between $\langle P_L^\mu \rangle$ and $\langle P_L^e \rangle$ is $10\% - 30\%$. One sees that the lepton-mass effect in the transverse polarization is much more significant than that in the longitudinal one. This is true for both $P \to P'$ and $P \to V$ transitions. Note that the values of $\langle \mathcal{A}_{FB}^{e} \rangle$ and $\langle P_{L(T)}^{e} \rangle$ for the rare decays $D_{(s)}^+ \to D^0 e^+ \nu_e$ are quite different in comparison with other $P \to P'$ transitions due to their extremely small kinematical regions.

We expect BESIII and other experiments such as LHC-b, Belle, CLEO and PANDA collaborations to throw more light in search of these transitions.

Chapter 6

Conclusion and Future Scopes

6.1 Conclusion

In this thesis, we have studied the mass spectra and decay properties of hadrons in the light, heavy and mixed (open) flavor sectors. In chapter 1, we have provided brief review of the recent development reported by experiments as well as the theoretical groups. We have also listed various issues, challenges and attempts made in the understanding the dynamics of heavy as well as open flavor sectors.

Chapter 2 corresponds to the spectroscopy of heavy quarkonia that includes charmonia ($c\bar{c}$), bottomonia ($b\bar{b}$) and B_c ($c\bar{b}$) mesons. We have reported a comprehensive study of heavy quarkonia in the framework of nonrelativistic potential model considering the Cornell potential with least possible number of free model parameters such as confinement strength and quark masses. These parameters are fine tuned to obtain the corresponding spin averaged ground state masses of quarkonia determined from experimental data. Further, we predict the masses of excited states including spin dependent part of confined one gluon exchange potential perturbatively. We have also computed the pseudoscalar and vector decay constants, different annihilation widths such as $\gamma\gamma$, gg, $\ell^+\ell^-$, $\gamma\gamma\gamma$, ggg and γgg of heavy quarkonia using nonrelativistic Van-Royen Weiskopf formulae. The first order radiative corrections in computation of these decays provide satisfactory results for the charmonia while no such correction is needed in case of bottomonia for being purely nonrelativistic system. We compute B_c mass spectra employing the quark masses and mean value of confinement strength of charmonia and bottomonia. We have also computed the weak decays of B_c mesons and the computed life time is also consistent with the

PDG data and other theoretical approaches. It is interesting to note here that despite having a c quark, the nonrelativistic calculation of B_c spectroscopy is in very good agreement with experimental data and other theoretical approaches.

In chapter 3, we have computed the masses and decay properties of doubly heavy baryons. We have reported the masses, magnetic moments and radiative decays of doubly heavy baryons in the extended relativistic harmonic confinement model (ERHM). ERHM uses the nonrelativistic reduction of the Dirac equation to study the masses of doubly heavy baryons. This model treats quark and antiquarks on equal basis. The spin averaged masses of the doubly heavy baryons are computed by solving the Dirac equation for harmonic confinement part of the potential. The expectation value of the Coulomb repulsion term is computed perturbatively using the Harmonic oscillator wave function. The spin dependent part of confined one gluon exchange interaction is computed perturbatively for determining the masses of spin $1/2^+$ and $3/2^+$ baryons. The masses are compared with different theoretical approaches and our results are in good accordance with the relativistic quark model and LQCD results. Our prediction on the mass of Ξ_{cc}^{++} match precisely with the LHCb data. We have also computed the magnetic moments using the spin flavor wave function of the respective baryons and compare with other theoretical approaches. Next, we have computed the radiative decay widths ($3/2^+ \to 1/2^+$) in terms of transition magnetic moments. While the radiative decays are yet to be identified experimentally and also there are wide range of results available in the literature, our results are consistently found to be within the range predicted by different theoretical approaches. We expect the experimental facilities to provide more results not only for the masses of the doubly heavy baryons but also for their decay properties.

In chapter 4, we have presented the mass and decay properties of exotic four quark states. In the literature, there are different models available that consider these states to be independent tetra quark states, dimeson molecules, hadro-charmonium etc. We have considered the Z_c, Z_b and Z_b' to be the dimeson molecules of $D^+\bar{D}^*$, $B\bar{B}^*$ and $B^*\bar{B}^*$ respectively. We consider the modified Woods-Saxon potential to compute the interaction between these mesons. The bound state masses are obtained by solving the Schrödinger equation numerically. It is observed that the computed masses are found to be sensitive to the variation in radius/size of the molecule for generalized Woods-Saxon potential unlike the standard Woods-Saxon potential. We

also compute the strong two body decay widths in the phenomenological Lagrangian mechanism. Our results of masses and decay widths are found to be consistent with the experimental data and other theoretical approaches.

While we have employed the nonrelativistic approach for studying the quarkonium, doubly heavy baryons and exotic states in chapters 2, 3 and 4 respectively, we have studied the weak decays of open flavor mesons in chapter 5. We have investigated the leptonic and semileptonic decays of D and D_s mesons within the framework of covariant confined quark model (CCQM) with in-built infrared confinement. The transition form factors have been calculated in the entire physical range of momentum transfer. We have also provided a brief comparison of the form factors with the other theoretical predictions. The parametrization of the form factors is done using the double pole approximation. These form factors are then used in computations of semileptonic branching fractions. We compared our results of the leptonic and semileptonic branching fractions with the recent BESIII, CLEO, *BABAR* data along with the light cone sum rules results and other theoretical predictions. Our results are in good agreement with the experimental data within 10% except for the channel $D_s \to K^0 \ell^+ \nu_\ell$. Our predictions for ratios of the branching fractions are also in excellent agreement with the experimental data. The ratios of the branching fractions for muon channel to electron channel $\mathcal{R}_{\mu/e} \sim 1$ which is consistent with the standard model prediction suggests no violation of lepton flavor universality. For the rare semileptonic decays $D^+_{(s)} \to D^0 \ell^+ \nu_\ell$, our results match with the theoretical predictions and also satisfies the experimental constraint. Low phase space gives a very small branching fraction that makes it difficult to probe experimentally. Experimentally, only BESIII have reported the upper bound on the branching fractions at 90% confidence level. We expect BESIII and other experiments such as LHCb, Belle, CLEO and PANDA collaborations to throw more light in search of these transitions.

6.2 Future Scope

In chapter 2, we have computed the spectroscopy of heavy quarkonia using Cornell potential. This work can be further extended incorporating the velocity dependent potentials together with the spin dependent ones at order $1/m^2$. Also the spectra can be computed using the pNRQCD potentials. The relativistic approach can give

better estimation for mass spectra and decay properties. Further, the same can also be applied for computing the mass spectra for the heavy baryons as well as for exotic states too.

In chapter 5, we have computed the decay properties of $D_{(s)}$ mesons in covariant confined quark model formalism. This study can further be utilised for the comprehensive review for the semileptonic D and D_s meson decays to probe for the probable search for lepton flavor universality. This method is also applicable to the computation of the semileptonic decays of B and B_s meson decays. The decays involving flavor changing neutral currents (FCNC) are the best tool to probe for the new physics beyond standard model because these decays are highly suppressed according to the Standard Model. The FCNCs are yet to be fully explored in the charm decays and CCQM is a promising tool for these decays. This includes the study of rare $D^+ \to \pi^+ \ \ell^+\ell^-$ decay and at quark level this can be induced by $c \to u\ell^+\ell^-$ for $\ell = e$ and μ transition. The new physics in decays involving FCNC can be introduced by the phenomenology of leptoquark, minimal supersymmetric standard models and other approaches. CCQM is the general formalism which can be applied to multiquark states also. Therefore CCQM can be employed for the studying decay properties of baryons as well as exotic states viz. tetraquark, pentaquark hadrons.

Bibliography

[1] M. Tanabashi *et al.* (Particle Data Group), Phys. Rev. D **98**, 030001 (2018).

[2] J. J. Dudek, R. G. Edwards, N. Mathur and D. G. Richards, "Charmonium excited state spectrum in lattice QCD", Phys. Rev. D **77**, 034501 (2008).

[3] S. Meinel, "The Bottomonium spectrum from lattice QCD with 2+1 flavors of domain wall fermions", Phys. Rev. D **79**, 094501 (2009).

[4] T. Burch, C. DeTar, M. Di Pierro, A. X. El-Khadra, E. D. Freeland, S. Gottlieb, A. S. Kronfeld, L. Levkova, P. B. Mackenzie and J. N. Simone, "Quarkonium mass splittings in three-flavor lattice QCD", Phys. Rev. D **81**, 034508 (2010).

[5] L. Liu, G. Moir, M. Peardon, S. M. Ryan, C. E. Thomas, P. Vilaseca, J. J. Dudek, R. G. Edwards, B. Joo and D. G. Richards (Hadron Spectrum Collaboration), "Excited and exotic charmonium spectroscopy from lattice QCD", JHEP **07**, 126 (2012).

[6] C. McNeile, C. T. H. Davies, E. Follana, K. Hornbostel and G. P. Lepage, "Heavy meson masses and decay constants from relativistic heavy quarks in full lattice QCD", Phys. Rev. D **86**, 074503 (2012).

[7] J. O. Daldrop, C. T. H. Davies and R. J. Dowdall (HPQCD Collaboration), "Prediction of the bottomonium D-wave spectrum from full lattice QCD", Phys. Rev. Lett. **108**, 102003 (2012).

[8] T. Kawanai and S. Sasaki, "Heavy quarkonium potential from Bethe-Salpeter wave function on the lattice", Phys. Rev. D **89**, 054507 (2014).

[9] T. Kawanai and S. Sasaki, "Interquark potential with finite quark mass from lattice QCD", Phys. Rev. Lett. **107**, 091601 (2011).

[10] Y. Burnier, O. Kaczmarek and A. Rothkopf, "Quarkonium at finite temperature: Towards realistic phenomenology from first principles", JHEP **12**, 101 (2015).

[11] M. Kalinowski and M. Wagner, "Masses of D mesons, D_s mesons and charmonium states from twisted mass lattice QCD", Phys. Rev. D **92**, 094508 (2015).

[12] Y. Burnier, O. Kaczmarek and A. Rothkopf, "In-medium P-wave quarkonium from the complex lattice QCD potential", JHEP **10**, 032 (2016).

[13] D. Bečirević, G. Duplančić, B. Klajn, B. Melić and F. Sanfilippo, "Lattice QCD and QCD sum rule determination of the decay constants of η_c, J/ψ and h_c states", Nucl. Phys. B **883**, 306 (2014).

[14] B. Colquhoun, R. J. Dowdall, C. T. H. Davies, K. Hornbostel and G. P. Lepage, "Υ and Υ' Leptonic Widths, a_μ^b and m_b from full lattice QCD", Phys. Rev. D **91**, 074514 (2015).

[15] N. Brambilla *et al.*, "QCD and Strongly Coupled Gauge Theories: Challenges and Perspectives", Eur. Phys. J. C **74**, 2981 (2014).

[16] N. Brambilla *et al.*, "Heavy quarkonium: progress, puzzles, and opportunities", Eur. Phys. J. C **71**, 1534 (2011).

[17] V. Lubicz, L. Riggio, G. Salerno, S. Simula and C. Tarantino (ETM Collaboration), "Scalar and vector form factors of $D \to \pi(K)\ell\nu$ decays with $N_f = 2 + 1 + 1$ twisted fermions", Phys. Rev. D **96**, 054514 (2017).

[18] V. Lubicz, L. Riggio, G. Salerno, S. Simula and C. Tarantino (ETM Collaboration), "Tensor form factor of $D \to \pi(K)\ell\nu$ and $D \to \pi(K)\ell\ell$ decays with $N_f = 2 + 1 + 1$ twisted-mass fermions", Phys. Rev. D **98**, 014516 (2018).

[19] L. Riggio, G. Salerno and S. Simula, "Extraction of $|V_{cd}|$ and $|V_{cs}|$ from experimental decay rates using lattice QCD $D \to \pi(K)\ell\nu$ form factors", Eur. Phys. J. C **78**, 501 (2018).

[20] S. Aoki *et al.*, "Review of lattice results concerning low-energy particle physics", Eur. Phys. J. C **77**, 112 (2017).

[21] G. C. Donald, C. T. H. Davies, J. Koponen and G. P. Lepage (HPQCD Collaboration), "V_{cs} from $D_s \to \phi\ell\nu$ semileptonic decay and full lattice QCD", Phys. Rev. D **90**, 074506 (2014).

[22] G. S. Bali, S. Collins, S. Dürr and I. Kanamori, "$D_s \to \eta, \eta'$ semileptonic decay form factors with disconnected quark loop contributions", Phys. Rev. D **91**, 014503 (2015).

[23] H. Garcilazo, A. Valcarce and J. Vijande, "Doubly heavy baryon spectra guided by lattice QCD", Phys. Rev. D **94**, 074003 (2016).

[24] Z. S. Brown, W. Detmold, S. Meinel and K. Orginos, "Charmed bottom baryon spectroscopy from lattice QCD", Phys. Rev. D **90**, 094507 (2014).

[25] M. Padmanath, R. G. Edwards, N. Mathur and M. Peardon, "Spectroscopy of doubly-charmed baryons from lattice QCD", Phys. Rev. D **91**, 094502 (2015).

[26] C. Alexandrou, V. Drach, K. Jansen, C. Kallidonis and G. Koutsou, "Baryon spectrum with $N_f = 2+1+1$ twisted mass fermions", Phys. Rev. D **90**, 074501 (2014).

[27] P. Pérez-Rubio, S. Collins and G. S. Bali, "Charmed baryon spectroscopy and light flavor symmetry from lattice QCD", Phys. Rev. D **92**, 034504 (2015).

[28] K. U. Can, G. Erkol, M. Oka and T. T. Takahashi, "Look inside charmed-strange baryons from lattice QCD", Phys. Rev. D **92**, 114515 (2015).

[29] M. A. Shifman, A. I. Vainshtein and V. I. Zakharov, "QCD and Resonance Physics. Theoretical Foundations", Nucl. Phys. B **147**, 385 (1979).

[30] W. E. Caswell and G. P. Lepage, "Effective Lagrangians for Bound State Problems in QED, QCD, and Other Field Theories", Phys. Lett. **B167**, 437 (1986).

[31] G. T. Bodwin, E. Braaten and G. P. Lepage, "Rigorous QCD analysis of inclusive annihilation and production of heavy quarkonium", Phys. Rev. D **51**, 1125 (1995), [Erratum: Phys. Rev.D55,5853(1997)].

[32] A. Pineda and J. Soto, "Effective field theory for ultrasoft momenta in NRQCD and NRQED", Nucl. Phys. Proc. Suppl. **64**, 428 (1998), [,428(1997)].

[33] N. Brambilla, A. Pineda, J. Soto and A. Vairo, "Potential NRQCD: An Effective theory for heavy quarkonium", Nucl. Phys. B **566**, 275 (2000).

[34] A. Chodos, R. L. Jaffe, K. Johnson, C. B. Thorn and V. F. Weisskopf, "A New Extended Model of Hadrons", Phys. Rev. D **9**, 3471 (1974).

[35] E. Eichten, K. Gottfried, T. Kinoshita, K. D. Lane and T.-M. Yan, "Charmonium: The Model", Phys. Rev. D **17**, 3090 (1978), [Erratum: Phys. Rev.D21,313(1980)].

[36] A. Martin, "A FIT of Upsilon and Charmonium Spectra", Phys. Lett. **B93**, 338 (1980).

[37] C. Quigg and J. L. Rosner, "Quantum Mechanics with Applications to Quarkonium", Phys. Rept. **56**, 167 (1979).

[38] P. C. Vinodkumar, J. N. Pandya, V. M. Bannur and S. B. Khadkikar, "A unified scheme for flavoured mesons and baryons", Eur. Phys. J. A **4**, 83 (1999).

[39] J. N. Pandya and P. C. Vinodkumar, "Masses of S and P wave mesons and pseudoscalar decay constants using a confinement scheme", Pramana **57**, 821 (2001).

[40] S. B. Khadkikar and P. C. Vinodkumar, "Confinement Models For Gluons", Pramana **29**, 39 (1987).

[41] P. C. Vinodkumar, K. B. Vijayakumar and S. B. Khadkikar, "Effect of the confined gluons in quark quark interaction", Pramana **39**, 47 (1992).

[42] P. C. Vinodkumar and S. B. Khadkikar, "Gauge constraints: A Probable basis for phenomenological confinement models", Phys. Lett. **B329**, 81 (1994), [Erratum: Phys. Lett.B340,264(1994)].

[43] W. Buchmuller and S. H. H. Tye, "Quarkonia and Quantum Chromodynamics", Phys. Rev. D **24**, 132 (1981).

[44] C. Quigg and J. L. Rosner, "Quarkonium Level Spacings", Phys. Lett. **B71**, 153 (1977).

[45] S. S. Gershtein, V. V. Kiselev, A. K. Likhoded and A. V. Tkabladze, "B_c spectroscopy", Phys. Rev. D **51**, 3613 (1995).

[46] A. K. Rai, R. H. Parmar and P. C. Vinodkumar, "Masses and decay constants of heavy-light flavor mesons in a variational scheme", J. Phys. G **28**, 2275 (2002).

[47] A. Kumar Rai, P. C. Vinodkumar and J. N. Pandya, "Decay rates of quarkonia and potential models", J. Phys. G **31**, 1453 (2005).

[48] A. K. Rai and P. C. Vinodkumar, "Properties of B_c meson", Pramana **66**, 953 (2006).

[49] A. K. Rai, B. Patel and P. C. Vinodkumar, "Properties of $Q\bar{Q}$ mesons in non-relativistic QCD formalism", Phys. Rev. C **78**, 055202 (2008).

[50] A. Parmar, B. Patel and P. C. Vinodkumar, "Two-Photon, Two-gluon and Radiative Decays of Heavy Flavoured Mesons", Nucl. Phys. A **848**, 299 (2010).

[51] S. K. Choi *et al.* (Belle Collaboration), "Observation of a narrow charmonium - like state in exclusive $B^{\pm} \to K^{\pm}\pi + \pi - J/\psi$ decays", Phys. Rev. Lett. **91**, 262001 (2003).

[52] B. Aubert *et al.* (BABAR Collaboration), "Study of the $B \to J/\psi K^-\pi^+\pi^-$ decay and measurement of the $B \to X(3872)K^-$ branching fraction", Phys. Rev. D **71**, 071103 (2005).

[53] B. Aubert *et al.* (BABAR Collaboration), "Study of $J/\psi\pi^+\pi^-$ states produced in $B^0 \to J/\psi\pi^+\pi^-K^0$ and $B^- \to J/\psi\pi^+\pi^-K^-$", Phys. Rev. D **73**, 011101 (2006).

[54] D. Acosta *et al.* (CDF Collaboration), "Observation of the narrow state $X(3872) \to J/\psi\pi^+\pi^-$ in $\bar{p}p$ collisions at $\sqrt{s} = 1.96$ TeV", Phys. Rev. Lett. **93**, 072001 (2004).

[55] R. Aaij *et al.* (LHCb Collaboration), "Observation of $X(3872)$ production in pp collisions at $\sqrt{s} = 7$ TeV", Eur. Phys. J. C **72**, 1972 (2012).

[56] R. Aaij *et al.* (LHCb Collaboration), "Determination of the X(3872) meson quantum numbers", Phys. Rev. Lett. **110**, 222001 (2013).

[57] G. V. Efimov and M. A. Ivanov, "Confinement and Quark Structure of Light Hadrons", Int. J. Mod. Phys. A **4**, 2031 (1989).

[58] G. V. Efimov and M. A. Ivanov, *The Quark confinement model of hadrons*, (IOP, Bristol1993).

[59] S. Weinberg, "Elementary particle theory of composite particles", Phys. Rev. **130**, 776 (1963).

[60] A. Salam, "Lagrangian theory of composite particles", Nuovo Cim. **25**, 224 (1962).

[61] J. J. Aubert *et al.* (E598 Collaboration), "Experimental Observation of a Heavy Particle J", Phys. Rev. Lett. **33**, 1404 (1974).

[62] T. A. Armstrong *et al.* (E760 Collaboration), "Study of the χ_1 and χ_2 charmonium states formed in $\bar{p}p$ annihilations", Nucl. Phys. B **373**, 35 (1992).

[63] M. Ablikim *et al.* (BESIII Collaboration), "Observation of the $\psi(1^3D_2)$ state in $e^+e^- \to \pi^+\pi^-\gamma\chi_{c1}$ at BESIII", Phys. Rev. Lett. **115**, 011803 (2015).

[64] S. W. Herb *et al.*, "Observation of a Dimuon Resonance at 9.5-GeV in 400-GeV Proton-Nucleus Collisions", Phys. Rev. Lett. **39**, 252 (1977).

[65] W. R. Innes *et al.*, "Observation of Structure in the Υ Region", Phys. Rev. Lett. **39**, 1240 (1977), [Erratum: Phys. Rev. Lett.39,1640(1977)].

[66] R. Mizuk *et al.* (Belle Collaboration), "Evidence for the $\eta_b(2S)$ and observation of $h_b(1P) \to \eta_b(1S)\gamma$ and $h_b(2P) \to \eta_b(1S)\gamma$", Phys. Rev. Lett. **109**, 232002 (2012).

[67] J. P. Lees *et al.* (BABAR Collaboration), "Study of radiative bottomonium transitions using converted photons", Phys. Rev. D **84**, 072002 (2011).

[68] S. Dobbs, Z. Metreveli, K. K. Seth, A. Tomaradze and T. Xiao, "Observation of $\eta_b(2S)$ in $\Upsilon(2S) \to \gamma\eta_b(2S)$, $\eta_b(2S) \to$ hadrons, and Confirmation of $\eta_b(1S)$", Phys. Rev. Lett. **109**, 082001 (2012).

[69] S. Sandilya *et al.* (Belle Collaboration), "Search for Bottomonium States in Exclusive Radiative $\Upsilon(2S)$ Decays", Phys. Rev. Lett. **111**, 112001 (2013).

[70] W.-k. Kwong and J. L. Rosner, "Masses of new particles containing b quarks", Phys. Rev. D **44**, 212 (1991).

[71] E. J. Eichten and C. Quigg, "Mesons with beauty and charm: Spectroscopy", Phys. Rev. D **49**, 5845 (1994).

[72] F. Abe *et al.* (CDF Collaboration), "Observation of the B_c meson in $p\bar{p}$ collisions at $\sqrt{s} = 1.8$ TeV", Phys. Rev. Lett. **81**, 2432 (1998).

[73] V. M. Abazov *et al.* (D0 Collaboration), "Observation of the B_c Meson in the Exclusive Decay $B_c \to J/\psi\pi$", Phys. Rev. Lett. **101**, 012001 (2008).

[74] R. Aaij *et al.* (LHCb Collaboration), "Measurements of B_c^+ production and mass with the $B_c^+ \to J/\psi\pi^+$ decay", Phys. Rev. Lett. **109**, 232001 (2012).

[75] R. Aaij *et al.* (LHCb Collaboration), "Measurement of the B_c^+ meson lifetime using $B_c^+ \to J/\psi\mu^+\nu_\mu X$ decays", Eur. Phys. J. C **74**, 2839 (2014).

[76] G. Aad *et al.* (ATLAS Collaboration), "Observation of an Excited $B_c^{\pm}$ Meson State with the ATLAS Detector", Phys. Rev. Lett. **113**, 212004 (2014).

[77] E. Eichten, S. Godfrey, H. Mahlke and J. L. Rosner, "Quarkonia and their transitions", Rev. Mod. Phys. **80**, 1161 (2008).

[78] S. Godfrey and S. L. Olsen, "The Exotic XYZ Charmonium-like Mesons", Ann. Rev. Nucl. Part. Sci. **58**, 51 (2008).

[79] T. Barnes and S. L. Olsen, "Charmonium spectroscopy", Int. J. Mod. Phys. A **24S1**, 305 (2009).

[80] A. Andronic *et al.*, "Heavy-flavour and quarkonium production in the LHC era: from proton–proton to heavy-ion collisions", Eur. Phys. J. C **76**, 107 (2016).

[81] S. Cho, K. Hattori, S. H. Lee, K. Morita and S. Ozaki, "Charmonium Spectroscopy in Strong Magnetic Fields by QCD Sum Rules: S-Wave Ground States", Phys. Rev. D **91**, 045025 (2015).

[82] T. Hilger, C. Popovici, M. Gomez-Rocha and A. Krassnigg, "Spectra of heavy quarkonia in a Bethe-Salpeter-equation approach", Phys. Rev. D **91**, 034013 (2015).

[83] M. B. Voloshin, "Charmonium", Prog. Part. Nucl. Phys. **61**, 455 (2008).

[84] Y. Kiyo and Y. Sumino, "Perturbative heavy quarkonium spectrum at next-to-next-to-next-to-leading order", Phys. Lett. **B730**, 76 (2014).

[85] T. Liu, A. A. Penin and A. Rayyan, "Coulomb Artifacts and Bottomonium Hyperfine Splitting in Lattice NRQCD", JHEP **02**, 084 (2017).

[86] R. J. Dowdall, C. T. H. Davies, T. Hammant and R. R. Horgan (HPQCD Collaboration), "Bottomonium hyperfine splittings from lattice nonrelativistic QCD including radiative and relativistic corrections", Phys. Rev. D **89**, 031502 (2014), [Erratum: Phys. Rev.D92,039904(2015)].

[87] M. Neubert, "Heavy quark symmetry", Phys. Rept. **245**, 259 (1994).

[88] D. Ebert, R. N. Faustov and V. O. Galkin, "Spectroscopy and Regge trajectories of heavy quarkonia and B_c mesons", Eur. Phys. J. C **71**, 1825 (2011).

[89] D. Ebert, R. N. Faustov and V. O. Galkin, "Mass spectra and Regge trajectories of light mesons in the relativistic quark model", Phys. Rev. D **79**, 114029 (2009).

[90] D. Ebert, R. N. Faustov and V. O. Galkin, "Masses and electroweak properties of light mesons in the relativistic quark model", Eur. Phys. J. C **47**, 745 (2006).

[91] D. Ebert, R. N. Faustov and V. O. Galkin, "Properties of heavy quarkonia and B_c mesons in the relativistic quark model", Phys. Rev. D **67**, 014027 (2003).

[92] D. Ebert, R. N. Faustov and V. O. Galkin, "Hyperfine splitting and leptonic decay rates in heavy quarkonia", Mod. Phys. Lett. A **18**, 1597 (2003).

[93] D. Ebert, R. N. Faustov and V. O. Galkin, "Two photon decay rates of heavy quarkonia in the relativistic quark model", Mod. Phys. Lett. A **18**, 601 (2003).

[94] D. Ebert, R. N. Faustov and V. O. Galkin, "Quark - anti-quark potential with retardation and radiative contributions and the heavy quarkonium mass spectra", Phys. Rev. D **62**, 034014 (2000).

[95] S. N. Gupta and S. F. Radford, "Quark – quark and quark – antiquark Potentials", Phys. Rev. D **24**, 2309 (1981).

[96] S. N. Gupta, S. F. Radford and W. W. Repko, "Quarkonium Spectra and Quantum Chromodynamics", Phys. Rev. D **26**, 3305 (1982).

[97] S. N. Gupta and S. F. Radford, "Remarks on quark-quarks and quark-antiquark potentials", Phys. Rev. D **25**, 3430 (1982).

[98] J. T. Pantaleone, S. H. H. Tye and Y. J. Ng, "Spin Splittings in Heavy Quarkonia", Phys. Rev. D **33**, 777 (1986).

[99] K. M. Maung, D. E. Kahana and J. W. Norbury, "Solution of two-body relativistic bound state equations with confining plus Coulomb interactions", Phys. Rev. D **47**, 1182 (1993).

[100] S. F. Radford and W. W. Repko, "Potential model calculations and predictions for heavy quarkonium", Phys. Rev. D **75**, 074031 (2007).

[101] S. F. Radford and W. W. Repko, "Hyperfine splittings in the $b\bar{b}$ system", Nucl. Phys. A **865**, 69 (2011).

[102] S. N. Gupta, S. F. Radford and W. W. Repko, "Semirelativistic Potential Model for Heavy Quarkonia", Phys. Rev. D **34**, 201 (1986).

[103] N. Devlani, V. Kher and A. K. Rai, "Masses and electromagnetic transitions of the B_c mesons", Eur. Phys. J. A **50**, 154 (2014).

[104] B. Patel and P. C. Vinodkumar, "Properties of $Q\bar{Q}$ ($Q \in b, c$) mesons in Coulomb plus Power potential (CPP$_\nu$)", J. Phys. G **36**, 035003 (2009).

[105] M. Fabre De La Ripelle, "A Confining Potential for Quarks", Phys. Lett. **B205**, 97 (1988).

[106] E. Eichten, K. Gottfried, T. Kinoshita, J. B. Kogut, K. D. Lane and T.-M. Yan, "The Spectrum of Charmonium", Phys. Rev. Lett. **34**, 369 (1975), [Erratum: Phys. Rev. Lett.36,1276(1976)].

[107] E. Eichten, K. Gottfried, T. Kinoshita, K. D. Lane and T.-M. Yan, "Charmonium: Comparison with Experiment", Phys. Rev. D **21**, 203 (1980).

[108] E. Eichten and F. Feinberg, "Spin Dependent Forces in QCD", Phys. Rev. D **23**, 2724 (1981).

[109] T. Barnes, S. Godfrey and E. S. Swanson, "Higher charmonia", Phys. Rev. D **72**, 054026 (2005).

[110] V. Sauli, "Bethe-Salpeter Study of Radially Excited Vector Quarkonia", Phys. Rev. D **86**, 096004 (2012).

[111] S. Leitão, A. Stadler, M. T. Peña and E. P. Biernat, "Linear confinement in momentum space: singularity-free bound-state equations", Phys. Rev. D **90**, 096003 (2014).

[112] S. Godfrey and N. Isgur, "Mesons in a Relativized Quark Model with Chromodynamics", Phys. Rev. D **32**, 189 (1985).

[113] S. Godfrey, "Spectroscopy of B_c mesons in the relativized quark model", Phys. Rev. D **70**, 054017 (2004).

[114] S. Godfrey and K. Moats, "Bottomonium Mesons and Strategies for their Observation", Phys. Rev. D **92**, 054034 (2015).

[115] W.-J. Deng, H. Liu, L.-C. Gui and X.-H. Zhong, "Charmonium spectrum and their electromagnetic transitions with higher multipole contributions", Phys. Rev. D **95**, 034026 (2017).

[116] W.-J. Deng, H. Liu, L.-C. Gui and X.-H. Zhong, "Spectrum and electromagnetic transitions of bottomonium", Phys. Rev. D **95**, 074002 (2017).

[117] C. S. Fischer, S. Kubrak and R. Williams, "Spectra of heavy mesons in the Bethe-Salpeter approach", Eur. Phys. J. A **51**, 10 (2015).

[118] O. Lakhina and E. S. Swanson, "Dynamic properties of charmonium", Phys. Rev. D **74**, 014012 (2006).

[119] J. Segovia, P. G. Ortega, D. R. Entem and F. Fernández, "Bottomonium spectrum revisited", Phys. Rev. D **93**, 074027 (2016).

[120] S. Patel, P. C. Vinodkumar and S. Bhatnagar, "Decay rates of charmonia within a quark-antiquark confining potential", Chin. Phys. C **40**, 053102 (2016).

[121] C. Bonati, M. D'Elia and A. Rucci, "Heavy quarkonia in strong magnetic fields", Phys. Rev. D **92**, 054014 (2015).

[122] T. Gutsche, V. E. Lyubovitskij, I. Schmidt and A. Vega, "Light-front potential for heavy quarkonia constrained by the holographic soft-wall model", Phys. Rev. D **90**, 096007 (2014).

[123] M. Shah, A. Parmar and P. C. Vinodkumar, "Leptonic and Digamma decay Properties of S-wave quarkonia states", Phys. Rev. D **86**, 034015 (2012).

[124] H. Negash and S. Bhatnagar, "Spectroscopy of ground and excited states of pseudoscalar and vector charmonium and bottomonium", Int. J. Mod. Phys. E **25**, 1650059 (2016).

[125] Bhaghyesh, K. B. Vijaya Kumar and A. P. Monteiro, "Heavy quarkonium spectra and its decays in a nonrelativistic model with Hulthen potential", J. Phys. G **38**, 085001 (2011).

[126] B.-Q. Li and K.-T. Chao, "Higher Charmonia and X,Y,Z states with Screened Potential", Phys. Rev. D **79**, 094004 (2009).

[127] B.-Q. Li and K.-T. Chao, "Bottomonium Spectrum with Screened Potential", Commun. Theor. Phys. **52**, 653 (2009).

[128] G. S. Bali, B. Bolder, N. Eicker, T. Lippert, B. Orth, P. Ueberholz, K. Schilling and T. Struckmann (TXL, T(X)L Collaboration), "Static potentials and glueball masses from QCD simulations with Wilson sea quarks", Phys. Rev. D **62**, 054503 (2000).

[129] G. S. Bali, "QCD forces and heavy quark bound states", Phys. Rept. **343**, 1 (2001).

[130] C. Alexandrou, P. de Forcrand and O. Jahn, "The Ground state of three quarks", Nucl. Phys. Proc. Suppl. **119**, 667 (2003).

[131] N. R. Soni, B. R. Joshi, R. P. Shah, H. R. Chauhan and J. N. Pandya, "$Q\bar{Q}$ ($Q \in \{b, c\}$) spectroscopy using the Cornell potential", Eur. Phys. J. C **78**, 592 (2018).

[132] A. K. Rai, J. N. Pandya and P. C. Vinodkummar, "Multiquark states as di-hadronic molecules", Nucl. Phys. A **782**, 406 (2007).

[133] A. K. Rai, J. N. Pandya and P. C. Vinodkumar, "Low-lying di-hadronic states in relativistic harmonic model", Indian J. Phys. A **80**, 387 (2006).

[134] J. N. Pandya, N. R. Soni, N. Devlani and A. K. Rai, "Decay rates and electromagnetic transitions of heavy quarkonia", Chin. Phys. C **39**, 123101 (2015).

[135] N. Isgur and G. Karl, "P Wave Baryons in the Quark Model", Phys. Rev. D **18**, 4187 (1978).

[136] K. B. Vijaya Kumar, A. K. Rath and S. B. Khadkikar, "Meson spectroscopy with confined one gluon exchange potential", Pramana **48**, 997 (1997).

[137] W. Lucha and F. F. Schoberl, "Solving the Schrodinger equation for bound states with Mathematica 3.0", Int. J. Mod. Phys. C **10**, 607 (1999).

[138] A. P. Monteiro, M. Bhat and K. B. Vijaya Kumar, "$c\bar{b}$ spectrum and decay properties with coupled channel effects", Phys. Rev. D **95**, 054016 (2017).

[139] S. B. Khadkikar and S. K. Gupta, "Magnetic Moments of Light Baryons in the Harmonic Model", Phys. Lett. **B124**, 523 (1983).

[140] S. K. Gupta and S. B. Khadkikar, "Precision Description of the Octet Baryon Magnetic Moments", Phys. Rev. D **36**, 307 (1987).

[141] R. Van Royen and V. F. Weisskopf, "Hadron Decay Processes and the Quark Model", Nuovo Cim. A **50**, 617 (1967), [Erratum: Nuovo Cim.A51,583(1967)].

[142] E. Braaten and S. Fleming, "QCD radiative corrections to the leptonic decay rate of the B(c) meson", Phys. Rev. D **52**, 181 (1995).

[143] A. V. Berezhnoy, V. V. Kiselev and A. K. Likhoded, "Photonic production of S- and P wave B_c states and doubly heavy baryons", Z. Phys. A **356**, 89 (1996).

[144] A. Krassnigg, M. Gomez-Rocha and T. Hilger, "Leptonic decays of D-wave vector quarkonia", J. Phys. Conf. Ser. **742**, 012032 (2016).

[145] G.-L. Wang, "Decay constants of heavy vector mesons in relativistic Bethe-Salpeter method", Phys. Lett. **B633**, 492 (2006).

[146] K. M. Ecklund *et al.* (CLEO Collaboration), "Two-Photon Widths of the χ_{cJ} States of Charmonium", Phys. Rev. D **78**, 091501 (2008).

[147] J. P. Lees *et al.* (BABAR Collaboration), "Measurement of the $\gamma\gamma^* \to \eta_c$ transition form factor", Phys. Rev. D **81**, 052010 (2010).

[148] M. Ablikim *et al.* (BESIII Collaboration), "Two-photon widths of the χ_{cJ} states of charmonium", Phys. Rev. D **85**, 112008 (2012).

[149] J. J. Dudek and R. G. Edwards, "Two Photon Decays of Charmonia from Lattice QCD", Phys. Rev. Lett. **97**, 172001 (2006).

[150] T. Chen *et al.* (CLQCD Collaboration), "Two-photon decays of η_c from lattice QCD", Eur. Phys. J. C **76**, 358 (2016).

[151] H. Khan and P. Hoodbhoy, "A Systematic gauge invariant approach to heavy quarkonium decays", Phys. Rev. D **53**, 2534 (1996).

[152] G. A. Schuler, F. A. Berends and R. van Gulik, "Meson photon transition form-factors and resonance cross-sections in e^+e^- collisions", Nucl. Phys. B **523**, 423 (1998).

[153] G. T. Bodwin, D. Kang and J. Lee, "Potential-model calculation of an order-v^2 nonrelativistic QCD matrix element", Phys. Rev. D **74**, 014014 (2006).

[154] G. T. Bodwin, H. S. Chung, D. Kang, J. Lee and C. Yu, "Improved determination of color-singlet nonrelativistic QCD matrix elements for S-wave charmonium", Phys. Rev. D **77**, 094017 (2008).

[155] J. P. Lansberg and T. N. Pham, "Effective Lagrangian for Two-photon and Two-gluon Decays of P-wave Heavy Quarkonium $\chi_{c0,2}$ and $\chi_{b0,2}$ states", Phys. Rev. D **79**, 094016 (2009).

[156] J. P. Lansberg and T. N. Pham, "Two-photon width of η_c and η_c' from heavy-quark spin symmetry", Phys. Rev. D **74**, 034001 (2006).

[157] W.-L. Sang, F. Feng, Y. Jia and S.-R. Liang, "Next-to-next-to-leading-order QCD corrections to $\chi_{c0,2} \to \gamma\gamma$", Phys. Rev. D **94**, 111501 (2016).

[158] C. S. Kim, T. Lee and G.-L. Wang, "Annihilation rate of heavy 0^{-+} quarkonium in relativistic Salpeter method", Phys. Lett. **B606**, 323 (2005).

[159] V. Kher and A. K. Rai, "Spectroscopy and decay properties of charmonium", Chin. Phys. C **42**, 083101 (2018).

[160] L. D. Landau, "On the angular momentum of a system of two photons", Dokl. Akad. Nauk Ser. Fiz. **60**, 207 (1948).

[161] C.-N. Yang, "Selection Rules for the Dematerialization of a Particle Into Two Photons", Phys. Rev. **77**, 242 (1950).

[162] W. Kwong, P. B. Mackenzie, R. Rosenfeld and J. L. Rosner, "Quarkonium Annihilation Rates", Phys. Rev. D **37**, 3210 (1988).

[163] E. J. Eichten, K. Lane and C. Quigg, "B Meson Gateways to Missing Charmonium Levels", Phys. Rev. Lett. **89**, 162002 (2002).

[164] R. Barbieri, M. Caffo, R. Gatto and E. Remiddi, "QCD Corrections to P wave quarkonium decays", Nucl. Phys. B **192**, 61 (1981).

[165] M. L. Mangano and A. Petrelli, "An update on χ_c decays: Perturbative QCD versus data", Phys. Lett. **B352**, 445 (1995).

[166] S. N. Gupta, J. M. Johnson and W. W. Repko, "Relativistic two photon and two gluon decay rates of heavy quarkonia", Phys. Rev. D **54**, 2075 (1996).

[167] P. Gonzalez, A. Valcarce, H. Garcilazo and J. Vijande, "Heavy meson description with a screened potential", Phys. Rev. D **68**, 034007 (2003).

[168] N. Brambilla, Y. Jia and A. Vairo, "Model-independent study of magnetic dipole transitions in quarkonium", Phys. Rev. D **73**, 054005 (2006).

[169] D.-M. Li, P.-F. Ji and B. Ma, "The newly observed open-charm states in quark model", Eur. Phys. J. C **71**, 1582 (2011).

[170] A. Abd El-Hady, M. A. K. Lodhi and J. P. Vary, "B_c mesons in a Bethe-Salpeter model", Phys. Rev. D **59**, 094001 (1999).

[171] S. N. Gupta and J. M. Johnson, "B_c spectroscopy in a quantum chromodynamic potential model", Phys. Rev. D **53**, 312 (1996).

[172] H.-X. Chen, W. Chen, X. Liu, Y.-R. Liu and S.-L. Zhu, "A review of the open charm and open bottom systems", Rept. Prog. Phys. **80**, 076201 (2017).

[173] E. Klempt and J.-M. Richard, "Baryon spectroscopy", Rev. Mod. Phys. **82**, 1095 (2010).

[174] M. Gell-Mann, "A Schematic Model of Baryons and Mesons", Phys. Lett. **8**, 214 (1964).

[175] M. Mattson *et al.* (SELEX Collaboration), "First Observation of the Doubly Charmed Baryon Ξ_{cc}^{+}", Phys. Rev. Lett. **89**, 112001 (2002).

[176] A. Ocherashvili *et al.* (SELEX Collaboration), "Confirmation of the double charm baryon $\Xi_{cc}^{+}(3520)$ via its decay to $pD^{+}K^{-}$", Phys. Lett. **B628**, 18 (2005).

[177] R. Aaij *et al.* (LHCb Collaboration), "Observation of the doubly charmed baryon Ξ_{cc}^{++}", Phys. Rev. Lett. **119**, 112001 (2017).

[178] R. Aaij *et al.* (LHCb Collaboration), "Measurement of the Lifetime of the Doubly Charmed Baryon Ξ_{cc}^{++}", Phys. Rev. Lett. **121**, 052002 (2018).

[179] R. Aaij *et al.* (LHCb Collaboration), "Search for the doubly charmed baryon Ξ_{cc}^{+}", JHEP **12**, 090 (2013).

[180] Q.-X. Yu and X.-H. Guo, "Masses of doubly heavy baryons in the Bethe-Salpeter equation approach", `arXiv:1810.00437`.

[181] Q.-F. Lü, K.-L. Wang, L.-Y. Xiao and X.-H. Zhong, "Mass spectra and radiative transitions of doubly heavy baryons in a relativized quark model", Phys. Rev. D **96**, 114006 (2017).

[182] D. Ebert, R. N. Faustov, V. O. Galkin and A. P. Martynenko, "Mass spectra of doubly heavy baryons in the relativistic quark model", Phys. Rev. D **66**, 014008 (2002).

[183] S. S. Gershtein, V. V. Kiselev, A. K. Likhoded and A. I. Onishchenko, "Spectroscopy of doubly heavy baryons", Phys. Rev. D **62**, 054021 (2000).

[184] H.-S. Li, L. Meng, Z.-W. Liu and S.-L. Zhu, "Radiative decays of the doubly charmed baryons in chiral perturbation theory", Phys. Lett. **B777**, 169 (2018).

[185] H.-S. Li, L. Meng, Z.-W. Liu and S.-L. Zhu, "Magnetic moments of the doubly charmed and bottom baryons", Phys. Rev. D **96**, 076011 (2017).

[186] L. Meng, H.-S. Li, Z.-W. Liu and S.-L. Zhu, "Magnetic moments of the spin-$\frac{3}{2}$ doubly heavy baryons", Eur. Phys. J. C **77**, 869 (2017).

[187] D.-L. Yao, "Masses and sigma terms of doubly charmed baryons up to $\mathcal{O}(p^4)$ in manifestly Lorentz-invariant baryon chiral perturbation theory", Phys. Rev. D **97**, 034012 (2018).

[188] M.-Z. Liu, Y. Xiao and L.-S. Geng, "Magnetic moments of the spin-1/2 doubly charmed baryons in covariant baryon chiral perturbation theory", Phys. Rev. D **98**, 014040 (2018).

[189] V. V. Kiselev, A. V. Berezhnoy and A. K. Likhoded, "Quark–Diquark Structure and Masses of Doubly Charmed Baryons", Phys. Atom. Nucl. **81**, 369 (2018), [Yad. Fiz.81,no.3,356(2018)].

[190] A. Bernotas and V. Šimonis, "Radiative M1 transitions of heavy baryons in the bag model", Phys. Rev. D **87**, 074016 (2013).

[191] V. Simonis, "Improved predictions for magnetic moments and M1 decay widths of heavy hadrons", (2018), arXiv:1803.01809.

[192] Yu. A. Simonov, J. A. Tjon and J. Weda, "Baryon magnetic moments in the effective quark Lagrangian approach", Phys. Rev. D **65**, 094013 (2002).

[193] N. Sharma, H. Dahiya, P. K. Chatley and M. Gupta, "Spin $1/2^+$, spin $3/2^+$ and transition magnetic moments of low lying and charmed baryons", Phys. Rev. D **81**, 073001 (2010).

[194] A. Faessler, T. Gutsche, M. A. Ivanov, J. G. Korner, V. E. Lyubovitskij, D. Nicmorus and K. Pumsa-ard, "Magnetic moments of heavy baryons in the relativistic three-quark model", Phys. Rev. D **73**, 094013 (2006).

[195] T. Branz, A. Faessler, T. Gutsche, M. A. Ivanov, J. G. Korner, V. E. Lyubovitskij and B. Oexl, "Radiative decays of double heavy baryons in a relativistic constituent three–quark model including hyperfine mixing", Phys. Rev. D **81**, 114036 (2010).

[196] X.-Z. Weng, X.-L. Chen and W.-Z. Deng, "Masses of doubly heavy-quark baryons in an extended chromomagnetic model", Phys. Rev. D **97**, 054008 (2018).

[197] W. Roberts and M. Pervin, "Heavy baryons in a quark model", Int. J. Mod. Phys. A **23**, 2817 (2008).

[198] C. Albertus, E. Hernandez, J. Nieves and J. M. Verde-Velasco, "Static properties and semileptonic decays of doubly heavy baryons in a nonrelativistic quark model", Eur. Phys. J. A **32**, 183 (2007), [Erratum: Eur. Phys. J.A36,119(2008)].

[199] R. Dhir and R. C. Verma, "Magnetic Moments of ($J^P = 3/2^+$) Heavy Baryons Using Effective Mass Scheme", Eur. Phys. J. A **42**, 243 (2009).

[200] R. Dhir, C. S. Kim and R. C. Verma, "Magnetic Moments of Bottom Baryons: Effective mass and Screened Charge", Phys. Rev. D **88**, 094002 (2013).

[201] B. Patel, A. K. Rai and P. C. Vinodkumar, "Masses and magnetic moments of heavy flavour baryons in hyper central model", J. Phys. G **35**, 065001 (2008), [J. Phys. Conf. Ser.110,122010(2008)].

[202] Z. Shah, K. Thakkar and A. K. Rai, "Excited State Mass spectra of doubly heavy baryons Ω_{cc}, Ω_{bb} and Ω_{bc}", Eur. Phys. J. C **76**, 530 (2016).

[203] Z. Shah and A. K. Rai, "Excited state mass spectra of doubly heavy Ξ baryons", Eur. Phys. J. C **77**, 129 (2017).

[204] Z. Shah and A. K. Rai, "Masses and Regge trajectories of triply heavy Ω_{ccc} and Ω_{bbb} baryons", Eur. Phys. J. A **53**, 195 (2017).

[205] T. M. Aliev, K. Azizi and M. Savci, "The masses and residues of doubly heavy spin-3/2 baryons", J. Phys. G **40**, 065003 (2013).

[206] T. M. Aliev, K. Azizi and M. Savci, "Doubly Heavy Spin–1/2 Baryon Spectrum in QCD", Nucl. Phys. A **895**, 59 (2012).

[207] J.-R. Zhang and M.-Q. Huang, "Doubly heavy baryons in QCD sum rules", Phys. Rev. D **78**, 094007 (2008).

[208] Z.-G. Wang, "Analysis of the $\frac{1}{2}^+$ doubly heavy baryon states with QCD sum rules", Eur. Phys. J. A **45**, 267 (2010).

[209] V. V. Kiselev and A. I. Onishchenko, "Doubly heavy baryons in sum rules of NRQCD", Nucl. Phys. **B581**, 432 (2000).

[210] U. Özdem, "Magnetic moments of doubly heavy baryons in light-cone QCD", J. Phys. G **46**, 035003 (2019).

[211] K.-W. Wei, B. Chen and X.-H. Guo, "Masses of doubly and triply charmed baryons", Phys. Rev. D **92**, 076008 (2015).

[212] K.-W. Wei, B. Chen, N. Liu, Q.-Q. Wang and X.-H. Guo, "Spectroscopy of singly, doubly, and triply bottom baryons", Phys. Rev. D **95**, 116005 (2017).

[213] P. C. Vinodkumar, K. B. Vijayakumar and S. B. Khadkikar, "Effect of the confined gluons in quark quark interaction", Pramana **39**, 47 (1992).

[214] A. Majethiya, B. Patel and P. C. Vinodkumar, "Radiative decays of single heavy flavour baryons", Eur. Phys. J. A **42**, 213 (2009).

[215] L.-Y. Xiao, K.-L. Wang, Q.-f. Lu, X.-H. Zhong and S.-L. Zhu, "Strong and radiative decays of the doubly charmed baryons", Phys. Rev. D **96**, 094005 (2017).

[216] M. Ablikim *et al.* (BESIII Collaboration), "Observation of a Charged Charmoniumlike Structure in $e^+e^- \to \pi^+\pi^- J/\psi$ at $\sqrt{s}$=4.26 GeV", Phys. Rev. Lett. **110**, 252001 (2013).

[217] Z. Q. Liu *et al.* (Belle Collaboration), "Study of $e^+e^- \to \pi^+\pi^- J/\psi$ and Observation of a Charged Charmoniumlike State at Belle", Phys. Rev. Lett. **110**, 252002 (2013).

[218] T. Xiao, S. Dobbs, A. Tomaradze and K. K. Seth, "Observation of the Charged Hadron $Z_c^{\pm}(3900)$ and Evidence for the Neutral $Z_c^0(3900)$ in $e^+e^- \to \pi\pi J/\psi$ at $\sqrt{s} = 4170$ MeV", Phys. Lett. **B727**, 366 (2013).

[219] M. Ablikim *et al.* (BESIII Collaboration), "Determination of the Spin and Parity of the $Z_c(3900)$", Phys. Rev. Lett. **119**, 072001 (2017).

[220] A. Bondar *et al.* (Belle Collaboration), "Observation of two charged bottomonium-like resonances in $\Upsilon(5S)$ decays", Phys. Rev. Lett. **108**, 122001 (2012).

[221] A. Garmash *et al.* (Belle Collaboration), "Amplitude analysis of $e^+e^- \to \Upsilon(nS)\pi^+\pi^-$ at $\sqrt{s} = 10.865$ GeV", Phys. Rev. D **91**, 072003 (2015).

[222] A. Garmash *et al.* (Belle Collaboration), "Observation of $Z_b(10610)$ and $Z_b(10650)$ Decaying to B Mesons", Phys. Rev. Lett. **116**, 212001 (2016).

[223] R. L. Jaffe, "Multi-Quark Hadrons. 1. The Phenomenology of $Q^2\bar{Q}^2$ Mesons", Phys. Rev. D **15**, 267 (1977).

[224] R. L. Jaffe, "$Q^2\bar{Q}^2$ Resonances in the Baryon - antiBaryon System", Phys. Rev. D **17**, 1444 (1978).

[225] L. Maiani, F. Piccinini, A. D. Polosa and V. Riquer, "Diquark-antidiquarks with hidden or open charm and the nature of X(3872)", Phys. Rev. D **71**, 014028 (2005).

[226] A. V. Manohar and M. B. Wise, "Exotic $QQ\overline{qq}$ states in QCD", Nucl. Phys. B **399**, 17 (1993).

[227] F. S. Navarra, M. Nielsen and J.-M. Richard, "Exotic Charmonium and Bottomonium-like Resonances", J. Phys. Conf. Ser. **348**, 012007 (2012).

[228] T. Guo, L. Cao, M.-Z. Zhou and H. Chen, "The Possible candidates of tetraquark: $Z_b(10610)$ and $Z_b(10650)$", (2011), `arXiv:1106.2284`.

[229] L. Zhao, W.-Z. Deng and S.-L. Zhu, "Hidden-Charm Tetraquarks and Charged Z_c States", Phys. Rev. D **90**, 094031 (2014).

[230] S. Patel, M. Shah and P. C. Vinodkumar, "Mass spectra of four-quark states in the hidden charm sector", Eur. Phys. J. A **50**, 131 (2014).

[231] S. Patel and P. C. Vinodkumar, "Tetraquark states in the bottom sector and the status of the Y_b (10890) state", Eur. Phys. J. C **76**, 356 (2016).

[232] I. V. Danilkin, V. D. Orlovsky and Yu. A. Simonov, "Hadron interaction with heavy quarkonia", Phys. Rev. D **85**, 034012 (2012).

[233] S. Dubynskiy and M. B. Voloshin, "Hadro-Charmonium", Phys. Lett. **B666**, 344 (2008).

[234] M. Alberti, G. S. Bali, S. Collins, F. Knechtli, G. Moir and W. Söldner, "Hadroquarkonium from lattice QCD", Phys. Rev. D **95**, 074501 (2017).

[235] Y. Dong, A. Faessler, T. Gutsche and V. E. Lyubovitskij, "Decays of Z_b^+ and $Z_b'^+$ as Hadronic Molecules", J. Phys. G **40**, 015002 (2013).

[236] Y. Dong, A. Faessler, T. Gutsche and V. E. Lyubovitskij, "Strong decays of molecular states Z_c^+ and $\mathrm{Z}_c'^+$", Phys. Rev. D **88**, 014030 (2013).

[237] A. E. Bondar, A. Garmash, A. I. Milstein, R. Mizuk and M. B. Voloshin, "Heavy quark spin structure in Z_b resonances", Phys. Rev. D **84**, 054010 (2011).

[238] M. B. Voloshin, "Radiative transitions from $\Upsilon(5S)$ to molecular bottomonium", Phys. Rev. D **84**, 031502 (2011).

[239] J.-R. Zhang, M. Zhong and M.-Q. Huang, "Could $Z_b(10610)$ be a $B^*\bar{B}$ molecular state?", Phys. Lett. **B704**, 312 (2011).

[240] C.-Y. Cui, Y.-L. Liu and M.-Q. Huang, "Investigating different structures of the Z_b (10610) and Z_b (10650)", Phys. Rev. D **85**, 074014 (2012).

[241] Y. Yang, J. Ping, C. Deng and H.-S. Zong, "Possible interpretation of the $Z_b(10610)$ and $Z_b(10650)$ in a chiral quark model", J. Phys. G **39**, 105001 (2012).

[242] Z.-F. Sun, J. He, X. Liu, Z.-G. Luo and S.-L. Zhu, "$Z_b(10610)^{\pm}$ and $Z_b(10650)^{\pm}$ as the $B^*\bar{B}$ and $B^*\bar{B}^*$ molecular states", Phys. Rev. D **84**, 054002 (2011).

[243] M. Cleven, F.-K. Guo, C. Hanhart and U.-G. Meissner, "Bound state nature of the exotic Z_b states", Eur. Phys. J. A **47**, 120 (2011).

[244] X.-H. Liu, L. Ma, L.-P. Sun, X. Liu and S.-L. Zhu, "Resolving the puzzling decay patterns of charged Z_c and Z_b states", Phys. Rev. D **90**, 074020 (2014).

[245] L. Ma, X.-H. Liu, X. Liu and S.-L. Zhu, "Strong decays of the XYZ states", Phys. Rev. D **91**, 034032 (2015).

[246] H.-X. Chen, W. Chen, X. Liu and S.-L. Zhu, "The hidden-charm pentaquark and tetraquark states", Phys. Rept. **639**, 1 (2016).

[247] F. E. Close and P. R. Page, "The $D^{*0}\bar{D}^0$ threshold resonance", Phys. Lett. **B578**, 119 (2004).

[248] M. T. Li, W. L. Wang, Y. B. Dong and Z. Y. Zhang, "$Z_b(10650)$ and $Z_b(10610)$ States in A Chiral Quark Model", J. Phys. G **40**, 015003 (2013).

[249] G.-J. Wang, X.-H. Liu, L. Ma, X. Liu, X.-L. Chen, W.-Z. Deng and S.-L. Zhu, "The strong decay patterns of Z_c and Z_b states in the relativized quark model", `arXiv:1811.10339`.

[250] W.-S. Huo and G.-Y. Chen, "The nature of Z_b states from a combined analysis of $\Upsilon(5S) \to h_b(mP)\pi^+\pi^-$ and $\Upsilon(5S) \to B^{(*)}\bar{B}^{(*)}\pi$", Eur. Phys. J. C **76**, 172 (2016).

[251] M. Cleven, Q. Wang, F.-K. Guo, C. Hanhart, U.-G. Meissner and Q. Zhao, "Confirming the molecular nature of the $Z_b(10610)$ and the $Z_b(10650)$", Phys. Rev. D **87**, 074006 (2013).

[252] T. Gutsche, V. E. Lyubovitskij and I. Schmidt, "Tetraquarks in holographic QCD", Phys. Rev. D **96**, 034030 (2017).

[253] Z.-G. Wang and T. Huang, "The $Z_b(10610)$ and $Z_b(10650)$ as axial-vector tetraquark states in the QCD sum rules", Nucl. Phys. A **930**, 63 (2014).

[254] F.-K. Guo, C. Hanhart, U.-G. Meißner, Q. Wang, Q. Zhao and B.-S. Zou, "Hadronic molecules", Rev. Mod. Phys. **90**, 015004 (2018).

[255] A. Ali, J. S. Lange and S. Stone, "Exotics: Heavy Pentaquarks and Tetraquarks", Prog. Part. Nucl. Phys. **97**, 123 (2017).

[256] N. R. Soni, R. R. Chaturvedi, A. K. Rai and J. N. Pandya, "Mass and Hadronic Decay Widths of Z States as Di-meson Molecule", Springer Proc. Phys. **203**, 729 (2018).

[257] R. D. Woods and D. S. Saxon, "Diffuse Surface Optical Model for Nucleon-Nuclei Scattering", Phys. Rev. **95**, 577 (1954).

[258] C. Berkdemir, A. Berkdemir and R. Sever, "Polynomial solutions of the Schrodinger equation for the generalized Woods-Saxon potential", Phys. Rev. C **72**, 027001 (2005).

[259] I. Adachi (Belle Collaboration), "Observation of two charged bottomonium-like resonances", `arXiv:1105.4583`.

[260] S. Patel, M. Shah, K. Thakkar and P. C. Vinodkumar, "Decay widths of Di-mesonic molecular states as candidates for Z_c and Z_b", PoS **Hadron2013**, 189 (2013).

[261] H.-W. Ke, Z.-T. Wei and X.-Q. Li, "Is $Z_c(3900)$ a molecular state", Eur. Phys. J. C **73**, 2561 (2013).

[262] F. Goerke, T. Gutsche, M. A. Ivanov, J. G. Körner and V. E. Lyubovitskij, "$Z_b(10610)$ and $Z_b'(10650)$ decays in a covariant quark model", Phys. Rev. D **96**, 054028 (2017).

[263] J. D. Richman and P. R. Burchat, "Leptonic and semileptonic decays of charm and bottom hadrons", Rev. Mod. Phys. **67**, 893 (1995).

[264] A. Ryd and A. A. Petrov, "Hadronic D and D_s Meson Decays", Rev. Mod. Phys. **84**, 65 (2012).

[265] M. K. Gaillard and B. W. Lee, "Rare Decay Modes of the K-Mesons in Gauge Theories", Phys. Rev. D **10**, 897 (1974).

[266] J. P. Lees *et al.* (BABAR Collaboration), "Measurement of the $D^0 \to \pi^- e^+ \nu_e$ differential decay branching fraction as a function of q^2 and study of form factor parameterizations", Phys. Rev. D **91**, 052022 (2015).

[267] B. Aubert *et al.* (BABAR Collaboration), "Study of the decay $D_s^+ \to K^+ K^- e^+ \nu_e$", Phys. Rev. D **78**, 051101 (2008).

[268] L. Widhalm *et al.* (Belle Collaboration), "Measurement of $D^0 \to \pi \ell \nu (K \ell \nu)$ Form Factors and Absolute Branching Fractions", Phys. Rev. Lett. **97**, 061804 (2006).

[269] M. Ablikim *et al.* (BESIII Collaboration), "Study of Dynamics of $D^0 \to K^- e^+ \nu_e$ and $D^0 \to \pi^- e^+ \nu_e$ Decays", Phys. Rev. D **92**, 072012 (2015).

[270] D. Besson *et al.* (CLEO Collaboration), "Improved measurements of D meson semileptonic decays to π and K mesons", Phys. Rev. D **80**, 032005 (2009).

[271] P. Colangelo and F. De Fazio, "D_s decays to eta and eta-prime final states: A Phenomenological analysis", Phys. Lett. **B520**, 78 (2001).

[272] D.-S. Du, J.-W. Li and M.-Z. Yang, "Form-factors and semileptonic decay of $D_s^+ \to \phi \bar{l} \nu$ from QCD sum rule", Eur. Phys. J. C **37**, 173 (2004).

[273] K. Azizi, R. Khosravi and F. Falahati, "Exclusive $D_s \to (\eta, \eta')l\nu$ decays in light cone QCD", J. Phys. G **38**, 095001 (2011).

[274] N. Offen, F. A. Porkert and A. Schäfer, "Light-cone sum rules for the $D_{(s)} \to \eta^{(\prime)} l \nu_l$ form factor", Phys. Rev. D **88**, 034023 (2013).

[275] U.-G. Meißner and W. Wang, "Generalized Heavy-to-Light Form Factors in Light-Cone Sum Rules", Phys. Lett. **B730**, 336 (2014).

[276] G. Duplancic and B. Melic, "Form factors of B, $B_s \to \eta(\prime)$ and D, $D_s \to \eta(\prime)$ transitions from QCD light-cone sum rules", JHEP **11**, 138 (2015).

[277] Y.-L. Wu, M. Zhong and Y.-B. Zuo, "$B_{(s)}, D_{(s)} \to \pi, K, \eta, \rho, K*, \omega, \phi$ Transition Form Factors and Decay Rates with Extraction of the CKM parameters $|V_{(ub)}|$, $|V_{(cs)}|$, $|V_{(cd)}|$", Int. J. Mod. Phys. A **21**, 6125 (2006).

[278] H.-B. Fu, X. Yang, R. Lü, L. Zeng, W. Cheng and X.-G. Wu, "The $D \to \rho$ transition form factors within the QCD light-cone sum rules and the D-meson semileptonic decays $D^0 \to \rho^- e^+ \nu_e$ and $D^+ \to \rho^0 e^+ \nu_e$", (2018), `arXiv:1808.06412`.

[279] J. Charles, A. Le Yaouanc, L. Oliver, O. Pene and J. C. Raynal, "Heavy to light form-factors in the heavy mass to large energy limit of QCD", Phys. Rev. D **60**, 014001 (1999).

[280] D. Melikhov and B. Stech, "Weak form-factors for heavy meson decays: An Update", Phys. Rev. D **62**, 014006 (2000).

[281] T. Palmer and J. O. Eeg, "Form factors for semileptonic D decays", Phys. Rev. D **89**, 034013 (2014).

[282] J. Bijnens and I. Jemos, "Vector Formfactors in Hard Pion Chiral Perturbation Theory", Nucl. Phys. **B846**, 145 (2011).

[283] S. Fajfer and J. F. Kamenik, "Charm meson resonances in $D \to P\ell\nu$ decays", Phys. Rev. D **71**, 014020 (2005).

[284] S. Fajfer and J. F. Kamenik, "Charm meson resonances and $D \to V$ semileptonic form-factors", Phys. Rev. D **72**, 034029 (2005).

[285] Z.-T. Wei, H.-W. Ke and X.-F. Yang, "Interpretation of the "f_{D_s} puzzle" in SM and beyond", Phys. Rev. D **80**, 015022 (2009).

[286] R. C. Verma, "Decay constants and form factors of s-wave and p-wave mesons in the covariant light-front quark model", J. Phys. G **39**, 025005 (2012).

[287] H.-Y. Cheng and X.-W. Kang, "Branching fractions of semileptonic D and D_s decays from the covariant light-front quark model", Eur. Phys. J. C **77**, 587 (2017).

[288] T. Sekihara and E. Oset, "Investigating the nature of light scalar mesons with semileptonic decays of D mesons", Phys. Rev. D **92**, 054038 (2015).

[289] T. Branz, A. Faessler, T. Gutsche, M. A. Ivanov, J. G. Korner and V. E. Lyubovitskij, "Relativistic constituent quark model with infrared confinement", Phys. Rev. D **81**, 034010 (2010).

[290] M. Ablikim *et al.* (BESIII Collaboration), "Search for the rare decay $D^+ \to D^0 e^+ \nu_e$", Phys. Rev. D **96**, 092002 (2017).

[291] H.-B. Li and M.-Z. Yang, "Rare Semileptonic Decays of Heavy Mesons with Flavor SU(3) Symmetry", Eur. Phys. J. C **59**, 841 (2009).

[292] S. Faller and T. Mannel, "Light-Quark Decays in Heavy Hadrons", Phys. Lett. **B750**, 653 (2015).

[293] N. R. Soni and J. N. Pandya, "Decay $D \to K^{(*)} \ell^+ \nu_\ell$ in covariant quark model", Phys. Rev. D **96**, 016017 (2017).

[294] N. R. Soni, M. A. Ivanov, J. G. Körner, J. N. Pandya, P. Santorelli and C. T. Tran, "Semileptonic $D_{(s)}$-meson decays in the light of recent data", Phys. Rev. D **98**, 114031 (2018).

[295] J. A. M. Vermaseren, "The FORM project", Nucl. Phys. Proc. Suppl. **183**, 19 (2008).

[296] R. P. Feynman, "Space - time approach to quantum electrodynamics", Phys. Rev. **76**, 769 (1949), [,99(1949)].

[297] W.-P. Chen, Y.-C. Chen, T.-W. Chiu, H.-Y. Chou, T.-S. Guu and T.-H. Hsieh (TWQCD Collaboration), "Decay Constants of Pseudoscalar D-mesons in Lattice QCD with Domain-Wall Fermion", Phys. Lett. **B736**, 231 (2014).

[298] Z.-G. Wang, "Analysis of the masses and decay constants of the heavy-light mesons with QCD sum rules", Eur. Phys. J. C **75**, 427 (2015).

[299] R. J. Dowdall, C. T. H. Davies, G. P. Lepage and C. McNeile, "V_{us} from π and K decay constants in full lattice QCD with physical u, d, s and c quarks", Phys. Rev. D **88**, 074504 (2013).

[300] H. Na, C. T. H. Davies, E. Follana, G. P. Lepage and J. Shigemitsu, "The $D \to K, l\nu$ Semileptonic Decay Scalar Form Factor and $|V_{cs}|$ from Lattice QCD", Phys. Rev. D **82**, 114506 (2010).

[301] D. Becirevic, V. Lubicz, F. Sanfilippo, S. Simula and C. Tarantino, "D-meson decay constants and a check of factorization in non-leptonic B-decays", JHEP **02**, 042 (2012).

[302] P. Ball, G. W. Jones and R. Zwicky, "$B \to V\gamma$ beyond QCD factorisation", Phys. Rev. D **75**, 054004 (2007).

[303] W. Sun, A. Alexandru, Y. Chen, T. Draper, Z. Liu, Y.-B. Yang and Yang (QCD Collaboration), "Anatomy of the ρ resonance from lattice QCD at the physical point", Chin. Phys. C **42**, 063102 (2018).

[304] B. Chakraborty, C. T. H. Davies, G. C. Donald, J. Koponen and G. P. Lepage (HPQCD Collaboration), "Nonperturbative comparison of clover and highly improved staggered quarks in lattice QCD and the properties of the ϕ meson", Phys. Rev. D **96**, 074502 (2017).

[305] M. Wirbel, B. Stech and M. Bauer, "Exclusive Semileptonic Decays of Heavy Mesons", Z. Phys. C **29**, 637 (1985).

[306] M. A. Ivanov, J. G. Körner and C. T. Tran, "Exclusive decays $B \to \ell^- \bar{\nu}$ and $B \to D^{(*)} \ell^- \bar{\nu}$ in the covariant quark model", Phys. Rev. D **92**, 114022 (2015).

[307] T. Gutsche, M. A. Ivanov, J. G. Körner, V. E. Lyubovitskij, P. Santorelli and N. Habyl, "Semileptonic decay $\Lambda_b \to \Lambda_c + \tau^- + \bar{\nu_\tau}$ in the covariant confined quark model", Phys. Rev. D **91**, 074001 (2015), [Erratum: Phys. Rev.D91,no.11,119907(2015)].

[308] S. Bifani, S. Descotes-Genon, A. Romero Vidal and M.-H. Schune, "Review of Lepton Universality tests in B decays", J. Phys. G **46**, 023001 (2019).

[309] M. A. Ivanov, J. G. Körner and C.-T. Tran, "Probing new physics in $\bar{B}^0 \to D^{(*)} \tau^- \bar{\nu}_\tau$ using the longitudinal, transverse, and normal polarization components of the tau lepton", Phys. Rev. D **95**, 036021 (2017).

[310] Q.-Y. Hu, X.-Q. Li and Y.-D. Yang, "$b \to c\tau\nu$ Transitions in the Standard Model Effective Field Theory", `arXiv:1810.04939`.

[311] P. Asadi, M. R. Buckley and D. Shih, "Asymmetry Observables and the Origin of $R_{D^{(*)}}$ Anomalies", Phys. Rev. D **99**, 035015 (2019).

[312] N. Rajeev and R. Dutta, "Impact of vector new physics couplings on $B_s \to (K, K^*)\tau\nu$ and $B \to \pi\tau\nu$ decays", Phys. Rev. D **98**, 055024 (2018).

[313] F. Feruglio, P. Paradisi and O. Sumensari, "Implications of scalar and tensor explanations of $R_{D^{(*)}}$", JHEP **11**, 191 (2018).

[314] M. Ablikim *et al.* (BESIII Collaboration), "First measurement of the form factors in $D_s^+ \to K^0 e^+ \nu_e$ and $D_s^+ \to K^{*0} e^+ \nu_e$ decays", Phys. Rev. Lett. **122**, 061801 (2019).

[315] T. Feldmann, P. Kroll and B. Stech, "Mixing and decay constants of pseudoscalar mesons", Phys. Rev. D **58**, 114006 (1998).

[316] M. Ablikim *et al.* (BESIII Collaboration), "Measurement of the form factors in the decay $D^+ \to \omega e^+ \nu_e$ and search for the decay $D^+ \to \phi e^+ \nu_e$", Phys. Rev. D **92**, 071101 (2015).

[317] M. Ablikim *et al.* (BESIII Collaboration), "Study of the $D^0 \to K^- \mu^+ \nu_\mu$ dynamics and test of lepton flavor universality with $D^0 \to K^- \ell^+ \nu_\ell$ decays", Phys. Rev. Lett. **122**, 011804 (2019).

[318] M. Ablikim *et al.* (BESIII Collaboration), "Measurement of the branching fraction for the semi-leptonic decay $D^{0(+)} \to \pi^{-(0)} \mu^+ \nu_\mu$ and test of lepton universality", Phys. Rev. Lett. **121**, 171803 (2018).

[319] M. Ablikim *et al.* (BESIII Collaboration), "Study of the decay $D^0 \to \bar{K}^0 \pi^- e^+ \nu_e$", Phys. Rev. D **99**, 011103 (2019).

[320] T. E. Coan *et al.* (CLEO Collaboration), "Absolute branching fraction measurements of exclusive D0 semileptonic decays", Phys. Rev. Lett. **95**, 181802 (2005).

[321] M. Ablikim *et al.* (BESIII Collaboration), "First Observation of $D^+ \to f_0(500) e^+ \nu_e$ and Improved Measurements of $D \to \rho e^+ \nu_e$", Phys. Rev. Lett. **122**, 062001 (2019).

[322] S. Dobbs *et al.* (CLEO Collaboration), "First Measurement of the Form Factors in the Decays $D^0 \to \rho^- e^+ \nu_e$ and $D^+ \to \rho^0 e^+ \nu_e$", Phys. Rev. Lett. **110**, 131802 (2013).

[323] D. Scora and N. Isgur, "Semileptonic meson decays in the quark model: An update", Phys. Rev. D **52**, 2783 (1995).

[324] M. Ablikim *et al.* (BESIII Collaboration), "Analysis of $D^+ \to \bar{K}^0 e^+ \nu_e$ and $D^+ \to \pi^0 e^+ \nu_e$ semileptonic decays", Phys. Rev. D **96**, 012002 (2017).

[325] M. Ablikim *et al.* (BESIII Collaboration), "Improved measurement of the absolute branching fraction of $D^+ \to \bar{K}^0 \mu^+ \nu_\mu$", Eur. Phys. J. C **76**, 369 (2016).

[326] M. Ablikim *et al.* (BESIII Collaboration), "Study of the decays $D^+ \to \eta^{(\prime)} e^+ \nu_e$", Phys. Rev. D **97**, 092009 (2018).

[327] J. Yelton *et al.* (CLEO Collaboration), "Studies of $D^+ \to \eta^{'}, \eta, \phi e^+ \nu_e$", Phys. Rev. D **84**, 032001 (2011).

[328] J. Hietala, D. Cronin-Hennessy, T. Pedlar and I. Shipsey, "Exclusive D_s semileptonic branching fraction measurements", Phys. Rev. D **92**, 012009 (2015).

[329] M. Ablikim *et al.* (BESIII Collaboration), "Measurements of the branching fractions for the semi-leptonic decays $D_s^+ \to \phi e^+ \nu_e$, $\phi \mu^+ \nu_\mu$, $\eta \mu^+ \nu_\mu$ and $\eta' \mu^+ \nu_\mu$", Phys. Rev. D **97**, 012006 (2018).

[330] M. Ablikim *et al.* (BESIII Collaboration), "Measurements of the absolute branching fractions for $D_s^+ \to \eta e^+ \nu_e$ and $D_s^+ \to \eta' e^+ \nu_e$", Phys. Rev. D **94**, 112003 (2016).

[331] M. Ablikim *et al.* (BES Collaboration), "Direct measurement of the branching fraction for the decay of $D^+ \to \bar{K}^0 e^+ \nu_e$ and determination of $\Gamma(D^0 \to K^- e^+ \nu_e)/\Gamma(D^+ \to \bar{K}^0 e^+ \nu_e)$", Phys. Lett. **B608**, 24 (2005).

[332] S. Dobbs *et al.* (CLEO Collaboration), "A Study of the semileptonic charm decays $D^0 \to \pi^- e^+ \nu_e$, $D^+ \to \pi^0 e^+ \nu_e$, $D^0 \to K^- e^+ \nu_e$, $D^+ \to \bar{K}^0 e^+ \nu_e$", Phys. Rev. D **77**, 112005 (2008).

[333] J. Yelton *et al.* (CLEO Collaboration), "Absolute Branching Fraction Measurements for Exclusive D_s Semileptonic Decays", Phys. Rev. D **80**, 052007 (2009).

[334] J. G. Körner and G. A. Schuler, "Exclusive Semileptonic Heavy Meson Decays Including Lepton Mass Effects", Z. Phys. C **46**, 93 (1990).

List of Publications

Papers in peer reviewed Journals

1. J. N. Pandya, N. R. Soni, N. Devlani, A. K. Rai, "Decay rates and electromagnetic transitions of heavy quarkonia", Chin. Phys. C **39**, 123101 (2015).

2. N. R. Soni and J. N. Pandya, "Decay $D \to K^{(*)}\ell^+\nu_\ell$ in covariant quark model", Phys. Rev. D **96**, 016017 (2017) [Erratum: Phys. Rev. D **99**, 059901 (2019)].

3. N. R. Soni, B. R. Joshi, R. P. Shah, H. R. Chauhan, J. N. Pandya "$Q\bar{Q}(Q \in \{b, c\})$ spectroscopy using Cornell potential", Eur. Phys. J. C **78**, 592 (2018).

4. N. R. Soni, M. A. Ivanov, J. G. Körner, J. N. Pandya, P. Santorelli, C. T. Tran, "Semileptonic $D_{(s)}$-meson decays in the light of recent data", Phys. Rev. D **98**, 114031 (2018).

Papers in Conference Proceedings

1. N. R. Soni and J. N. Pandya, "Masses and radiative leptonic decay properties of B_c meson", DAE Symp. Nucl. Phys. **58**, 674 (2013).

2. N. R. Soni and J. N. Pandya, "Semileptonic and pionic decays of doubly strange baryons", DAE Symp. Nucl. Phys. **60**, 694 (2015).

3. A. N. Gadaria, N. R. Soni, J. N. Pandya, "Masses and magnetic moment of doubly heavy baryons", DAE Symp. Nucl. Phys. **61**, 698 (2016).

4. N. R. Soni, J. N. Pandya, "Masses and radiative decay of Ω_{cc}^+ baryon", DAE Symp. Nucl. Phys. **62**, 770 (2017).

5. N. R. Soni, R. R. Chaturvedi. A. K. Rai, J. N. Pandya, "Mass and Hadronic Decay Widths of Z States as Di-meson Molecule", Springer Proc. Phys. **203**, 729 (2018).

6. A. N. Gadaria, N. R. Soni, Raghav Chaturvedi, A. K. Rai, J. N. Pandya, "Decay Properties of Ξ_{cc}^{++} baryons", DAE symp. on Nucl. Phys. **63**, 912 (2018).

Decay rates and electromagnetic transitions of heavy quarkonia *

J. N. Pandya[1;1)] N. R. Soni[1] N. Devlani[2] A. K. Rai[3]

[1] Applied Physics Department, Faculty of Technology & Engineering, The M S University of Baroda, Vadodara 390001, Gujarat, INDIA
[2] Applied Physics Department, Polytechnic, The M S University of Baroda, Vadodara 390002, Gujarat, INDIA
[3] Department of Applied Physics, Sardar Vallabhbhai National Institute of Technology, Surat 395007, Gujarat, INDIA

Abstract: The electromagnetic radiative transition widths for heavy quarkonia, as well as digamma and digluon decay widths, are computed in the framework of the extended harmonic confinement model (ERHM) and Coulomb plus power potential (CPP$_\nu$) with varying potential index ν. The outcome is compared with the values obtained from other theoretical models and experimental results. While the mass spectra, digamma and digluon widths from ERHM as well as CPP$_{\nu=1}$ are in good agreement with experimental data, the electromagnetic transition widths span over a wide range for the potential models considered here making it difficult to prefer a particular model over the others because of the lack of experimental data for most transition widths.

Key words: heavy quarkonia, radiative decays, electromagnetic transitions

PACS: 12.39.Jh, 12.39.Pn, 13.20.Gd **DOI:** 10.1088/1674-1137/39/12/123101

1 Introduction

Decay properties of mesons are of special experimental and theoretical interest because they provide us with further insights into the dynamics of these systems in addition to the knowledge we have gained from the spectra of these families. A large number of experimental facilities worldwide have provided and continue to provide enormous amounts of data which need to be interpreted using the available theoretical approaches [1]. Many phenomenological studies on numerous observables of the $c\bar{c}$ and $b\bar{b}$ bound states have established that the non-relativistic nature appears to be an essential ingredient to understand the dynamics of heavy quarkonia [2]. Thus, the heavy quarkonium spectroscopy is mostly dependent on the quark mass m, the momentum mv and the binding energy mv^2 in the non-relativistic limit. Two effective field theories, non-relativistic QCD (NRQCD) [3, 4] and potential NRQCD (pNRQCD) [5, 6], have been developed leading to a large number of new results for several observables in quarkonium physics [7].

Radiative transitions in heavy quarkonia have been a subject of interest as the CLEO-c experiment has measured the magnetic dipole (M1) transitions $J/\psi(1S)\to\gamma\eta_c(1S)$ and $J/\psi(2S)\to\gamma\eta_c(1S)$ using a combination of inclusive and exclusive techniques and reconciling with theoretical calculations of lattice QCD and effective field theory techniques [8, 9]. M1 transition rates are normally weaker than E1 rates, but they are of more interest because they may allow access to spin-singlet states that are very difficult to produce otherwise. It is also interesting that the known M1 rates show serious disagreement between theory and experiment when it comes to potential models. This is in part due to the fact that M1 transitions between different spatial multiplets, such as $J/\psi(1S)\to\gamma\eta_c(2S\to1S)$ are nonzero only due to small relativistic corrections to a vanishing lowest-order M1 matrix element [10].

We use the spectroscopic parameters of the extended harmonic confinement model (ERHM), which has been successful in predictions of masses of open flavour mesons from light to heavy flavour sectors [11–13]. The mass spectra of charmonia and bottomonia predicted by this model, and a Coulomb plus power potential (CPP$_\nu$) with varying potential index ν (from 0.5 to 2.0), employing a non-relativistic treatment for heavy quarks [14–17], have been utilized for the present computations along with other theoretical and experimental results.

2 Theoretical framework

One of the tests for the success of any theoretical

Received 23 December 2014, Revised 26 June 2015

∗ Supported by University Grants Commission, India for Major Research Project F. No.42-775/2013(SR) (J N Pandya) and Dept. of Science and Technology, India under SERC fast track scheme SR/FTP/PS-152/2012 (A K Rai)

1) E-mail: jnpandya-apphy@msubaroda.ac.in

model for mesons is the correct prediction of their decay rates. Many phenomenological models predict the masses correctly but overestimate the decay rates [14, 15, 18]. We have successfully employed a phenomenological harmonic potential scheme and CPP$_\nu$ potential with varying potential index for different confinement strengths to compute masses of bound states of heavy quarkonia, and the resulting parameters and wave functions have been used to study various decay properties [13].

The choice of scalar plus vector potential for quark confinement has been successful in predictions of the low lying hadronic properties in the relativistic schemes for quark confinement [19–21], which have been extended to accommodate multiquark states from lighter to heavier flavour sectors with unequal quark masses [11, 12]. The coloured quarks are assumed to be confined through a Lorentz scalar plus a vector potential of the form

$$V(r)=\frac{1}{2}(1+\gamma_0)A^2r^2+B, \tag{1}$$

where A and B are the model parameters and γ_0 is the Dirac matrix.

The wave functions for quarkonia are constructed here by retaining the nature of the single particle wave function but with a two particle size parameter $\Omega_N(q_iq_j)$,

$$R_{n\ell}(r) = \left[\frac{\Omega_{\rm N}^{3/2}}{2\pi}\frac{n!}{\Gamma\left(n+\ell+\frac{3}{2}\right)}\right]^{\frac{1}{2}}(\Omega_{\rm N}^{1/2}r)^{\ell} \times\exp\left(\frac{-\Omega_{\rm N}\ r^2}{2}\right)L_n^{\ell+\frac{1}{2}}(\Omega_{\rm N}r^2). \tag{2}$$

The Coulombic part of the energy is computed using the residual Coulomb potential using the colour dielectric "coefficient", which is found to be state dependent [11], so as to get a consistent Coulombic contribution to the excited states of the hadrons. This is a measure of the confinement strength through the non-perturbative contributions to the confinement scale at the respective threshold energies of the quark-antiquark excitations.

The spin average (center of weight) masses of the $c\bar{c}$ and $b\bar{b}$ ground states are obtained by choosing the model parameters m_c=1.428 GeV, m_b=4.637 GeV, k= 0.1925 and the confinement parameter A=0.0685 GeV$^{3/2}$ [11, 12].

In the other approach using the CPP$_\nu$ scheme for the heavy-heavy bound state systems such as $c\bar{c}$ and $b\bar{b}$, we treat the motion of both the quarks and antiquarks nonrelativistically [13]. The CPP$_\nu$ potential is given by

$$V(r)=\frac{-\alpha_c}{r}+Ar^\nu, \tag{3}$$

Here, for the study of heavy flavoured mesons, $\alpha_c = 4\alpha_s/3$, α_s being the strong running coupling constant, A is the potential parameter and ν is a general power, such that the choice $\nu=1$ corresponds to the Coulomb plus linear potential.

We have employed the hydrogenic trial wave function here for the present calculations. For excited states we consider the wave function multiplied by an appropriate orthogonal polynomial function such that the generalized variational wave function gets orthonormalized. Thus, the trial wave function for the (n,l) state is assumed to be the form given by

$$R_{nl}(r)=\left(\frac{\mu^3(n-l-1)!}{2n(n+l)!}\right)^{\frac{1}{2}}(\mu\ r)^l{\rm e}^{-\mu r/2}L_{n-l-1}^{2l+1}(\mu r). \tag{4}$$

Here, μ is the variational parameter and $L_{n-l-1}^{2l+1}(\mu r)$ is a Laguerre polynomial.

For a chosen value of ν, the variational parameter μ is determined for each state using the virial theorem

$$\langle KE\rangle=\frac{1}{2}\left\langle\frac{r{\rm d}V}{{\rm d}r}\right\rangle. \tag{5}$$

The potential index ν is chosen to vary from 0.5 to 2.

Table 1. Digamma decay width of charmonia (keV).

	1^1S_0	2^1S_0	3^1S_0	4^1S_0	1^3P_0	1^3P_2	2^3P_0	2^3P_2
ERHM	8.76	5.94	3.05	1.43	69.97	73.93	6.93	6.98
ERHM(corr)	6.21	4.21	2.17	1.01	71.04	75.06	5.87	5.91
CPP$_{\nu=0.5}$	12.85	3.47	1.83	1.24	5.74	1.54	21.11	5.69
CPP$_{\nu=0.5}$(corr)	7.32	1.98	1.04	0.71	5.84	1.19	21.59	4.40
CPP$_{\nu=1.0}$	22.79	9.88	6.73	5.28	27.29	7.45	143.30	39.41
CPP$_{\nu=1.0}$(corr)	12.99	5.63	3.84	3.01	27.91	5.76	146.57	30.49
CPP$_{\nu=1.5}$	30.84	17.55	14.16	12.65	63.35	17.52	511.88	144.33
CPP$_{\nu=1.5}$(corr)	17.58	10.00	8.07	7.21	64.79	13.56	523.53	111.66
CPP$_{\nu=2.0}$	37.43	25.11	22.88	22.43	108.06	30.26	1058.7	305.98
CPP$_{\nu=2.0}$(corr)	21.34	14.31	13.04	12.79	110.52	23.41	1082.8	236.72
[29]	10.38	3.378	1.9	1.288	–	–	–	–
[30]	8.5	2.4	0.88	–	2.5	0.31	1.7	0.23
[31]	7.8	3.5	–	–	–	–	–	–
[32]	11.8	–	–	–	–	–	–	–

Table 2. Digluon decay width of charmonia (MeV).

	1^1S_0	2^1S_0	3^1S_0	4^1S_0	1^3P_0	1^3P_2	2^3P_0	2^3P_2
ERHM	13.48	9.14	4.7	2.19	0.11	0.11	9.07	9.13
ERHM(corr)	19.04	12.91	6.64	3.1	0.19	0.2	5.31	5.43
$\mathrm{CPP}_{\nu=0.5}$	43.41	11.73	6.17	4.19	0.019	3.71	0.07	13.74
$\mathrm{CPP}_{\nu=0.5}$(corr)	69.94	18.89	9.94	6.76	0.040	1.43	0.15	5.29
$\mathrm{CPP}_{\nu=1.0}$	77.01	33.37	22.74	17.84	0.092	17.99	0.48	95.21
$\mathrm{CPP}_{\nu=1.0}$(corr)	124.08	53.77	36.64	28.74	0.195	6.93	1.02	36.69
$\mathrm{CPP}_{\nu=1.5}$	104.18	59.28	47.85	42.73	0.214	42.33	1.73	348.66
$\mathrm{CPP}_{\nu=1.5}$(corr)	167.85	95.51	77.09	68.85	0.453	16.31	3.66	134.38
$\mathrm{CPP}_{\nu=2}$	126.46	84.83	77.29	75.79	0.365	73.11	3.58	739.15
$\mathrm{CPP}_{\nu=2.0}$(corr)	203.75	136.67	124.53	122.12	0.773	28.18	7.57	284.88
[22]	26.7±3.0	–	–	–	10.2±0.7	2.034±0.12	–	–
[23]	48.927	–	–	–	38.574	4.396	–	–
[33]pert.	15.70	–	–	–	4.68	1.72	–	–
[33]nonpert.	10.57	–	–	–	4.88	0.69	–	–

Table 3. Digamma decay width of bottomonia (keV).

	1^1S_0	2^1S_0	3^1S_0	4^1S_0	1^3P_0	1^3P_2	2^3P_0	2^3P_2
ERHM	0.47	0.26	0.12	0.01	1.37	1.39	0.12	0.12
ERHM(corr)	0.35	0.20	0.09	0.07	1.39	1.40	0.10	0.10
$\mathrm{CPP}_{\nu=0.5}$	0.36	0.06	0.03	0.038	0.02	0.005	0.057	0.015
$\mathrm{CPP}_{\nu=0.5}$(corr)	0.24	0.04	0.02	0.026	0.02	0.004	0.058	0.013
$\mathrm{CPP}_{\nu=1.0}$	0.55	0.15	0.09	0.080	0.08	0.022	0.42	0.11
$\mathrm{CPP}_{\nu=1.0}$(corr)	0.37	0.10	0.06	0.054	0.08	0.018	0.43	0.09
$\mathrm{CPP}_{\nu=1.5}$	0.71	0.27	0.18	0.123	0.20	0.055	1.34	0.36
$\mathrm{CPP}_{\nu=1.5}$(corr)	0.48	0.18	0.12	0.084	0.21	0.045	1.36	0.30
$\mathrm{CPP}_{\nu=2.0}$	0.84	0.38	0.29	0.165	0.35	0.095	2.83	0.76
$\mathrm{CPP}_{\nu=2.0}$(corr)	0.57	0.26	0.20	0.112	0.36	0.078	2.88	0.63
[29]	0.496	0.212	0.135	0.099	–	–	–	–
[30]	0.527	0.263	0.172	–	0.037	0.0066	0.037	0.0067
[31]	0.460	0.20	–	–	–	–	–	–
[32]	0.580	–	–	–	–	–	–	–

Table 4. Digluon decay width of bottomonia (MeV).

	1^1S_0	2^1S_0	3^1S_0	4^1S_0	1^3P_0	1^3P_2	2^3P_0	2^3P_2
ERHM	7.61	4.31	1.99	1.58	22.45	22.68	1.93	1.94
ERHM(corr)	9.95	5.64	2.61	2.07	38.17	38.57	1.92	1.92
$\mathrm{CPP}_{\nu=0.5}$	10.92	1.77	0.78	1.17	0.61	0.16	1.74	0.46
$\mathrm{CPP}_{\nu=0.5}$(corr)	15.51	2.51	1.11	1.66	1.20	0.16	3.40	0.46
$\mathrm{CPP}_{\nu=1.0}$	16.71	4.65	2.72	2.43	2.51	0.67	12.81	3.42
$\mathrm{CPP}_{\nu=1.0}$(corr)	23.72	6.61	3.86	3.45	4.90	0.66	25.04	3.39
$\mathrm{CPP}_{\nu=1.5}$	21.53	8.14	5.60	3.76	6.22	1.67	40.70	10.91
$\mathrm{CPP}_{\nu=1.5}$(corr)	30.58	11.55	7.95	5.34	12.16	1.65	79.57	10.81
$\mathrm{CPP}_{\nu=2.0}$	25.55	11.66	8.95	5.03	10.74	2.88	86.12	23.15
$\mathrm{CPP}_{\nu=2.0}$(corr)	36.29	16.56	12.72	7.14	21.00	2.85	168.36	22.93
[23]	14.64	–	–	–	2.745	0.429	–	–
[33]pert.	11.49	–	–	–	0.96	0.33	–	–
[33]nonpert.	12.39	–	–	–	2.74	0.25	–	–
[39]	12.46	–	–	–	2.15	0.22	–	–

Quark mass parameters are fitted to get the experimental ground state masses of m_c=1.31 GeV, m_b=4.66 GeV, α_c=0.4 (for $c\bar{c}$) and α_c=0.3 (for $b\bar{b}$). The potential parameter A also varies with ν [16].

We have done a completely parameter-free computation of digamma and digluon decay widths and radiative electric and magnetic dipole transition widths using the parameters of these phenomenological models that were fixed to obtain the ground state masses of the quarkonia systems.

Table 5. E1 transition partial widths of $c\bar{c}$ (keV).

transitions	ERHM	CPP$_\nu$				[34]	[35]	[23]	[36]	[30]	[22]
		ν=0.5	ν=1.0	ν=1.5	ν=2.0						
$2^3S_1\to1^3P_0$	9.2	6.7	38.2	89.2	145.8	51.7	45	–	47	74	29.8±1.29
$2^3S_1\to1^3P_1$	18.6	13.8	73.6	164.6	259.7	44.9	40.9	–	42.8	62	28.2±1.47
$2^3S_1\to1^3P_2$	11.3	8.4	37.2	72.4	100.3	30.9	26.5	–	30.1	43	26.5±1.3
$3^3S_1\to2^3P_0$	16.4	5.9	51.4	164.3	349.2	–	87.3	–	–	–	
$3^3S_1\to2^3P_1$	43.3	8.4	65.2	192.7	382.9	65.7	–	–	–	–	
$3^3S_1\to2^3P_2$	54.2	1.6	4	4.1	3.1	–	31.6	–	–	–	
$3^3S_1\to1^3P_0$	129.4	105.1	583.9	1389	2274	–	1.2	–	–	–	
$3^3S_1\to1^3P_1$	336.4	281.5	1531	3607	5863	–	2.5	–	–	–	
$3^3S_1\to1^3P_2$	410.1	1897	4379	6998	–	–	3.3	–	–	–	
$1^3P_2\to1^3S_1$	680.7	168	421	652	828	448	390.6	250	315	424	390±26
$1^3P_1\to1^3S_1$	426.2	127	269	363	409	333	287	229	41	314	299±22
$1^3P_0\to1^3S_1$	325.9	110	209	256	264	161	142	173	120	152	133±9
$1^1P_1\to1^1S_0$	1076.2	401	1015	1569	2000	723	610	451	482	498	
$2^3P_2\to2^3S_1$	325.3	151	701	1707	2883	–	358.6	83	–	225	
$2^3P_1\to2^3S_1$	258.9	92	316	596	824	–	208.3	73.8	–	103	
$2^3P_0\to2^3S_1$	231.0	68	190	291	322	–	53.6	49.4	–	61	
$2^1P_1\to2^1S_0$	611.7	184	843	1961	3219	–	–	146.9	–	309	
$2^3P_2\to1^3S_1$	700.1	187	1279	3510	5896	–	33	140	–	101	
$2^3P_1\to1^3S_1$	661.3	160	962	2352	3590	–	28	133	–	83	
$2^3P_0\to1^3S_1$	643.5	146	822	1880	2683	–	21	114	–	74	
$2^3P_1\to1^1S_0$	951.6	93	549	1321	2013	–	–	227	–	134	

Table 6. E1 transition partial widths of $b\bar{b}$ (keV).

transitions	ERHM	CPP$_\nu$				[34]	[35]	[23]	[36]	[30]	[22]
		ν=0.5	ν=1.0	ν=1.5	ν=2.0						
$2^3S_1\to1^3P_0$	0.24	0.06	0.4	1.08	1.63	1.65	1.15	–	1.29	1.67	1.21±0.16
$2^3S_1\to1^3P_1$	0.40	0.12	0.74	1.75	2.71	2.57	1.87	–	2.0	2054	2.21±0.22
$2^3S_1\to1^3P_2$	0.12	0.04	0.38	1.39	3.03	2.53	1.88	–	2.04	2.62	2.29±0.22
$3^3S_1\to2^3P_0$	0.35	0.04	0.32	1.03	2.16	1.65	1.67	–	1.35	1.83	1.2±0.16
$3^3S_1\to2^3P_1$	0.82	0.08	0.62	1.78	3.60	2.65	2.74	–	2.20	2.96	2.56±0.34
$3^3S_1\to2^3P_2$	0.80	0.06	0.30	0.62	0.98	2.89	2.80	–	2.40	3.23	2.66±0.41
$3^3S_1\to1^3P_0$	3.91	2.38	15.4	40.4	72.0	0.124	0.03	–	0.001	0.07	0.055±0.08
$3^3S_1\to1^3P_1$	9.50	6.38	41.1	106.8	188.8	0.307	0.09	–	0.008	0.17	<0.018±0.001
$3^3S_1\to1^3P_2$	9.86	8.22	54.7	153.7	290.8	0.445	0.13	–	0.015	0.25	<0.2±0.32
$1^3P_2\to1^3S_1$	61.96	11.3	26.7	40.1	48.8	42.7	31	44.0	31.6	38	
$1^3P_1\to1^3S_1$	39.58	09.4	21.3	33.3	43.5	37.1	27	42.0	27.8	34	
$1^3P_0\to1^3S_1$	30.72	08.6	18.7	27.8	35.0	29.5	22	37.0	22.0	27	
$1^1P_1\to1^3S_0$	62.70	15.7	37.7	60.4	81.6	–	38	60.0	–	56.8	
$2^3P_2\to2^3S_1$	14.57	04.9	23.4	55.5	96.1	18.8	17	20.4	14.5	18.8	
$2^3P_1\to2^3S_1$	10.65	04.3	18.2	39.5	63.7	15.9	14	12.5	12.4	15.9	
$2^3P_0\to2^3S_1$	8.98	03.9	15.9	32.8	51.1	11.7	10	4.4	9.2	11.7	
$2^1P_1\to2^1S_0$	15.67	05.4	25.4	60.0	102.1	23.6	–	25.8	–	24.7	
$2^3P_2\to1^3S_1$	45.03	09.0	33.0	67.2	104.0	8.41	7.74	20.8	12.7	13	
$2^3P_1\to1^3S_1$	41.71	08.6	30.2	58.9	88.0	8.01	7.31	19.9	12.7	12.4	
$2^3P_0\to1^3S_1$	40.12	08.4	28.8	55.0	80.8	7.36	6.69	14.1	10.9	11.4	
$2^1P_1\to1^1S_1$	49.57	0.3	01.7	04.5	08.2	9.9	–	14.1	10.9	15.9	

3 Digamma and digluon decay widths

Using the model parameters and the radial wave functions, we compute the digamma ($\Gamma_{\gamma\gamma}(\eta_Q)$) and digluon ($\Gamma_{gg}(\chi_Q)$) decay widths. The digamma decay width of the P-wave $Q\bar{Q}$ state χ_{Q1} is forbidden according to the Landau-Yang theorem. Most of the quark model predictions for the S-wave $\eta_Q\to\gamma\gamma$ width are comparable with the experimental result, while the theoretical predictions for the P-wave ($\chi_{Q0,2}\to\gamma\gamma$) widths differ significantly

Table 7. Radiative M1 transition widths of $c\bar{c}$ in (keV).

transition	$1^3S_1\to1^1S_0$	$2^3S_1\to2^1S_0$	$3^3S_1\to3^1S_0$	$2^3S_1\to1^1S_0$
ERHM	0.703 (110)	0.151 (62)	0.023 (17)	20.521 (654)
$CPP_{\nu=0.5}$	1.86	0.03	0.004	16.52
$CPP_{\nu=1.0}$	9.68	0.55	0.135	58.13
$CPP_{\nu=1.5}$	20.45	2.60	0.942	108.44
$CPP_{\nu=2.0}$	38.35	6.92	3.241	157.23
[9]	1.5±1.0	–	–	–
[10]NR	2.90 (116)	0.21 (48)	0.046 (29)	–
[23]	1.29	0.12	0.04	–
[35]	2.7	1.2	–	–
[22]	1.21±0.37	< 0.67	–	3000±500

Table 8. Radiative M1 transition widths of $b\bar{b}$ in (eV).

transition	$1^3S_1\to1^1S_0$	$2^3S_1\to2^1S_0$	$3^3S_1\to3^1S_0$	$2^3S_1\to1^1S_0$
ERHM	2.33 (36)	0.169 (15)	0.050 (10)	1395.9 (580)
$CPP_{\nu=0.5}$	2.51	0.01	0.001	223.23
$CPP_{\nu=1.0}$	9.13	0.17	0.036	799.45
$CPP_{\nu=1.5}$	19.12	0.98	0.244	1629.06
$CPP_{\nu=2.0}$	31.20	2.51	1.088	2514.04
[23]	7.28	0.67	0.19	–
[34]	5.8 (60)	1.40 (33)	0.80 (27)	–
[35]	4.0	0.5	–	–
[36]	8.95	1.51	0.826	–
[37]	9.2	0.6	0.6	–
[38]	7.7 (59)	0.53 (25)	0.13 (16)	–

from the experimental observations [22]. The contribution from QCD corrections takes care of this discrepancy. The one-loop QCD radiative corrections in the digamma decay widths of $^1S_0(\eta_Q)$, $^3P_0(\chi_{Q0})$ and $^3P_2(\chi_{Q2})$ are computed using the non relativistic expressions given by [23, 24]:

$$\Gamma_{\gamma\gamma}(\eta_Q) = \frac{3e_Q^4\alpha_{em}^2 M_{\eta_Q}|R_0(0)|^2}{2m_Q^3}\left[1-\frac{\alpha_s}{\pi}\frac{(20-\pi^2)}{3}\right], \quad (6)$$

$$\Gamma_{\gamma\gamma}(\chi_{Q0}) = \frac{27e_Q^4\alpha_{em}^2 M_{\chi_{Q0}}|R_1^{'}(0)|^2}{2m_Q^5}\left[1+B_0\frac{\alpha_s}{\pi}\right], \quad (7)$$

$$\Gamma_{\gamma\gamma}(\chi_{Q2}) = \frac{4}{15}\frac{27e_Q^4\alpha_{em}^2 M_{\chi_{Q2}}|R_1^{'}(0)|^2}{2m_Q^5}\left[1+B_2\frac{\alpha_s}{\pi}\right], \quad (8)$$

where $B_0=\pi^2/3-28/9$ and $B_2=-16/3$ are the next-to-leading-order (NLO) QCD radiative corrections [25–27].

Similarly, the digluon decay widths of the η_Q, χ_{Q0} and χ_{Q2} states are given by [28]:

$$\Gamma_{gg}(\eta_Q)=\frac{\alpha_s^2 M_{\eta_Q}|R_0(0)|^2}{3m_Q^3}[1+C_Q(\alpha_s/\pi)], \quad (9)$$

$$\Gamma_{gg}(\chi_{Q0})=\frac{3\alpha_s^2 M_{\chi_{Q0}}|R_1^{'}(0)|^2}{m_Q^5}[1+C_{0Q}(\alpha_s/\pi)]. \quad (10)$$

$$\Gamma_{gg}(\chi_{Q2})=\left(\frac{4}{15}\right)\frac{3\alpha_s^2 M_{\chi_{Q2}}|R_1^{'}(0)|^2}{m_Q^5}[1+C_{2Q}(\alpha_s/\pi)]. \quad (11)$$

Here, the quantities in the brackets are the NLO QCD radiative corrections [27] and the coefficients have values of $C_Q=4.4$, $C_{0Q}=10.0$ and $C_{2Q}=-0.1$ for the bottom quark.

4 Radiative E1 and M1 transitions

In the non-relativistic limit, the M1 transition width between two S-wave states is given by [9]

$$\Gamma_{n^3S_1\to n'^1S_0\gamma} = \frac{4}{3}\alpha e_Q^2\frac{k_\gamma^3}{m^2}\left|\int_0^\infty r^2 dr R_{n'0}(r)R_{n0}(r)j_0\left(\frac{k_\gamma r}{2}\right)\right|^2, \quad (12)$$

where e_Q is the fraction of electrical charge of the heavy quark ($e_b=-1/3$, $e_c=2/3$), α is the fine structure constant and $R_{nl}(r)$ are the radial Schrödinger wave functions. The photon energy k_γ is nearly equal to the mass difference of the two quarkonia, so it is of order mv^2 or smaller. This is unlike radiative transitions from a heavy quarkonium to a light meson, such as $J/\psi\to\eta\gamma$, where a hard photon is emitted. Since $r\sim 1/(mv)$, the spherical Bessel function is expanded as $j_0(k_\gamma r/2)=1-(k_\gamma r)^2/24+\cdots$ [9]. While the overlap integral in (12) is unity at leading order for $n=n'$ (allowed transitions), it vanishes for $n\neq n'$ (hindered transitions). The widths of hindered transitions are determined by higher-order and relativistic corrections only.

In the non-relativistic limit, radiative E1 and M1 transition partial widths are given by [9]

$$\Gamma_{n^{2S+1}L_{iJ_i}\to n'^{2S+1}L_{fJ_f}\gamma} = \frac{4\alpha e_Q^2 k_\gamma^3}{3}(2J'+1)\max(L_i,L_f) \times\begin{Bmatrix} J_i & 1 & J_f \\ L_f & S & L_i\end{Bmatrix}\times|\langle f|r|i\rangle|^2, \quad (13)$$

$$\Gamma_{n^3S_1\to n'^1S_0\gamma} = \frac{4}{3}\frac{2J'+1}{2L+1}\delta_{LL'}\delta_{S,S'\pm1}\alpha e_Q^2\frac{k_\gamma^3}{m^2} \times\left|\int_0^\infty r^2 dr R_{n'0}(r)R_{n0}(r)j_0\left(\frac{k_\gamma r}{2}\right)\right|^2. \quad (14)$$

The CLEO-c experiment has measured the magnetic dipole (M1) transitions $J/\psi(1S)\to\gamma\eta_c(1S)$ and $\psi(2S)\to\gamma\eta_c(1S)$ using a combination of inclusive and exclusive techniques reconciling with the theoretical calculations of lattice QCD and effective field theory techniques [8, 9]. M1 transition rates are normally weaker than E1 rates, but they are of more interest because they may allow access to spin-singlet states that are very difficult to produce otherwise. The spectroscopic parameters of ERHM and CPP_ν are utilized for the present computations.

5 Results and conclusions

In this paper, we have employed the masses of the pseudoscalar and vector mesons, their wave functions, and other input parameters from our earlier work [13] for the calculations of the digamma, digluon decay widths as well as E1 & M1 transitions. E1 and M1 radiative transitions of the $c\bar{c}$ and $b\bar{b}$ mesons in the ERHM and Coulomb plus power potential CPP_ν models and computed numerical results are tabulated in Tables 1–8. The digamma and digluon decay widths of the $c\bar{c}$ and $b\bar{b}$ mesons are computed with and without QCD corrections. The ERHM predictions of digamma decay widths of charmonia for the ground state are found to be comparable to the other theoretical results. In case of the CPP_ν model these values are fairly close around $\nu<1$. A similar trend is found in the case of digluon decay rates of charmonia. The digamma and digluon decay widths predicted by the ERHM and CPP_ν models are very close to the other theoretical predictions.

The computations of E1 transition widths are done without any relativistic correction terms. This indicates the possible inclusion of the same in the wave function with a single center size parameter. The E1 and M1 transitions of the $c\bar{c}$ and $b\bar{b}$ mesons have been calculated by several groups (See Tables 5–8) but their predictions are not in mutual agreement. The predictions from References [34, 35] and the CPP_ν model (at $\nu \simeq 1$ for $c\bar{c}$ and at $\nu \simeq 1.5$ for $b\bar{b}$ mesons) are in fair agreement with experimental values. One of the limitations of the CPP_ν model is the inability to obtain the mass spectra of the $c\bar{c}$ and $b\bar{b}$ mesons at the same potential index ν. The computed magnetic radiative transition rates are tabulated along with other theoretical predictions and available experimental values in Tables 7 and 8. The values in the parentheses are the energy of the photon in MeV. The transition widths obtained by the potential models show a large deviation from the experimental data; however, the values computed using effective mean field theories ($\Gamma_{J/\psi\to\eta_c\gamma} = 1.5\pm1.0$ keV and $\Gamma_{\Upsilon(1S)\to\eta_b\gamma} = 3.6\pm2.9$ eV [9]), are found to be nearly the same as the potential model results. The photon energies in all the models are found to be nearly the same as the mass splitting. The wide variation in predicted hyperfine splitting leads to considerable uncertainty in the predicted rates for these transitions. Differences in the theoretical assumptions of the potential models make it difficult to draw sharp conclusion about the validity of a particular model because of the lack of experimental data.

References

1 Wiedner U. Progress in Particle and Nucl. Phys. 2011, **66**: 477
2 Brambilla N et al. hep-ph/0412158
3 Caswell W E, Lepage G P. Phys. Lett. B, 1986, **167**: 437
4 Bodwin G T, Braaten E, Lepage G P. Phys. Rev. D, 1995, **51**: 1125; 1997, **55**: 5853
5 Pineda A, Soto J. Nucl. Phys. Proc. Suppl., 1998, **64**: 428 [arXiv:hep-ph/9707481]
6 Brambilla N, Pineda A, Soto J, Vairo A. Nucl. Phys. B, 2000, **566**: 275 [arXiv:hep-ph/9907240]
7 Brambilla N et al. Eur. Phys. J. C, 2011, **71**: 1534
8 Mitchell R E et al. (CLEO collaboration). Phys. Rev. Lett., 2009, **102**: 011801; Erratum-ibid., 2011, **106**: 159903
9 Brambilla N, JIA Y, Vairo A. Phys. Rev. D, 2006, **73**: 054005
10 Barnes T, Godfrey S, Swanon E S. Phys. Rev. D, 2005, **72**: 054026
11 Vinodkumar P C, Pandya J N, Bannur V M, Khadkikar S B. Eur. Phys. J., A, 1999, **4**: 83
12 Pandya J N, Vinodkumar P C. Pramana J. Phys., 2001 **57**: 821
13 Rai A K, Pandya J N, Vinodkumar P C. Eur. Phys. Jnl. A, 2008, **38**: 77; Jnl. Phys. G, 2005 **31**: 1453
14 Rai A K, Parmar R H, Vinodkumar P C. Jnl. Phys. G, 2002, **28**: 2275
15 Rai A K, Vinodkumar P C. Pramana J. Phys., 2006. **66**: 953
16 Rai A K, Patel B, Vinodkumar P C. Phys. Rev. C, 2008 **78**: 055202
17 Rai A K, Pandya J N, Vinodkumar P C. Nucl. Phys. A, 2007, **782**: 406; Indian J.Phys. A, 2006, **80**: 387
18 Buchmüller W, Tye S H H. Phys. Rev. D, 1981, **24**: 132
19 Khadkikar S B, Gupta S K. Phys. Lett. B, 1983, **124**: 523
20 Gupta S K, Khadkikar S B. Phys. Rev. D, 1987, **36**: 307
21 Jena S N, Behera M R, Panda S. Phys. Rev. D, 1996, **54**: 11
22 Olive K A et al. (Particle Data Group). Chin. Phys. C, 2014 **38**: 090001
23 Parmar A et al. Nucl. Phys. A, 2010, **848**: 299
24 Patel B, Vinodkumar P C. J. Phys. G: Nucl. Part. Phys. 2009 **36**: 035003
25 Kwong Waikwok et al. Phys. Rev. D, 1988 **37**: 3210
26 Barbieri R, Caffo M, Gatto R, Remiddi E. Nucl. Phys. B 1981 **192**: 61
27 Mangano M, Petrelli A. Phys. Lett. B, 1945, **352**: 445
28 Lansberg J P, Pham T N. Phys. Rev. D, 2009, **79**: 094016
29 Shah M, Parmar A, Vinodkumar P C. Phys. Rev. D, 2012, **86**: 034015
30 B. Quing Li, K. Ta Chao. Phys. Rev. D, 2009, **79**: 094004; Bai Quing Li, Kung- Ta Chao. Commun. Theor. Phys. 2009, **52**: 653
31 Schuler G A, Berends F A, van Gulik R. Nucl. Phys. B, 1998, **523**: 423
32 Ahmady M R, Mendel R R. Phys. Rev. D, 1995, **51**: 141
33 Laverty J T, Radford S F, Repko W W. arXiv:0901.3917 [hep-ph]
34 Ebert D, Faustov N, Galkin V O. Phys. Rev. D, 2003, **67**: 014027
35 Radford S F, Repko W W. Phys. Rev. D, 2007 **75**: 074031
36 Brambilla N et al. CERN Yellow Report 2005-005; arxiv://hep-ph/0412158
37 Anisovich V V, Dakhno L G, Matveev M A, Nikonov V A, Sarantsev A V. Phys. Atom. Nucl., 2007, **70**: 63
38 Lähde T A. Nucl.Phys. A, 2003, **714**: 183
39 Gupta Suraj N, Johnson James M, Repko Wayne W. Phys. Rev. D, 1996, **54**: 2075. arXiv:hep-ph/9606349

PHYSICAL REVIEW D **96,** 016017 (2017)

Decay $D \to K^{(*)}\ell^+\nu_\ell$ in covariant quark model

N. R. Soni* and J. N. Pandya†

Applied Physics Department, Faculty of Technology and Engineering,
The Maharaja Sayajirao University of Baroda, Vadodara 390001 Gujarat, India

(Received 6 June 2017; published 24 July 2017)

We study the leptonic and semileptonic D-meson decays ($D \to \ell^+\nu_\ell$ and $D \to K^{(*)}\ell^+\nu_\ell$) in the framework of covariant quark model with built-in infrared confinement. We compute the required form factors in the entire kinematical momentum transfer region. The calculated form factors are used to evaluate the branching fractions of these transitions. We determine the following ratios of the partial widths: $\Gamma(D^0 \to K^- e^+\nu_e)/\Gamma(D^+ \to \bar{K}^0 e^+\nu_e) = 1.02$, $\Gamma(D^0 \to K^-\mu^+\nu_\mu)/\Gamma(D^+ \to \bar{K}^0\mu^+\nu_\mu) = 0.99$ and $\Gamma(D^+ \to \bar{K}^0\mu^+\nu_\mu)/\Gamma(D^+ \to \bar{K}^0 e^+\nu_e) = 0.97$ which are in close resemblance with the isospin invariance and experimental results.

DOI: 10.1103/PhysRevD.96.016017

I. INTRODUCTION

The semileptonic decays involve strong as well as weak interactions. The extraction of Cabibbo-Kobayashi-Maskawa (CKM) matrix elements from these exclusive decays can be parametrized by form factor calculations. As $|V_{cd}|$ and $|V_{cs}|$ are constrained by CKM unitarity, the calculation of semileptonic decays of D-mesons can also be an important test to look for new physics. The decay $D \to K^{(*)}\ell^+\nu_\ell$ provides accurate determination of $|V_{cs}|$. Thus, the theoretical prediction for the form factors and their q^2-dependence need to be tested. A comprehensive review of experimental and theoretical challenges in study of hadronic decays of D and D_s mesons along with required experimental and theoretical tools [1] provide motivation to look into semileptonic decays in this paper.

Recently, BESIII [2–5] and *BABAR* [6] collaborations have reported precise and improved measurements on semileptonic form factors and branching fractions on decays of $D \to K\ell^+\nu_\ell$ and $D \to \pi\ell^+\nu_\ell$. A brief review of the earlier work and present experimental status of D-meson decays are given in [7]. Also there are variety of theoretical models available in the literature for the computation of hadronic form factors. One of the oldest models is based on the quark model known as ISGW model for CP violation in semileptonic B meson decays based on the nonrelativistic constituent quark picture [8]. The advanced version (ISGW2 model [9]) includes the heavy quark symmetry and has been used for semileptonic decays of $B_{(s)}$, $D_{(s)}$ and B_c mesons. The form factors are also calculated in lattice quantum chromodynamics (LQCD) [10–15], light-cone sum rules (LCSR) [16–18] and LCSR with heavy quark effective theory [19]. The form factor calculations from LCSR provide good results at low ($q^2 \simeq 0$) and high ($q^2 \simeq q^2_{\rm max}$) momentum transfers. The form factors have also been calculated for the process $D \to K\ell\nu_\ell$ in the entire momentum transfer range [15] using the LQCD. Also recently the Flavour Lattice Averaging Group (FLAG) have reported the latest lattice results for determination of CKM matrices within the standard model [20].

The form factors of $D, B \to P, V, S$ transitions with P, V and S corresponding to pseudoscalar, vector and scalar meson respectively have been evaluated in the light front quark model (LFQM) [21]. The form factors for $D \to P, V$ are also computed in the framework of chiral quark model (χQM) [22] as well in the phenomenological model based on heavy meson chiral theory (HMχT) [23,24]. The form factors of $B_{(s)}, D_{(s)} \to \pi, K, \eta$ have been evaluated in three flavor hard pion chiral perturbation theory [25]. The form factors for $D \to \pi e^+\nu_e$ have been computed in the framework of "charm-changing current" [26]. The authors of [27,28] have determined the form factors $f_+^{K(\pi)}$ by globally analyzing the available measurements of branching fractions for $D \to K(\pi)e^+\nu_e$. The vector form factors for $D \to K\ell\nu_\ell$ were also parameterized in [29]. The evaluation of transition form factors and decays of $B_{(s)}, D_{(s)} \to f_0(980), K_0^*(1430)\ell\nu_\ell$ has been done in [30,31] from QCD sum rules. The computation of differential branching fractions for $D_{(s)} \to (P, V, S)\ell\nu_\ell$ was also performed using chiral unitary approach [32,33], generalized linear sigma model [34,35] and sum rules [36]. Various decay properties of $D_{(s)}$ and $B_{(s)}$ are also studied in the formalism of semirelativistic [37–40] and relativistic [41–43] potential models.

In this paper, we employ the covariant constituent quark model (CQM) with built-in infrared confinement [44–49] to compute the leptonic and semileptonic decays. The form factors of these transitions are expressed through only few universal functions. One of the key features of CQM is access to the entire physical range of momentum transfer. Our aim is to perform independent calculations of these

*nrsoni-apphy@msubaroda.ac.in
†jnpandya-apphy@msubaroda.ac.in

decays including q^2 behavior of the transition form factors, leptonic decay constants of D and K mesons and ratios of branching fractions for the decay $D \to K^{(*)}\ell^+\nu_\ell$ and $D \to \pi\ell^+\nu_\ell$.

This paper is organized as follows. After a brief introduction of the semileptonic D-meson decays in Sec. I, in Sec. II we introduce the theoretical framework of CQM and also discuss the method of extracting the model parameters. In Sec. III, we give the definition of the form factors for the decays $D \to K^{(*)}\ell^+\nu_\ell$. In Sec. IV for numerical results, we first compute the leptonic branching fractions of D^+-meson. Next we give numerical results of the form factors. We also parametrize the form factors using double pole approximation. From the form factors, we compute the differential branching fraction for the $D \to K^{(*)}\ell^+\nu_\ell$, with $\ell = e$ and μ and the branching fractions. We also calculate the forward-backward asymmetry and convexity parameters. We compare our results with available experimental, lattice and other theoretical results. Finally, we summarize the present work in Sec. V.

II. MODEL

The CQM is an effective quantum field approach [44–49] for hadronic interactions based on an effective Lagrangian of hadrons interacting with their constituent quarks. In this paper, we restrict ourselves to weak decays of D-mesons only. The interaction Lagrangian describing the coupling of meson $M(q_1\bar{q}_2)$ to the constituent quarks q_1 and $\bar{q}_2$ in the framework of CQM is given by

$$\mathcal{L}_{\rm int} = g_M M(x) \int dx_1 dx_2 F_M(x; x_1, x_2)\bar{q}_2(x_2)\Gamma_M q_1(x_1) + \text{H.c.} \quad (1)$$

where Γ_M is the Dirac matrix and projects onto the spin quantum number of relevant mesonic field $M(x)$. g_M is the coupling constant and F_M is the vertex function that is related to the scalar part of the Bethe-Salpeter amplitude. F_M also characterizes the finite size of the mesons. We choose the vertex function that satisfies the Lorentz invariance of the Lagrangian Eq. (1),

$$F_M(x, x_1, x_2) = \delta\left(x - \sum_{i=1}^{2} w_i x_i\right)\Phi_M((x_1 - x_2)^2) \quad (2)$$

with Φ_M is the correlation function of two constituent quarks with masses m_{q_1} and m_{q_2} and $w_{q_i} = m_{q_i}/(m_{q_1} + m_{q_2})$ such that $w_1 + w_2 = 1$. We choose Gaussian function for vertex function as

$$\tilde{\Phi}_M(-p^2) = \exp(p^2/\Lambda_M^2) \quad (3)$$

with the parameter Λ_M characterized by the finite size of the meson. In the Euclidian space, we can write $p^2 = -p_E^2$, so that the vertex function has the appropriate falloff behavior so as to remove the ultraviolet divergence in the loop integral.

We use the compositeness conditions [50,51] to determine the coupling strength g_M in Eq. (5) that requires the renormalization constant Z_M for the bare state to composite mesonic state $M(x)$ set to zero, i.e.,

$$Z_M = 1 - \tilde{\Pi}'_M(m_M^2) = 0, \quad (4)$$

where $\tilde{\Pi}'_M$ is the derivative of meson mass operator and Z_M is the wave function renormalization constant of the meson M. Here, $Z_M^{1/2}$ is the matrix element between the physical state and the corresponding bare state. The above condition guarantees that the physical state does not contain any bare quark state i.e. bound state. The constituents are virtual and are introduced to realize the interaction and as a result the physical state turns dressed and its mass and wave function are renormalized.

The meson mass operator Fig. 1 for any meson is defined as

$$\tilde{\Pi}_M(p^2) = N_c g_M^2 \int \frac{d^4k}{(2\pi)^4 i}\tilde{\Phi}_M^2(-k^2) \times \text{tr}(\Gamma_1 S_1(k + w_1 p)\Gamma_2 S_2(k - w_2 p)) \quad (5)$$

where $N_c = 3$ is the number of colors. Γ_1, Γ_2 are the Dirac matrices and for scalar, vector and pseudoscalar mesons, we choose the gamma matrices accordingly. $S's$ are the quark propagator and we use the free fermion propagator for the constituent quark. For the computation of loop integral in Eq. (5), we write the quark propagator in terms of Fock-Schwinger representation as

$$S_q(k+p) = \frac{1}{m_q - \not{k} - \not{p}} = \frac{m_q + \not{k} + \not{p}}{m_q^2 - (k+p)^2} = (m_q + \not{k} + \not{p})\int_0^\infty d\alpha e^{-\alpha[m_q^2 - (k+p)^2]}, \quad (6)$$

where k is the loop momentum and p is the external momentum. The use of Fock-Schwinger representation allows to do the tensor integral in an efficient way since

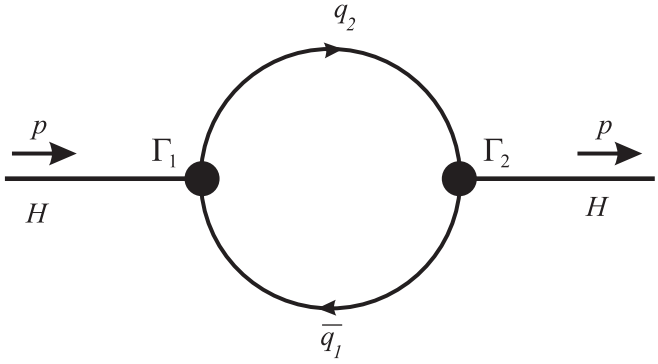

FIG. 1. Diagram describing meson mass operator.

the loop momenta can be converted into the derivative of exponential function [49]. All the necessary trace evaluation and loop integrals are done in FORM [52]. For the remaining integral over the Fock-Schwinger parameters $0 \le \alpha_i \le \infty$, we use an additional integration converting the Fock-Schwinger parameters into a simplex. The transformation reads [53]

$$\prod_{i=1}^{n}\int_0^\infty d\alpha_i f(\alpha_1,\ldots,\alpha_n) = \int_0^\infty dt t^{n-1}\prod_{i=1}^{n}\int d\alpha_i \delta\left(1-\sum_{i=1}^{n}\alpha_i\right) f(t\alpha_1,\ldots,t\alpha_n) \tag{7}$$

For meson case $n = 2$.

While the integral over t in Eq. (7) is convergent below the threshold $p^2 < (m_{q_1} + m_{q_2})^2$, its convergence above threshold $p^2 \ge (m_{q_1} + m_{q_2})^2$ is guaranteed by augmenting the quark mass by an imaginary part, i.e. $m_q \to m_q - i\epsilon, \epsilon > 0$, in the quark propagator Eq. (6). This makes it possible to rotate the integration variable t to the imaginary axis $t \to it$. The integral Eq. (7) in turn becomes convergent but obtains an imaginary part corresponding to quark pair production. However, by reducing the scale of integration at the upper limit corresponding to the introduction of an infrared cutoff

$$\int_0^\infty dt(\ldots) \to \int_0^{1/\lambda^2} dt(\ldots), \tag{8}$$

one can remove all possible thresholds present in the initial quark diagram [49]. Thus the infrared cutoff parameter λ effectively guarantees the confinement of quarks within hadrons.

Before going for the semileptonic decays, we need to specify the independent model parameters namely size parameter of meson Λ and constituent quark masses m_{q_i}. These model parameters are determined by fitting calculated decay constants of basic processes such as leptonic (Fig. 2) and radiative decays to available experimental data

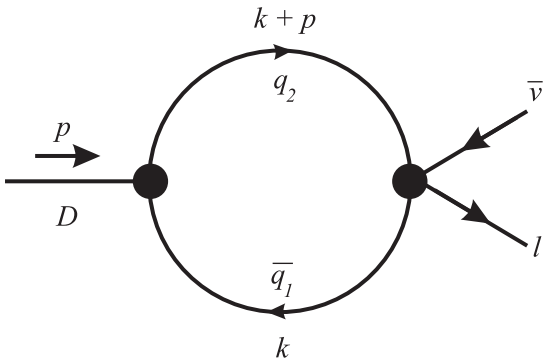

FIG. 2. Quark model diagrams for the D-meson leptonic decay.

TABLE I. Leptonic decay constants f_H (in MeV).

f_H	Present	Data	Reference
f_D	206.1	204.6 ± 5.0	PDG [57]
		207.4 (3.8)	LQCD [58]
		210 ± 11	QCDSR [59]
f_{D^*}	244.3	263 ± 21	QCDSR [59]
		$278 \pm 13 \pm 10$	LQCD [60]
f_{D_s}	257.5	257.5 ± 4.6	PDG [57]
		254 (2) (4)	LQCD [61]
		250.2 ± 3.6	LQCD [12]
		247.2 (4.1)	LQCD [58]
		259 ± 10	QCDSR [59]
$f_{D_s^*}$	272.0	308 ± 21	QCDSR [59]
		311 ± 9	LQCD [60]
f_{D_s}/f_D	1.249	1.258 ± 0.038	PDG [57]
		1.192 (0.22)	LQCD [58]
		1.23 ± 0.07	QCDSR [59]
f_K	156.0	155.0 (1.9)	LQCD [58]
		155.37 (34)	LQCD [62]
		157.9 ± 1.5	LQCD [12]
f_{K^*}	226.8	217 ± 7	PDG [57]
f_π	130.3	132.3 ± 1.6	LQCD [12]
		130.39 (20)	LQCD [62]

or LQCD for vector and pseudoscalar mesons. We use the updated least square fit performed in the recent papers of the model parameters [54–56] (all in GeV). We take the infrared cutoff parameter λ to be the same throughout this study.

$m_{u/d}$	m_s	m_c	m_b	λ	
0.241	0.428	1.67	5.05	0.181	GeV

and the size parameters

Λ_D	Λ_{D^*}	Λ_K	Λ_{K^*}	Λ_π	
1.6	1.53	1.01	0.80	0.87	GeV

We have listed our results for the leptonic decay constants of $D_{(s)}^{(*)}$, $K^{(*)}$ and π mesons in the Table I. The decay constants we use in our calculations match quite well with Particle Data Group (PDG), LQCD and QCD sum rules (QCDSR) results.

III. FORM FACTORS

In the standard model of particle physics, semileptonic decays of any meson is caused by weak force in which one lepton and corresponding neutrino is produced in addition to one or more hadrons (Fig. 3).

The invariant matrix element for the semileptonic $D \to K^{(*)}\ell^+\nu_\ell$ decay can be written as

$$M(D \to K^{(*)}\ell^+\nu_\ell) = \frac{G_F}{\sqrt{2}} V_{cs} \langle K^{(*)}|\bar{s}O^\mu c|D\rangle \ell^+ O^\mu \nu_\ell \tag{9}$$

where $O^\mu = \gamma^\mu(1-\gamma_5)$ is the weak Dirac matrix with left chirality. The matrix elements for the above semileptonic transitions in the covariant quark model are written as

$$\begin{aligned}\langle K_{[\bar{d}s]}(p_2)|\bar{s}O^\mu c|D_{[\bar{d}c]}(p_1)\rangle &= N_c g_D g_K \int \frac{d^4k}{(2\pi)^4 i}\tilde{\phi}_D(-(k+w_{13}p_1)^2)\tilde{\phi}_K(-(k+w_{23}p_2)^2) \\ &\times \mathrm{tr}[O^\mu S_1(k+p_1)\gamma^5 S_3(k)\gamma^5 S_2(k+p_2)] \\ &= F_+(q^2)P^\mu + F_-(q^2)q^\mu \end{aligned} \tag{10}$$

$$\begin{aligned}\langle K^*_{[\bar{d}s]}(p_2,\epsilon_\nu)|\bar{s}O^\mu c|D_{[\bar{d}c]}(p_1)\rangle &= N_c g_D g_{K^*} \int \frac{d^4k}{(2\pi)^4 i}\tilde{\phi}_D(-(k+w_{13}p_1)^2)\tilde{\phi}_{K^*}(-(k+w_{23}p_2)^2) \\ &\times \mathrm{tr}[O^\mu S_1(k+p_1)\gamma^5 S_3(k)\epsilon_\nu^\dagger S_2(k+p_2)] \\ &= \frac{\epsilon_\nu^\dagger}{m_1+m_2}[-g^{\mu\nu}P\cdot qA_0(q^2) + P^\mu P^\nu A_+(q^2) + q^\mu P^\nu A_-(q^2) + i\varepsilon^{\mu\nu\alpha\beta}P_\alpha q_\beta V(q^2)] \end{aligned} \tag{11}$$

with $P = p_1 + p_2$, $q = p_1 - p_2$ and ϵ_ν to be the polarization vector such that $\epsilon_\nu^\dagger \cdot p_2 = 0$ and on-shell conditions of particles require $p_1^2 = m_1^2 = m_D^2$ and $p_2^2 = m_2^2 = m_{K^{(*)}}^2$. Since there are three quarks involved in this transition, we use the notation $w_{ij} = m_{q_j}/(m_{q_i} + m_{q_j})$ $(i,\ j = 1,\ 2,\ 3)$ such that $w_{ij} + w_{ji} = 1$.

IV. NUMERICAL RESULTS

Having determined the necessary model parameters and form factors, we are now in position to present our numerical results. We first compute pure leptonic decays of D^+-meson and then using the form factors obtained in Sec. III, we compute branching fractions for semileptonic D-meson decays.

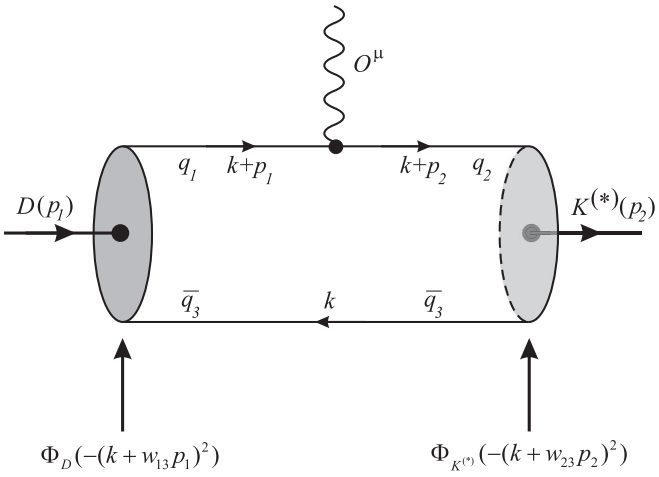

FIG. 3. Quark model diagrams for the D-meson semileptonic decay.

We compute the pure leptonic decays of $D^+ \to \ell^+\nu_\ell$ within the standard model. The branching fraction for leptonic decay is given by

$$\mathcal{B}(D^+ \to \ell^+\nu_\ell) = \frac{G_F^2}{8\pi} m_D m_\ell^2 \left(1 - \frac{m_\ell^2}{m_D^2}\right)^2 f_D^2 |V_{cd}|^2 \tau_D \tag{12}$$

where G_F is the fermi coupling constant, m_D and m_ℓ are the D-meson and lepton masses respectively and τ_D is the D-meson lifetime. f_D is the leptonic decay constant of D-meson from Table I. The resultant branching fractions for $\ell = \tau$, μ and e are given in Table II. It is important to note that the helicity flip factor $(1 - m_\ell^2/m_D^2)$ affects the leptonic branching fractions because of the different lepton masses. We also compare our results with the experimental data. The branching fraction for $D^+ \to \mu^+\nu_\mu$ shows very good agreement with BESIII [63] and CLEO-c [64] data. The branching fractions for $D^+ \to e^+\nu_e$ and $D^+ \to \tau^+\nu_\tau$ also fulfill the experimental constraints.

In Figs. 4 and 5, we plot our calculated form factors as a function of momentum transfer squared in the entire range $0 \le q^2 \le q^2_{\max} = (m_D - m_{K^{(*)}})^2$. The multidimensional integral (three-fold for semileptonic case) appearing in Eqs. (10) and (11) are computed numerically using

TABLE II. Leptonic D^+-decay branching fraction ($\tau_{D^+} = 1.040 \times 10^{-12}$ s [57]).

Channel	Present	Data	Reference
$D^+ \to e^+\nu_e$	8.953×10^{-9}	$<8.8 \times 10^{-6}$	PDG [57]
$D^+ \to \mu^+\nu_\mu$	3.803×10^{-4}	$(3.71 \pm 0.19) \times 10^{-4}$	BESIII [63]
		$(3.82 \pm 0.32) \times 10^{-4}$	CLEO-c [64]
$D^+ \to \tau^+\nu_\tau$	1.013×10^{-3}	$<1.2 \times 10^{-3}$	PDG [57]

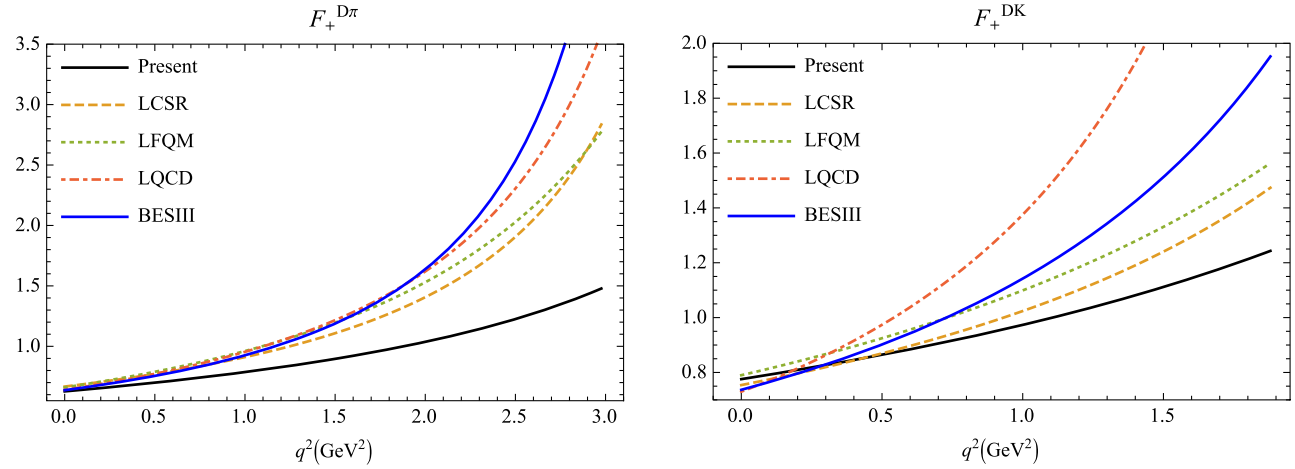

FIG. 4. The results for the form factors appearing in Eq. (10) for semileptonic $D \to \pi$ and $D \to K$ transitions. We compare our plot with the results from LCSR Ref. [18], LFQM Ref. [21], LQCD Ref. [10] as well with the BESIII data Ref. [4].

Mathematica. Our form factor results are also well represented by the double-pole parametrization

$$F(q^2) = \frac{F(0)}{1 - as + bs^2}, \qquad s = \frac{q^2}{m_1^2}. \tag{13}$$

The numerical results of form factors and associated double-pole parameters are listed in Table III. In Fig. 4, we plot the form factor F_+ for $D \to K(\pi)\ell^+\nu_\ell$ decays in the entire kinematical range of momentum transfer. We compare our plot with the results from LCSR Ref. [18], LFQM

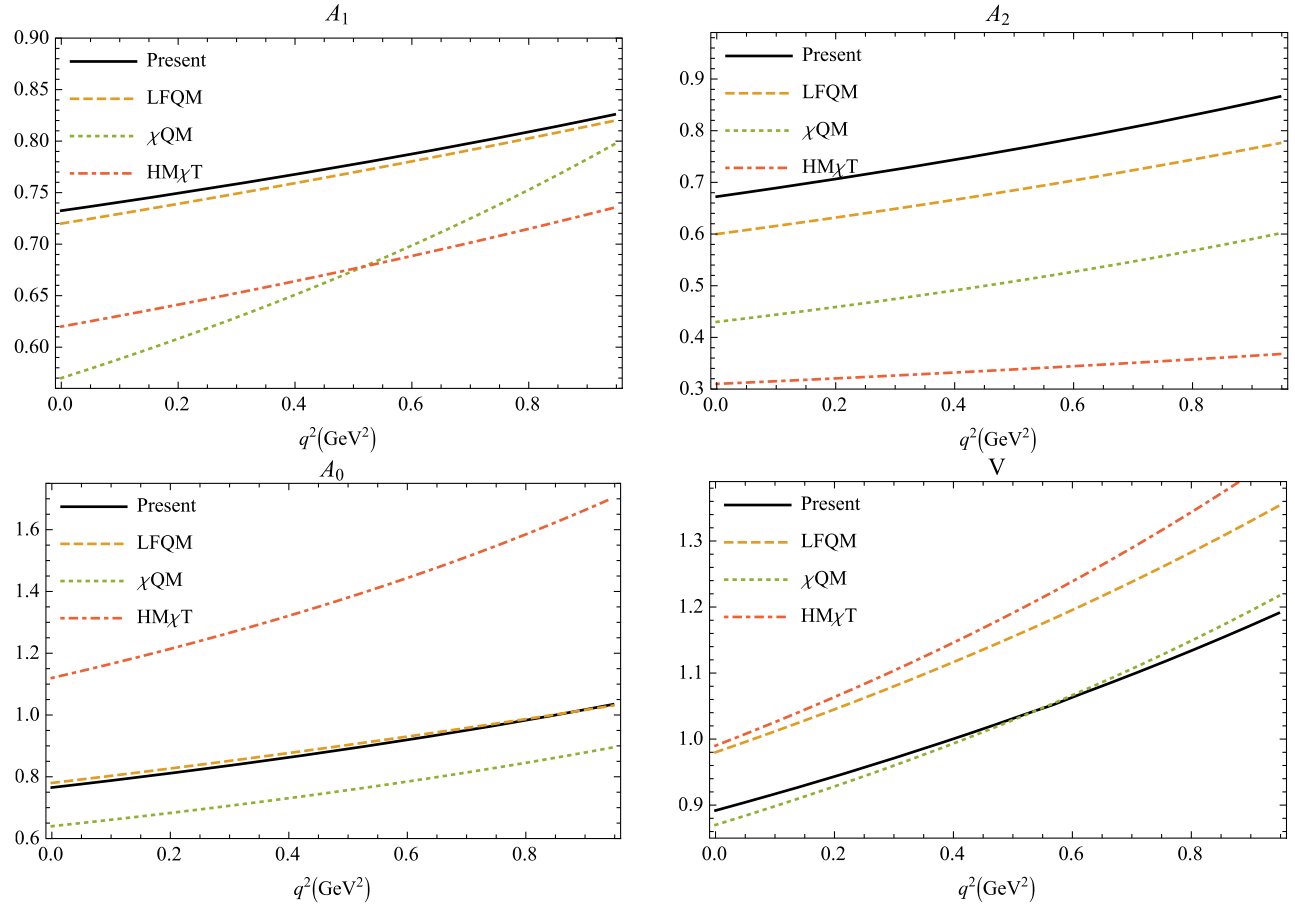

FIG. 5. The form factors appearing in Eq. (11) for semileptonic $D \to K^*$ transitions. We compare our results with LFQM Ref. [21], chiral quark model (χQM) Ref. [22] and heavy meson chiral theory (HMχT) [24].

TABLE III. Double pole parameters for the computation of form factors in Eq. (13).

	F_+	F_-	A_0	A_+	A_-	V
$F(0)$	0.76	−0.39	2.07	0.67	−0.90	0.89
a	0.72	0.75	0.39	0.84	0.95	0.96
b	0.046	0.032	−0.10	0.087	0.13	0.13

Ref. [21], LQCD Ref. [10] as well with the BESIII data Ref. [4]. Our results at maximum recoil point $q^2 \to 0$ are in very good agreement with the other approaches as well as with the experimental result. A similar plot can be obtained for form factor F_-. We also plot the vector form factors and for the comparison of the form factors for $D \to K^* \ell^+ \nu_\ell$ transition with other approaches, we need to write our form factors Eq. (11) in terms of those used in Ref. [17]. The relations read

$$A_0 = \frac{m_1 + m_2}{m_1 - m_2} A_1, \qquad A_+ = A_2,$$
$$A_- = \frac{2m_2(m_1 + m_2)}{q^2}(A_3 - A_0), \qquad V = V. \quad (14)$$

The form factors in Eq. (14) also satisfy the constraints

$$A_0(0) = A_3(0)$$
$$2m_2 A_3(q^2) = (m_1 + m_2)A_1(q^2) - (m_1 - m_2)A_2(q^2). \quad (15)$$

Figure 5 shows form factors from the present calculation along with the results from LFQM [21], chiral quark model (χQM) [22] and with heavy meson chiral theory (HMχT) [24]. The plot shows that our results of the form factors A_0, A_1 and A_2 match with LFQM [21] and the vector form factors match with the χQM [22] where the authors have used energy scaling parameters extracted from modified low energy effective theory in $H \to V$ transitions. Our results show little deviation from those obtained using HMχT [24]. In computation of form factors for $q^2 = 0$ using LCSR, the authors of [18] have used the $\overline{\text{MS}}$ scheme for c-quark mass and the computation of form factors for $q \geq 0$ is performed in the form of conformal mapping and series parametrization. In the LFQM [21], the authors have used the method of double pole approximation, where as in BESIII [4] and *BABAR* [6] experiment, the form factors are parametrized in terms of two and three parameters series expansion respectively.

The differential branching fractions for semileptonic $D \to K \ell^+ \nu_\ell$ decay are computed using [65,66]

$$\frac{d\Gamma(D \to K \ell^+ \nu_\ell)}{dq^2} = \frac{G_F^2 |V_{cs}|^2 |p_2| q^2 v^2}{12(2\pi)^3 m_1^2} \times ((1 + \delta_\ell)\mathcal{H}_L + 3\delta_\ell \mathcal{H}_{SL}) \quad (16)$$

where the helicity flip factor $\delta_\ell = m_\ell^2/2q^2$, $|p_2| = \lambda^2(m_1^2, m_2^2, q^2)/2m_1$ is momentum of K meson in the rest frame of D-meson and velocity-type parameter $v = 1 - m_\ell^2/q^2$.

The bilinear combinations of the helicity amplitudes $\mathcal{H}$ are defined as [48],

$$\mathcal{H}_L = |H_0|^2, \qquad \mathcal{H}_S = |H_t|^2, \qquad \mathcal{H}_{SL} = \text{Re}(H_0 H_t^\dagger) \quad (17)$$

and the helicity amplitudes are expressed via the form factor in the matrix element as,

$$H_t = \frac{1}{\sqrt{q^2}}(PqF_+ + q^2 F_-) \quad (18)$$

$$H_0 = \frac{2m_1|p_2|}{\sqrt{q^2}} F_+. \quad (19)$$

Similarly the differential branching fractions for semileptonic $D \to K^* \ell^+ \nu_\ell$ decay is computed by [65,66]

$$\frac{d\Gamma(D \to K^* \ell^+ \nu_\ell)}{dq^2} = \frac{G_F^2 |V_{cs}|^2 |p_2| q^2 v^2}{12(2\pi)^3 m_1^2} \times ((1 + \delta_\ell)(\mathcal{H}_U + \mathcal{H}_L) + 3\delta_\ell \mathcal{H}_S). \quad (20)$$

The bilinear combinations of the helicity amplitudes $\mathcal{H}$ are defined as [48]

$$\mathcal{H}_U = |H_{+1+1}|^2 + |H_{-1-1}|^2,$$
$$\mathcal{H}_P = |H_{+1+1}|^2 - |H_{-1-1}|^2,$$
$$\mathcal{H}_L = |H_{00}|^2, \qquad \mathcal{H}_S = |H_{t0}|^2,$$
$$\mathcal{H}_{SL} = \text{Re}(H_{00} H_{t0}^\dagger) \quad (21)$$

here also the helicity amplitudes are expressed via the form factor in the matrix element as

$$H_{t0} = \frac{1}{m_1 + m_2} \frac{m_1|p_2|}{m_2\sqrt{q^2}}(Pq(-A_0 + A_+) + q^2 A_-) \quad (22)$$

$$H_{\pm 1 \pm 1} = \frac{1}{m_1 + m_2}(-PqA_0 \pm 2m_1|p_2|V) \quad (23)$$

$$H_{00} = \frac{1}{m_1 + m_2} \frac{1}{2m_2\sqrt{q^2}} \times (-Pq(m_1^2 - m_2^2 - q^2)A_0 + 4m_1^2|p_2|^2 A_+). \quad (24)$$

In Fig. 6, we present our results for differential branching fractions of $D \to K^{(*)} \ell^+ \nu_\ell$ in the entire kinematical range of momentum transfer. The semileptonic branching

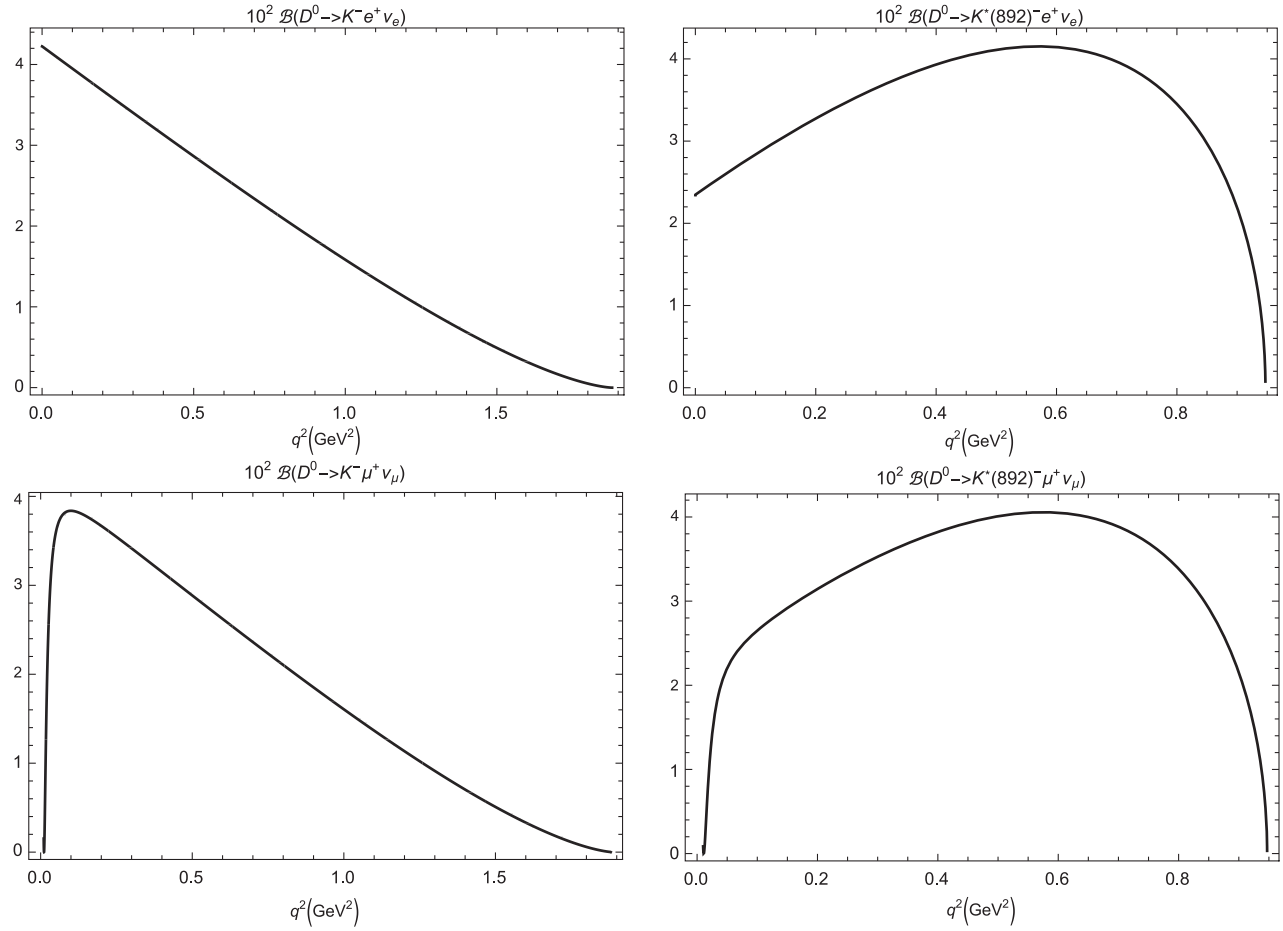

FIG. 6. Differential branching fractions of the decays $D \to K^{(*)}\ell^+\nu_\ell$.

TABLE IV. Branching fractions of $D \to K^{(*)}\ell^+\nu_\ell$ and $D \to \pi\ell^+\nu_\ell$ (in %).

Channel	Present	Data	Reference
$D^+ \to \bar{K}^0 e^+\nu_e$	8.84	$8.60 \pm 0.06 \pm 0.15$	BESIII [2]
		$8.83 \pm 0.10 \pm 0.20$	CLEO-c [72]
$D^+ \to \bar{K}^0\mu^+\nu_\mu$	8.60	$8.72 \pm 0.07 \pm 0.18$	BESIII [3]
$D^+ \to \pi^0 e^+\nu_e$	0.619	$0.363 \pm 0.08 \pm 0.05$	BESIII [2]
		$0.405 \pm 0.016 \pm 0.009$	CLEO-c [72]
$D^+ \to \pi^0\mu^+\nu_\mu$	0.607	–	–
$D^+ \to \bar{K}^*(892)^0 e^+\nu_e$	8.35	–	–
$D^+ \to \bar{K}^*(892)^0\mu^+\nu_\mu$	7.94	–	–
$D^0 \to K^- e^+\nu_e$	3.46	3.538 ± 0.033	PDG [57]
		$3.505 \pm 0.014 \pm 0.033$	BESIII [4]
		$3.50 \pm 0.03 \pm 0.04$	CLEO-c [72]
		$3.45 \pm 0.07 \pm 0.20$	Belle [73]
$D^0 \to K^-\mu^+\nu_\mu$	3.36	3.33 ± 0.13	PDG [57]
		$3.505 \pm 0.014 \pm 0.033$	BESIII
$D^0 \to \pi^- e^+\nu_e$	0.239	$0.2770 \pm 0.0068 \pm 0.0092$	*BABAR* [6]
		$0.295 \pm 0.004 \pm 0.003$	BESIII [4]
		$0.288 \pm 0.008 \pm 0.003$	CLEO-c [72]
		$0.255 \pm 0.019 \pm 0.016$	Belle [73]
$D^0 \to \pi^-\mu^+\nu_\mu$	0.235	0.238 ± 0.024	PDG [57]
$D^0 \to K^*(892)^- e^+\nu_e$	3.25	2.16 ± 0.16	PDG [57]
$D^0 \to K^*(892)^-\mu^+\nu_\mu$	3.09	1.92 ± 0.25	PDG [57]

TABLE V. Ratios of the semileptonic decays of D mesons.

Ratio	Value
$\Gamma(D^0 \to K^- e^+ \nu_e)/\Gamma(D^+ \to \bar{K}^0 e^+ \nu_e)$	1.02
$\Gamma(D^0 \to K^- \mu^+ \nu_\mu)/\Gamma(D^+ \to \bar{K}^0 \mu^+ \nu_\mu)$	0.99
$\Gamma(D^+ \to \bar{K}^0 \mu^+ \nu_\mu)/\Gamma(D^+ \to \bar{K}^0 e^+ \nu_e)$	0.97

fractions in Eqs. (16) and (20) are computed by numerically integrating the differential branching fractions shown in Fig. 6. The branching fractions for $D \to K^{(*)} \ell^+ \nu_\ell$ and $D \to \pi \ell^+ \nu_\ell$ are presented in Table IV. We also compare our results with experimental results. The results for $\mathcal{B}(D^+ \to \bar{K}^0 \ell^+ \nu_\ell)$ and $\mathcal{B}(D^0 \to K^- \ell^+ \nu_\ell)$, ($\ell = e$ and μ) show excellent agreement with the recent BESIII data [2–4] as well with the other experimental collaborations. Also the ratios of the different semileptonic decay widths for the channels $D \to K \ell^+ \nu_\ell$ are presented in Table V and our results are well within the isospin conservation rules given in Ref. [67]. We also present our results for $\mathcal{B}(D^0 \to K^*(892)^- \ell^+ \nu_e)$ but our results overestimate the data given in PDG [57]. This deviation of the present study within the standard model might be explained through hadronic uncertainty or ratios of differential distributions for longitudinal and transverse polarizations of these K^* mesons [68]. The FOCUS [69] and CLEO-c [70] experiments have also reported mixing of scalar amplitudes with dominant vector decays. These observations open up new possibilities of investigations in charm semileptonic decays. There have also been attempts to explain these exclusive decays using R-parity violating supersymmetric effects [71] and their direct correlation with possible supersymmetric signals expected from LHC and BESIII data. We predict the branching fractions for $D^+ \to \bar{K}^*(892)^0 \ell^+ \nu_e$ but we do not compare our results since no experimental results are available for this channel.

We also present our results for branching fractions of $D^+ \to \pi^0 \ell^+ \nu_\ell$ and $D^0 \to \pi^- \ell^+ \nu_\ell$ transitions. Our prediction for $\mathcal{B}(D^+ \to \pi^0 e^+ \nu_e)$ is higher than BESIII [2] and CLEO-c data [72] while the trend is opposite in the case of $\mathcal{B}(D^0 \to \pi^- e^+ \nu_e)$. The deviation of the $\mathcal{B}(D^+ \to \pi^0 e^+ \nu_e)$ from experimental and LQCD data might be attributed to the computed form factors. However, our $\mathcal{B}(D^0 \to \pi^- e^+ \nu_e)$ is in close proximity to that by Belle [73] and $\mathcal{B}(D^0 \to \pi^- \mu^+ \nu_\mu)$ is in excellent agreement with PDG data [57].

We also list some more physical observables in terms of helicity amplitudes. We have already shown the computed differential branching fractions in Fig. 6. Next, the helicity amplitudes defined above are used to plot the

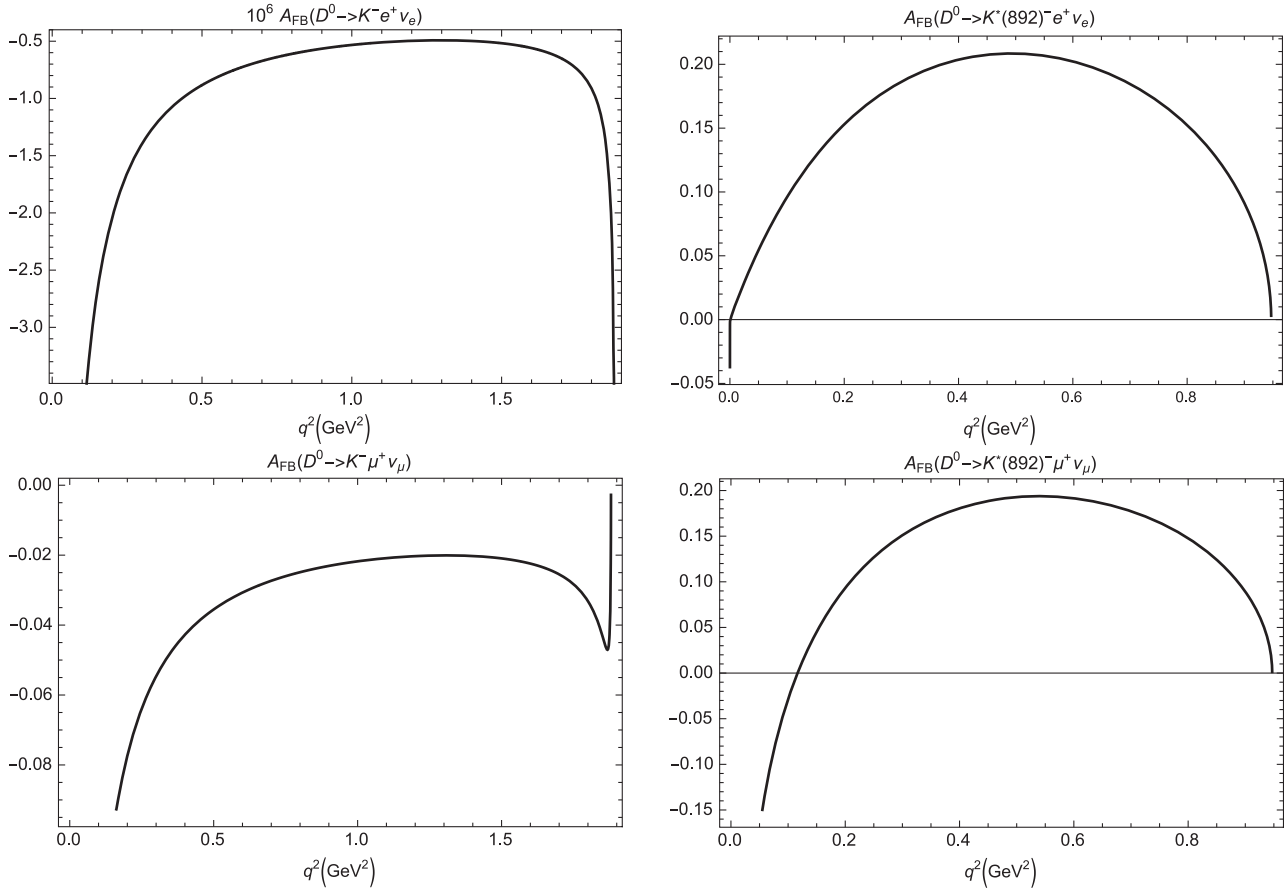

FIG. 7. Forward-backward asymmetries of the decays $D \to K^{(*)} \ell^+ \nu_\ell$.

TABLE VI. Averages of forward-backward asymmetry and convexity parameters.

Channel	ℓ	$\langle A_{FB}^{\ell}\rangle$	$\langle C_F^{\ell}\rangle$	$\langle C_F^{h}\rangle$
$D \to K$	e	-4.27×10^{-6}	-1.5	3
	μ	-0.058	-1.32	3
$D \to K^*$	e	0.17	-0.45	0.91
	μ	0.13	-0.37	0.89

forward-backward asymmetry in Fig. 7 for $D \to K^{(*)}\ell^+\nu_\ell$ in the entire kinematical range of momentum transfer. We use the following relation for plotting the forward-backward asymmetry (A_{FB}) [55,65]

$$\mathcal{A}_{FB}(q^2) = -\frac{3}{4}\frac{\mathcal{H}_P + 4\delta_\ell \mathcal{H}_{SL}}{(1+\delta_\ell)(\mathcal{H}_U + \mathcal{H}_L) + 3\delta_\ell \mathcal{H}_S}. \quad (25)$$

It is evident from Fig. 7 that the $A_{FB}(q^2)$ for $D \to K\ell^+\nu_\ell$ and $D \to K^*\ell^+\nu_\ell$ are similar for both e and μ modes. $A_{FB}(q^2) \to 0$ for in the both zero recoil and larger recoil limits because of the zero recoil relations of the helicity functions $\mathcal{H}_P = \mathcal{H}_{SL} = 0$ and longitudinal dominance in the partial rates at the maximum recoil.

Also the lepton and hadron side convexity parameter are defined as [55,65]

$$C_F^{\ell} = \frac{3}{4}\frac{(1-2\delta_\ell)(\mathcal{H}_U - 2\mathcal{H}_L)}{(1+\delta_\ell)(\mathcal{H}_U + \mathcal{H}_L) + 3\delta_\ell \mathcal{H}_S} \quad (26)$$

and

$$C_F^{h} = -\frac{3}{2}\frac{(1+\delta_\ell)(\mathcal{H}_U - 2\mathcal{H}_L) - 6\delta_\ell \mathcal{H}_S}{(1+\delta_\ell)(\mathcal{H}_U + \mathcal{H}_L) + 3\delta_\ell \mathcal{H}_S}. \quad (27)$$

The plot for the convexity parameters Eqs. (26) and (27) as a function of entire momentum transfer range can easily be obtained. In Table VI, we give the q^2 averages of the above observables. Note that in order to obtain the averages of these observables, we need to multiply the numerator and denominator by phase space factor $|p_2|q^2v^2$. Also in computation of leptonic and semileptonic branching fractions, forward-backward asymmetry and convexity parameters, the values of CKM matrices namely $|V_{cs}|$ and $|V_{cd}|$, meson masses, lepton masses and their lifetimes are taken from PDG [57].

V. CONCLUSION

In this article, we have analyzed the leptonic ($D^+ \to e^+\nu_e$) and semileptonic ($D \to K^{(*)}\ell^+\nu_\ell$, $D \to \pi\ell^+\nu_\ell$) decays using covariant quark model with infrared confinement within the standard model framework. The ratios of the partial widths are found to be consistent with the isospin conservation holding within uncertainties in experimental data. It is interesting to note here that the $\mathcal{B}(D^+ \to \pi^0\ell^+\nu_\ell)$ deviate from existing data while $\mathcal{B}(D^0 \to \pi^-\ell^+\nu_\ell)$ match well. Further exploration to this observation may lead to interesting outcome.

The deviation of branching fractions in case of $D \to K^*\ell\nu_\ell$ might be understood by underlying hadronic uncertainty or ratios of differential distributions for longitudinal and transverse polarizations of the K^* mesons. We are looking forward to analyzing $D \to K^*\ell^+\nu_\ell$ decay and expect the experimental facilities to throw more light on their form factor shapes in forthcoming attempts that will help in understanding the charm decays and possibly the dynamics of these systems beyond the standard model.

ACKNOWLEDGMENTS

We thank Prof. Mikhail A. Ivanov for the continuous support through out this work and providing critical remarks for improvement of the manuscript. N. R. S. would like to thank Bogoliubov Laboratory of Theoretial Physics, Joint Institute for Nuclear Research for warm hospitality during Helmholtz-DIAS International Summer School "Quantum Field Theory at the Limits: from Strong Field to Heavy Quarks" where this work was initiated. This work is done under Major Research Project F.No. 42-775/2013 (SR) with financial support from the University Grants Commission of India.

[1] A. Ryd and A. A. Petrov, Rev. Mod. Phys. **84**, 65 (2012).
[2] M. Ablikim *et al.* (BESIII Collaboration), arXiv:1703.09084.
[3] M. Ablikim *et al.* (BESIII Collaboration), Eur. Phys. J. C **76**, 369 (2016).
[4] M. Ablikim *et al.* (BESIII Collaboration), Phys. Rev. D **92**, 072012 (2015).
[5] M. Ablikim *et al.* (BESIII Collaboration), Phys. Rev. D **92**, 112008 (2015).
[6] J. P. Lees *et al.* (*BABAR* Collaboration), Phys. Rev. D **91**, 052022 (2015).
[7] Y. Amhis *et al.*, arXiv:1612.07233.
[8] N. Isgur, D. Scora, B. Grinstein, and M. B. Wise, Phys. Rev. D **39**, 799 (1989).
[9] D. Scora and N. Isgur, Phys. Rev. D **52**, 2783 (1995).
[10] C. Aubin *et al.* (Fermilab Lattice, HPQCD, MILC Collaboration), Phys. Rev. Lett. **94**, 011601 (2005).

[11] C. Bernard *et al.* (Fermilab Lattice and MILC Collaborations), Phys. Rev. D **80**, 034026 (2009).
[12] H. Na, C. T. H. Davies, E. Follana, G. P. Lepage, and J. Shigemitsu (HPQCD Collaboration), Phys. Rev. D **82**, 114506 (2010).
[13] A. Al-Haydari, A. Ali Khan, V. M. Braun, S. Collins, M. Göckeler, G. N. Lacagnina, M. Panero, A. Schäfer, and G. Schierholz (QCDSF Collaboration), Eur. Phys. J. A **43**, 107 (2010).
[14] H. Na, C. T. H. Davies, E. Follana, J. Koponen, G. P. Lepage, and J. Shigemitsu (HPQCD Collaboration), Phys. Rev. D **84**, 114505 (2011).
[15] J. Koponen, C. T. H. Davies, G. C. Donald, E. Follana, G. P. Lepage, H. Na, and J. Shigemitsu, arXiv:1305.1462.
[16] A. Khodjamirian, R. Ruckl, S. Weinzierl, C. W. Winhart, and O. I. Yakovlev, Phys. Rev. D **62**, 114002 (2000).
[17] A. Khodjamirian, T. Mannel, and N. Offen, Phys. Rev. D **75**, 054013 (2007).
[18] A. Khodjamirian, C. Klein, T. Mannel, and N. Offen, Phys. Rev. D **80**, 114005 (2009).
[19] W. Y. Wang, Y. L. Wu, and M. Zhong, Phys. Rev. D **67**, 014024 (2003).
[20] S. Aoki *et al.*, Eur. Phys. J. C **77**, 112 (2017).
[21] R. C. Verma, J. Phys. G **39**, 025005 (2012).
[22] T. Palmer and J. O. Eeg, Phys. Rev. D **89**, 034013 (2014).
[23] S. Fajfer and J. F. Kamenik, Phys. Rev. D **71**, 014020 (2005).
[24] S. Fajfer and J. F. Kamenik, Phys. Rev. D **72**, 034029 (2005).
[25] J. Bijnens and I. Jemos, Nucl. Phys. **B846**, 145 (2011).
[26] B. Ananthanarayan, I. Caprini, and I. Sentitemsu Imsong, Eur. Phys. J. A **47**, 147 (2011).
[27] G. Rong, Y. Fang, H. L. Ma, and J. Y. Zhao, Phys. Lett. B **743**, 315 (2015).
[28] Y. Fang, G. Rong, H. L. Ma, and J. Y. Zhao, Eur. Phys. J. C **75**, 10 (2015).
[29] S. Descotes-Genon and A. Le Yaouanc, J. Phys. G **35**, 115005 (2008).
[30] M.-Z. Yang, Phys. Rev. D **73**, 034027 (2006); **73**, 079901 (E) (2006).
[31] I. Bediaga, F. S. Navarra, and M. Nielsen, Phys. Lett. B **579**, 59 (2004).
[32] T. Sekihara and E. Oset, Phys. Rev. D **92**, 054038 (2015).
[33] J.-J. Xie, L.-R. Dai, and E. Oset, Phys. Lett. B **742**, 363 (2015).
[34] A. H. Fariborz, R. Jora, J. Schechter, and M. N. Shahid, Int. J. Mod. Phys. A **30**, 1550012 (2015).
[35] A. H. Fariborz, R. Jora, J. Schechter, and M. Naeem Shahid, Phys. Rev. D **84**, 094024 (2011).
[36] W. Wang and C.-D. Lü, Phys. Rev. D **82**, 034016 (2010).
[37] V. Kher, N. Devlani, and A. K. Rai, Chin. Phys. C **41**, 073101 (2017).
[38] N. Devlani and A. K. Rai, Int. J. Theor. Phys. **52**, 2196 (2013).
[39] N. Devlani and A. K. Rai, Eur. Phys. J. A **48**, 104 (2012).
[40] N. Devlani and A. K. Rai, Phys. Rev. D **84**, 074030 (2011).
[41] M. Shah, B. Patel, and P. C. Vinodkumar, Phys. Rev. D **93**, 094028 (2016).
[42] M. Shah, B. Patel, and P. C. Vinodkumar, Eur. Phys. J. C **76**, 36 (2016).
[43] M. Shah, B. Patel, and P. C. Vinodkumar, Phys. Rev. D **90**, 014009 (2014).
[44] G. V. Efimov and M. A. Ivanov, Int. J. Mod. Phys. A **04**, 2031 (1989).
[45] G. V. Efimov and M. A. Ivanov, *The Quark Confinement Model of Hadrons* (IOP, Bristol, 1993).
[46] M. A. Ivanov and P. Santorelli, Phys. Lett. B **456**, 248 (1999).
[47] M. A. Ivanov, P. Santorelli, and N. Tancredi, Eur. Phys. J. A **9**, 109 (2000).
[48] A. Faessler, T. Gutsche, M. A. Ivanov, J. G. Körner, and V. E. Lyubovitskij, Eur. Phys. J. direct C **4**, 1 (2002).
[49] T. Branz, A. Faessler, T. Gutsche, M. A. Ivanov, J. G. Korner, V. E. Lyubovitskij, and B. Oexl, Phys. Rev. D **81**, 114036 (2010).
[50] A. Salam, Nuovo Cimento **25**, 224 (1962).
[51] S. Weinberg, Phys. Rev. **130**, 776 (1963).
[52] J. A. M. Vermaseren, Nucl. Phys. B, Proc. Suppl. **183**, 19 (2008).
[53] R. P. Feynman, Phys. Rev. **76**, 769 (1949).
[54] S. Dubnička, A. Z. Dubničková, A. Issadykov, M. A. Ivanov, A. Liptaj, and S. K. Sakhiyev, Phys. Rev. D **93**, 094022 (2016).
[55] T. Gutsche, M. A. Ivanov, J. G. Körner, V. E. Lyubovitskij, P. Santorelli, and N. Habyl, Phys. Rev. D **91**, 074001 (2015); **91**, 119907(E).
[56] G. Ganbold, T. Gutsche, M. A. Ivanov, and V. E. Lyubovitskij, J. Phys. G **42**, 075002 (2015).
[57] C. Patrignani *et al.* (Particle Data Group), Chin. Phys. C **40**, 100001 (2016).
[58] N. Carrasco *et al.* (ETM Collaboration), Phys. Rev. D **91**, 054507 (2015).
[59] Z.-G. Wang, Eur. Phys. J. C **75**, 427 (2015).
[60] D. Becirevic, V. Lubicz, F. Sanfilippo, S. Simula, and C. Tarantino, J. High Energy Phys. 02 (2012) 042.
[61] Y.-B. Yang *et al.*, Phys. Rev. D **92**, 034517 (2015),
[62] R. J. Dowdall, C. T. H. Davies, G. P. Lepage, and C. McNeile, Phys. Rev. D **88**, 074504 (2013).
[63] M. Ablikim *et al.* (BESIII Collaboration), Phys. Rev. D **89**, 051104 (2014).
[64] B. I. Eisenstein *et al.* (CLEO Collaboration), Phys. Rev. D **78**, 052003 (2008).
[65] M. A. Ivanov, J. G. Körner, and C. T. Tran, Phys. Rev. D **92**, 114022 (2015).
[66] M. A. Ivanov, J. G. Körner, and C. T. Tran, Phys. Rev. D **94**, 094028 (2016).
[67] J. G. Körner and G. A. Schuler, Z. Phys. C **46**, 93 (1990).
[68] S. Fajfer, I. Nišandžić, and U. Rojec, Phys. Rev. D **91**, 094009 (2015).
[69] J. M. Link *et al.* (FOCUS Collaboration), Phys. Lett. B **535**, 43 (2002).
[70] M. R. Shepherd *et al.* (CLEO Collaboration), Phys. Rev. D **74**, 052001 (2006).
[71] R.-M. Wang, J. Zhu, J.-H. Sheng, M.-L. Liu, and Y.-G. Xu, Nucl. Phys. **B901**, 22 (2015).
[72] D. Besson *et al.* (CLEO Collaboration), Phys. Rev. D **80**, 032005 (2009).
[73] L. Widhalm *et al.* (Belle Collaboration), Phys. Rev. Lett. **97**, 061804 (2006).

Erratum: Decay $D \to K^{(*)}\ell^+\nu_\ell$ in covariant quark model [Phys. Rev. D 96, 016017 (2017)]

N. R. Soni and J. N. Pandya

(Received 15 February 2019; published 4 March 2019)

DOI: 10.1103/PhysRevD.99.059901

For computing the branching fraction for $D^+ \to \pi^0\ell^+\nu_\ell$ using Eq. (20), there was a factor of $1/2$ missing. The updated correct results of the branching fraction (Table IV) should read $\mathcal{B}(D^+ \to \pi^0 e^+\nu_e) = 0.309\%$ and $\mathcal{B}(D^+ \to \pi^0\mu^+\nu_\mu) = 0.303\%$. Accordingly, in the numerical results section, the statement, "Our prediction for $\mathcal{B}(D^+ \to \pi^0 e^+\nu_e)$ is higher than BESIII [2] and CLEO-c data [72] while the trend is opposite in the case of $\mathcal{B}(D^0 \to \pi^- e^+\nu_e)$." (on page 8) should be read as, "Our predictions for $\mathcal{B}(D^+ \to \pi^0 e^+\nu_e)$ and $\mathcal{B}(D^0 \to \pi^- e^+\nu_e)$ are lower than BESIII [2] and CLEO-c data [72] data." The other numerical results of the paper are not affected by this unintended error. The conclusion remains unchanged.

Eur. Phys. J. C (2018) 78:592
https://doi.org/10.1140/epjc/s10052-018-6068-6

THE EUROPEAN PHYSICAL JOURNAL C

Regular Article - Theoretical Physics

$Q\bar{Q}$ ($Q \in \{b, c\}$) spectroscopy using the Cornell potential

N. R. Soni[a], **B. R. Joshi, R. P. Shah, H. R. Chauhan, J. N. Pandya**[b]

Applied Physics Department, Faculty of Technology and Engineering, The Maharaja Sayajirao University of Baroda, Vadodara, Gujarat 390001, India

Received: 17 November 2017 / Accepted: 13 July 2018

Abstract The mass spectra and decay properties of heavy quarkonia are computed in nonrelativistic quark-antiquark Cornell potential model. We have employed the numerical solution of Schrödinger equation to obtain their mass spectra using only four parameters namely quark mass (m_c, m_b) and confinement strength ($A_{c\bar{c}}$, $A_{b\bar{b}}$). The spin hyperfine, spin-orbit and tensor components of the one gluon exchange interaction are computed perturbatively to determine the mass spectra of excited S, P, D and F states. Digamma, digluon and dilepton decays of these mesons are computed using the model parameters and numerical wave functions. The predicted spectroscopy and decay properties for quarkonia are found to be consistent with available data from experiments, lattice QCD and other theoretical approaches. We also compute mass spectra and life time of the B_c meson without additional parameters. The computed electromagnetic transition widths of heavy quarkonia and B_c mesons are in tune with available experimental data and other theoretical approaches.

1 Introduction

Mesonic bound states having both heavy quark and antiquark ($c\bar{c}$, $b\bar{b}$ and $c\bar{b}$) are among the best tools for understanding the quantum chromodynamics. Many experimental groups such as CLEO, LEP, CDF, D0 and NA50 have provided data and *BABAR*, Belle, CLEO-III, ATLAS, CMS and LHCb are producing and expected to produce more precise data in upcoming experiments. Comprehensive reviews on the status of experimental heavy quarkonium physics are found in literature [1–6].

Within open flavor threshold, the heavy quarkonia have very rich spectroscopy with narrow and experimentally characterized states. The potential between the interacting quarks within the hadrons demands the understanding of underlying physics of strong interactions. In PDG [7], large amount of experimental data is available for masses along with different decay modes. There are many theoretical groups viz. the lattice quantum chromodynamics (LQCD) [8–18], QCD [19,20], QCD sum rules [21,22], perturbative QCD [23], lattice NRQCD [24,25] and effective field theories [26] that have attempted to explain the production and decays of these states. Others include phenomenological potential models such as the relativistic quark model based on quasi-potential approach [27–33], where the relativistic quasi-potential including one loop radiative corrections reproduce the mass spectrum of quarkonium states. The quasi-potential has also been employed along with leading order radiative correction to heavy quark potential [34–37], relativistic potential model [38–40] as well as semirelativistic potential model [41]. In nonrelativistic potential models, there exist several forms of quark antiquark potentials in the literature. The most common among them is the coulomb repulsive plus quark confinement interaction potential. In our previous work [42–45], we have employed the confinement scheme based on harmonic approximation along with Lorentz scalar plus vector potential. The authors of [46–52] have considered the confinement of power potential Ar^{ν} with ν varying from 0.1 to 2.0 and the confinement strength A to vary with potential index ν. Confinement of the order $r^{2/3}$ have also been attempted [53]. Linear confinement of quarks has been considered by many groups [54–66] and they have provided good agreement with the experimental data for quarkonium spectroscopy along with decay properties. The Bethe–Salpeter approach was also employed for the mass spectroscopy of charmonia and bottomonia [60,61,67]. The quarkonium mass spectrum was also computed in the nonrelativistic quark model [68], screened potential model [65,66] and constituent quark model [69]. There are also other nonlinear potential models that predict the mass spectra of the heavy quarkonia successfully [70–80].

In 90's, the nonrelativistic potential models predicted not only the ground state mass of the tightly bound state of c

[a] e-mail: nrsoni-apphy@msubaroda.ac.in

[b] e-mail: jnpandya-apphy@msubaroda.ac.in

Published online: 21 July 2018

and $\bar{b}$ in the range of 6.2–6.3 GeV [81,82] but also predicted to have very rich spectroscopy. In 1998, CDF collaboration [83] reported B_c mesons in $p\bar{p}$ collisions at $\sqrt{s} = 1.8$ TeV and was later confirmed by D0 [84] and LHCb [85] collaborations. The LHCb collaboration has also made the most precise measurement of the life time of B_c mesons [86]. The first excited state is also reported by ATLAS Collaborations [87] in $p\bar{p}$ collisions with significance of 5.2σ.

It is important to show that any given potential model should be able to compute mass spectra and decay properties of B_c meson using parameters fitted for heavy quarkonia. Attempts in this direction have been made in relativistic quark model based on quasi-potential along with one loop radiative correction [27], quasistatic and confinement QCD potential with confinement parameters along with quark masses [88] and rainbow-ladder approximation of Dyson–Schwinger and Bethe–Salpeter equations [67].

The interaction potential for mesonic states is difficult to derive for full range of quark antiquark separation from first principles of QCD. So most forms of QCD inspired potential would result in uncertainties in the computation of spectroscopic properties particularly in the intermediate range. Different potential models may produce similar mass spectra matching with experimental observations but they may not be in mutual agreement when it comes to decay properties like decay constants, leptonic decays or radiative transitions. Moreover, the mesonic states are identified with masses along with certain decay channels, therefore the test for any successful theoretical model is to reproduce the mass spectrum along with decay properties. Relativistic as well as nonrelativistic potential models have successfully predicted the spectroscopy but they are found to differ in computation of the decay properties [22,47–51,55,78–80]. In this article, we employ nonrelativistic potential with one gluon exchange (essentially Coulomb like) plus linear confinement (Cornell potential) as this form of the potential is also supported by LQCD [89–91]. We solve the Schrödinger equation numerically for the potential to get the spectroscopy of the quarkonia. We first compute the mass spectra of charmonia and bottomonia states to determine quark masses and confinement strengths after fitting the spin-averaged ground state masses with experimental data of respective mesons. Using the potential parameters and numerical wave function, we compute the decay properties such as leptonic decay constants, digamma, dilepton, digluon decay width using the Van-Royen Weiskopf formula. These parameters are then used to compute the mass spectra and life-time of B_c meson. We also compute the electromagnetic ($E1$ and $M1$) transition widths of heavy quarkonia and B_c mesons.

2 Methodology

Bound state of two body system within relativistic quantum field is described in Bethe–Salpeter formalism. However, the Bethe–Salpeter equation is solved only in the ladder approximations. Also, Bethe–Salpeter approach in harmonic confinement is successful in low flavor sectors [92,93]. Therefore the alternative treatment for the heavy bound state is nonrelativistic. Significantly low momenta of quark and antiquark compared to mass of quark-antiquark system $m_{Q,\bar{Q}} \gg \Lambda_{QCD} \sim |\mathbf{p}|$ also constitutes the basis of the nonrelativistic treatment for the heavy quarkonium spectroscopy. Here, for the study of heavy bound state of mesons such as $c\bar{c}$, $c\bar{b}$ and $b\bar{b}$, the nonrelativistic Hamiltonian is given by

$$H = M + \frac{p^2}{2M_{cm}} + V_{\text{Cornell}}(r) + V_{SD}(r) \tag{1}$$

where

$$M = m_Q + m_{\bar{Q}} \quad \text{and} \quad M_{cm} = \frac{m_Q m_{\bar{Q}}}{m_Q + m_{\bar{Q}}} \tag{2}$$

where m_Q and $m_{\bar{Q}}$ are the masses of quark and antiquark respectively, $\mathbf{p}$ is the relative momentum of the each quark and $V_{\text{Cornell}}(r)$ is the quark-antiquark potential of the type coulomb plus linear confinement (Cornell potential) given by

$$V_{\text{Cornell}}(r) = -\frac{4}{3}\frac{\alpha_s}{r} + Ar. \tag{3}$$

Here, $1/r$ term is analogous to the Coulomb type interaction corresponding to the potential induced between quark and antiquark through one gluon exchange that dominates at small distances. The second term is the confinement part of the potential with the confinement strength A as the model parameter. The confinement term becomes dominant at the large distances. α_s is a strong running coupling constant and can be computed as

$$\alpha_s(\mu^2) = \frac{4\pi}{\left(11 - \frac{2}{3}n_f\right)\ln\left(\mu^2/\Lambda^2\right)} \tag{4}$$

where n_f is the number of flavors, μ is renormalization scale related to the constituent quark masses as $\mu = 2m_Q m_{\bar{Q}}/(m_Q + m_{\bar{Q}})$ and Λ is a QCD scale which is taken as 0.15 GeV by fixing $\alpha_s = 0.1185$ [7] at the Z-boson mass.

The confinement strengths with respective quark masses are fine tuned to reproduce the experimental spin averaged ground state masses of both $c\bar{c}$ and $b\bar{b}$ mesons and they are given in Table 1. We compute the masses of radially and orbitally excited states without any additional parameters. Similar work has been done by [47,51,52] and they have considered different values of confinement strengths for different potential indices. The Cornell potential has been shown to be

Table 1 Parameters for quarkonium spectroscopy

m_c	m_c	A_{cc}	A_{bb}
1.317 GeV	4.584 GeV	0.18 GeV^2	0.25 GeV^2

independently successful in computing the spectroscopy of ψ and Υ families. In this article, we compute the mass spectra of the ψ and Υ families along with B_c meson with minimum number of parameters.

Using the parameters defined in Table 1, we compute the spin averaged masses of quarkonia. In order to compute masses of different $n^m L_J$ states according to different J^{PC} values, we use the spin dependent part of one gluon exchange potential (OGEP) $V_{SD}(r)$ perturbatively. The OGEP includes spin-spin, spin-orbit and tensor terms given by [20,22,59,68]

$$V_{SD}(r) = V_{SS}(r)\left[S(S+1) - \frac{3}{2}\right] + V_{LS}(r)(\mathbf{L}\cdot\mathbf{S}) + V_T(r)\left[S(S+1) - 3(S\cdot\hat{r})(S\cdot\hat{r})\right] \quad (5)$$

The spin-spin interaction term gives the hyper-fine splitting while spin-orbit and tensor terms gives the fine structure of the quarkonium states. The coefficients of spin dependent terms of the Eq. (5) can be written as [20]

$$V_{SS}(r) = \frac{1}{3m_Q m_{\bar{Q}}}\nabla^2 V_V(r) = \frac{16\pi\alpha_s}{9m_Q m_{\bar{Q}}}\delta^3(\mathbf{r}) \quad (6)$$

$$V_{LS}(r) = \frac{1}{2m_Q m_{\bar{Q}} r}\left(3\frac{dV_V(r)}{dr} - \frac{dV_S(r)}{dr}\right) \quad (7)$$

$$V_T(r) = \frac{1}{6m_Q m_{\bar{Q}}}\left(3\frac{dV_V^2(r)}{dr^2} - \frac{1}{r}\frac{dV_V(r)}{dr}\right) \quad (8)$$

Where $V_V(r)$ and $V_S(r)$ correspond to the vector and scalar part of the Cornell potential in Eq. (3) respectively. Using all the parameters defined above, the Schrödinger equation is numerically solved using *Mathematica* notebook utilizing the Runge–Kutta method [94]. It is generally believed that the charmonia need to be treated relativistically due to their lighter masses, but we note here that the computed wave functions of charmonia using relativistic as well as nonrelativistic approaches do not show significant difference [33]. So we choose to compute the charmonium mass spectra nonrelativistically in present study. The computed mass spectra of heavy quarkonia and B_c mesons are listed in Tables 2, 3, 4, 5, 6 and 7.

3 Decay properties

The mass spectra of the hadronic states are experimentally determined through detection of energy and momenta of daughter particles in various decay channels. Generally, most phenomenological approaches obtain their model parameters like quark masses and confinement/Coulomb strength by fitting with the experimental ground states. So it becomes necessary for any phenomenological model to validate their fitted parameters through proper evaluation of various decay rates in general and annihilation rates in particular. In the nonrelativistic limit, the decay properties are dependent on the wave function. In this section, we test our parameters and wave functions to determine various annihilation widths and electromagnetic transitions.

3.1 Leptonic decay constants

The leptonic decay constants of heavy quarkonia play very important role in understanding the weak decays. The matrix elements for leptonic decay constants of pseudoscalar and vector mesons are given by

$$\langle 0|\bar{Q}\gamma^\mu\gamma_5 Q|P_\mu(k)\rangle = if_P k^\mu \quad (9)$$

$$\langle 0|\bar{Q}\gamma^\mu Q|P_\mu(k)\rangle = if_V M_V \epsilon^{*\mu} \quad (10)$$

where k is the momentum of pseudoscalar meson, $\epsilon^{*\mu}$ is the polarization vector of meson. In the nonrelativistic limit, the decay constants of pseudoscalar and vector mesons are given by Van Royen-Weiskopf formula [96]

$$f^2_{P/V} = \frac{3|R_{nsP/V}(0)|^2}{\pi M_{nsP/V}}\bar{C}^2(\alpha_S). \quad (11)$$

Here the QCD correction factor $\bar{C}^2(\alpha_S)$ [97,98]

$$\bar{C}^2(\alpha_S) = 1 - \frac{\alpha_s}{\pi}\left(\delta^{P,V} - \frac{m_Q - m_{\bar{Q}}}{m_Q + m_{\bar{Q}}}\ln\frac{m_Q}{m_{\bar{Q}}}\right). \quad (12)$$

With $\delta^P = 2$ and $\delta^V = 8/3$. Using the above relations, we compute the leptonic decay constants f_p and f_v for charmonia, bottomonia and B_c mesons. The results are listed in Tables 8, 9, 10, 11, 12 and 13 in comparison with other models including LQCD.

3.2 Annihilation widths of heavy quarkonia

Digamma, digluon and dilepton annihilation decay widths of heavy quarkonia are very important in understanding the dynamics of heavy quarks within the mesons. The measurement of digamma decay widths provides the information regarding the internal structure of meson. The decay $\eta_c \to \gamma\gamma$, $\chi_{c0,2} \to \gamma\gamma$ was reported by CLEO-c [103], *BABAR* [104] and then BESIII [105] collaboration have reported high accuracy data. LQCD is found to underestimate the decay widths of $\eta_c \to \gamma\gamma$ and $\chi_{c0} \to \gamma\gamma$ when compared to experimental data [106,107]. Other approaches to attempt computation of annihilation rates of heavy quarkonia include NRQCD [108–112], relativistic quark model [31,32], effective Lagrangian [113,114] and next-to-next-to

Table 2 Mass spectrum of S and P-wave charmonia (in GeV)

State	Present	[27]	[65]	[67]	[76]	[39]	[73]	[59]	[68]	[70]	LQCD [17]	PDG [7]
1^1S_0	2.989	2.981	2.984	2.925	2.979	2.980	2.980	2.982	3.088	2.979	2.884	2.984
1^3S_1	3.094	3.096	3.097	3.113	3.097	3.097	3.097	3.090	3.168	3.096	3.056	3.097
2^1S_0	3.602	3.635	3.637	3.684	3.623	3.597	3.633	3.630	3.669	3.600	3.535	3.639
2^3S_1	3.681	3.685	3.679	3.676	3.673	3.685	3.690	3.672	3.707	3.680	3.662	3.686
3^1S_0	4.058	3.989	4.004	–	3.991	4.014	3.992	4.043	4.067	4.011	–	–
3^3S_1	4.129	4.039	4.030	3.803	4.022	4.095	4.030	4.072	4.094	4.077	–	4.039
4^1S_0	4.448	4.401	4.264	–	4.250	4.433	4.244	4.384	4.398	4.397	–	–
4^3S_1	4.514	4.427	4.281	–	4.273	4.477	4.273	4.406	4.420	4.454	–	4.421
5^1S_0	4.799	4.811	4.459	–	4.446	–	4.440	–	–	–	–	–
5^3S_1	4.863	4.837	4.472	–	4.463	–	4.464	–	–	–	–	–
6^1S_0	5.124	5.155	–	–	4.595	–	4.601	–	–	–	–	–
6^3S_1	5.185	5.167	–	–	4.608	–	4.621	–	–	–	–	–
1^3P_0	3.428	3.413	3.415	3.323	3.433	3.416	3.392	3.424	3.448	3.488	3.412	3.415
1^3P_1	3.468	3.511	3.521	3.489	3.510	3.508	3.491	3.505	3.520	3.514	3.480	3.511
1^1P_1	3.470	3.525	3.526	3.433	3.519	3.527	3.524	3.516	3.536	3.539	3.494	3.525
1^3P_2	3.480	3.555	3.553	3.550	3.556	3.558	3.570	3.556	3.564	3.565	3.536	3.556
2^3P_0	3.897	3.870	3.848	3.833	3.842	3.844	3.845	3.852	3.870	3.947	–	3.918
2^3P_1	3.938	3.906	3.914	3.672	3.901	3.940	3.902	3.925	3.934	3.972	–	–
2^1P_1	3.943	3.926	3.916	3.747	3.908	3.960	3.922	3.934	3.950	3.996	–	–
2^3P_2	3.955	3.949	3.937	–	3.937	3.994	3.949	3.972	3.976	4.021	4.066	3.927
3^3P_0	4.296	4.301	4.146	–	4.131	–	4.192	4.202	4.214	–	–	–
3^3P_1	4.338	4.319	4.192	3.912	4.178	–	4.178	4.271	4.275	–	–	–
3^1P_1	4.344	4.337	4.193	–	4.184	–	4.137	4.279	4.291	–	–	–
3^3P_2	4.358	4.354	4.211	–	4.208	–	4.212	4.317	4.316	–	–	–
4^3P_0	4.653	4.698	–	–	–	–	–	–	–	–	–	–
4^3P_1	4.696	4.728	–	–	–	–	–	–	–	–	–	–
4^1P_1	4.704	4.744	–	–	–	–	–	–	–	–	–	–
4^3P_2	4.718	4.763	–	–	–	–	–	–	–	–	–	–
5^3P_0	4.983	–	–	–	–	–	–	–	–	–	–	–
5^3P_1	5.026	–	–	–	–	–	–	–	–	–	–	–
5^1P_1	5.034	–	–	–	–	–	–	–	–	–	–	–
5^3P_2	5.049	–	–	–	–	–	–	–	–	–	–	–

leading order QCD correction to $\chi_{c0,2} \to \gamma\gamma$ in the framework of nonrelativistic QCD factorization [115].

The meson decaying into digamma suggests that the spin can never be one [116,117]. Corresponding digamma decay width of a pseudoscalar meson in nonrelativistic limit is given by Van Royen-Weiskopf formula [96,118]

$$\Gamma_{n^1S_0\to\gamma\gamma} = \frac{3\alpha_e^2 e_Q^4 |R_{nsP}(0)|^2}{m_Q^2}\left[1+\frac{\alpha_s}{\pi}\left(\frac{\pi^2-20}{3}\right)\right] \tag{13}$$

$$\Gamma_{n^3P_0\to\gamma\gamma} = \frac{27\alpha_e^2 e_Q^4 |R'_{nP}(0)|^2}{M_Q^4}\left[1+\frac{\alpha_s}{\pi}\left(\frac{3\pi^2-28}{9}\right)\right] \tag{14}$$

$$\Gamma_{n^3P_2\to\gamma\gamma} = \frac{36\alpha_e^2 e_Q^4 |R'_{nP}(0)|^2}{5M_Q^4}\left[1-\frac{16}{3}\frac{\alpha_s}{\pi}\right] \tag{15}$$

where the bracketed quantities are QCD next-to-leading order radiative corrections [118,119].

Digluon annihilation of quarkonia is not directly observed in detectors as digluonic state decays into various hadronic states making it a bit complex to compute digluon annihilation widths from nonrelativistic approximations derived from first principles. The digluon decay width of pseudoscalar meson along with the QCD leading order radiative correction is given by [113,118–120]

Table 3 Mass spectrum of D and F-wave charmonia (in GeV)

State	Present	[27]	[65]	[67]	[76]	[39]	[73]	[59]	[68]	[70]
1^3D_3	3.755	3.813	3.808	3.869	3.799	3.831	3.844	3.806	3.809	3.798
1^1D_2	3.765	3.807	3.805	3.739	3.796	3.824	3.802	3.799	3.803	3.796
1^3D_2	3.772	3.795	3.807	3.550	3.798	3.824	3.788	3.800	3.804	3.794
1^3D_1	3.775	3.783	3.792	–	3.787	3.804	3.729	3.785	3.789	3.792
2^3D_3	4.176	4.220	4.112	3.806	4.103	4.202	4.132	4.167	4.167	4.425
2^1D_2	4.182	4.196	4.108	–	4.099	4.191	4.105	4.158	4.158	4.224
2^3D_2	4.188	4.190	4.109	–	4.100	4.189	4.095	4.158	4.159	4.223
2^3D_1	4.188	4.105	4.095	–	4.089	4.164	4.057	4.142	4.143	4.222
3^3D_3	4.549	4.574	4.340	–	4.331	–	4.351	–	–	–
3^1D_2	4.553	3.549	4.336	–	4.326	–	4.330	–	–	–
3^3D_2	4.557	4.544	4.337	–	4.327	–	4.322	–	–	–
3^3D_1	4.555	4.507	4.324	–	4.317	–	4.293	–	–	–
4^3D_3	4.890	4.920	–	–	–	–	4.526	–	–	–
4^1D_2	4.892	4.898	–	–	–	–	4.509	–	–	–
4^3D_2	4.896	4.896	–	–	–	–	4.504	–	–	–
4^3D_1	4.891	4.857	–	–	–	–	4.480	–	–	–
1^3F_2	3.990	4.041	–	–	–	4.068	–	4.029	–	–
1^3F_3	4.012	4.068	–	3.999	–	4.070	–	4.029	–	–
1^1F_3	4.017	4.071	–	4.037	–	4.066	–	4.026	–	–
1^3F_4	4.036	4.093	–	–	–	4.062	–	4.021	–	–
2^3F_2	4.378	4.361	–	–	–	–	–	4.351	–	–
2^3F_3	4.396	4.400	–	–	–	–	–	3.352	–	–
2^1F_3	4.400	4.406	–	–	–	–	–	4.350	–	–
2^3F_4	4.415	4.434	–	–	–	–	–	4.348	–	–
3^3F_2	4.730	–	–	–	–	–	–	–	–	–
3^3F_3	4.746	–	–	–	–	–	–	–	–	–
3^1F_3	4.749	–	–	–	–	–	–	–	–	–
3^3F_4	4.761	–	–	–	–	–	–	–	–	–

$$\Gamma_{n^1S_0\to gg} = \frac{2\alpha_s^2|R_{nsP}(0)|^2}{3m_Q^2}[1+C_Q(\alpha_s/\pi)] \tag{16}$$

$$\Gamma_{n^3P_0\to gg} = \frac{6\alpha_s^2|R'_{nP}(0)|^2}{m_Q^4}[1+C_{0Q}(\alpha_s/\pi)] \tag{17}$$

$$\Gamma_{n^3P_2\to gg} = \frac{4\alpha_s^2|R'_{nP}(0)|^2}{5m_Q^4}[1+C_{2Q}(\alpha_s/\pi)] \tag{18}$$

Here, the coefficients in the bracket have values of $C_Q = 4.8$, $C_{0Q} = 9.5$, $C_{2Q} = -2.2$ for the charm quark and $C_Q = 4.4$, $C_{0Q} = 10.0$, $C_{2Q} = -0.1$ for the bottom quark [118].

The vector mesons have quantum numbers 1^{--} and can annihilate into dilepton. The dileptonic decay of vector meson along with one loop QCD radiative correction is given by [96,118]

$$\Gamma_{n^3S_1\to\ell^+\ell^-} = \frac{4\alpha_e^2e_Q^2|R_{nsV}(0)|^2}{M_{nsV}^2}\left[1-\frac{16\alpha_s}{3\pi}\right] \tag{19}$$

Here, α_e is the electromagnetic coupling constant, α_s is the strong running coupling constant in Eq. (4) and e_Q is the charge of heavy quark in terms of electron charge. In above relations, $|R_{nsP/V}(0)|$ corresponds to the wave function of S-wave at origin for pseudoscalar and vector mesons while $|R'_{nP}(0)|$ is the derivative of P-wave function at origin. The annihilation rates of heavy quarkonia are listed in Tables 14, 15, 16, 17, 18 and 19.

3.3 Electromagnetic transition widths

The electromagnetic transitions can be determined broadly in terms of electric and magnetic multipole expansions and their study can help in understanding the non-perturbative regime of QCD. We consider the leading order terms i.e. electric ($E1$) and magnetic ($M1$) dipoles with selection rules $\Delta L = \pm 1$ and $\Delta S = 0$ for the $E1$ transitions while $\Delta L = 0$ and $\Delta S = \pm 1$ for $M1$ transitions. We now employ the numerical

Table 4 Mass spectrum of S and P-wave bottomonia (in GeV)

State	Present	[64]	[27]	[66]	[67]	[77]	[40]	[73]	[69]	PDG [7]
1^1S_0	9.428	9.402	9.398	9.390	9.414	9.389	9.393	9.392	9.455	9.398
1^3S_1	9.463	9.465	9.460	9.460	9.490	9.460	9.460	9.460	9.502	9.460
2^1S_0	9.955	9.976	9.990	9.990	9.987	9.987	9.987	9.991	9.990	9999
2^3S_1	9.979	10.003	10.023	10.015	10.089	10.016	10.023	10.024	10.015	10.023
3^1S_0	10.338	10.336	10.329	10.326	–	10.330	10.345	10.323	10.330	–
3^3S_1	10.359	10.354	10.355	10.343	10.327	10.351	10.364	10.346	10.349	10.355
4^1S_0	10.663	10.523	10.573	10.584	–	10.595	10.623	10.558	–	–
4^3S_1	10.683	10.635	10.586	10.597	–	10.611	10.643	10.575	10.607	10.579
5^1S_0	10.956	10.869	10.851	10.800	–	10.817	–	10.741	–	–
5^3S_1	10.975	10.878	10.869	10.811	–	10.831	–	10.755	10.818	10.876
6^1S_0	11.226	11.097	11.061	10.997	–	11.011	–	10.892	–	–
6^3S_1	11.243	11.102	11.088	10.988	–	11.023	–	10.904	10.995	11.019
1^3P_0	9.806	9.847	9.859	9.864	9.815	9.865	9.861	9.862	9.855	9.859
1^3P_1	9.819	9.876	9.892	9.903	9.842	9.897	9.891	9.888	9.874	9.893
1^1P_1	9.821	9.882	9.900	9.909	9.806	9.903	9.900	9.896	9.879	9.899
1^3P_2	9.825	9.897	9.912	9.921	9.906	9.918	9.912	9.908	9.886	9.912
2^3P_0	10.205	10.226	10.233	10.220	10.254	10.226	10.230	10.241	10.221	10.232
2^3P_1	10.217	10.246	10.255	10.249	10.120	10.251	10.255	10.256	10.236	10.255
2^1P_1	10.220	10.250	10.260	10.254	10.154	10.256	10.262	10.261	10.240	10.260
2^3P_2	10.224	10.261	10.268	10.264	–	10.269	10.271	10.268	10.246	10.269
3^3P_0	10.540	10.552	10.521	10.490	–	10.502	–	10.511	10.500	–
3^3P_1	10.553	10.538	10.541	10.515	10.303	10.524	–	10.507	10.513	–
3^1P_1	10.556	10.541	10.544	10.519	–	10.529	–	10.497	10.516	–
3^3P_2	10.560	10.550	10.550	10.528	–	10.540	–	10.516	10.521	–
4^3P_0	10.840	10.775	10.781	–	–	10.732	–	–	–	–
4^3P_1	10.853	10.788	10.802	–	–	10.753	–	–	–	–
4^1P_1	10.855	10.790	10.804	–	–	10.757	–	–	–	–
4^3P_2	10.860	10.798	10.812	–	–	10.767	–	–	–	–
5^3P_0	11.115	11.004	–	–	–	10.933	–	–	–	–
5^3P_1	11.127	11.014	–	–	–	10.951	–	–	–	–
5^1P_1	11.130	11.016	–	–	–	10.955	–	–	–	–
5^3P_2	11.135	11.022	–	–	–	10.965	–	–	–	–

wave function for computing the electromagnetic transition widths among quarkonia and B_c meson states in order to test parameters used in present work. For $M1$ transition, we restrict our calculations for transitions among S-waves only. In the nonrelativistic limit, the radiative $E1$ and $M1$ widths are given by [4,54,55,124,125]

$$\Gamma\left(n^{2S+1}L_{iJ_i} \to n'^{2S+1}L_{fJ_f} + \gamma\right) = \frac{4\alpha_e\langle e_Q\rangle^2\omega^3}{3}(2J_f+1)S_{if}^{E1}|M_{if}^{E1}|^2 \tag{20}$$

$$\Gamma\left(n^3S_1 \to n'^1S_0 + \gamma\right) = \frac{\alpha_e\mu^2\omega^3}{3}(2J_f+1)|M_{if}^{M1}|^2 \tag{21}$$

where, mean charge content $\langle e_Q\rangle$ of the $Q\bar{Q}$ system, magnetic dipole moment μ and photon energy ω are given by

$$\langle e_Q\rangle = \left|\frac{m_{\bar{Q}}e_Q - e_{\bar{Q}}m_Q}{m_Q + m_{\bar{Q}}}\right| \tag{22}$$

$$\mu = \frac{e_Q}{m_Q} - \frac{e_{\bar{Q}}}{m_{\bar{Q}}} \tag{23}$$

and

$$\omega = \frac{M_i^2 - M_f^2}{2M_i} \tag{24}$$

Table 5 Mass spectrum of D and F-wave bottomonia (in GeV)

State	Present	[64]	[27]	[66]	[67]	[77]	[40]	[73]	[69]	PDG [7]
1^3D_3	10.073	10.115	10.166	10.157	10.232	10.156	10.163	10.177	10.127	–
1^1D_2	10.074	10.148	10.163	10.153	10.194	10.152	10.158	10.166	10.123	–
1^3D_2	10.075	10.147	10.161	10.153	10.145	10.151	10.157	10.162	10.122	10.163
1^3D_1	10.074	10.138	10.154	10.146	–	10.145	10.149	10.147	10.117	–
2^3D_3	10.423	10.455	10.449	10.436	–	10.442	10.456	10.447	10.422	–
2^1D_2	10.424	10.450	10.445	10.432	–	10.439	10.452	10.440	10.419	–
2^3D_2	10.424	10.449	10.443	10.432	–	10.438	10.450	10.437	10.418	–
2^3D_1	10.423	10.441	10.435	10.425	–	10.432	10.443	10.428	10.414	–
3^3D_3	10.733	10.711	10.717	–	–	10.680	–	10.652	–	–
3^1D_2	10.733	10.706	10.713	–	–	10.677	–	10.646	–	–
3^3D_2	10.733	10.705	10.711	–	–	10.676	–	10.645	–	–
3^3D_1	10.731	10.698	10.704	–	–	10.670	–	10.637	–	–
4^3D_3	11.015	10.939	10.963	–	–	10.886	–	10.817	–	–
4^1D_2	11.015	10.935	10.959	–	–	10.883	–	10.813	–	–
4^3D_2	11.016	10.934	10.957	–	–	10.882	–	10.811	–	–
4^3D_1	11.013	10.928	10.949	–	–	10.877	–	10.805	–	–
1^3F_2	10.283	10.350	10.343	10.338	–	–	10.353	–	10.315	–
1^3F_3	10.287	10.355	10.346	10.340	10.302	–	10.356	–	10.321	–
1^1F_3	10.288	10.355	10.347	10.339	10.319	–	10.356	–	10.322	–
1^3F_4	10.291	10.358	10.349	10.340	–	–	10.357	–	–	–
2^3F_2	10.604	10.615	10.610	–	–	–	10.610	–	–	–
2^3F_3	10.607	10.619	10.614	–	–	–	10.613	–	–	–
2^1F_3	10.607	10.619	10.647	–	–	–	10.613	–	–	–
2^3F_4	10.609	10.622	10.617	–	–	–	10.615	–	–	–
3^3F_2	10.894	10.850	–	–	–	–	–	–	–	–
3^3F_3	10.896	10.853	–	–	–	–	–	–	–	–
3^1F_3	10.897	10.853	–	–	–	–	–	–	–	–
3^3F_4	10.898	10.856	–	–	–	–	–	–	–	–

respectively. Also the symmetric statistical factor is given by

$$S_{if}^{E1} = \max(L_i, L_f) \begin{Bmatrix} J_i & 1 & J_f \\ L_f & S & L_i \end{Bmatrix}^2. \tag{25}$$

The matrix element $|M_{if}|$ for $E1$ and $M1$ transition can be written as

$$\left|M_{if}^{E1}\right| = \frac{3}{\omega}\left\langle f \left| \frac{\omega r}{2} j_0\left(\frac{\omega r}{2}\right) - j_1\left(\frac{\omega r}{2}\right)\right| i\right\rangle \tag{26}$$

and

$$\left|M_{if}^{M1}\right| = \left\langle f \left| j_0\left(\frac{\omega r}{2}\right)\right| i\right\rangle \tag{27}$$

The electromagnetic transition widths are listed in Tables 20, 21, 22, 23, 24 and 25 and also compared with experimental results as well as theoretical predictions.

3.4 Weak decays of B_c mesons

The decay modes of B_c mesons are different from charmonia and bottomonia because of the inclusion of different flavor quarks. Their decay properties are very important probes for the weak interaction as B_c meson decays only through weak decays, therefore have relatively quite long life time. The pseudoscalar state can not decay via strong or electromagnetic decays because of this flavor asymmetry.

In the spectator model [126], the total decay width of B_c meson can be broadly classified into three classes. (i) Decay of b quark considering c quark as a spectator, (ii) Decay of c quark considering b quark as a spectator and (iii) Annihilation channel $B_c \to \ell^+\nu_\ell$. The total width is given by

$$\Gamma(B_c \to X) = \Gamma(b \to X) + \Gamma(c \to X) + \Gamma(Anni) \tag{28}$$

In the calculations of total width we have not considered the interference among them as all these decays lead to different

Table 6 Mass spectrum of S and P-wave B_c meson (in GeV)

State	Present	[46]	[27]	[63]	[95]	PDG [7]
1^1S_0	6.272	6.278	6.272	6.271	6.275	6.275
1^3S_1	6.321	6.331	6.333	6.338	6.314	–
2^1S_0	6.864	6.863	6.842	6.855	6.838	6.842
2^3S_1	6.900	6.873	6.882	6.887	6.850	–
3^1S_0	7.306	7.244	7.226	7.250	–	–
3^3S_1	7.338	7.249	7.258	7.272	–	–
4^1S_0	7.684	7.564	7.585	–	–	–
4^3S_1	7.714	7.568	7.609	–	–	–
5^1S_0	8.025	7.852	7.928	–	–	–
5^3S_1	8.054	7.855	7.947	–	–	–
6^1S_0	8.340	8.120	–	–	–	–
6^3S_1	8.368	8.122	–	–	–	–
1^3P_0	6.686	6.748	6.699	6.706	6.672	–
1^3P_1	6.705	6.767	6.750	6.741	6.766	–
1^1P_1	6.706	6.769	6.743	6.750	6.828	–
1^3P_2	6.712	6.775	6.761	6.768	6.776	–
2^3P_0	7.146	7.139	7.094	7.122	6.914	–
2^3P_1	7.165	7.155	7.134	7.145	7.259	–
2^1P_1	7.168	7.156	7.094	7.150	7.322	–
2^3P_2	7.173	7.162	7.157	7.164	7.232	–
3^3P_0	7.536	7.463	7.474	–	–	–
3^3P_1	7.555	7.479	7.510	–	–	–
3^1P_1	7.559	7.479	7.500	–	–	–
3^3P_2	7.565	7.485	7.524	–	–	–
4^3P_0	7.885	–	7.817	–	–	–
4^3P_1	7.905	–	7.853	–	–	–
4^1P_1	7.908	–	7.844	–	–	–
4^3P_2	7.915	–	7.867	–	–	–
5^3P_0	8.207	–	–	–	–	
5^3P_1	8.226	–	–	–	–	
5^1P_1	8.230	–	–	–	–	
5^3P_2	8.237	–	–	–	–	

Table 7 Mass spectrum of D and F-wave B_c meson (in GeV)

State	Present	[46]	[27]	[63]	[95]
1^3D_3	6.990	7.026	7.029	7.045	6.980
1^1D_2	6.994	7.035	7.026	7.041	7.009
1^3D_2	6.997	7.025	7.025	7.036	7.154
1^3D_1	6.998	7.030	7.021	7.028	7.078
2^3D_3	7.399	7.363	7.405	–	–
2^1D_2	7.401	7.370	7.400	–	–
2^3D_2	7.403	7.361	7,399	–	–
2^3D_1	7.403	7.365	7.392	–	–
3^3D_3	7.761	–	7.750	–	–
3^1D_2	7.762	–	7.743	–	–
3^3D_2	7.764	–	7.741	–	–
3^3D_1	7.762	–	7.732	–	–
4^3D_3	8.092	–	–	–	–
4^1D_2	8.093	–	–	–	–
4^3D_2	8.094	–	–	–	–
4^3D_1	8.091	–	–	–	–
1^3F_2	7.234	–	7.273	7.269	–
1^3F_3	7.242	–	7.269	7.276	–
1^1F_3	7.241	–	7.268	7.266	–
1^3F_4	7.244	–	7.277	7.271	–
2^3F_2	7.607	–	7.618	–	–
2^3F_3	7.615	–	7.616	–	–
2^1F_3	7.614	–	7.615	–	–
2^3F_4	7.617	–	7.617	–	–
3^3F_2	7.946	–	–	–	–
3^3F_3	7.954	–	–	–	–
3^1F_3	7.953	–	–	–	–
3^3F_4	7.956	–	–	–	–

channel. In the spectator approximation, the inclusive decay width of b and c quark is given by

$$\Gamma(b \to X) = \frac{9G_F^2|V_{cb}|^2 m_b^5}{192\pi^3} \tag{29}$$

$$\Gamma(c \to X) = \frac{9G_F^2|V_{cs}|^2 m_c^5}{192\pi^3} \tag{30}$$

$$\Gamma(Anni) = \frac{G_F^2}{8\pi}|V_{bc}|^2 f_{B_c}^2 M_{B_c} m_q^2 \left(1 - \frac{m_q^2}{M_{B_c^2}}\right)^2 C_q \tag{31}$$

where $C_q = 3|V_{cs}|$ for D_s mesons and m_q is the mass of heaviest fermions. V_{cs} and V_{cb} are the CKM matrices and we have taken the value of CKM matrices from the PDG. G_f is the Fermi coupling constant. Here we have used the model quark masses, B_c meson mass and decay constants for the computation of total width. Here we compute the decay width of B_c meson using Eq. (28) and corresponding life time. The computed life time comes out to be 0.539×10^{-12} s which is in very good agreement with the world averaged mean life time $(0.507 \pm 0.009) \times 10^{-12}$ s [7].

4 Numerical results and discussion

Having determined the confinement strengths and quark masses, we are now in position to present our numerical results. We first compute the mass spectra of heavy quarkonia and B_c meson. In most of the potential model computations, the confinement strength is fixed by experimental ground state masses for $c\bar{c}$, $b\bar{b}$ and $c\bar{b}$ independently. We observe here that the confinement strength A for B_c meson is arithmetic mean of those for $c\bar{c}$ and $b\bar{b}$ which discards the

Table 8 Pseudoscalar decay constant of charmonia (in MeV)

State	f_p	[52]	[99]	[68]	LQCD [100]	QCDSR [100]	PDG [7]
$1S$	350.314	363	378	402	387(7)(2)	309 ± 39	335 ± 75
$2S$	278.447	275	82	240	–	–	–
$3S$	249.253	239	206	193	–	–	–
$4S$	231.211	217	87	–	–	–	–
$5S$	218.241	202	–	–	–	–	
$6S$	208.163	197	–	–	–	–	–

Table 9 Vector decay constant of charmonia (in MeV)

State	f_v	[52]	[99]	[68]	LQCD [100]	QCDSR [100]	PDG [7]
$1S$	325.876	338	411	393	418(8)(5)	401 ± 46	416 ± 6
$2S$	257.340	254	155	293	–	–	304 ± 4
$3S$	229.857	220	188	258	–	–	–
$4S$	212.959	200	262	–	–	–	–
$5S$	200.848	186	–	–	–	–	–
$6S$	191.459	175	–	–	–	–	–

Table 10 Pseudoscalar decay constant of bottomonia (in MeV)

State	f_p	[52]	[99]	[43]	[68]
$1S$	646.025	744	756	711	599
$2S$	518.803	577	285	–	411
$3S$	474.954	511	333	–	354
$4S$	449.654	471	40	–	–
$5S$	432.072	443	–	–	–
$6S$	418.645	422	–	–	–

Table 11 Vector decay constant of bottomonia (in MeV)

State	f_v	[52]	[99]	[68]	[101]	LQCD [102]	PDG [7]
$1S$	647.250	706	707	665	$498 \pm (20)$	649(31)	715 ± 5
$2S$	519.436	547	393	475	$366 \pm (27)$	481(39)	498 ± 8
$3S$	475.440	484	9	418	$304 \pm (27)$	–	430 ± 4
$4S$	450.066	446	20	388	$259 \pm (22)$	–	336 ± 18
$5S$	432.437	419	–	367	$228 \pm (16)$	–	–
$6S$	418.977	399	–	351	–	–	–

Table 12 Pseudoscalar decay constant of B_c meson (in MeV)

State	f_p	[52]	[30]	[22]	[82]	[95]
$1S$	432.955	465	503	$460 \pm (60)$	500	554.125
$2S$	355.504	361	–	–	–	
$3S$	325.659	319	–	–	–	
$4S$	307.492	293	–	–	–	
$5S$	294.434	275	–	–	–	
$6S$	284.237	261	–	–	–	

Table 13 Vector decay constant of B_c meson (in MeV)

State	f_v	[52]	[30]	[22]	[82]
$1S$	434.642	435	433	$460 \pm (60)$	500
$2S$	356.435	337	–	–	–
$3S$	326.374	297	–	–	–
$4S$	308.094	273	–	–	–
$5S$	294.962	256	–	–	–
$6S$	284.709	243	–	–	–

Table 14 Digamma decay width of S and P-wave charmonia (in keV)

State	$\Gamma_{\gamma\gamma}$	[76]	[32]	[68]	[121]	PDG [7]
1^1S_0	7.231	8.5	5.5	7.18	7.14 ± 0.95	5.1 ± 0.4
2^1S_0	5.507	2.4	1.8	1.71	4.44 ± 0.48	2.15 ± 1.58
3^1S_0	4.971	0.88	–	1.21	–	–
4^1S_0	4.688	–	–	–	–	–
5^1S_0	4.507	–	–	–	–	–
6^1S_0	4.377	–	–	–	–	–
1^3P_0	8.982	2.5	2.9	3.28	–	2.34 ± 0.19
1^3P_2	1.069	0.31	0.50	–	–	0.53 ± 0.4
2^3P_0	9.111	1.7	1.9	–	–	–
2^3P_2	1.084	0.23	0.52	–	–	–
3^3P_0	9.104	1.2	–	–	–	–
3^3P_2	1.0846	0.17	–	–	–	–
4^3P_0	9.076	–	–	–	–	–
4^3P_2	1.080	–	–	–	–	–
5^3P_0	9.047	–	–	–	–	–
5^3P_2	1.077	–	–	–	–	–

Table 15 Digamma decay width of S and P-wave bottomonia (in keV)

State	$\Gamma_{\gamma\gamma}$	[77]	[62]	[32]	[68]	[121]
1^1S_0	0.387	0.527	0.214	0.35	0.23	0.384 ± 0.047
2^1S_0	0.263	0.263	0.121	0.15	0.07	0.191 ± 0.025
3^1S_0	0.229	0.172	0.906	0.10	0.04	–
4^1S_0	0.212	0.105	0.755	–	–	–
5^1S_0	0.201	0.121	–	–	–	–
6^1S_0	0.193	0.050	–	–	–	–
1^3P_0	0.0196	0.050	0.0208	0.038	–	–
1^3P_2	0.0052	0.0066	0.0051	0.008	–	–
2^3P_0	0.0195	0.037	0.0227	0.029	–	–
2^3P_2	0.0052	0.0067	0.0062	0.006	–	–
3^3P_0	0.0194	0.037	–	–	–	–
3^3P_2	0.0051	0.0064	–	–	–	–
4^3P_0	0.0192	–	–	–	–	–
4^3P_2	0.0051	–	–	–	–	–
5^3P_0	0.0191	–	–	–	–	–
5^3P_2	0.0050	–	–	–	–	–

Table 16 Digluon decay width of S and P-wave charmonia (in MeV)

State	Γ_{gg}	[70]	[121]	PDG [7]
1^1S_0	35.909	22.37	19.60	26.7 ± 3.0
2^1S_0	27.345	16.74	12.1	14.7 ± 0.7
3^1S_0	24.683	14.30	–	–
4^1S_0	23.281	–	–	–
5^1S_0	22.379	–	–	–
6^1S_0	23.736	–	–	–
1^3P_0	37.919	9.45	–	10.4 ± 0.7
1^3P_2	3.974	2.81	–	2.03 ± 0.12
2^3P_0	38.462	10.09	–	–
2^3P_2	4.034	7.34	–	–
3^3P_0	38.433	–	–	–
3^3P_2	4.028	–	–	–
4^3P_0	38.315	–	–	–
4^3P_2	4.016	–	–	–
5^3P_0	39.191	–	–	–
5^3P_2	4.003	–	–	–

Table 17 Digluon decay width of S and P-wave bottomonia (in MeV)

State	Γ_{gg}	[47]	[121]	[122]
1^1S_0	5.448	17.945	6.98	12.46
2^1S_0	3.710	–	3.47	–
3^1S_0	3.229	–	–	–
4^1S_0	2.985	–	–	–
5^1S_0	2.832	–	–	–
6^1S_0	2.274	–	–	–
1^3P_0	0.276	5.250	–	2.15
1^3P_2	0.073	0.822	–	0.22
2^3P_0	0.275	–	–	–
2^3P_2	0.073	–	–	–
3^3P_0	0.273	–	–	–
3^3P_2	0.072	–	–	–
4^3P_0	0.271	–	–	–
4^3P_2	0.072	–	–	–
5^3P_0	0.269	–	–	–
5^3P_2	0.071	–	–	–

need to introduce additional confinement strength parameter for computation of B_c spectra. Similar approach has been used earlier within QCD potential model [88]. Using model parameters and numerical wave function we compute the various decay properties of heavy quarkonia and B_c mesons namely leptonic decay constants, annihilation widths and electromagnetic transitions. In Tables 2 and 3, we present our result for charmonium mass spectra. We compare our results with PDG data [7], lattice QCD [17] data, relativistic quark model [27], nonrelativistic quark model [65,68], QCD relativistic functional approach [67], relativistic potential model [39] and nonrelativistic potential models [59,70,73,76]. Our results for S-wave are in excellent agreement with the experimental data [7]. We determine the mass difference for S-wave charmonia i.e. $M_{J/\psi} - M_{\eta_c} = 105$ MeV and $M_{\psi(2S)} - M_{\eta_c(2S)} = 79$ MeV while that from experimental data are 113 and 47 MeV respectively [7]. Our results for P-waves are also consistent with the PDG data [7] as well

Table 18 Dilepton decay width of charmonia (in keV)

State	$\Gamma_{\ell^+\ell^-}$	[73]	[52]	[39]	[31]	PDG [7]
$1S$	2.925	4.95	6.99	1.89	5.4	5.547 ± 0.14
$2S$	1.533	1.69	3.38	1.04	2.4	2.359 ± 0.04
$3S$	1.091	0.96	2.31	0.77	–	0.86 ± 0.07
$4S$	0.856	0.65	1.78	0.65	–	0.58 ± 0.07
$5S$	0.707	0.49	1.46	–	–	–
$6S$	0.602	0.39	1.24	–	–	–

Table 19 Dilepton decay width of bottomonia (in keV)

State	$\Gamma_{\ell^+\ell^-}$	[73]	[40]	[52]	[31]	[123]	PDG [7]
$1S$	1.098	1.20	1.33	1.61	1.3	0.98	1.340 ± 0.018
$2S$	0.670	0.52	0.62	0.87	0.5	0.41	0.612 ± 0.011
$3S$	0.541	0.33	0.48	0.66	–	0.27	0.443 ± 0.008
$4S$	0.470	0.24	0.40	0.53	–	0.20	0.272 ± 0.029
$5S$	0.422	0.19	–	0.44	–	0.16	–
$6S$	0.387	0.16	–	0.39	–	0.12	–

Table 20 $E1$ transition width of charmonia (in keV)

Transition	Present	[39]	[30]	[76]	[65]	PDG [7]
$2^3S_1 \to 1^3P_0$	21.863	45.0	51.7	74	22	29.8 ± 1.5
$2^3S_1 \to 1^3P_1$	43.292	40.9	44.9	62	42	27.9 ± 1.5
$2^3S_1 \to 1^3P_2$	62.312	26.5	30.9	43	38	26 ± 1.5
$2^1S_0 \to 1^1P_1$	36.197	8.3	8.6	146	49	–
$3^3S_1 \to 2^3P_0$	31.839	87.3	–	–	–	–
$3^3S_1 \to 2^3P_1$	64.234	65.7	–	–	–	–
$3^3S_1 \to 2^3P_2$	86.472	31.6	–	–	–	–
$3^1S_0 \to 2^1P_1$	51.917	–	–	–	–	–
$3^3S_1 \to 1^3P_0$	46.872	1.2	–	–	–	–
$3^3S_1 \to 1^3P_1$	107.088	2.5	–	–	–	–
$3^3S_1 \to 1^3P_2$	163.485	3.3	–	–	–	–
$3^1S_0 \to 1^1P_1$	178.312	–	–	–	–	–
$1^3P_0 \to 1^3S_1$	112.030	142.2	161	167	284	119.5 ± 8
$1^3P_1 \to 1^3S_1$	146.317	287.0	333	354	306	295 ± 13
$1^3P_2 \to 1^3S_1$	157.225	390.6	448	473	172	384.2 ± 16
$1^1P_1 \to 1^1S_0$	247.971	610.0	723	764	361	357 ± 280
$2^3P_0 \to 2^3S_1$	70.400	53.6	–	61	–	–
$2^3P_1 \to 2^3S_1$	102.672	208.3	–	103	–	–
$2^3P_2 \to 2^3S_1$	116.325	358.6	–	225	–	–
$2^1P_1 \to 2^1S_0$	163.646	–	–	309	–	–
$2^3P_0 \to 1^3S_1$	173.324	20.8	–	74	–	–
$2^3P_1 \to 1^3S_1$	210.958	28.4	–	83	–	–
$2^3P_2 \to 1^3S_1$	227.915	33.2	–	101	–	–
$2^1P_1 \to 1^1S_0$	329.384	–	–	134	–	–
$1^3D_1 \to 1^3P_0$	161.504	–	423	486	272	172 ± 30
$1^3D_1 \to 1^3P_1$	93.775	–	142	150	138	70 ± 17
$1^3D_1 \to 1^3P_2$	5.722	–	5.8	5.8	7.1	≤ 21
$1^3D_2 \to 1^3P_1$	165.176	317.3	297	342	285	–
$1^3D_2 \to 1^3P_2$	50.317	65.7	62	70	91	–
$1^3D_3 \to 1^3P_2$	175.212	62.7	252	284	350	–
$1^1D_2 \to 1^1P_1$	205.93	–	335	575	362	–

as LQCD [17] with less than 2% deviation. Since experimental/LQCD results are not available for P-wave charmonia beyond $n = 2$ states, we compare our results with the relativistic quark model [27] and it is also observed to have 1–2 % deviation throughout the spectra. For charmonia, only $1P$ states are available and for $2P$ only one state is available namely χ_{c2}. Our results for $1P$ and $2P$ states are also satisfactory. We also list the mass spectra of D and F wave and find it to be consistent with the theoretical predictions. Overall, computed charmonium spectra is consistent with PDG and other theoretical models.

In Tables 4 and 5, we compare our results of bottomonium spectra with PDG data [7], relativistic quark model [27,64], nonrelativistic quark model [66], QCD relativistic functional approach [67], relativistic potential model [40], nonrelativistic potential models [73,77] and covariant constituent quark model [69]. Similarly for S-wave bottomonia, up to $n = 3$ vector states are known experimentally and for pseudoscalar states, only $n = 1$ and 2 are available. Our results for $\Upsilon(1S)$ and $\Upsilon(3S)$ are in good agreement with the PDG data while for $\Upsilon(2S)$, $\Upsilon(4S)$ and $\Upsilon(5S)$, slight deviation (within 1%) is observed. Our results for $\eta_b(1S)$ and $\eta_b(3S)$ also match well with less than 0.5% deviation. We obtain $M_{\Upsilon(1S)} - M_{\eta_b} = 35$ MeV and for $M_{\Upsilon(2S)} - M_{\eta_b(2S)} = 24$ MeV against the PDG data of 62 and 24 MeV respectively. For P-wave, $1P$ and $2P$ states are reported and for $3P$, only χ_{b1} is reported. Our results for $1P$ bottomonia deviate by $\simeq 0.3\%$ from the experimental results but for $2P$, they are quite satisfactory and devi-

Table 21 $E1$ transition width of bottomonia (in keV)

Transition	Present	[39]	[30]	[77]	[66]	PDG [7]
$2^3S_1 \to 1^3P_0$	2.377	1.15	1.65	1.67	1.09	1.22 ± 0.11
$2^3S_1 \to 1^3P_1$	5.689	1.87	2.57	2.54	2.17	2.21 ± 0.19
$2^3S_1 \to 1^3P_2$	8.486	1.88	2.53	2.62	2.62	2.29 ± 0.20
$2^1S_0 \to 1^1P_1$	10.181	4.17	3.25	6.10	3.41	–
$3^3S_1 \to 2^3P_0$	3.330	1.67	1.65	1.83	1.21	1.20 ± 0.12
$3^3S_1 \to 2^3P_1$	7.936	2.74	2.65	2.96	2.61	2.56 ± 0.26
$3^3S_1 \to 2^3P_2$	11.447	2.80	2.89	3.23	3.16	2.66 ± 0.27
$3^3S_1 \to 1^3P_0$	0.594	0.03	0.124	0.07	0.097	0.055 ± 0.010
$3^3S_1 \to 1^3P_1$	1.518	0.09	0.307	0.17	0.0005	0.018 ± 0.010
$3^3S_1 \to 1^3P_2$	2.354	0.13	0.445	0.15	0.14	0.20 ± 0.03
$3^1S_0 \to 1^1P_1$	3.385	0.03	0.770	1.24	0.67	–
$3^1S_0 \to 2^1P_1$	13.981	–	3.07	11.0	4.25	–
$1^3P_2 \to 1^3S_1$	57.530	31.2	29.5	38.2	31.8	–
$1^3P_1 \to 1^3S_1$	54.927	27.3	37.1	33.6	31.9	–
$1^3P_0 \to 1^3S_1$	49.530	22.1	42.7	26.6	27.5	–
$1^1P_1 \to 1^1S_0$	72.094	37.9	54.4	55.8	35.8	–
$2^3P_2 \to 2^3S_1$	28.848	16.8	18.8	18.8	15.5	15.1 ± 5.6
$2^3P_1 \to 2^3S_1$	26.672	13.7	15.9	15.9	15.3	19.4 ± 5.0
$2^3P_0 \to 2^3S_1$	23.162	9.90	11.7	11.7	14.4	–
$2^1P_1 \to 2^1S_0$	35.578	–	23.6	24.7	16.2	–
$2^3P_2 \to 1^3S_1$	29.635	7.74	8.41	13.0	12.5	9.8 ± 2.3
$2^3P_1 \to 1^3S_1$	28.552	7.31	8.01	12.4	10.8	8.9 ± 2.2
$2^3P_0 \to 1^3S_1$	26.769	6.69	7.36	11.4	5.4	–
$2^1P_1 \to 1^1S_0$	34.815	–	9.9	15.9	16.1	–
$1^3D_1 \to 1^3P_0$	9.670	–	24.2	23.6	19.8	–
$1^3D_1 \to 1^3P_1$	6.313	–	12.9	12.3	13.3	–
$1^3D_1 \to 1^3P_2$	0.394	–	0.67	0.65	1.02	–
$1^3D_2 \to 1^3P_1$	11.489	19.3	24.8	23.8	21.8	–
$1^3D_2 \to 1^3P_2$	3.583	5.07	6.45	6.29	7.23	–
$1^3D_3 \to 1^3P_2$	14.013	21.7	26.7	26.4	32.1	–
$1^1D_2 \to 1^1P_1$	14.821	–	30.2	42.3	30.3	–

ating by 0.2% only from the PDG data. Our result for $\Upsilon(1D)$ also agrees well with the experimental data with 0.8% deviation. The F-wave mass spectra is also in good agreement with the theoretical predictions. Looking at the comparison with PDG data Ref. [7] and relativistic quark model Ref. [27], present quarkonium mass spectra deviate less than 2% for charmonia and less than 1% for bottomonia.

We now employ the quark masses and confinement strengths used for computing mass spectra of quarkonia to predict the spectroscopy of B_c mesons without introducing any additional parameter. Our results are tabulated in Tables 6 and 7. For B_c mesons, only 0^{-+} states are experimentally observed for $n = 1$ and 2 and our results are in very good agreement with the experimental results with less than 0.3 % error.

We note here that the masses of orbitally excited states (especially $n = 1$ states) of charmonia are systematically lower than the other models and experimental data. This tendency decreases as one moves to higher n states. Absence of similar trend in case of B_c and bottomonia systems suggests that relativistic treatment might improve the results in lower energy regime of charmonia.

Using the mass spectra of heavy quarkonia and B_c meson, we plot the Regge trajectories in (J, M^2) and (n_r, M^2) planes where $n_r = n - 1$. We use the following relations [27]

$$J = \alpha M^2 + \alpha_0 \tag{32}$$

$$n_r = \beta M^2 + \beta_0 \tag{33}$$

Table 22 $E1$ transition width of B_c meson (in keV)

Transition	Present	[30]	[63]	[46]
$2^3S_1 \to 1^3P_0$	4.782	5.53	2.9	0.94
$2^3S_1 \to 1^3P_1$	11.156	7.65	4.7	1.45
$2^3S_1 \to 1^3P_2$	16.823	7.59	5.7	2.28
$2^1S_0 \to 1^1P_1$	18.663	4.40	6.1	3.03
$3^3S_1 \to 2^3P_0$	7.406	–	–	–
$3^3S_1 \to 2^3P_1$	17.049	–	–	–
$3^3S_1 \to 2^3P_2$	25.112	–	–	–
$3^3S_1 \to 1^3P_0$	6.910	–	–	–
$3^3S_1 \to 1^3P_1$	17.563	–	–	–
$3^3S_1 \to 1^3P_2$	27.487	–	–	–
$3^1S_0 \to 1^1P_1$	38.755	–	–	–
$3^1S_0 \to 2^1P_1$	27.988	–	–	–
$1^3P_2 \to 1^3S_1$	55.761	122	83	64.24
$1^3P_1 \to 1^3S_1$	53.294	87.1	11	51.14
$1^3P_0 \to 1^3S_1$	46.862	75.5	55	58.55
$1^1P_1 \to 1^1S_0$	71.923	18.4	80	72.28
$2^3P_2 \to 2^3S_1$	41.259	75.3	55	64.92
$2^3P_1 \to 2^3S_1$	38.533	45.3	45	50.40
$2^3P_0 \to 2^3S_1$	38.308	34.0	42	55.05
$2^1P_1 \to 2^1S_0$	52.205	13.8	52	56.28
$2^3P_2 \to 1^3S_1$	60.195	–	14	–
$2^3P_1 \to 1^3S_1$	57.839	–	5.4	–
$2^3P_0 \to 1^3S_1$	52.508	–	1.0	–
$2^1P_1 \to 1^1S_0$	74.211	–	19	–
$1^3D_1 \to 1^3P_0$	44.783	133	55	–
$1^3D_1 \to 1^3P_1$	28.731	65.3	28	–
$1^3D_1 \to 1^3P_2$	1.786	3.82	1.8	–
$1^3D_2 \to 1^3P_1$	51.272	139	64	–
$1^3D_2 \to 1^3P_2$	16.073	23.6	15	–
$1^3D_3 \to 1^3P_2$	60.336	149	78	–
$1^1D_2 \to 1^1P_1$	66.020	143	63	–

Table 23 $M1$ transition width of charmonia (in keV)

Transition	Present	[39]	[30]	[65]	[75]	PDG [7]
$1^3S_1 \to 1^1S_0$	2.722	2.7	1.05	2.39	3.28	1.58 ± 0.37
$2^3S_1 \to 2^1S_0$	1.172	1.2	0.99	0.19	1.45	0.21 ± 0.15
$2^3S_1 \to 1^1S_0$	7.506	0.0	0.95	7.80	–	1.24 ± 0.29
$3^3S_1 \to 3^1S_0$	9.927	–	–	0.088	–	–

Table 24 $M1$ transition width of bottomonia (in eV)

Transition	Present	[39]	[30]	[66]	[75]	PDG [7]
$1^3S_1 \to 1^1S_0$	37.668	4.0	5.8	10	15.36	–
$2^3S_1 \to 2^1S_0$	5.619	0.05	1.40	0.59	1.82	–
$2^3S_1 \to 1^1S_0$	77.173	0.0	6.4	66	–	12.5 ± 4.9
$3^3S_1 \to 3^1S_0$	2.849	–	0.8	3.9	–	–
$3^3S_1 \to 2^1S_0$	36.177	–	1.5	11	–	≤ 14
$3^3S_1 \to 1^1S_0$	76.990	–	10.5	71	–	10 ± 2

Table 25 $M1$ transition width of B_c meson (in eV)

Transition	Present	[30]	[63]	[46]
$1^3S_1 \to 1^1S_0$	53.109	33	80	2.2
$2^3S_1 \to 2^1S_0$	21.119	17	10	0.014
$2^3S_1 \to 1^1S_0$	481.572	428	600	495
$2^1S_0 \to 1^3S_1$	568.346	488	300	1092

where α, β are slopes and α_0, β_0 are the intercepts that can be computed using the methods given in Ref. [27]. In Figs. 1, 2 and 3, we plot the Regge trajectories. Regge trajectories from present approach and relativistic quark model [27] show similar trend i.e. for charmonium spectra, the computed mass square fits very well to a linear trajectory and found to be almost parallel and equidistant in both the planes. Also, for bottomonia and B_c mesons, we observe the nonlinearity in the parent trajectories. The nonlinearity increases as we go from $c\bar{b}$ to $b\bar{b}$ mesons indicating increasing contribution from the inter-quark interaction over confinement.

According to the first principles of QCD, while the one-gluon-exchange interaction gives rise to employment of Coulomb potential with a strength proportional to the strong running coupling constant at very short distances, nonperturbative effect like confinement becomes prominent at larger distances. Charmonium belongs to neither purely nonrelativistic nor the relativistic regime where chiral symmetry breaking is more significant from physics point of view. Though Lattice QCD calculations in the quenched approximation have suggested a linearly increasing potential in the confinement range [8–18], a specific form of interaction potential in the full range is not yet known. At short distances relativistic effects are more important as they give rise to quark-antiquark pairs from the vacuum that in turn affect the nonrelativistic Coulomb interaction in the presence of sea quarks. The mass spectra of quarkonia is not sensitive to these relativistic effects at short distances. However, the decay properties show significant difference with inclusion of relativistic corrections. We have used the most accepted available correction terms for computation of decay properties [113,118–120] that improves the results significantly in most cases.

Using the potential parameters and numerical wave function, we compute the various decay properties of heavy quarkonia. We first compute the leptonic decay constants of pseudoscalar and vector mesons and our numerical results are tabulated in Tables 8, 9, 10, 11, 12 and 13. For the case

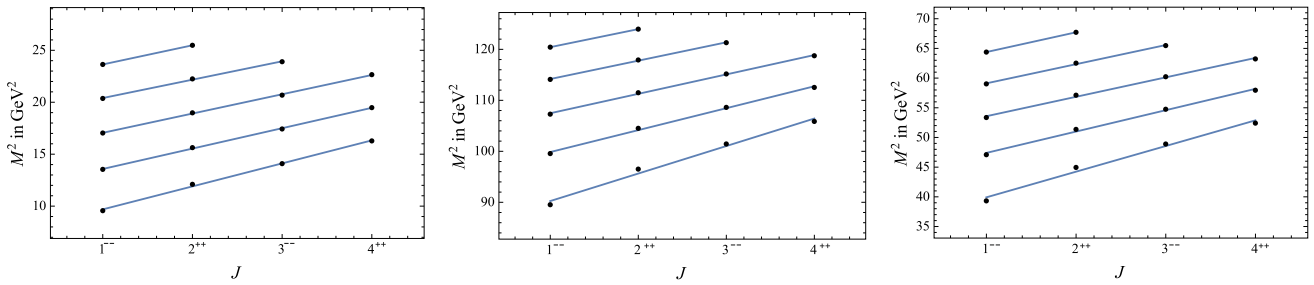

Fig. 1 Parent and daughter Regge trajectories (J, M^2) for charmonia (left), bottomonia (middle) and B_c (right) mesons with natural parity $(P = (-1)^J)$

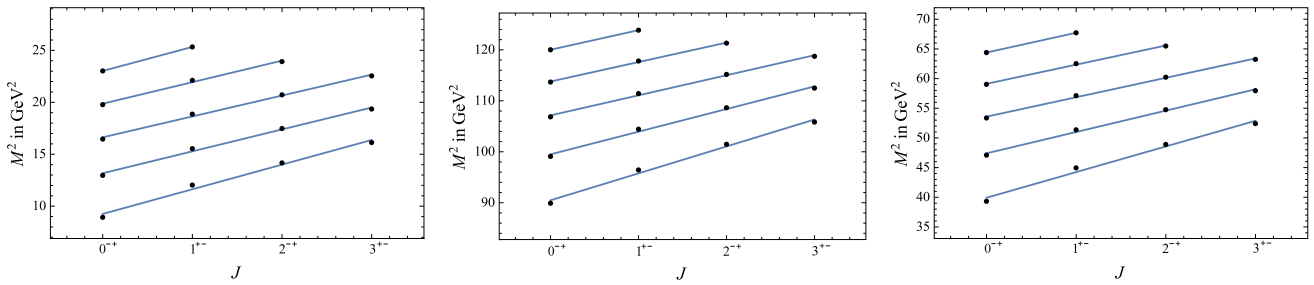

Fig. 2 Parent and daughter Regge trajectories (J, M^2) for charmonia (left), bottomonia (middle) and B_c (right) mesons with unnatural parity $(P = (-1)^{J+1})$

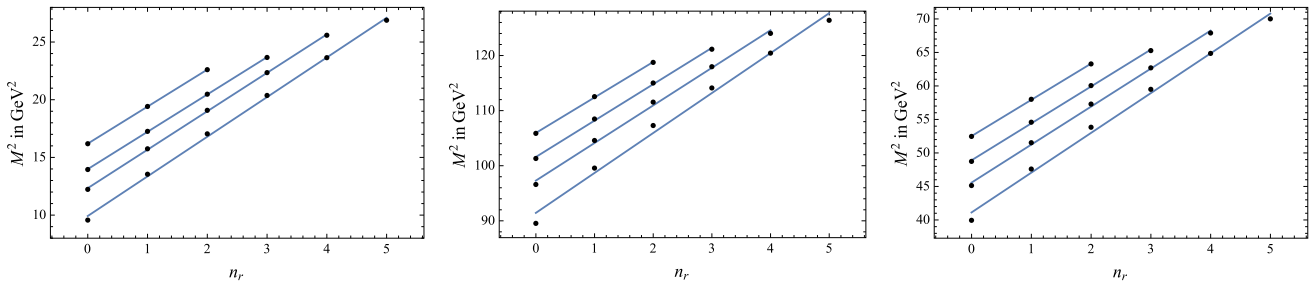

Fig. 3 Parent and daughter Regge trajectories $(n_r \rightarrow M^2)$ for charmonia (left), bottomonia (middle) and B_c (right) mesons

of charmonia, our results are higher than those using LQCD and QCDSR [100]. In order to overcome this discrepancy, we include the QCD correction factors given in Ref. [97] and the results are tabulated in Tables 8 and 9. After introducing the correction factors our results match with PDG, LQCD and QCDSR [100] along with other theoretical models. We also compute the decay constants for excited S-wave charmonia and we found that our results are consistent with the other theoretical predictions. We also compute the decay constants of bottomonia and B_c mesons. In this case, our results match with other theoretical predictions without incorporating the relativistic corrections. In the case of vector decay constants of bottomonia, our results are very close to experimental results as well as those obtained in LQCD Ref. [102]. For the decay constants of B_c mesons, we compare our results with nonrelativistic potential models [52,95].

Next we compute the digamma, digluon and dilepton decay widths using the relations Eqs. (13)–(16). Where the bracketed quantities are the first order radiative corrections to the decay widths. We compare our results with the available experimental results. We also compare our results with the theoretical models such as screened potential model [76,77], Martin-like potential model [73], relativistic quark model (RQM) [31,32], heavy quark spin symmetry [114], relativistic Salpeter model [121] and other theoretical data.

Tables 14 and 15 we present our results for digamma decay widths for charmonia and bottomonia. Our results for $\Gamma(\eta_c \rightarrow \gamma\gamma)$ and $\Gamma(\eta_c(2S) \rightarrow \gamma\gamma)$ are higher than the experimental results. Experimental observation of the two photon decays of pseudoscalar states are considered as an important probe for identification of flavour as well as internal structure of mesons. The first order radiative correction [bracketed terms in Eq. (13)] was utilized to incorporate the difference and it is observed that our results along with the correction match with the experimental results [7]. We also compute the digamma decay width of excited charmonia.

Our results for P-wave charmonia are higher than that of screened potential model [76] and relativistic quark model [32]. Our results for $\Gamma(\eta_b \rightarrow \gamma\gamma)$ match quite well with the experimental data while computed $\Gamma(\eta_b(2S) \rightarrow \gamma\gamma)$ value is overestimated when compared with the PDG data. For the excited state of S-wave bottomonia, our results fall in between those obtained in screened potential model [77] and relativistic quark model with linear confinement [64]. The scenario is similar with P-wave bottomonia and charmonia.

Di-gluon decay has substantial contribution to hadronic decay of quarkonia below $c\bar{c}$ and $b\bar{b}$ threshold. In Tables 16 and 17 we represent our results for digluon decay width of charmonia and bottomonia respectively. Our results for $\Gamma(\eta_c \rightarrow gg)$ match perfectly with the PDG data [7] but in the case of $\Gamma(\eta_c(2S) \rightarrow gg)$ our result is higher than the PDG data. We also compare the results obtained with that of the relativistic Salpeter method [121] and an approximate potential model [70]. It is seen from Table 16 that the relativistic corrections provide better results in case of P-wave charmonia where as that for bottomonia are underestimated in present calculations when compared to relativistic QCD potential model [122] and power potential model [47]. As the experimental data of digluon annihilation of bottomonia are not available, the validity of either of the approaches can be validated only after observations in forthcoming experiments.

We present the result of dilepton decay widths in the Tables 18 and 19 and it is observed that our results matches with the PDG data [7] upto $n = 3$ for both charmonia and bottomonia. The contribution of the correction factor is more significant in the excited states with compared to that in the ground states of the quarkonia, indicating different dynamics in the intermediate quark-antiquark distance. Our results are also in good accordance with the other theoretical models.

We present our results of $E1$ transitions in Tables 20, 21 and 22 in comparison with theoretical attempts such as relativistic potential model [39], quark model [30], nonrelativistic screened potential model [66,76,77]. We also compare our results of charmonia transitions with available experimental results. Our result for $\Gamma(\psi(2S) \rightarrow \chi_{cJ}(1P) + \gamma)$ is in good agreement with the experimental result for $J = 0$ but our results for $J = 1, 2$ are higher than the PDG data. Our results also agree well for the transition $\Gamma(\chi_{c2}(1P) \rightarrow J/\psi + \gamma)$. We also satisfy the experimental constraints for the transition $\Gamma(1^3D_1 \rightarrow \chi_{cJ} + \gamma)$ for $J = 0, 1, 2$. Our results share the same range with the results computed in other theoretical models. The $E1$ transitions of bottomonia agree fairly well except for the channel $\Gamma(\Upsilon(3S) \rightarrow \chi_{bJ}(3P))$, where our results are higher than the experimental results. The comparison of our results of $E1$ transitions in B_c mesons with relativistic quark model [30,63] and power potential model [46] are found to be in good agreement. In Tables 23, 24 and 25, we present our results of $M1$ transitions and also compared with relativistic potential model [39], quark model [30,64], nonrelativistic screened potential model [65,66], power potential [46] as well as with available experimental results. Our results of $\Gamma(\mathrm{n}\psi \rightarrow \mathrm{n}'\eta_c + \gamma)$ are in very good agreement with the PDG data as well with the other theoretical predictions. Computed $M1$ transitions in B_c mesons are also within the results obtained from theoretical predictions. The computed $M1$ transition of bottomonia are found to be higher than the PDG data and also theoretical predictions.

5 Conclusion

In this article, we have reported a comprehensive study of heavy quarkonia in the framework of nonrelativistic potential model considering linear confinement with least number of free model parameters such as confinement strength and quark mass. They are fine tuned to obtain the corresponding spin averaged ground state masses of charmonia and bottomonia determined from experimental data. The parameters are then used to predict the masses of excited states. In order to compute mass spectra of orbitally excited states, we incorporate contributions from the spin dependent part of confined one gluon exchange potential perturbatively.

Our results are found to be consistent with available PDG data, LQCD, relativistic quark model and other theoretical potential models. We also compute the digamma, digluon and dilepton decay widths of heavy quarkonia using nonrelativistic Van-Royen Weiskopf formula. The first order radiative corrections in calculation of these decays provide satisfactory results for the charmonia while no such correction is needed in case of bottomonia for being purely nonrelativistic system. We employ our parameters in computation of B_c spectroscopy employing the quark masses and mean value of confinement strength of charmonia and bottomonia and our results are also consistent with the PDG data. We also compute the weak decays of B_c mesons and the computed life time is also consistent with the PDG data. It is interesting to note here that despite having a c quark, the nonrelativistic calculation of B_c spectroscopy is in very good agreement with experimental and other theoretical models.

Acknowledgements J.N.P. acknowledges the support from the University Grants Commission of India under Major Research Project F.No. 42-775/2013(SR).

Funded by SCOAP[3].

References

1. E. Eichten, S. Godfrey, H. Mahlke, J.L. Rosner, Rev. Mod. Phys. **80**, 1161 (2008). https://doi.org/10.1103/RevModPhys.80.1161
2. S. Godfrey, S.L. Olsen, Ann. Rev. Nucl. Part. Sci. **58**, 51 (2008). https://doi.org/10.1146/annurev.nucl.58.110707.171145
3. T. Barnes, S.L. Olsen, Int. J. Mod. Phys. A **24S1**, 305 (2009). https://doi.org/10.1142/S0217751X09046576
4. N. Brambilla et al., Eur. Phys. J. C **71**, 1534 (2011). https://doi.org/10.1140/epjc/s10052-010-1534-9
5. N. Brambilla et al., Eur. Phys. J. C **74**(10), 2981 (2014). https://doi.org/10.1140/epjc/s10052-014-2981-5
6. A. Andronic et al., Eur. Phys. J. C **76**, 107 (2016). https://doi.org/10.1140/epjc/s10052-015-3819-59
7. C. Patrignani et al., Chin. Phys. C **40**(10), 100001 (2016). https://doi.org/10.1088/1674-1137/40/10/100001
8. J.J. Dudek, R.G. Edwards, N. Mathur, D.G. Richards, Phys. Rev. D **77**, 034501 (2008). https://doi.org/10.1103/PhysRevD.77.034501
9. S. Meinel, Phys. Rev. D **79**, 094501 (2009). https://doi.org/10.1103/PhysRevD.79.094501
10. T. Burch, C. DeTar, M. Di Pierro, A.X. El-Khadra, E.D. Freeland, S. Gottlieb, A.S. Kronfeld, L. Levkova, P.B. Mackenzie, J.N. Simone, Phys. Rev. D **81**, 034508 (2010). https://doi.org/10.1103/PhysRevD.81.034508
11. L. Liu, G. Moir, M. Peardon, S.M. Ryan, C.E. Thomas, P. Vilaseca, J.J. Dudek, R.G. Edwards, B. Joo, D.G. Richards, JHEP **07**, 126 (2012). https://doi.org/10.1007/JHEP07(2012)126
12. C. McNeile, C.T.H. Davies, E. Follana, K. Hornbostel, G.P. Lepage, Phys. Rev. D **86**, 074503 (2012). https://doi.org/10.1103/PhysRevD.86.074503
13. J.O. Daldrop, C.T.H. Davies, R.J. Dowdall, Phys. Rev. Lett. **108**, 102003 (2012). https://doi.org/10.1103/PhysRevLett.108.102003
14. T. Kawanai, S. Sasaki, Phys. Rev. D **89**(5), 054507 (2014). https://doi.org/10.1103/PhysRevD.89.054507
15. T. Kawanai, S. Sasaki, Phys. Rev. Lett. **107**, 091601 (2011). https://doi.org/10.1103/PhysRevLett.107.091601
16. Y. Burnier, O. Kaczmarek, A. Rothkopf, JHEP **12**, 101 (2015). https://doi.org/10.1007/JHEP12(2015)101
17. M. Kalinowski, M. Wagner, Phys. Rev. D **92**(9), 094508 (2015). https://doi.org/10.1103/PhysRevD.92.094508
18. Y. Burnier, O. Kaczmarek, A. Rothkopf, JHEP **10**, 032 (2016). https://doi.org/10.1007/JHEP10(2016)032
19. T. Hilger, C. Popovici, M. Gomez-Rocha, A. Krassnigg, Phys. Rev. D **91**(3), 034013 (2015). https://doi.org/10.1103/PhysRevD.91.034013
20. M.B. Voloshin, Prog. Part. Nucl. Phys. **61**, 455 (2008). https://doi.org/10.1016/j.ppnp.2008.02.001
21. S. Cho, K. Hattori, S.H. Lee, K. Morita, S. Ozaki, Phys. Rev. D **91**(4), 045025 (2015). https://doi.org/10.1103/PhysRevD.91.045025
22. S.S. Gershtein, V.V. Kiselev, A.K. Likhoded, A.V. Tkabladze, Phys. Rev. D **51**, 3613 (1995). https://doi.org/10.1103/PhysRevD.51.3613
23. Y. Kiyo, Y. Sumino, Phys. Lett. B **730**, 76 (2014). https://doi.org/10.1016/j.physletb.2014.01.030
24. T. Liu, A.A. Penin, A. Rayyan, JHEP **02**, 084 (2017). https://doi.org/10.1007/JHEP02(2017)084
25. R.J. Dowdall, C.T.H. Davies, T. Hammant, R.R. Horgan, Phys. Rev. D **89**(3), 031502 (2014). https://doi.org/10.1103/PhysRevD.92.039904, https://doi.org/10.1103/PhysRevD.89.031502. [Erratum: Phys. Rev. D **92**, 039904 (2015)]
26. M. Neubert, Phys. Rep. **245**, 259 (1994). https://doi.org/10.1016/0370-1573(94)90091-4
27. D. Ebert, R.N. Faustov, V.O. Galkin, Eur. Phys. J. C **71**, 1825 (2011). https://doi.org/10.1140/epjc/s10052-011-1825-9
28. D. Ebert, R.N. Faustov, V.O. Galkin, Phys. Rev. D **79**, 114029 (2009). https://doi.org/10.1103/PhysRevD.79.114029
29. D. Ebert, R.N. Faustov, V.O. Galkin, Eur. Phys. J. C **47**, 745 (2006). https://doi.org/10.1140/epjc/s2006-02601-0
30. D. Ebert, R.N. Faustov, V.O. Galkin, Phys. Rev. D **67**, 014027 (2003). https://doi.org/10.1103/PhysRevD.67.014027
31. D. Ebert, R.N. Faustov, V.O. Galkin, Mod. Phys. Lett. A **18**, 1597 (2003). https://doi.org/10.1142/S0217732303011307
32. D. Ebert, R.N. Faustov, V.O. Galkin, Mod. Phys. Lett. A **18**, 601 (2003). https://doi.org/10.1142/S021773230300971X
33. D. Ebert, R.N. Faustov, V.O. Galkin, Phys. Rev. D **62**, 034014 (2000). https://doi.org/10.1103/PhysRevD.62.034014
34. S.N. Gupta, S.F. Radford, Phys. Rev. D **24**, 2309 (1981). https://doi.org/10.1103/PhysRevD.24.2309
35. S.N. Gupta, S.F. Radford, W.W. Repko, Phys. Rev. D **26**, 3305 (1982). https://doi.org/10.1103/PhysRevD.26.3305
36. S.N. Gupta, S.F. Radford, Phys. Rev. D **25**, 3430 (1982). https://doi.org/10.1103/PhysRevD.25.3430
37. J.T. Pantaleone, S.H.H. Tye, Y.J. Ng, Phys. Rev. D **33**, 777 (1986). https://doi.org/10.1103/PhysRevD.33.777
38. K.M. Maung, D.E. Kahana, J.W. Norbury, Phys. Rev. D **47**, 1182 (1993). https://doi.org/10.1103/PhysRevD.47.1182
39. S.F. Radford, W.W. Repko, Phys. Rev. D **75**, 074031 (2007). https://doi.org/10.1103/PhysRevD.75.074031
40. S.F. Radford, W.W. Repko, Nucl. Phys. A **865**, 69 (2011). https://doi.org/10.1016/j.nuclphysa.2011.06.032
41. S.N. Gupta, S.F. Radford, W.W. Repko, Phys. Rev. D **34**, 201 (1986). https://doi.org/10.1103/PhysRevD.34.201
42. P.C. Vinodkumar, J.N. Pandya, V.M. Bannur, S.B. Khadkikar, Eur. Phys. J. A **4**, 83 (1999). https://doi.org/10.1007/s100500050206
43. J.N. Pandya, P.C. Vinodkumar, Pramana **57**, 821 (2001). https://doi.org/10.1007/s12043-001-0031-y
44. A.K. Rai, J.N. Pandya, P.C. Vinodkumar, Eur. Phys. J. A **38**, 77 (2008). https://doi.org/10.1140/epja/i2008-10639-9
45. J.N. Pandya, N.R. Soni, N. Devlani, A.K. Rai, Chin. Phys. C **39**(12), 123101 (2015). https://doi.org/10.1088/1674-1137/39/12/123101
46. N. Devlani, V. Kher, A.K. Rai, Eur. Phys. J. A **50**(10), 154 (2014). https://doi.org/10.1140/epja/i2014-14154-2
47. A. Parmar, B. Patel, P.C. Vinodkumar, Nucl. Phys. A **848**, 299 (2010). https://doi.org/10.1016/j.nuclphysa.2010.08.016
48. A.K. Rai, R.H. Parmar, P.C. Vinodkumar, J. Phys. G **28**, 2275 (2002). https://doi.org/10.1088/0954-3899/28/8/313
49. A. Kumar Rai, P.C. Vinodkumar, J.N. Pandya, J. Phys. G **31**, 1453 (2005). https://doi.org/10.1088/0954-3899/31/12/007
50. A.K. Rai, P.C. Vinodkumar, Pramana **66**, 953 (2006). https://doi.org/10.1007/BF02704795
51. A.K. Rai, B. Patel, P.C. Vinodkumar, Phys. Rev. C **78**, 055202 (2008). https://doi.org/10.1103/PhysRevC.78.055202
52. B. Patel, P.C. Vinodkumar, J. Phys. G **36**, 035003 (2009). https://doi.org/10.1088/0954-3899/36/3/035003
53. M. Fabre De La Ripelle, Phys. Lett. B **205**, 97 (1988). https://doi.org/10.1016/0370-2693(88)90406-6
54. E. Eichten, K. Gottfried, T. Kinoshita, J.B. Kogut, K.D. Lane, T.M. Yan, Phys. Rev. Lett. **34**, 369 (1975). https://doi.org/10.1103/PhysRevLett.34.369. [Erratum: Phys. Rev. Lett. **36**, 1276 (1976)]
55. E. Eichten, K. Gottfried, T. Kinoshita, K.D. Lane, T.M. Yan, Phys. Rev. D **17**, 3090 (1978). https://doi.org/10.1103/PhysRevD.17.3090, https://doi.org/10.1103/PhysRevD.21.313. [Erratum: Phys. Rev. D **21**, 313 (1980)]
56. E. Eichten, K. Gottfried, T. Kinoshita, K.D. Lane, T.M. Yan, Phys. Rev. D **21**, 203 (1980). https://doi.org/10.1103/PhysRevD.21.203

57. C. Quigg, J.L. Rosner, Phys. Rep. **56**, 167 (1979). https://doi.org/10.1016/0370-1573(79)90095-4
58. E. Eichten, F. Feinberg, Phys. Rev. D **23**, 2724 (1981). https://doi.org/10.1103/PhysRevD.23.2724
59. T. Barnes, S. Godfrey, E.S. Swanson, Phys. Rev. D **72**, 054026 (2005). https://doi.org/10.1103/PhysRevD.72.054026
60. V. Sauli, Phys. Rev. D **86**, 096004 (2012). https://doi.org/10.1103/PhysRevD.86.096004
61. S. Leitão, A. Stadler, M.T. Peña, E.P. Biernat, Phys. Rev. D **90**(9), 096003 (2014). https://doi.org/10.1103/PhysRevD.90.096003
62. S. Godfrey, N. Isgur, Phys. Rev. D **32**, 189 (1985). https://doi.org/10.1103/PhysRevD.32.189
63. S. Godfrey, Phys. Rev. D **70**, 054017 (2004). https://doi.org/10.1103/PhysRevD.70.054017
64. S. Godfrey, K. Moats, Phys. Rev. D **92**(5), 054034 (2015). https://doi.org/10.1103/PhysRevD.92.054034
65. W.J. Deng, H. Liu, L.C. Gui, X.H. Zhong, Phys. Rev. D **95**(3), 034026 (2017). https://doi.org/10.1103/PhysRevD.95.034026
66. W.J. Deng, H. Liu, L.C. Gui, X.H. Zhong, Phys. Rev. D **95**(7), 074002 (2017). https://doi.org/10.1103/PhysRevD.95.074002
67. C.S. Fischer, S. Kubrak, R. Williams, Eur. Phys. J. A **51**, 10 (2015). https://doi.org/10.1140/epja/i2015-15010-7
68. O. Lakhina, E.S. Swanson, Phys. Rev. D **74**, 014012 (2006). https://doi.org/10.1103/PhysRevD.74.014012
69. J. Segovia, P.G. Ortega, D.R. Entem, F. Fernández, Phys. Rev. D **93**(7), 074027 (2016). https://doi.org/10.1103/PhysRevD.93.074027
70. S. Patel, P.C. Vinodkumar, S. Bhatnagar, Chin. Phys. C **40**(5), 053102 (2016). https://doi.org/10.1088/1674-1137/40/5/053102
71. C. Bonati, M. D'Elia, A. Rucci, Phys. Rev. D **92**(5), 054014 (2015). https://doi.org/10.1103/PhysRevD.92.054014
72. T. Gutsche, V.E. Lyubovitskij, I. Schmidt, A. Vega, Phys. Rev. D **90**(9), 096007 (2014). https://doi.org/10.1103/PhysRevD.90.096007
73. M. Shah, A. Parmar, P.C. Vinodkumar, Phys. Rev. D **86**, 034015 (2012). https://doi.org/10.1103/PhysRevD.86.034015
74. H. Negash, S. Bhatnagar, Int. J. Mod. Phys. E **25**(08), 1650059 (2016). https://doi.org/10.1142/S0218301316500592
75. K.B.Vijaya Bhaghyesh, A.P.Monteiro Kumar, Phys. G **38**, 085001 (2011). https://doi.org/10.1088/0954-3899/38/8/085001
76. B.Q. Li, K.T. Chao, Phys. Rev. D **79**, 094004 (2009). https://doi.org/10.1103/PhysRevD.79.094004
77. B.Q. Li, K.T. Chao, Commun. Theor. Phys. **52**, 653 (2009). https://doi.org/10.1088/0253-6102/52/4/20
78. C. Quigg, J.L. Rosner, Phys. Lett. B **71**, 153 (1977). https://doi.org/10.1016/0370-2693(77)90765-1
79. A. Martin, Phys. Lett. B **93**(3), 338 (1980). https://doi.org/10.1016/0370-2693(80)90527-4
80. W. Buchmuller, S.H.H. Tye, Phys. Rev. D **24**, 132 (1981). https://doi.org/10.1103/PhysRevD.24.132
81. Wk Kwong, J.L. Rosner, Phys. Rev. D **44**, 212 (1991). https://doi.org/10.1103/PhysRevD.44.212
82. E.J. Eichten, C. Quigg, Phys. Rev. D **49**, 5845 (1994). https://doi.org/10.1103/PhysRevD.49.5845
83. F. Abe et al., Phys. Rev. Lett. **81**, 2432 (1998). https://doi.org/10.1103/PhysRevLett.81.2432
84. V.M. Abazov et al., Phys. Rev. Lett. **101**, 012001 (2008). https://doi.org/10.1103/PhysRevLett.101.012001
85. R. Aaij et al., Phys. Rev. Lett. **109**, 232001 (2012). https://doi.org/10.1103/PhysRevLett.109.232001
86. R. Aaij et al., Eur. Phys. J. C **74**(5), 2839 (2014). https://doi.org/10.1140/epjc/s10052-014-2839-x
87. G. Aad et al., Phys. Rev. Lett. **113**(21), 212004 (2014). https://doi.org/10.1103/PhysRevLett.113.212004
88. S.N. Gupta, J.M. Johnson, Phys. Rev. D **53**, 312 (1996). https://doi.org/10.1103/PhysRevD.53.312
89. G.S. Bali, B. Bolder, N. Eicker, T. Lippert, B. Orth, P. Ueberholz, K. Schilling, T. Struckmann, Phys. Rev. D **62**, 054503 (2000). https://doi.org/10.1103/PhysRevD.62.054503
90. G.S. Bali, Phys. Rep. **343**, 1 (2001). https://doi.org/10.1016/S0370-1573(00)00079-X
91. C. Alexandrou, P. de Forcrand, O. Jahn, Nucl. Phys. Proc. Suppl. **119**, 667 (2003)
92. N. Isgur, G. Karl, Phys. Rev. D **18**, 4187 (1978). https://doi.org/10.1103/PhysRevD.18.4187
93. K.B. Vijaya Kumar, A.K. Rath, S.B. Khadkikar, Pramana **48**, 997 (1997). https://doi.org/10.1007/BF02847459
94. W. Lucha, F.F. Schoberl, Int. J. Mod. Phys. C **10**, 607 (1999). https://doi.org/10.1142/S0129183199000450
95. A.P. Monteiro, M. Bhat, K.B. Vijaya Kumar, Phys. Rev. D **95**(5), 054016 (2017). https://doi.org/10.1103/PhysRevD.95.054016
96. R. Van Royen, V.F. Weisskopf, Nuovo Cim. A **50**, 617 (1967). https://doi.org/10.1007/BF02823542. [Erratum: Nuovo Cim. A **51**, 583 (1967)]
97. E. Braaten, S. Fleming, Phys. Rev. D **52**, 181 (1995). https://doi.org/10.1103/PhysRevD.52.181
98. A.V. Berezhnoy, V.V. Kiselev, A.K. Likhoded, Z. Phys. A **356**, 89 (1996). https://doi.org/10.1007/s002180050152
99. A. Krassnigg, M. Gomez-Rocha, T. Hilger, J. Phys. Conf. Ser. **742**(1), 012032 (2016). https://doi.org/10.1088/1742-6596/742/1/012032
100. D. Bečirević, G. Duplančić, B. Klajn, B. Melić, F. Sanfilippo, Nucl. Phys. B **883**, 306 (2014). https://doi.org/10.1016/j.nuclphysb.2014.03.024
101. G.L. Wang, Phys. Lett. B **633**, 492 (2006). https://doi.org/10.1016/j.physletb.2005.12.005
102. B. Colquhoun, R.J. Dowdall, C.T.H. Davies, K. Hornbostel, G.P. Lepage, Phys. Rev. D **91**(7), 074514 (2015). https://doi.org/10.1103/PhysRevD.91.074514
103. K.M. Ecklund et al., Phys. Rev. D **78**, 091501 (2008). https://doi.org/10.1103/PhysRevD.78.091501
104. J.P. Lees et al., Phys. Rev. D **81**, 052010 (2010). https://doi.org/10.1103/PhysRevD.81.052010
105. M. Ablikim et al., Phys. Rev. D **85**, 112008 (2012). https://doi.org/10.1103/PhysRevD.85.112008
106. J.J. Dudek, R.G. Edwards, Phys. Rev. Lett. **97**, 172001 (2006). https://doi.org/10.1103/PhysRevLett.97.172001
107. T. Chen et al., Eur. Phys. J. C **76**(7), 358 (2016). https://doi.org/10.1140/epjc/s10052-016-4212-8
108. G.T. Bodwin, E. Braaten, G.P. Lepage, Phys. Rev. D **51**, 1125 (1995). https://doi.org/10.1103/PhysRevD.55.5853, https://doi.org/10.1103/PhysRevD.51.1125. [Erratum: Phys. Rev. D **55**, 5853 (1997)]
109. H. Khan, P. Hoodbhoy, Phys. Rev. D **53**, 2534 (1996). https://doi.org/10.1103/PhysRevD.53.2534
110. G.A. Schuler, F.A. Berends, R. van Gulik, Nucl. Phys. B **523**, 423 (1998). https://doi.org/10.1016/S0550-3213(98)00128-X
111. G.T. Bodwin, D. Kang, J. Lee, Phys. Rev. D **74**, 014014 (2006). https://doi.org/10.1103/PhysRevD.74.014014
112. G.T. Bodwin, H.S. Chung, D. Kang, J. Lee, C. Yu, Phys. Rev. D **77**, 094017 (2008). https://doi.org/10.1103/PhysRevD.77.094017
113. J.P. Lansberg, T.N. Pham, Phys. Rev. D **79**, 094016 (2009). https://doi.org/10.1103/PhysRevD.79.094016
114. J.P. Lansberg, T.N. Pham, Phys. Rev. D **74**, 034001 (2006). https://doi.org/10.1103/PhysRevD.74.034001
115. W.L. Sang, F. Feng, Y. Jia, S.R. Liang, Phys. Rev. D **94**(11), 111501 (2016). https://doi.org/10.1103/PhysRevD.94.111501
116. L.D. Landau, Dokl. Akad. Nauk Ser. Fiz. **60**(2), 207 (1948). https://doi.org/10.1016/B978-0-08-010586-4.50070-5
117. C.N. Yang, Phys. Rev. **77**, 242 (1950). https://doi.org/10.1103/PhysRev.77.242

118. W. Kwong, P.B. Mackenzie, R. Rosenfeld, J.L. Rosner, Phys. Rev. D **37**, 3210 (1988). https://doi.org/10.1103/PhysRevD.37.3210
119. R. Barbieri, M. Caffo, R. Gatto, E. Remiddi, Nucl. Phys. B **192**, 61 (1981). https://doi.org/10.1016/0550-3213(81)90192-9
120. M.L. Mangano, A. Petrelli, Phys. Lett. B **352**, 445 (1995). https://doi.org/10.1016/0370-2693(95)00516-N
121. C.S. Kim, T. Lee, G.L. Wang, Phys. Lett. B **606**, 323 (2005). https://doi.org/10.1016/j.physletb.2004.11.084
122. S.N. Gupta, J.M. Johnson, W.W. Repko, Phys. Rev. D **54**, 2075 (1996). https://doi.org/10.1103/PhysRevD.54.2075
123. P. Gonzalez, A. Valcarce, H. Garcilazo, J. Vijande, Phys. Rev. D **68**, 034007 (2003). https://doi.org/10.1103/PhysRevD.68.034007
124. N. Brambilla, Y. Jia, A. Vairo, Phys. Rev. D **D73**, 054005 (2006). https://doi.org/10.1103/PhysRevD.73.054005
125. D.M. Li, P.F. Ji, B. Ma, Eur. Phys. J. C **71**, 1582 (2011). https://doi.org/10.1140/epjc/s10052-011-1582-9
126. A. Abd El-Hady, M.A.K. Lodhi, J.P. Vary, Phys. Rev. D **59**, 094001 (1999). https://doi.org/10.1103/PhysRevD.59.094001

Semileptonic $D_{(s)}$-meson decays in the light of recent data

N. R. Soni,[1,*] M. A. Ivanov,[2,†] J. G. Körner,[3,‡] J. N. Pandya,[1,§] P. Santorelli,[4,5,‖] and C. T. Tran[6,4,¶]

[1]*Applied Physics Department, Faculty of Technology and Engineering, The Maharaja Sayajirao University of Baroda, Vadodara 390001, Gujarat, India*

[2]*Bogoliubov Laboratory of Theoretical Physics, Joint Institute for Nuclear Research, 141980 Dubna, Russia*

[3]*PRISMA Cluster of Excellence, Institut für Physik, Johannes Gutenberg-Universität, D-55099 Mainz, Germany*

[4]*Dipartimento di Fisica "E. Pancini," Università di Napoli Federico II, Complesso Universitario di Monte S. Angelo, Via Cintia, Edificio 6, 80126 Napoli, Italy*

[5]*Istituto Nazionale di Fisica Nucleare, Sezione di Napoli, 80126 Napoli, Italy*

[6]*Institute of Research and Development, Duy Tan University, 550000 Da Nang, Vietnam*

(Received 1 November 2018; published 26 December 2018)

Inspired by recent improved measurements of charm semileptonic decays at BESIII, we study a large set of $D(D_s)$-meson semileptonic decays where the hadron in the final state is one of D^0, ρ, ω, $\eta^{(\prime)}$ in the case of D^+ decays, and D^0, ϕ, K^0, $K^*(892)^0$, $\eta^{(\prime)}$ in the case of D_s^+ decays. The required hadronic form factors are computed in the full kinematical range of momentum transfer by employing the covariant confined quark model developed by us. A detailed comparison of the form factors with those from other approaches is provided. We calculate the decay branching fractions and their ratios, which show good agreement with available experimental data. We also give predictions for the forward-backward asymmetry and the longitudinal and transverse polarizations of the charged lepton in the final state.

DOI: 10.1103/PhysRevD.98.114031

I. INTRODUCTION

Semileptonic $D(D_s)$-meson decays provide a good platform to study both the weak and strong interactions in the charm sector (for a review, see e.g., Ref. [1]). Measurements of their decay rates allow a direct determination of the Cabibbo-Kobayashi-Maskawa (CKM) matrix elements $|V_{cs}|$ and $|V_{cd}|$. In particular, the average of the measurements of *BABAR* [2,3], Belle [4], BESIII [5], and CLEO [6] of the decays $D \to \pi(K)\ell\nu$ was used to extract the elements $|V_{cd(s)}|$, as recently reported by the Particle Data Group (PDG) [7]. Such extraction of the CKM matrix elements from experiments requires theoretical knowledge of the hadronic form factors which take into account the nonperturbative quantum chromodynamics (QCD) effects.

The elements $|V_{cs}|$ and $|V_{cd}|$ can also be determined indirectly by using the unitarity constraint on the CKM matrix. This method was very useful in the past when the direct measurements still suffered from large uncertainties, both experimental and theoretical. Once these matrix elements are determined, whether directly or indirectly, one can in reverse study the strong interaction effects in various charm semileptonic channels to reveal the decay dynamics. One can also test the predictions of different theoretical approaches, such as the form factors and the branching fractions. In this manner, the study of semileptonic charm decays can indirectly contribute to a more precise determination of other CKM matrix elements such as $|V_{ub}|$, in the sense that constraints provided by charm decays can improve the theoretical inputs needed for extracting $|V_{ub}|$ from exclusive charmless B semileptonic decays.

Recent progresses in experimental facilities and theoretical studies have made more and more stringent tests of the standard model (SM) available in the charm sector and have opened a new window through which to look for possible new physics effects beyond the SM. These tests include the CKM matrix unitarity, charge-conjugation-parity violation, isospin symmetry, and lepton flavor universality (LFU). Notably, the BESIII collaboration has reported recently measurements of many semimuonic

*nrsoni-apphy@msubaroda.ac.in
†ivanovm@theor.jinr.ru
‡jukoerne@uni-mainz.de
§jnpandya-apphy@msubaroda.ac.in
‖Pietro.Santorelli@na.infn.it
¶corresponding author.
tranchienthang1347@gmail.com

charm decays [8–10], some for the first time and some with much improved precision. This paves the way to the search for signals of LFU violations in these channels. In addition, the study of the decays $D_s \to \eta^{(\prime)}\ell^+\nu_\ell$ provides information about the $\eta-\eta'$ mixing angle and helps probe the interesting $\eta-\eta'$-glueball mixing [11,12].

From the theoretical point of view, the calculation of hadronic form factors plays a crucial role in the study of charm semileptonic decays. This calculation is carried out by nonperturbative methods including lattice QCD (LQCD) [13–15], QCD sum rules [16–18], light-cone sum rules (LCSR) [19–25], and phenomenological quark models. Regarding the quark models used in studies of semileptonic D decays, one can mention the Isgur-Scora-Grinstein-Wise (ISGW) model [26] and its updated version ISGW2 [27], the constituent quark model (CQM) [28], the relativistic quark model based on the quasipotential approach [29], the chiral quark model [30], the light-front quark model (LFQM) [31–33], and the model based on the combination of heavy meson and chiral symmetries (HMχT) [34,35]. Several semileptonic decay channels of the $D_{(s)}$ mesons were also studied in the large energy effective theory [36], chiral perturbation theory [37], the so-called chiral unitary approach (χUA) [38], and a new approach assuming pure heavy quark symmetry [39]. Recently, a simple expression for $D \to K$ semileptonic form factors was studied in Ref. [40]. We also mention here early attempts to account for flavor symmetry breaking in pseudoscalar meson decay constants by the authors of Ref. [41]. It is worth noting that each method has only a limited range of applicability, and their combination will give a better picture of the underlined physics [28].

In this paper, we compute the form factors of the semileptonic $D(D_s)$ decays in the framework of the covariant confined quark model (CCQM) [42–45]. To be more specific, we study the decays $D^+ \to (D^0,\rho^0,\omega,\eta,\eta')\ell^+\nu_\ell$, $D_s^+ \to (D^0,\phi,K^0,K^*(892)^0,\eta,\eta')\ell^+\nu_\ell$, and $D^0 \to \rho^-\ell^+\nu_\ell$. This paper follows our previous study [46] in which some of us have considered the decays $D \to K^{(*)}\ell^+\nu_\ell$ and $D \to \pi\ell^+\nu_\ell$ in great detail. Our aim is to provide a systematic and independent study of $D_{(s)}$ semileptonic channels in the same theoretical framework. This will shed more light on the theoretical study of the charm decays, especially on the shape of the corresponding form factors, since the CCQM predicts the form factors in the whole physical range of momentum transfer without using any extrapolations. Besides, many of the studies mentioned in the previous paragraph were done about a decade ago, with the main focus on the branching fraction. In light of recent data, more up-to-date predictions are necessary, not only for the branching fraction but also for other physical observables such as the forward-backward asymmetry and the lepton polarization. Finally, such a systematic study is necessary to test our model's predictions and to better estimate its theoretical error.

The rest of the paper is organized as follows. In Sec. II, we briefly provide the definitions of the semileptonic matrix element and hadronic form factors. Then we give the decay distribution in terms of the helicity amplitudes. In Sec. III, we introduce the essential ingredients of the covariant confined quark model and describe in some detail the calculation of the form factors in our approach. Numerical results for the form factors, the decay branching fractions, and other physical observables are presented in Sec. IV. We compare our findings with other theoretical approaches as well as experimental data including recent LQCD calculations and BESIII data. Finally, the conclusion is given in Sec. V.

II. MATRIX ELEMENT AND DECAY DISTRIBUTION

Within the SM, the matrix element for semileptonic decays of the $D_{(s)}$ meson to a pseudoscalar (P) or a vector (V) meson in the final state is written as

$$\mathcal{M}(D_{(s)} \to (P,V)\ell^+\nu_\ell) = \frac{G_F}{\sqrt{2}} V_{cq} \langle (P,V)|\bar{q}O^\mu c|D_{(s)}\rangle [\ell^+ O_\mu \nu_\ell], \tag{1}$$

where $O^\mu = \gamma^\mu(1-\gamma_5)$, and $q = d, s$. The hadronic part in the matrix element is parametrized by the invariant form factors which depend on the momentum transfer squared q^2 between the two mesons as follows:

$$\begin{aligned}
\langle P(p_2)|\bar{q}O^\mu c|D_{(s)}(p_1)\rangle &= F_+(q^2)P^\mu + F_-(q^2)q^\mu,\\
\langle V(p_2,\epsilon_2)|\bar{q}O^\mu c|D_{(s)}(p_1)\rangle &= \frac{\epsilon_{2\alpha}^\dagger}{M_1+M_2}[-g^{\mu\alpha}PqA_0(q^2)\\
&\quad + P^\mu P^\alpha A_+(q^2) + q^\mu P^\alpha A_-(q^2)\\
&\quad + i\varepsilon^{\mu\alpha Pq}V(q^2)],
\end{aligned} \tag{2}$$

where $P = p_1 + p_2$, $q = p_1 - p_2$, and ϵ_2 is the polarization vector of the vector meson V, so that $\epsilon_2^\dagger \cdot p_2 = 0$. The mesons are on shell: $p_1^2 = m_{D_{(s)}}^2 = M_1^2$, $p_2^2 = m_{P,V}^2 = M_2^2$.

For later comparison of the form factors with other studies, we relate our form factors defined in Eq. (2) to the well-known Bauer-Stech-Wirbel (BSW) form factors [47], namely, $F_{+,0}$ for $D_{(s)} \to P$ and $A_{0,1,2}$ and V for $D_{(s)} \to V$. Note that in Ref. [47] the notation F_1 was used instead of F_+. The relations read

$$\begin{aligned}
&\tilde{A}_2 = A_+, \qquad \tilde{V} = V, \qquad \tilde{F}_+ = F_+,\\
&\tilde{A}_1 = \frac{M_1-M_2}{M_1+M_2}A_0, \qquad \tilde{F}_0 = F_+ + \frac{q^2}{M_1^2-M_2^2}F_-,\\
&\tilde{A}_0 = \frac{M_1-M_2}{2M_2}\left(A_0 - A_+ - \frac{q^2}{M_1^2-M_2^2}A_-\right).
\end{aligned} \tag{3}$$

Here, the BSW form factors are denoted with a tilde to distinguish from our form factors. However, for simplicity, we will omit the tilde in what follows. In all comparisons of the form factors to appear below, we use the BSW ones.

Once the form factors are known, one can easily calculate the semileptonic decay rates. However, it is more convenient to write down the differential decay width in terms of the so-called helicity amplitudes which are combinations of the form factors. This is known as the helicity technique, first described in Ref. [48] and further discussed in our recent papers [49,50]. One has

$$\frac{d\Gamma(D_{(s)}\to(P,V)\ell^+\nu_\ell)}{dq^2} = \frac{G_F^2|V_{cq}|^2|\mathbf{p_2}|q^2}{96\pi^3 M_1^2}\left(1-\frac{m_\ell^2}{q^2}\right)^2 \times\left[\left(1+\frac{m_\ell^2}{2q^2}\right)(|H_+|^2+|H_-|^2+|H_0|^2)+\frac{3m_\ell^2}{2q^2}|H_t|^2\right], \quad (4)$$

where $|\mathbf{p_2}|=\lambda^{1/2}(M_1^2,M_2^2,q^2)/2M_1$ is the momentum of the daughter meson in the rest frame of the parent meson. Here, the helicity amplitudes for the decays $D_{(s)}\to V\ell^+\nu_\ell$ are defined as

$$\begin{aligned} H_\pm &= \frac{1}{M_1+M_2}(-PqA_0 \pm 2M_1|\mathbf{p_2}|V), \\ H_0 &= \frac{1}{M_1+M_2}\frac{1}{2M_2\sqrt{q^2}}[-Pq(M_1^2-M_2^2-q^2)A_0 \\ &\quad + 4M_1^2|\mathbf{p_2}|^2A_+], \\ H_t &= \frac{1}{M_1+M_2}\frac{M_1|\mathbf{p_2}|}{M_2\sqrt{q^2}}[Pq(-A_0+A_+)+q^2A_-]. \end{aligned} \quad (5)$$

In the case of the decays $D_{(s)}\to P\ell^+\nu_\ell$ one has

$$\begin{aligned} H_\pm &= 0, \qquad H_0 = \frac{2M_1|\mathbf{p_2}|}{\sqrt{q^2}}F_+, \\ H_t &= \frac{1}{\sqrt{q^2}}(PqF_+ + q^2F_-). \end{aligned} \quad (6)$$

In order to study the lepton-mass effects, one can define several physical observables such as the forward-backward asymmetry $\mathcal{A}_{\rm FB}^\ell(q^2)$ and the longitudinal $P_L^\ell(q^2)$ and transverse $P_T^\ell(q^2)$ polarization of the charged lepton in the final state. This requires the angular decay distribution, which was described elsewhere [50]. In short, one can write down these observables in terms of the helicity amplitudes as follows:

$$\mathcal{A}_{\rm FB}^\ell(q^2) = -\frac{3}{4}\frac{|H_+|^2-|H_-|^2+4\delta_\ell H_0H_t}{(1+\delta_\ell)\sum|H_n|^2+3\delta_\ell|H_t|^2}, \quad (7)$$

$$P_L^\ell(q^2) = -\frac{(1-\delta_\ell)\sum|H_n|^2-3\delta_\ell|H_t|^2}{(1+\delta_\ell)\sum|H_n|^2+3\delta_\ell|H_t|^2}, \quad (8)$$

$$P_T^\ell(q^2) = -\frac{3\pi}{4\sqrt{2}}\frac{\sqrt{\delta_\ell}(|H_+|^2-|H_-|^2-2H_0H_t)}{(1+\delta_\ell)\sum|H_n|^2+3\delta_\ell|H_t|^2}, \quad (9)$$

where $\delta_\ell=m_\ell^2/2q^2$ is the helicity-flip factor, and the index n runs through $(+,-,0)$. The average of these observables over the q^2 range is better suited for experimental measurements with low statistics. To calculate the average one has to multiply the numerator and denominator of e.g., Eq. (7) by the phase-space factor $C(q^2)=|\mathbf{p_2}|(q^2-m_\ell^2)^2/q^2$ and integrate them separately. These observables are sensitive to contributions of physics beyond the SM and can be used to test LFU violations [51–57].

III. FORM FACTORS IN THE COVARIANT CONFINED QUARK MODEL

In this study, the semileptonic form factors are calculated in the framework of the CCQM [42,43]. The CCQM is an effective quantum field approach to the calculation of hadronic transitions. The model is built on the assumption that hadrons interact via constituent quark exchange only. This is realized by adopting a relativistic invariant Lagrangian that describes the coupling of a hadron to its constituent quarks. This approach can be used to treat not only mesons [58–62], but also baryons [63–65], tetraquarks [66–68], and other multiquark states [69] in a consistent way. For a detailed description of the model and the calculation techniques we refer the reader to the references mentioned above. We list below only several key features of the CCQM for completeness.

For the simplest hadronic system, i.e., a meson M, the interaction Lagrangian is given by

$$\mathcal{L}_{\rm int} = g_M M(x)\int dx_1dx_2F_M(x;x_1,x_2) \times\bar{q}_2(x_2)\Gamma_M q_1(x_1)+{\rm H.c.}, \quad (10)$$

where g_M is the quark-meson coupling and Γ_M is the Dirac matrix. For a pseudoscalar (vector) meson $\Gamma_M=\gamma_5$ ($\Gamma_M=\gamma_\mu$). The vertex function $F_M(x,x_1,x_2)$ effectively describes the quark distribution in the meson and is given by

$$F_M(x,x_1,x_2)=\delta\left(x-\sum_{i=1}^2 w_ix_i\right)\cdot\Phi_M((x_1-x_2)^2), \quad (11)$$

where $w_{q_i}=m_{q_i}/(m_{q_1}+m_{q_2})$ such that $w_1+w_2=1$. The function Φ_M depends on the effective size of the meson. In order to avoid ultraviolet divergences in the quark loop integrals, it is required that the Fourier transform of Φ_M has an appropriate falloff behavior in the Euclidean region. Since the final results are not sensitive to the specific form of Φ_M, for simplicity, we choose a Gaussian form as follows:

$$\tilde{\Phi}_M(-p^2) = \int dx e^{ipx} \Phi_M(x^2) = e^{p^2/\Lambda_M^2}, \quad (12)$$

where the parameter Λ_M characterizes the finite size of the meson.

The coupling strength g_M is determined by the compositeness condition $Z_M = 0$ [70], where Z_M is the wave function renormalization constant of the meson. This condition ensures the absence of any bare quark state in the physical mesonic state and, therefore, helps avoid double counting and provides an effective description of a bound state.

In order to calculate the form factors, one first writes down the matrix element of the hadronic transition. In the CCQM, the hadronic matrix element is described by the one-loop Feynman diagram depicted in Fig. 1 and is constructed from the convolution of quark propagators and vertex functions as follows:

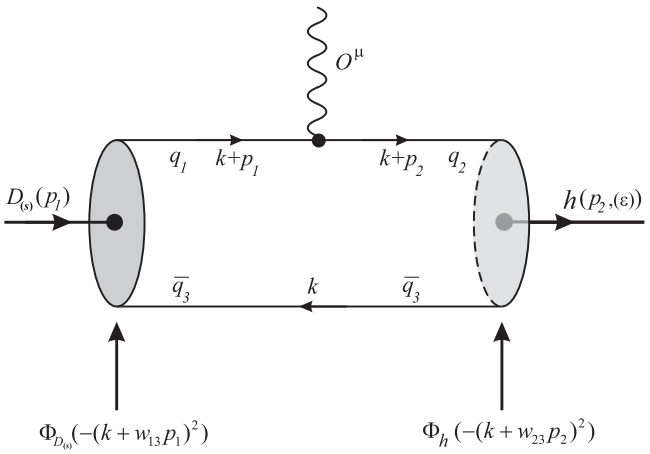

FIG. 1. Quark model diagram for the $D_{(s)}$-meson semileptonic decay.

$$\langle P(p_2)|\bar{q}O^\mu c|D_{(s)}(p_1)\rangle = N_c g_{D_{(s)}} g_P \int \frac{d^4k}{(2\pi)^4 i} \tilde{\Phi}_{D_{(s)}}(-(k+w_{13}p_1)^2)\tilde{\Phi}_P(-(k+w_{23}p_2)^2) \times \mathrm{tr}[O^\mu S_1(k+p_1)\gamma^5 S_3(k)\gamma^5 S_2(k+p_2)], \quad (13)$$

$$\langle V(p_2,\epsilon_2)|\bar{q}O^\mu c|D_{(s)}(p_1)\rangle = N_c g_{D_{(s)}} g_V \int \frac{d^4k}{(2\pi)^4 i} \tilde{\Phi}_{D_{(s)}}(-(k+w_{13}p_1)^2)\tilde{\Phi}_V(-(k+w_{23}p_2)^2) \times \mathrm{tr}[O^\mu S_1(k+p_1)\gamma^5 S_3(k)\not{\epsilon}_2^\dagger S_2(k+p_2)], \quad (14)$$

where $N_c = 3$ is the number of colors, $w_{ij} = m_{q_j}/(m_{q_i} + m_{q_j})$, and $S_{1,2}$ are quark propagators, for which we use the Fock-Schwinger representation

$$S_i(k) = (m_{q_i} + \not{k}) \int_0^\infty d\alpha_i \exp[-\alpha_i(m_{q_i}^2 - k^2)]. \quad (15)$$

It should be noted that all loop integrations are carried out in Euclidean space.

Using various techniques described in our previous papers, a form factor F can be finally written in the form of a threefold integral

$$F = N_c g_{D_{(s)}} g_{(P,V)} \int_0^{1/\lambda^2} dt t \int_0^1 d\alpha_1 \times \int_0^1 d\alpha_2 \delta(1-\alpha_1-\alpha_2) f(t\alpha_1, t\alpha_2), \quad (16)$$

where $f(t\alpha_1, t\alpha_2)$ is the resulting integrand corresponding to the form factor F, and λ is the so-called infrared cutoff parameter, which is introduced to avoid the appearance of the branching point corresponding to the creation of free quarks and taken to be universal for all physical processes.

The model parameters, namely, the meson size parameters, the constituent quark masses, and the infrared cutoff parameter are determined by fitting the radiative and leptonic decay constants to experimental data or LQCD calculations. The model parameters required for the calculation in this paper are listed in Tables I and II. Other parameters such as the mass and lifetime of mesons and leptons, the CKM matrix elements, and physical constants are taken from the recent report of the PDG [7]. In particular, we adopt the following values for the CKM matrix elements: $|V_{cd}| = 0.218$ and $|V_{cs}| = 0.997$.

Once the model parameters are fixed, the form factors are obtained by calculating the threefold integral in Eq. (16).

TABLE I. Meson size parameters in GeV.

Λ_D	Λ_{D_s}	Λ_K	Λ_{K^*}	Λ_ϕ	Λ_ρ	Λ_ω	$\Lambda_\eta^{q\bar{q}}$	$\Lambda_\eta^{s\bar{s}}$	$\Lambda_{\eta'}^{q\bar{q}}$	$\Lambda_{\eta'}^{s\bar{s}}$
1.600	1.750	1.014	0.805	0.880	0.610	0.488	0.881	1.973	0.257	2.797

TABLE II. Quark masses and infrared cutoff parameter in GeV.

$m_{u/d}$	m_s	m_c	m_b	λ
0.241	0.428	1.672	5.05	0.181

This is done by using MATHEMATICA as well as FORTRAN code. In the CCQM, the form factors are calculable in the entire range of momentum transfer. The calculated form factors are very well represented by the double-pole parametrization

$$F(q^2) = \frac{F(0)}{1 - a\hat{s} + b\hat{s}^2}, \qquad \hat{s} = \frac{q^2}{m^2_{D_{(s)}}}. \tag{17}$$

Our results for the parameters $F(0)$, a, and b appearing in the parametrization Eq. (17) are given in Table III.

It is worth noting here that in the calculation of the $D_{(s)} \to \eta^{(\prime)}$ form factors one has to take into account the mixing of the light and the s-quark components. By assuming $m_u = m_d \equiv m_q$, the quark content can be written as

$$\begin{pmatrix} \eta \\ \eta' \end{pmatrix} = -\begin{pmatrix} \sin\delta & \cos\delta \\ -\cos\delta & \sin\delta \end{pmatrix} \begin{pmatrix} q\bar{q} \\ s\bar{s} \end{pmatrix},$$
$$q\bar{q} \equiv \frac{u\bar{u} + d\bar{d}}{\sqrt{2}}. \tag{18}$$

The angle δ is defined by $\delta = \theta_P - \theta_I$, where $\theta_I = \arctan(1/\sqrt{2})$ is the ideal mixing angle. We adopt the value $\theta_P = -15.4°$ from Ref. [71].

TABLE III. Parameters of the double-pole parametrization Eq. (17) for the form factors.

F	$F(0)$	a	b	F	$F(0)$	a	b
$A_+^{D\to\rho}$	0.57	0.96	0.15	$A_-^{D\to\rho}$	−0.74	1.11	0.22
$A_0^{D\to\rho}$	1.47	0.47	−0.10	$V^{D\to\rho}$	0.76	1.13	0.23
$A_+^{D\to\omega}$	0.55	1.01	0.17	$A_-^{D\to\omega}$	−0.69	1.17	0.26
$A_0^{D\to\omega}$	1.41	0.53	−0.10	$V^{D\to\omega}$	0.72	1.19	0.27
$A_+^{D_s\to\phi}$	0.67	1.06	0.17	$A_-^{D_s\to\phi}$	−0.95	1.20	0.26
$A_0^{D_s\to\phi}$	2.13	0.59	−0.12	$V^{D_s\to\phi}$	0.91	1.20	0.25
$A_+^{D_s\to K^*}$	0.57	1.13	0.21	$A_-^{D_s\to K^*}$	−0.82	1.32	0.34
$A_0^{D_s\to K^*}$	1.53	0.61	−0.11	$V^{D_s\to K^*}$	0.80	1.32	0.33
$F_+^{D\to\eta}$	0.67	0.93	0.12	$F_-^{D\to\eta}$	−0.37	1.02	0.18
$F_+^{D\to\eta'}$	0.76	1.23	0.23	$F_-^{D\to\eta'}$	−0.064	2.29	1.71
$F_+^{D\to D^0}$	0.91	5.88	4.40	$F_-^{D\to D^0}$	−0.026	6.32	8.37
$F_+^{D_s\to\eta}$	0.78	0.69	0.002	$F_-^{D_s\to\eta}$	−0.42	0.74	0.008
$F_+^{D_s\to\eta'}$	0.73	0.88	0.018	$F_-^{D_s\to\eta'}$	−0.28	0.92	0.009
$F_+^{D_s\to K}$	0.60	1.05	0.18	$F_-^{D_s\to K}$	−0.38	1.14	0.24
$F_+^{D_s\to D^0}$	0.92	5.08	2.25	$F_-^{D_s\to D^0}$	−0.34	6.79	8.91

IV. RESULTS AND DISCUSSION

A. Form factors

In this subsection, we compare our form factors with those from other theoretical approaches and from experimental measurements. For convenience, we relate all form factors from different studies to the BSW form factors, as mentioned in Sec. II. In the SM, the hadronic matrix element between two mesons is parametrized by two form factors (F_+ and F_0) for the $P \to P'$ transition and four form factors ($A_{0,1,2}$ and V) for the $P \to V$ one. However, in semileptonic decays of D and D_s mesons, the form factors F_0 and A_0 are less interesting because their contributions to the decay rate vanish in the zero lepton-mass limit (the tau mode is kinematically forbidden). Therefore, we focus more on the form factors F_+, A_1, A_2, and V. We note that the uncertainties of our form factors mainly come from the errors of the model parameters. These parameters are determined from a least-squares fit to available experimental data and some lattice calculations. We have observed that the errors of the fitted parameters are within 10%. We then calculated the propagation of these errors on the form factors and found the uncertainties on the form factors to be of order 20% at small q^2 and 30% at high q^2. At maximum recoil $q^2 = 0$, the form factor uncertainties are of order 15%.

We start with the $D_{(s)} \to P$ transition form factor $F_+(q^2)$. In Table IV, we compare the maximum-recoil values $F_+(q^2 = 0)$ with other theoretical approaches. It is observed that our results are in good agreement with other quark models, especially with the CQM [28] and the LFQM [32]. Besides, quark model predictions for $F_+(0)$ of the $D_{(s)} \to \eta^{(\prime)}$ channels are in general higher than those obtained by LCSR [22,24] and LQCD [14]. This suggests that more studies of these form factors are needed. For example, a better LQCD calculation of $F_+(0)$ is expected. Note that the authors of Ref. [14] considered their LQCD calculation as a pilot study rather than a conclusive one.

Regarding the $D_{(s)} \to V$ transition form factors A_1, A_2, and V, it is more interesting to compare their ratios at maximum recoil. The ratios are defined as follows:

$$r_2 = \frac{A_2(q^2 = 0)}{A_1(q^2 = 0)}, \qquad r_V = \frac{V(q^2 = 0)}{A_1(q^2 = 0)}. \tag{19}$$

In Table V, we compare these ratios with the world average given by the PDG [7] and with other theoretical results obtained in CQM [28], LFQM [32], HMχT [35], and LQCD [13]. Our results for the form factor ratios r_2 and r_V agree well with the PDG data within uncertainty except for the ratio $r_V(D_s^+ \to \phi)$, for which our prediction is much lower than that from PDG. Note that our prediction $r_V(D_s^+ \to \phi) = 1.34$ is close to the value 1.42 from the LFQM [32]. It is also seen that for most cases, the HMχT predictions [35] for the ratios at $q^2 = 0$ are largely different

TABLE IV. Comparison of $F_+(0)$ for $D_{(s)} \to P$ transitions.

	$D \to \eta$	$D \to \eta'$	$D_s \to \eta$	$D_s \to \eta'$	$D_s \to K^0$
Present	0.67 ± 0.10	0.76 ± 0.11	0.78 ± 0.12	0.73 ± 0.11	0.60 ± 0.09
CQM [28]	⋯	⋯	0.78	0.78	0.72
LFQM [32]	0.71	⋯	0.76	⋯	0.66
LQCD$_{M_\pi=470\ \mathrm{MeV}}$[14]	⋯	⋯	0.564(11)	0.437(18)	⋯
LQCD$_{M_\pi=370\ \mathrm{MeV}}$[14]	⋯	⋯	0.542(13)	0.404(25)	⋯
LCSR [22]	0.552 ± 0.051	0.458 ± 0.105	0.432 ± 0.033	0.520 ± 0.080	⋯
LCSR [24]	$0.429^{+0.165}_{-0.141}$	$0.292^{+0.113}_{-0.104}$	$0.495^{+0.030}_{-0.029}$	$0.558^{+0.047}_{-0.045}$	⋯

TABLE V. Ratios of the $D_{(s)} \to V$ transition form factors at maximum recoil.

Channel	Ratio	Present	PDG [7]	LQCD [13]	CQM [28]	LFQM [32]	HMχT [35]
$D \to \rho$	r_2	0.93 ± 0.19	0.83 ± 0.12	⋯	0.83	0.78	0.51
	r_V	1.26 ± 0.25	1.48 ± 0.16	⋯	1.53	1.47	1.72
$D^+ \to \omega$	r_2	0.95 ± 0.19	1.06 ± 0.16	⋯	⋯	0.84	0.51
	r_V	1.24 ± 0.25	1.24 ± 0.11	⋯	⋯	1.47	1.72
$D_s^+ \to \phi$	r_2	0.99 ± 0.20	0.84 ± 0.11	0.74(12)	0.73	0.86	0.52
	r_V	1.34 ± 0.27	1.80 ± 0.08	1.72(21)	1.72	1.42	1.80
$D_s^+ \to K^{*0}$	r_2	0.99 ± 0.20	⋯	⋯	0.74	0.82	0.55
	r_V	1.40 ± 0.28	⋯	⋯	1.82	1.55	1.93

from the PDG values, demonstrating the fact that this model is more suitable for the high q^2 region.

In order to have a better picture of the form factors in the whole q^2 range $0 \le q^2 \le q^2_{\mathrm{max}} = (m_{D_{(s)}} - m_{P/V})^2$ we plot in Figs. 2–5 their q^2 dependence from various studies. It is very interesting to note that, in all cases, our form factors are close to those obtained in the covariant LFQM [32], and this is not for the first time such a good agreement is observed. In a previous study of the semileptonic decays $B_c \to J/\psi(\eta_c)\ell\nu$ [72] it was seen that the corresponding form factors agree very well between our model and the covariant LFQM [73]. This suggests that a comparison of the two models in more detail may be fruitful. It is also worth noting that the HMχT [35] prediction for the form factor $A_0(q^2)$ is systematically much higher than that from other theoretical calculations.

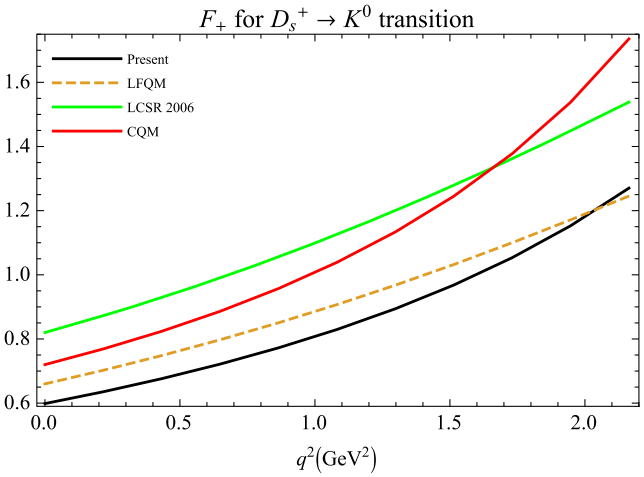

FIG. 2. Form factor $F_+(q^2)$ for $D_s^+ \to K^0$ in our model, LFQM [32], LCSR [20], and CQM [28].

Very recently, the ETM collaboration has provided the lattice determination [75] for the full set of the form factors characterizing the semileptonic $D \to \pi(K)\ell\nu$ and rare $D \to \pi(K)\ell\ell$ decays within and beyond the SM, when an additional tensor coupling is considered. As mentioned before, the decays $D \to \pi(K)\ell\nu$ have been studied in our model already [46]. However, we compute the $D \to \pi(K)\ell\nu$ form factors including the tensor one in this paper, in order to compare with the recent ETM results. This demonstrates the fidelity of the CCQM predictions for the hadronic form factors and helps us better estimate the theoretical uncertainties of our model. Moreover, the tensor and scalar form factors are essential for the study of possible new physics in these decays [for more detail we refer to a similar calculation of the full set of $B \to D^{(*)}$ and $B \to \pi(\rho)$ form factors in our model [76,77]].

The new tensor form factor is defined by

$$\langle P(p_2)|\bar{q}\sigma^{\mu\nu}(1-\gamma^5)c|D(p_1)\rangle = \frac{iF^T(q^2)}{M_1+M_2}(P^\mu q^\nu - P^\nu q^\mu + i\epsilon^{\mu\nu Pq}). \quad (20)$$

Note that we obtained $F_0(q^2)$ by using the form factors $F_+(q^2)$ and $F_-(q^2)$ defined in Eq. (2), with the help of the relation

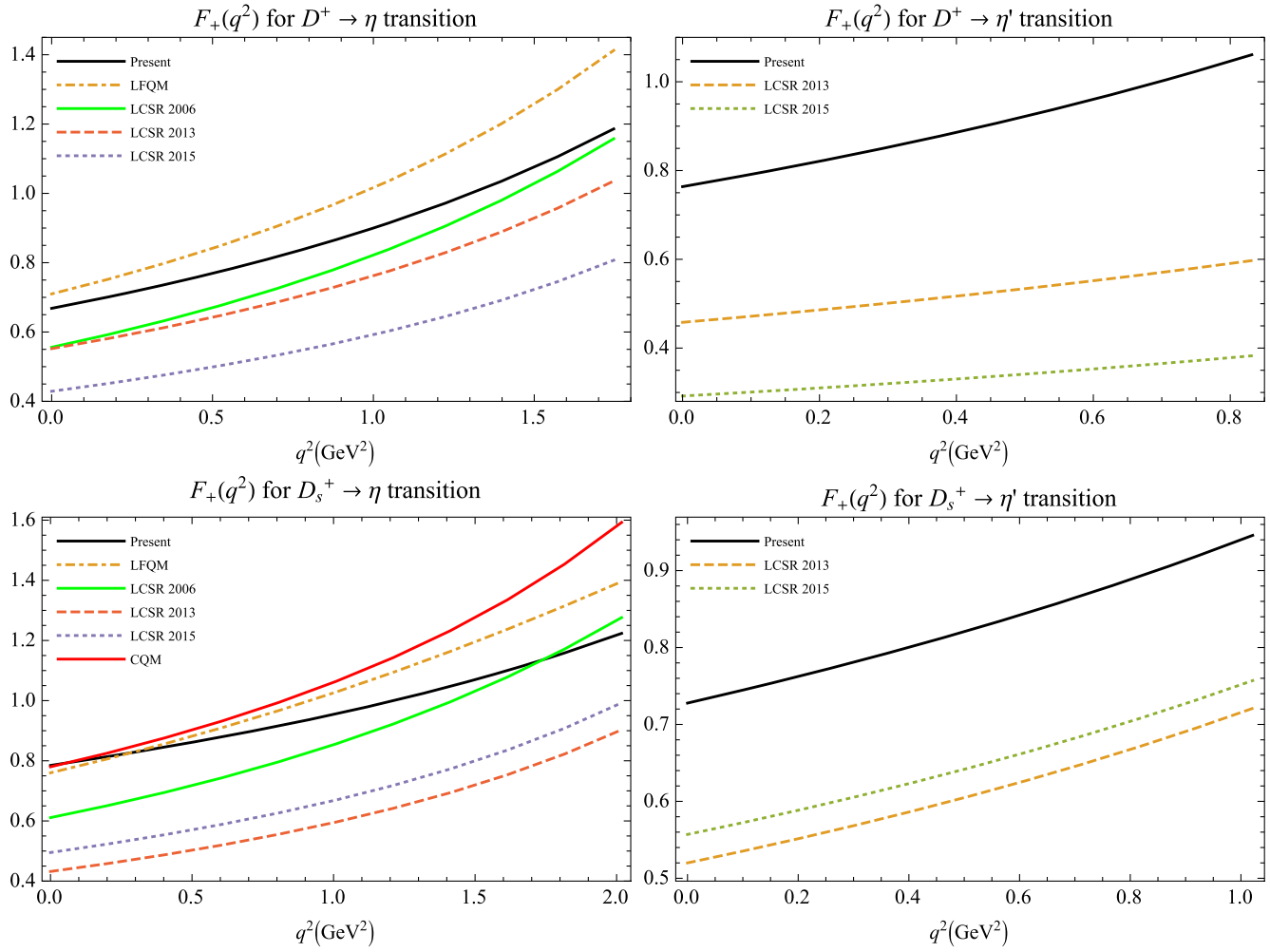

FIG. 3. Form factor $F_+(q^2)$ for $D^+_{(s)} \to \eta^{(\prime)}$ in our model, LCSR [20,22,24], and CQM [28].

$$F_0(q^2) = F_+(q^2) + \frac{q^2}{M_1^2 - M_2^2} F_-(q^2). \tag{21}$$

Meanwhile, the ETM collaboration directly calculated the scalar matrix element $\langle P(p_2)|\bar{q}c|D(p_1)\rangle$ and then determined $F_0(q^2)$ using the equation of motion. In this way, the final result becomes sensitive to the quark mass difference.

In Fig. 6 we compare the form factors $F_0(q^2)$, $F_+(q^2)$, and $F_T(q^2)$ of the $D \to \pi(K)\ell\nu$ transitions with those obtained by the ETM collaboration. It is seen that our $F_0(q^2)$ agrees well with the ETM only in the low q^2 region. However, our results for $F_+(q^2)$ are very close to those of the ETM. Note that the determination of $F_+(q^2)$ by the ETM is dependent on $F_0(q^2)$. It is interesting that the tensor form factors between the two studies are in perfect agreement. Even though this form factor does not appear within the SM, this agreement has an important meaning because, in both approaches, the tensor form factor is determined directly from the corresponding matrix element without any additional assumptions. In Table VI, we present the values of the form factors and their ratios at maximum recoil. One sees that our results agree with the ETM calculation within uncertainty.

B. Branching fractions and other observables

In Tables VII and VIII, we summarize our predictions for the semileptonic branching fractions of the D and D_s mesons, respectively. For comparison, we also list results of other theoretical calculations and the most recent experimental data given by the CLEO and BESIII collaborations. Note that the uncertainties of our predictions for the branching fractions and other polarization observables are of order 50%, taking into account only the main source of uncertainties related to the form factors.

In general, our results for the branching fractions are consistent with experimental data as well as with other theoretical calculations. It is worth mentioning that, for such a large set of decays considered in this study, our branching fractions agree very well with all available experimental data except for one channel, the $D_s^+ \to K^0\ell^+\nu_\ell$. In this case, our prediction is nearly twice

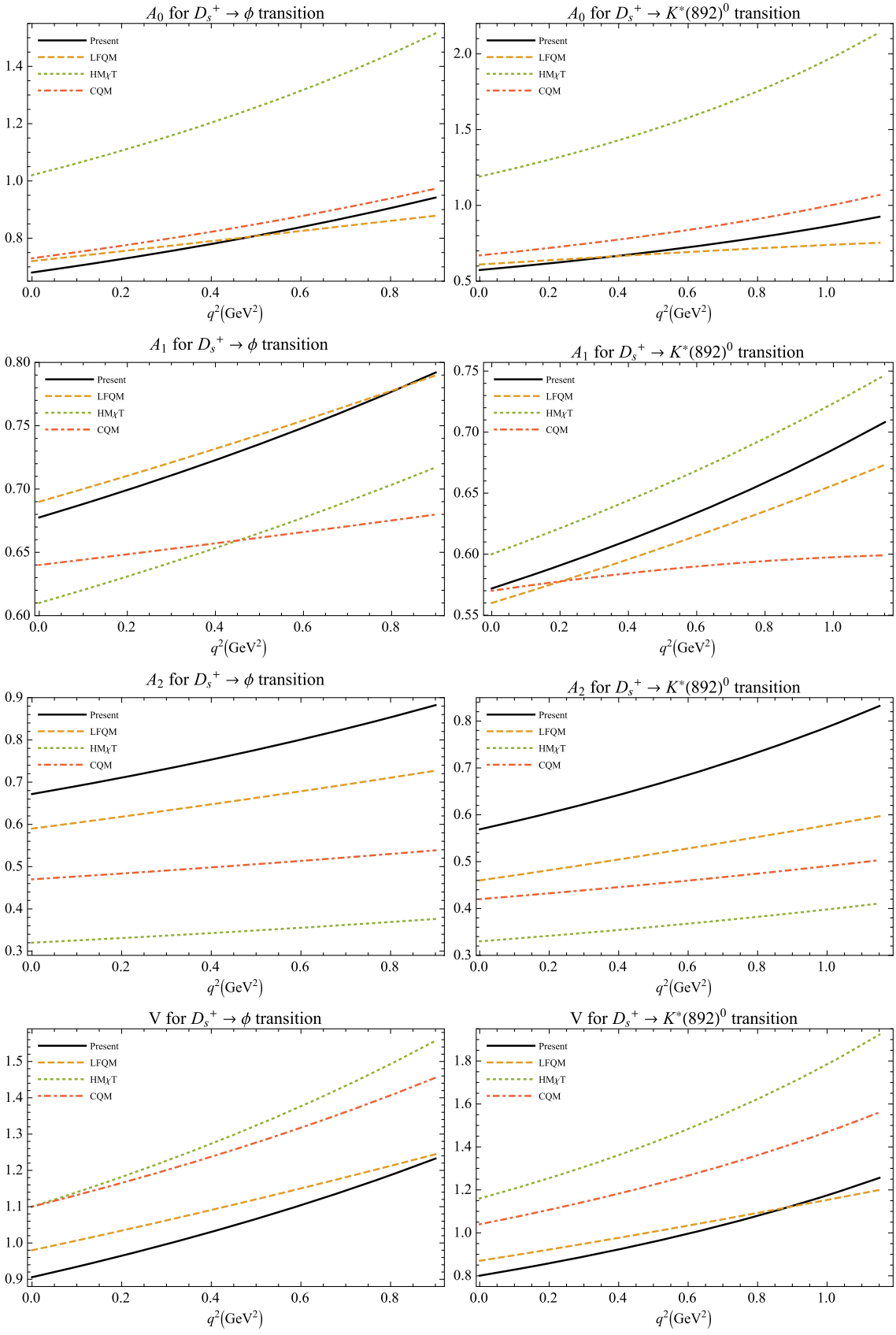

FIG. 4. Form factors for $D_s^+ \to \phi$ (left) and $D_s^+ \to K^*(892)^0$ (right) in our model, LFQM [32], HMχT [35], and CQM [28].

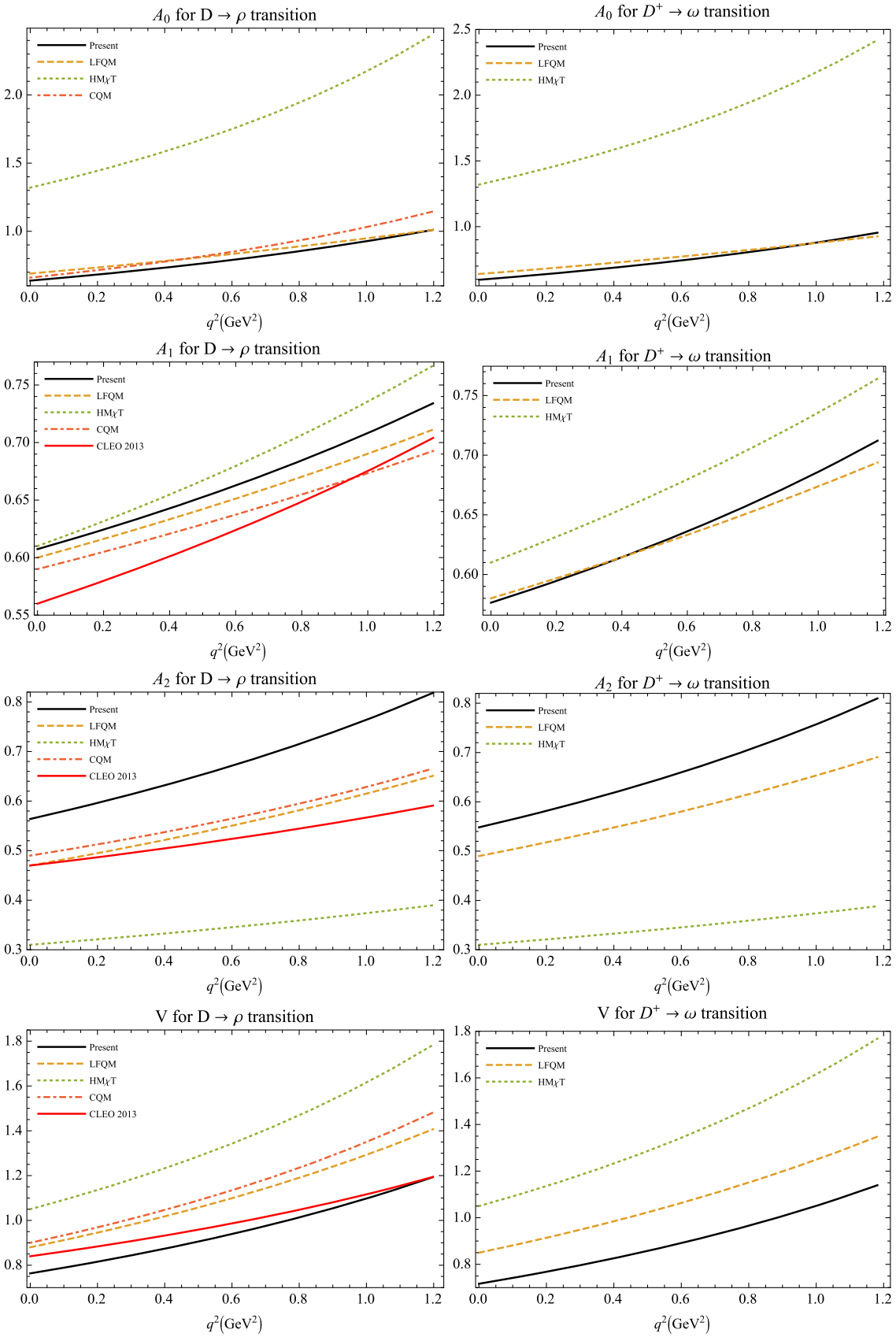

FIG. 5. Form factors for $D \to \rho$ (left) and $D^+ \to \omega$ (right) in our model, LFQM [32], HMχT [35], CQM [28], and CLEO data [74].

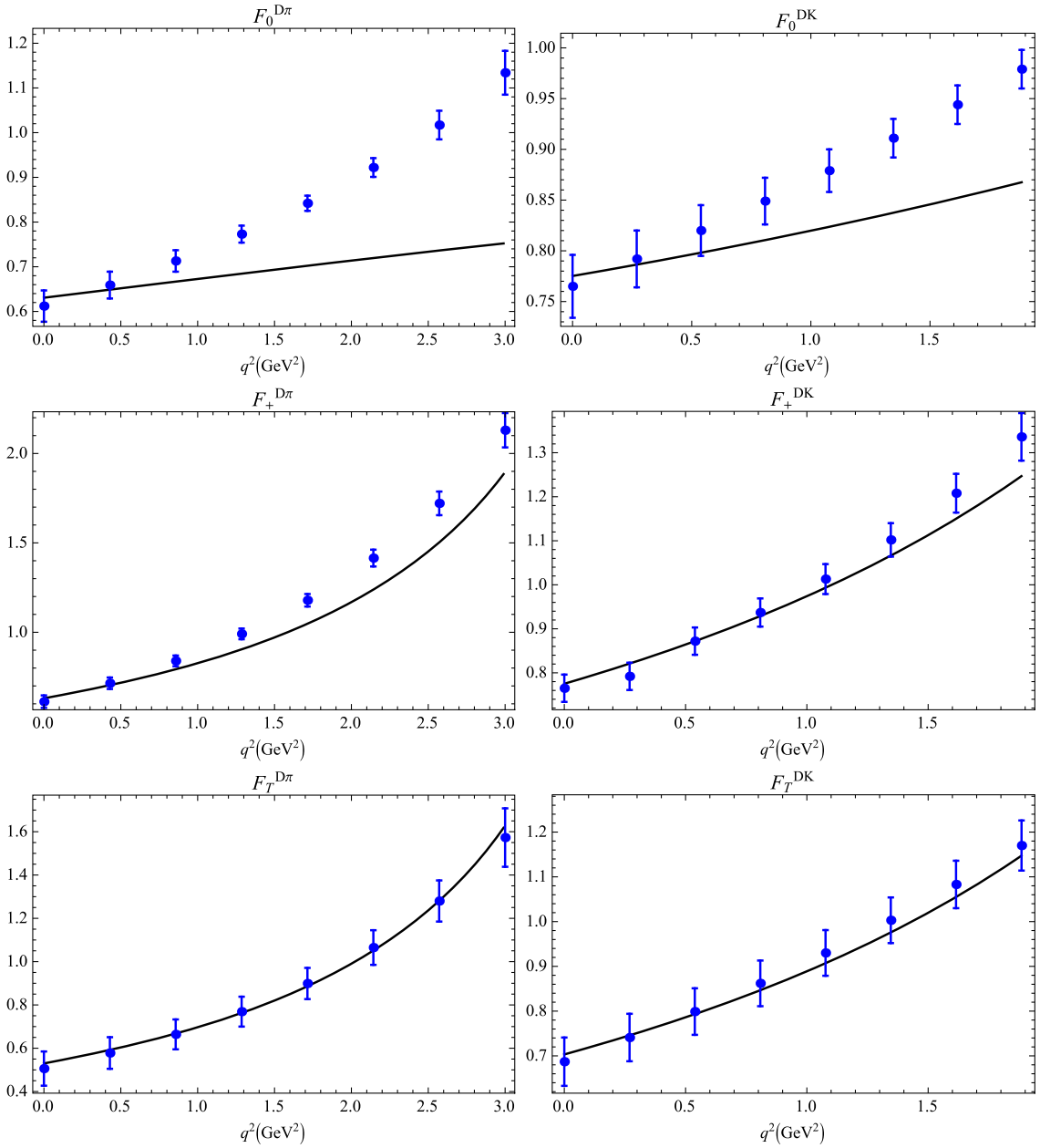

FIG. 6. $D \to \pi(K)\ell\nu$ form factors obtained in our model (solid lines) and in lattice calculation (dots with error bars) by the ETM collaboration [75].

as small as the CLEO central value [83] and about 30% smaller than the LFQM prediction [33].

We also give prediction for the ratio $\Gamma(D^0 \to \rho^- e^+ \nu_e)/2\Gamma(D^+ \to \rho^0 e^+ \nu_e)$ which should be equal to unity in the SM, assuming isospin invariance. Our calculation yields 0.98, in agreement with CLEO's result of $1.03 \pm 0.09^{+0.08}_{-0.02}$ [74]. Besides, our ratio of branching fractions $\mathcal{B}(D_s^+ \to \eta' e^+ \nu_e)/\mathcal{B}(D_s^+ \to \eta e^+ \nu_e) = 0.37$ coincides with the result 0.36 ± 0.14 obtained by CLEO [85] and the more recent value 0.40 ± 0.14 by BESIII [84].

TABLE VI. $D \to \pi(K)\ell\nu$ form factors and their ratios at $q^2 = 0$.

	$f_+^{D\pi}(0)$	$f_+^{DK}(0)$	$f_T^{D\pi}(0)$	$f_T^{DK}(0)$	$f_T^{D\pi}(0)/f_+^{D\pi}(0)$	$f_T^{DK}(0)/f_+^{DK}(0)$
Present	0.63	0.78	0.53	0.70	0.84	0.90
ETM [75]	0.612(35)	0.765(31)	0.506(79)	0.687(54)	0.827(114)	0.898(50)

TABLE VII. Branching fractions of $D^+(D^0)$-meson semileptonic decays.

Channel	Unit	Present	Other	Reference	Data	Reference
$D^0 \to \rho^- e^+ \nu_e$	10^{-3}	1.62	1.97	χUA [38]	$1.445 \pm 0.058 \pm 0.039$	BESIII [78]
			$1.749^{+0.421}_{-0.297} \pm 0.006$	LCSR [25]	$1.77 \pm 0.12 \pm 0.10$	CLEO [74]
			2.0	HMχT [35]		
$D^0 \to \rho^- \mu^+ \nu_\mu$	10^{-3}	1.55	1.84	χUA [38]		
$D^+ \to \rho^0 e^+ \nu_e$	10^{-3}	2.09	2.54	χUA [38]	$1.860 \pm 0.070 \pm 0.061$	BESIII [78]
			$2.217^{+0.534}_{-0.376} \pm 0.015$	LCSR [25]	$2.17 \pm 0.12^{+0.12}_{-0.22}$	CLEO [74]
			2.5	HMχT [35]		
$D^+ \to \rho^0 \mu^+ \nu_\mu$	10^{-3}	2.01	2.37	χUA [38]	2.4 ± 0.4	PDG [7]
$D^+ \to \omega e^+ \nu_e$	10^{-3}	1.85	2.46	χUA [38]	$1.63 \pm 0.11 \pm 0.08$	BESIII [79]
			2.5	HMχT [35]	$1.82 \pm 0.18 \pm 0.07$	CLEO [74]
			2.1 ± 0.2	LFQM [33]		
$D^+ \to \omega \mu^+ \nu_\mu$	10^{-3}	1.78	2.29	χUA [38]		
			2.0 ± 0.2	LFQM [33]		
$D^+ \to \eta e^+ \nu_e$	10^{-4}	9.37	12 ± 1	LFQM [33]	$10.74 \pm 0.81 \pm 0.51$	BESIII [80]
			24.5 ± 5.26	LCSR [22]	$11.4 \pm 0.9 \pm 0.4$	CLEO [81]
			14.24 ± 10.98	LCSR [24]		
$D^+ \to \eta \mu^+ \nu_\mu$	10^{-4}	9.12	12 ± 1	LFQM [33]		
$D^+ \to \eta' e^+ \nu_e$	10^{-4}	2.00	1.8 ± 0.2	LFQM [33]	$1.91 \pm 0.51 \pm 0.13$	BESIII [80]
			3.86 ± 1.77	LCSR [22]	$2.16 \pm 0.53 \pm 0.07$	CLEO [81]
			1.52 ± 1.17	LCSR [24]		
$D^+ \to \eta' \mu^+ \nu_\mu$	10^{-4}	1.90	1.7 ± 0.2	LFQM [33]		

TABLE VIII. Branching fractions of D_s-meson semileptonic decays (in %).

Channel	Present	Other	Reference	Data	Reference
$D_s^+ \to \phi e^+ \nu_e$	3.01	2.12	χUA [38]	$2.26 \pm 0.45 \pm 0.09$	BESIII [9]
		3.1 ± 0.3	LFQM [33]	$2.61 \pm 0.03 \pm 0.08 \pm 0.15$	*BABAR* [82]
		2.4	HMχT [35]	$2.14 \pm 0.17 \pm 0.08$	CLEO [83]
$D_s^+ \to \phi \mu^+ \nu_\mu$	2.85	1.94	χUA [38]		
		2.9 ± 0.3	LFQM [33]	$1.94 \pm 0.53 \pm 0.09$	BESIII [9]
$D_s^+ \to K^0 e^+ \nu_e$	0.20	0.27 ± 0.02	LFQM [33]	$0.39 \pm 0.08 \pm 0.03$	CLEO [83]
$D_s^+ \to K^0 \mu^+ \nu_\mu$	0.20	0.26 ± 0.02	LFQM [33]		
$D_s^+ \to K^{*0} e^+ \nu_e$	0.18	0.202	χUA [38]	$0.18 \pm 0.04 \pm 0.01$	CLEO [83]
		0.19 ± 0.02	LFQM [33]		
		0.22	HMχT [35]		
$D_s^+ \to K^{*0} \mu^+ \nu_\mu$	0.17	0.189	χUA [38]		
		0.19 ± 0.02	LFQM [33]		
$D_s^+ \to \eta e^+ \nu_e$	2.24	2.26 ± 0.21	LFQM [33]	$2.30 \pm 0.31 \pm 0.08$	BESIII [84]
		2.00 ± 0.32	LCSR [22]	$2.28 \pm 0.14 \pm 0.19$	CLEO [83]
		2.40 ± 0.28	LCSR [24]		
$D_s^+ \to \eta \mu^+ \nu_\mu$	2.18	2.22 ± 0.20	LFQM [33]	$2.42 \pm 0.46 \pm 0.11$	BESIII [9]
$D_s^+ \to \eta' e^+ \nu_e$	0.83	0.89 ± 0.09	LFQM [33]	$0.93 \pm 0.30 \pm 0.05$	BESIII [84]
		0.75 ± 0.23	LCSR [22]	$0.68 \pm 0.15 \pm 0.06$	CLEO [83]
		0.79 ± 0.14	LCSR [24]		
$D_s^+ \to \eta' \mu^+ \nu_\mu$	0.79	0.85 ± 0.08	LFQM [33]	$1.06 \pm 0.54 \pm 0.07$	BESIII [9]

TABLE IX. Semileptonic branching fractions for $D^+_{(s)} \to D^0 \ell^+ \nu_\ell$.

Channel	Present	Other	Reference	Data	Reference
$D^+ \to D^0 e^+ \nu_e$	2.23×10^{-13}	2.78×10^{-13}	[88]	$< 1.0 \times 10^{-4}$	BESIII [87]
		2.71×10^{-13}	[89]		
$D_s^+ \to D^0 e^+ \nu_e$	2.52×10^{-8}	$(2.97 \pm 0.03) \times 10^{-8}$	[88]	...	...
		3.34×10^{-8}	[89]		

TABLE X. Forward-backward asymmetry and lepton polarization components.

	$\langle \mathcal{A}^e_{\rm FB} \rangle$	$\langle \mathcal{A}^\mu_{\rm FB} \rangle$	$\langle P^e_L \rangle$	$\langle P^\mu_L \rangle$	$\langle P^e_T \rangle$	$\langle P^\mu_T \rangle$
$D^0 \to \rho^- \ell^+ \nu_\ell$	0.21	0.19	−1.00	−0.92	1.4×10^{-3}	0.22
$D^+ \to \rho^0 \ell^+ \nu_\ell$	0.22	0.19	−1.00	−0.92	1.4×10^{-3}	0.22
$D^+ \to \omega \ell^+ \nu_\ell$	0.21	0.19	−1.00	−0.92	1.4×10^{-3}	0.22
$D^+ \to \eta \ell^+ \nu_\ell$	-6.4×10^{-6}	−0.06	−1.00	−0.83	2.8×10^{-3}	0.44
$D^+ \to \eta' \ell^+ \nu_\ell$	-13.0×10^{-6}	−0.10	−1.00	−0.70	4.2×10^{-3}	0.59
$D^+ \to D^0 \ell^+ \nu_\ell$	−0.10	...	−0.72	...	0.56	...
$D_s^+ \to \phi \ell^+ \nu_\ell$	0.18	0.15	−1.00	−0.91	1.5×10^{-3}	0.23
$D_s^+ \to K^{*0} \ell^+ \nu_\ell$	0.22	0.20	−1.00	−0.92	1.4×10^{-3}	0.22
$D_s^+ \to K^0 \ell^+ \nu_\ell$	-5.0×10^{-6}	−0.05	−1.00	−0.86	2.4×10^{-3}	0.39
$D_s^+ \to \eta \ell^+ \nu_\ell$	-6.0×10^{-6}	−0.06	−1.00	−0.84	2.7×10^{-3}	0.42
$D_s^+ \to \eta' \ell^+ \nu_\ell$	-11.2×10^{-6}	−0.09	−1.00	−0.75	3.8×10^{-3}	0.54
$D_s^+ \to D^0 \ell^+ \nu_\ell$	-7.37×10^{-4}	...	−1.00	...	0.038	...

Finally, we predict $\mathcal{B}(D^+ \to \eta' e^+ \nu_e)/\mathcal{B}(D^+ \to \eta e^+ \nu_e) = 0.21$, which agrees very well with the values 0.19 ± 0.05 and 0.18 ± 0.05 we got from experimental data by CLEO [81] and BESIII [80], respectively. It is worth mentioning here that very recently, the BESIII collaboration has reported their measurement of $\mathcal{B}(D^0 \to K^- \mu^+ \nu_\mu)$ [86] with significantly improved precision. In their paper, they also approved the prediction of our model for the ratio $\mathcal{B}(D^0 \to K^- \mu^+ \nu_\mu)/\mathcal{B}(D^0 \to K^- e^+ \nu_e)$ provided in Ref. [46].

In Table IX, we present our results for the semileptonic decays $D^+_{(s)} \to D^0 e^+ \nu_e$, which are rare in the SM due to phase-space suppression. These decays are of particular interest since they are induced by the light quark decay, while the heavy quark acts as the spectator. Besides, the small phase space helps reduce the theoretical errors. The first experimental constraint on the branching fraction $\mathcal{B}(D^+ \to D^0 e^+ \nu_e)$ was recently obtained by the BESIII collaboration [87]. However, the experimental upper limit is still far above the SM predictions. The branching fractions obtained in our model are comparable with other theoretical calculations using the flavor SU(3) symmetry in the light quark sector [88,89].

Finally, in Table X we list our predictions for the forward-backward asymmetry $\langle \mathcal{A}^\ell_{\rm FB} \rangle$, the longitudinal polarization $\langle P^\ell_L \rangle$, and the transverse polarization $\langle P^\ell_T \rangle$ of the charged lepton in the final state. It is seen that, for the $P \to V$ transitions, the lepton-mass effect in $\langle \mathcal{A}^\ell_{\rm FB} \rangle$ is small, resulting in a difference of only 10%–15% between the corresponding electron and muon modes. For the $P \to P'$ transitions, $\langle \mathcal{A}^\mu_{\rm FB} \rangle$ are about 10^4 times larger than $\langle \mathcal{A}^e_{\rm FB} \rangle$. This is readily seen from Eq. (7): for $P \to P'$ transitions the two helicity amplitudes $H_\pm$ vanish and the forward-backward asymmetry is proportional to the lepton mass squared. Regarding the longitudinal polarization, the difference between $\langle P^\mu_L \rangle$ and $\langle P^e_L \rangle$ is 10%–30%. One sees that the lepton-mass effect in the transverse polarization is much more significant than that in the longitudinal one. This is true for both $P \to P'$ and $P \to V$ transitions. Note that the values of $\langle \mathcal{A}^e_{\rm FB} \rangle$ and $\langle P^e_{L(T)} \rangle$ for the rare decays $D^+_{(s)} \to D^0 e^+ \nu_e$ are quite different in comparison with other $P \to P'$ transitions due to their extremely small kinematical regions.

V. SUMMARY AND CONCLUSION

We have presented a systematic study of the D and D_s semileptonic decays within the framework of the CCQM. All the relevant form factors are calculated in the entire range of momentum transfer squared. We have also provided a detailed comparison of the form factors with other theoretical predictions and, in some cases, with available experimental data. In particular, we have observed a good agreement with the form factors obtained in the covariant LFQM, for all decays. It is worth noting that our tensor form factors for the $D \to \pi(K) \ell \nu$ decays are in perfect agreement with the recent LQCD calculation by the ETM collaboration [75].

We have given our predictions for the semileptonic branching fractions and their ratios. In general, our results are in good agreement with other theoretical approaches and with recent experimental data obtained by *BABAR*, CLEO, and BESIII. In all cases, our predictions for the

branching fractions agree with experimental data within 10%, except for the $D_s^+ \to K^0 \ell^+ \nu_\ell$ channel. Our predictions for the ratios of branching fractions are in full agreement with experimental data. To conclude, we have provided the first ever theoretical predictions for the forward-backward asymmetries and lepton longitudinal and transverse polarizations, which are important for future experiments.

ACKNOWLEDGMENTS

J. N. P. acknowledges financial support from University Grants Commission of India under Major Research Project F.No. 42-775/2013(SR). P. S. acknowledges support from Istituto Nazionale di Fisica Nucleare, I. S. QFT_HEP. M. A. I., J. G. K., and C. T. T. thank Heisenberg-Landau Grant for providing support for their collaboration. M. A. I. acknowledges financial support of PRISMA Cluster of Excellence at University of Mainz. N. R. S. thanks Bogoliubov Laboratory of Theoretical Physics, Joint Institute for Nuclear Research for warm hospitality during Helmholtz-DIAS International Summer School "Quantum Field Theory at the Limits: from Strong Field to Heavy Quarks" where this work was initiated. C. T. T. acknowledges support from Duy Tan University during the beginning stage of this work. M. A. I. and C. T. T. appreciate warm hospitality of Mainz Institute for Theoretical Physics at University of Mainz, where part of this work was done.

Note added.—Recently, we became aware of the paper [90] where the BESIII collaboration reported their new measurements of the branching fractions for the decays $D_s^+ \to K^0 e^+ \nu_e$ and $D_s^+ \to K^{*0} e^+ \nu_e$ with improved precision. They also obtained for the first time the values of the form factors at maximum recoil. Our predictions for the branching fraction $\mathcal{B}(D_s^+ \to K^{*0} e^+ \nu_e)$ as well as the form factor parameters $f_+^{D_s K}(0)$, $r_V^{D_s K^*}(0)$, and $r_2^{D_s K^*}(0)$ agree with the new BESIII results. Regarding their result $\mathcal{B}(D_s^+ \to K^0 e^+ \nu_e) = (3.25 \pm 0.41) \times 10^{-3}$, the central value is closer to our prediction, in comparison with the CLEO result [83]. However, the BESIII result is still at 1σ larger than ours.

[1] J. D. Richman and P. R. Burchat, Rev. Mod. Phys. **67**, 893 (1995).
[2] J. P. Lees *et al.* (*BABAR* Collaboration), Phys. Rev. D **91**, 052022 (2015).
[3] B. Aubert *et al.* (*BABAR* Collaboration), Phys. Rev. D **76**, 052005 (2007).
[4] L. Widhalm *et al.* (Belle Collaboration), Phys. Rev. Lett. **97**, 061804 (2006).
[5] M. Ablikim *et al.* (BESIII Collaboration), Phys. Rev. D **92**, 072012 (2015).
[6] D. Besson *et al.* (CLEO Collaboration), Phys. Rev. D **80**, 032005 (2009).
[7] M. Tanabashi *et al.* (Particle Data Group), Phys. Rev. D **98**, 030001 (2018).
[8] M. Ablikim *et al.* (BESIII Collaboration), Eur. Phys. J. C **76**, 369 (2016).
[9] M. Ablikim *et al.* (BESIII Collaboration), Phys. Rev. D **97**, 012006 (2018).
[10] M. Ablikim *et al.* (BESIII Collaboration), Phys. Rev. Lett. **121**, 171803 (2018).
[11] V. V. Anisovich, D. V. Bugg, D. I. Melikhov, and V. A. Nikonov, Phys. Lett. B **404**, 166 (1997).
[12] C. Di Donato, G. Ricciardi, and I. Bigi, Phys. Rev. D **85**, 013016 (2012).
[13] G. C. Donald, C. T. H. Davies, J. Koponen, and G. P. Lepage (HPQCD Collaboration), Phys. Rev. D **90**, 074506 (2014).
[14] G. S. Bali, S. Collins, S. Dürr, and I. Kanamori, Phys. Rev. D **91**, 014503 (2015).
[15] S. Aoki *et al.*, Eur. Phys. J. C **77**, 112 (2017).
[16] P. Ball, Phys. Rev. D **48**, 3190 (1993).
[17] P. Colangelo and F. De Fazio, Phys. Lett. B **520**, 78 (2001).
[18] D. S. Du, J. W. Li, and M. Z. Yang, Eur. Phys. J. C **37**, 173 (2004).
[19] A. Khodjamirian, R. Ruckl, S. Weinzierl, C. W. Winhart, and O. I. Yakovlev, Phys. Rev. D **62**, 114002 (2000).
[20] Y. L. Wu, M. Zhong, and Y. B. Zuo, Int. J. Mod. Phys. A **21**, 6125 (2006).
[21] K. Azizi, R. Khosravi, and F. Falahati, J. Phys. G **38**, 095001 (2011).
[22] N. Offen, F. A. Porkert, and A. Schäfer, Phys. Rev. D **88**, 034023 (2013).
[23] U. G. Meißner and W. Wang, Phys. Lett. B **730**, 336 (2014).
[24] G. Duplancic and B. Melic, J. High Energy Phys. 11 (2015) 138.
[25] H. B. Fu, X. Yang, R. Lü, L. Zeng, W. Cheng, and X. G. Wu, arXiv:1808.06412.
[26] N. Isgur, D. Scora, B. Grinstein, and M. B. Wise, Phys. Rev. D **39**, 799 (1989).
[27] D. Scora and N. Isgur, Phys. Rev. D **52**, 2783 (1995).
[28] D. Melikhov and B. Stech, Phys. Rev. D **62**, 014006 (2000).
[29] R. N. Faustov, V. O. Galkin, and A. Y. Mishurov, Phys. Rev. D **53**, 1391 (1996).
[30] T. Palmer and J. O. Eeg, Phys. Rev. D **89**, 034013 (2014).
[31] Z. T. Wei, H. W. Ke, and X. F. Yang, Phys. Rev. D **80**, 015022 (2009).
[32] R. C. Verma, J. Phys. G **39**, 025005 (2012).
[33] H. Y. Cheng and X. W. Kang, Eur. Phys. J. C **77**, 587 (2017); **77**, 863(E) (2017).
[34] S. Fajfer and J. F. Kamenik, Phys. Rev. D **71**, 014020 (2005).

[35] S. Fajfer and J. F. Kamenik, Phys. Rev. D **72**, 034029 (2005).
[36] J. Charles, A. Le Yaouanc, L. Oliver, O. Pene, and J. C. Raynal, Phys. Rev. D **60**, 014001 (1999).
[37] J. Bijnens and I. Jemos, Nucl. Phys. **B846**, 145 (2011).
[38] T. Sekihara and E. Oset, Phys. Rev. D **92**, 054038 (2015).
[39] L. R. Dai, X. Zhang, and E. Oset, Phys. Rev. D **98**, 036004 (2018).
[40] T. N. Pham, Int. J. Mod. Phys. A **33**, 1850160 (2018).
[41] S. S. Gershtein and M. Y. Khlopov, Pis'ma Zh. Eksp. Teor. Fiz. **23**, 374 (1976); M. Y. Khlopov, Yad. Fiz. **28**, 1134 (1978) [Sov. J. Nucl. Phys. **28**, 583 (1978)].
[42] G. V. Efimov and M. A. Ivanov, Int. J. Mod. Phys. A **04**, 2031 (1989); *The Quark Confinement Model of Hadrons* (CRC Press, Boca Raton, 1993).
[43] T. Branz, A. Faessler, T. Gutsche, M. A. Ivanov, J. G. Körner, and V. E. Lyubovitskij, Phys. Rev. D **81**, 034010 (2010).
[44] M. A. Ivanov, J. G. Körner, S. G. Kovalenko, P. Santorelli, and G. G. Saidullaeva, Phys. Rev. D **85**, 034004 (2012).
[45] T. Gutsche, M. A. Ivanov, J. G. Körner, V. E. Lyubovitskij, and P. Santorelli, Phys. Rev. D **86**, 074013 (2012).
[46] N. R. Soni and J. N. Pandya, Phys. Rev. D **96**, 016017 (2017).
[47] M. Wirbel, B. Stech, and M. Bauer, Z. Phys. C **29**, 637 (1985).
[48] J. G. Körner and G. A. Schuler, Z. Phys. C **38**, 511 (1988); **41**, 690(E) (1989); Phys. Lett. B **231**, 306 (1989); Z. Phys. C **46**, 93 (1990).
[49] T. Gutsche, M. A. Ivanov, J. G. Körner, V. E. Lyubovitskij, P. Santorelli, and N. Habyl, Phys. Rev. D **91**, 074001 (2015); **91**, 119907(E) (2015).
[50] M. A. Ivanov, J. G. Körner, and C. T. Tran, Phys. Rev. D **92**, 114022 (2015).
[51] S. Bifani, S. Descotes-Genon, A. Romero Vidal, and M. H. Schune, arXiv:1809.06229.
[52] M. A. Ivanov, J. G. Körner, and C. T. Tran, Phys. Rev. D **95**, 036021 (2017).
[53] Q. Y. Hu, X. Q. Li, and Y. D. Yang, arXiv:1810.04939.
[54] P. Asadi, M. R. Buckley, and D. Shih, arXiv:1810.06597.
[55] N. Rajeev and R. Dutta, Phys. Rev. D **98**, 055024 (2018).
[56] F. Feruglio, P. Paradisi, and O. Sumensari, arXiv:1806.10155.
[57] R. Alonso, J. Martin Camalich, and S. Westhoff, arXiv:1811.05664.
[58] M. A. Ivanov and P. Santorelli, Phys. Lett. B **456**, 248 (1999).
[59] A. Faessler, T. Gutsche, M. A. Ivanov, J. G. Körner, and V. E. Lyubovitskij, Eur. Phys. J. Direct **4**, 1 (2002).
[60] M. A. Ivanov, J. G. Körner, and P. Santorelli, Phys. Rev. D **73**, 054024 (2006).
[61] M. A. Ivanov and C. T. Tran, Phys. Rev. D **92**, 074030 (2015).
[62] S. Dubnička, A. Z. Dubničková, M. A. Ivanov, A. Liptaj, P. Santorelli, and C. T. Tran, arXiv:1808.06261.
[63] T. Gutsche, M. A. Ivanov, J. G. Körner, V. E. Lyubovitskij, and P. Santorelli, Phys. Rev. D **87**, 074031 (2013).
[64] T. Gutsche, M. A. Ivanov, J. G. Körner, and V. E. Lyubovitskij, Phys. Rev. D **96**, 054013 (2017).
[65] T. Gutsche, M. A. Ivanov, J. G. Körner, V. E. Lyubovitskij, P. Santorelli, and C. T. Tran, Phys. Rev. D **98**, 053003 (2018).
[66] S. Dubnicka, A. Z. Dubnickova, M. A. Ivanov, J. G. Körner, P. Santorelli, and G. G. Saidullaeva, Phys. Rev. D **84**, 014006 (2011).
[67] F. Goerke, T. Gutsche, M. A. Ivanov, J. G. Körner, V. E. Lyubovitskij, and P. Santorelli, Phys. Rev. D **94**, 094017 (2016).
[68] F. Goerke, T. Gutsche, M. A. Ivanov, J. G. Körner, and V. E. Lyubovitskij, Phys. Rev. D **96**, 054028 (2017).
[69] T. Gutsche, M. A. Ivanov, J. G. Körner, V. E. Lyubovitskij, and K. Xu, Phys. Rev. D **96**, 114004 (2017).
[70] A. Salam, Nuovo Cimento **25**, 224 (1962); S. Weinberg, Phys. Rev. **130**, 776 (1963).
[71] T. Feldmann, P. Kroll, and B. Stech, Phys. Rev. D **58**, 114006 (1998).
[72] C. T. Tran, M. A. Ivanov, J. G. Körner, and P. Santorelli, Phys. Rev. D **97**, 054014 (2018).
[73] W. Wang, Y. L. Shen, and C. D. Lu, Phys. Rev. D **79**, 054012 (2009).
[74] S. Dobbs *et al.* (CLEO Collaboration), Phys. Rev. Lett. **110**, 131802 (2013).
[75] V. Lubicz, L. Riggio, G. Salerno, S. Simula, and C. Tarantino (ETM Collaboration), Phys. Rev. D **96**, 054514 (2017); **98**, 014516 (2018).
[76] M. A. Ivanov, J. G. Körner, and C. T. Tran, Phys. Rev. D **94**, 094028 (2016).
[77] M. A. Ivanov, J. G. Körner, and C. T. Tran, Phys. Part. Nucl. Lett. **14**, 669 (2017).
[78] M. Ablikim *et al.* (BESIII Collaboration), arXiv:1809.06496.
[79] M. Ablikim *et al.* (BESIII Collaboration), Phys. Rev. D **92**, 071101 (2015).
[80] M. Ablikim *et al.* (BESIII Collaboration), Phys. Rev. D **97**, 092009 (2018).
[81] J. Yelton *et al.* (CLEO Collaboration), Phys. Rev. D **84**, 032001 (2011).
[82] B. Aubert *et al.* (*BABAR* Collaboration), Phys. Rev. D **78**, 051101 (2008).
[83] J. Hietala, D. Cronin-Hennessy, T. Pedlar, and I. Shipsey, Phys. Rev. D **92**, 012009 (2015).
[84] M. Ablikim *et al.* (BESIII Collaboration), Phys. Rev. D **94**, 112003 (2016).
[85] J. Yelton *et al.* (CLEO Collaboration), Phys. Rev. D **80**, 052007 (2009).
[86] M. Ablikim *et al.* (BESIII Collaboration), arXiv:1810.03127.
[87] M. Ablikim *et al.* (BESIII Collaboration), Phys. Rev. D **96**, 092002 (2017).
[88] H. B. Li and M. Z. Yang, Eur. Phys. J. C **59**, 841 (2009).
[89] S. Faller and T. Mannel, Phys. Lett. B **750**, 653 (2015).
[90] M. Ablikim *et al.* (BESIII Collaboration), arXiv:1811.02911.

Masses and radiative leptonic decay properties of Bc meson

N. R. Soni* and J. N. Pandya
Applied Physics Department, Faculty of Technology and Engineering,
The M S University of Baroda, Vadodara 390001, INDIA
**Email: nakulphy@gmail.com*

Introduction

We employ non-relativistic treatment with the help of Schrödinger equation in order to study the Bc spectroscopy. The Schrödinger equation for the bound state of Bc system is solved using numerical integration together with convexity arguments and nodal theorem for wave function [1]. The pure-leptonic decays of heavy mesons are very interesting from theoretical as well as experimental point of view [2,3]. In the present paper we have studied the decay constants and the leptonic decay width using the non-relativistic treatment.

Methodology

We solve the Schrödinger Equation numerically with the quark-antiquark potential of the form [4-6],

$$V(r) = -\frac{k\alpha_s}{r} + Ar^{\upsilon} + \mathrm{V_{SD}} \qquad (1)$$

Where A is the potential parameter, υ is a general potential index corresponding to the confining part of the potential. For present computation of masses and decay properties, we have taken as $\upsilon = 1$. α_s is the strong running coupling coefficient which can be determined from

$$\alpha_s(\mathrm{M}^2) = \frac{4\pi}{\left(11-\frac{2}{3}\mathrm{n_f}\right)\ln\frac{\mathrm{M}^2+\mathrm{M_b^2}}{\Lambda^2}} \qquad (2)$$

Where the scale is taken as $\mathrm{M}=2m_Q m_{\bar{q}}/(m_Q + m_{\bar{q}})$, $\mathrm{M_b}$=0.95 GeV, ∧=413 MeV. We fit the values of k and A for ground state of $b\bar{b}$ using experimental value of b quark mass and then determine the c quark mass by fitting $c\bar{c}$ ground state mass [7]. We choose the scale for the Bc system as α_s = 0.255. The obtained values for k = 1.173, A = 0.17, $\mathrm{m_b}$ = 4.66 GeV and $\mathrm{m_c}$ = 1.275 GeV are employed for further computation. $\mathrm{V_{SD}}$ is the spin dependent part of the potential [8].

$$\mathrm{V_{SD}} = V_{\mathrm{SS(r)}}\left[S(S+1) - \frac{3}{2}\right] + V_{LS}(r)(\vec{L}.\vec{S}) + V_T(r)\left[S(S+1) - \frac{3(\vec{S}.\vec{r})(\vec{S}.\vec{r})}{r^2}\right] \qquad (3)$$

The spin-orbit term containing $V_{LS}(r)$ and the tensor term $\mathrm{V_T(r)}$ describe the fine structure of the meson state, while the spin-spin term containing $\mathrm{V_{SS}(r)}$ proportional to $2(\overrightarrow{S_q}.\overrightarrow{S_{\bar{q}}})=S(S+1)-3/2$. The coefficient of these spin-dependent terms of Eq.3 can be written in terms of the vector and scalar parts of the static potential as [8]

$$V_{LS}(r) = \frac{1}{2m_1m_2r}\left(3\frac{dV_V}{dr} - \frac{dV_S}{dr}\right)$$

$$V_T(r) = \frac{1}{6\,m_1m_2r}\left(3\frac{d^2V_V}{dr^2} - \frac{1}{r}\frac{dV_S}{dr}\right) \qquad (5)$$

$$V_{SS}(r) = \frac{1}{3m_1m_2}\nabla^2 V_V$$

The Bc mass spectroscopy is computed with these parameters and the result is given in Table 1.

TABLE I: Masses of Bc Meson (GeV)

State n $^{2S+1}\mathrm{L_J}$	Present	[9]	[10]	[11]
1 $^1\mathrm{S_0}$	6.293	6.270	6.349	6.264
1 $^3\mathrm{S_1}$	6.317	6.332	6.373	6.337
2 $^1\mathrm{S_0}$	6.777	6.835	6.821	6.856
2 $^3\mathrm{S_1}$	6.811	6.881	6.855	6.899
3 $^1\mathrm{S_0}$	7.152	7.193	7.125	7.244
3 $^3\mathrm{S_1}$	7.187	7.235	7.210	7.280

Decay Constants

The pseudoscalar and vector decay constants are computed using the Van Royen Weisskopf formula for color are zero separation between the constituent quarks in ground state [12]

$$\mathrm{f_p} = \sqrt{\frac{3}{\pi M_p}}\,R_{1S}(0)\ ;\ \mathrm{f_v} = \sqrt{\frac{3}{\pi M_v}}\,R_{1S}(0) \qquad (5)$$

M_p and M_v are the masses of the pseudoscalar and vector meson respectively. The values of $\mathrm{f_p}$ and $\mathrm{f_V}$ are given in the Table II with the charge radii of the S-wave Bc mesons.

TABLE II: pseudoscalar and vector decay constants

State	Decay constant (MeV)				
	Present	[14]	[16]	[17]	[18]
$1\ ^1S_0$	412	350	360	456	607
$1\ ^3S_1$	411	--	--	--	604

Radiative Leptonic Decay Width

In this section, we compute the radiative decay width using the relation [13]

$$\Gamma(Bc \to l\overline{\gamma v}) = \frac{G_F^2|V_{cb}|^2}{8\pi^2} f_{Bc}^2 m_{Bc}^3 \frac{m_l^2}{m_{Bc}^2} \left(1 - \frac{m_l^2}{m_{Bc}^2}\right)^2$$

As the mass of the lepton is very low compared to the *Bc* meson, the decays of pseudoscalar mesons into light lepton pairs are helicity suppressed, i.e. their decay widths are suppressed m_l^2/m_{Bc}^2, therefore the above formula becomes

$$\Gamma(Bc \to \gamma l\bar{v}) = \frac{\alpha G_F^2|V_{cb}|^2}{2592\pi^2} f_{Bc}^2 m_{Bc}^3 [x_b + x_c] \quad (6)$$

Where $\alpha = 1/137$ is the electromagnetic coupling constant, G_F Fermi coupling constant = 1.66×10^{-5}, $|V_{cb}|$=0.044 [13] is the CKM matrix element. x_b and x_c is given by:

$$x_b = \left(3 - \frac{m_{Bc}}{m_b}\right)^2 \text{ and } \quad x_c = \left(3 - 2\,\frac{m_{Bc}}{m_b}\right)^2 \qquad (7)$$

The computed radiative leptonic decay width for S-wave *Bc* mesons is 1.59×10^{-17} GeV which is comparable in order with 6.44×10^{-17} GeV as obtained by C. Cheng et al. [16].

Summary

The results from Table (I) suggests that our results for the *Bc* meson S-wave masses are in good agreement with that by D. Ebert et al [9] with small deviation from other references. It is also evident from Table II that the decay constants are in tune with other theoretical models too. As the experimental results for the same are not available, we compare the outcome of the present work with existing phenomenological models. It is found that the present non-relativistic computation can provide good framework to study *Bc* meson as both the quarks can be treated non-relativistically. Further study on the decay properties using fine-tuned parameters is underway.

Acknowledgement

This work is supported by the University Grants Commission of India under Major Research Project F.No.42-775/2013(SR)

Reference

[1] Wolfgung LUCHA, Franz F. SCHOBERL, arXiv: hep-ph/9811453v2 9 Jan 1999, HEPHY-PUB 703/98 UWThPh-1998-58 October 1998
[2] C.-H. Chang and Y.-Q. Chen, Phys. Rev. D49 (1994) 3399.
[3] D.-S. Du, H.-Y. Jin and Y.-D. Yang, preprint BIHEP-Th/97-007, hep-ph/9705261
[4] A. K. Rai, R. H. Parmar, and P. C. Vinodkumar, J. Phys. G: Nucl. Part. Phys. 28, 2275 (2002),
[5] A. K. Rai, J. N. Pandya, and P. C. Vinodkumar, J. Phys. G: Nucl. Part. Phys. 31, 1453 (2005),
[6] A. K. Rai, B. Patel, and P. C. Vinodkumar, Phys. Rev. C 78, 055202 (2008).
[7] Particle Data Group, J. Beringer et al. (PR D86, 010001 (2012).
[8] Voloshin M B, Prog. Part. Nucl. Phys. 61, 455 (2008);arXiv:hep-ph/0711.4556v3.
[9] D Ebert, R N Faustov and V O Galkin, *Phys. Rev.* D67, 014027 (2003)
[10] A.K.Rai, P.C.Vinodkumar *Pramana J. Phys.*, Vol. 66, No. 5, May 2006
[11] V. O. Galkin, A. Yu. Mishurov and R. N. Faustov, Yad. Fiz. 55, 2175 (1992) [Sov. J. Nucl. Phys. 55, 1207 (1992)].
[12] E J Eichten and C Quigg, *Phys. Rev.* D49, 5845 (1994)
[13] Chao-Hsi Chang, Jian-Ping Cheng and Cai-Dian L¨u arXiv:hep-ph/9712325v2 21 Jan 1998, DESY 97-246 AS-ITP-97-027 December, 1997
[14] T.M. Aliev, M.Savci, Phys. Letts. B434 (1998) 358, hep-ph/9804407.
[15] C.-H. Chang, J-P Cheng and C-D L¨u, Phys. Letts. B425 (1998) 166, hep-ph/9712325.
[16] Chao-hsi Chang, Cai-Dian Lu, Guo-Li Wang, Hong-Shi Zong, Phys. Rev. D 60 (1999) 114013
[17] S S Gershtein, V V Kiselev, A K Likhoded and A V Tkabladze, *Phys. Rev.* **D51** (1995) 3613
[18] J N Pandya and P C Vinodkumar, Pramana J. Phys. 57(4) (2001) 821

Semi-leptonic and pionic decays of Doubly Strange baryons

N R Soni* and J N Pandya
Applied Physics Department, Faculty of Technology and Engineering, The M S University of Baroda, Vadodara, Gujarat, INDIA.

Introduction

The doubly strange b-baryon Ω_b^- was reported by $D0$ [1] and CDF [2] Collaboration through the channel $\Omega_b^- \rightarrow J/\psi\Omega^-$ at $\sqrt{1.96}$ TeV. Doubly strange c-baryon Ω_c^0 was observed by $E687$ [3] significantly in the channel of $\Omega_c^0 \rightarrow \Sigma^+K^-K^-\pi^+$ and later was confirmed by other groups [4]. We employ the extended harmonic confinement model in order to understand semi leptonic and pionic decay modes of these states to compute their masses and decay widths.

Methodology

The mass of baryon in the N energy eigenstate and J spin state can be computed as[5]

$$M_N^J = \sum_{i=1}^{3}\epsilon_N(q_i)_{conf} + \sum_{i<j=1}^{3}\epsilon(q_i,q_j)_{coul} + \sum_{i<j=1}^{3}\epsilon_N^J(q_i,q_j)_{S.D.} \quad (1)$$

where the first term is the confinement part, second term is due to the Coulomb interaction between the constituent quarks and the third term corresponds to the spin-dependent interactions.
The confinement energy of the baryonic system is given by [6],

$$\epsilon(q)_{conf} = \sqrt{(2N+3)\Omega_N(q) + M_q^2 - \frac{3M_q}{\sum_{i=1}^{3}M_{q_i}}}$$

where the size parameter, $\Omega_N(q)$ of RHM radial wave function is energy dependent and is given by

$$\Omega_N(q) = A\sqrt{E_N + M_q} \quad (2)$$

M_q is the constituent quark mass. The Coulomb of eq. 1 can be computed as

$$\epsilon(q_1,q_2)_{coul} = \left\langle NS\left|\frac{k\alpha_s^{eff}}{r}\right|NS\right\rangle \quad (3)$$

where α_s^{eff} is the strong running coupling coefficient. The spin-spin interaction is computed using the spin hyperfine interaction of the residual confined one gluon exchange potential [5–9]

$$V_{\sigma_i\cdot\sigma_j} = \frac{\alpha_s(\mu)N_i^2N_j^2}{4}\frac{\lambda_i\lambda_j}{[E_i+m_i][E_j+m_j]} \times\left[4\pi\delta^3(r) - C^4r^2D_1(r)\right]\left(-\frac{2}{3}\sigma_i\sigma_j\right)$$

where $N_{i/j}$ is the normalization constant, C is the confinement strength of the gluon, r is the inter-quark distance, $\lambda_i\lambda_j$ is the spin factor, $D_1(r)$ is the confined gluon propagator and can be fitted to $\sim \frac{k_1}{r}exp(-C^2r^2/2)$ [7, 8].

$$\epsilon_N^J(q_i,q_j)_{S.D.} = \langle NS|V_{SD}|NS\rangle \quad (4)$$

Here we have used $m_b = 4829$ MeV, $m_c = 1479$ MeV and $m_s = 410$ MeV. The potential parameters k, k_1 and C are fine tuned to obtain the experimental mass of Ω^-. The parameters used in this computation are $k = 0.006$, $k_1 = 21.36$ and $C = 100$ MeV.

Decay of Doubly strange baryons

In this section we compute the decay of Ω_c^0 and Ω_B^- baryon. The general definition for the semi-electronic decay width is given by [10]

*Electronic address: nakulphy@gmail.com

$$\frac{d\Gamma}{dw} = \frac{G_f^2 M^5}{192\pi^3}|V_{CKM}|^2\sqrt{w^2-1}P(w) \quad (5)$$

where $P(w)$ contains the hadronic and leptonic tensor. After evaluating the integration over $w = 1$ in the hadronic form factors one will get the following relation for the decay width for electronic $(1/2)^+ \to (1/2)^+$ transition [10]

$$\Gamma_{\Omega_{c/b}^{0/-}\to\Xi_{c/b}^{+/0}e^-\bar{\nu}} = \frac{G_f^2|V_{CKM}|^2}{15\pi^3}(M-m)^5 \quad (6)$$

where G_f is the Fermi coupling constant. The pionic decay width using the transition amplitude is computed using [10]

$$\Gamma_{\Omega_b^-\to\Xi_b^0\pi^-} = \frac{(\Delta M)^{\frac{3}{2}}}{192\pi M^7}|A((ss)_1 \to (us)_0\pi^-)|^2$$

here $\Delta M = [M^2-(m-m_\pi)^2][M^2-(m+m_\pi)^2]$ and the weak di-quark decay amplitude can be approximated with $|a_{weak}| \sim (1...2)\times 10^{-6}$ as [10]

$$A((ss)_1 \to (us)_0\pi^-) \sim 2MV_{us}V_{ud}^* a_{weak}$$

Where V_{us} and V_{ud} are the CKM matrices. We compute the semi-leptonic and pionic decay widths of Ω_c^0 and Ω_b^- without any additional parameters and the results are given in the table II.

Conclusion

The ground state masses of Ω_c^0 and Ω_b^- are computed using the methodology explained in the first section and compared with the experimental data. We also compute the semi-leptonic and pionic decay widths of Ω_c^0 and Ω_b^-. It is observed from table II that our results are well within the range as proposed by [10].

Acknowledgments

This work is supported by the University Grants Commission of India under Major Research Project F.No.42-775/2013(SR)

TABLE I: ground state masses in MeV

State	quark content	present	[11]
Ω_c^0	css	2694.63	2695.2 ± 1.7
Ω_b^-	bss	6049.58	6048.8 ± 3.2

TABLE II: baryonic decay widths in GeV

mode of decay	present	[10]
$\Omega_c^0 \to \Xi_c^+ e^- \bar{\nu}$	9.05×10^{-18}	2.6×10^{-18}
$\Omega_c^0 \to \Xi_c'^+ e^- \bar{\nu}$	3.65×10^{-19}	3.63×10^{-19}
$\Omega_b^0 \to \Xi_b^0 e^- \bar{\nu}$	16.17×10^{-18}	4.05×10^{-18}
$\Omega_b^- \to \Xi_b^0\pi^-$	0.93×10^{-18}	$(0.7...2.6)\times10^{-18}$
$\Omega_b^- \to \Xi_b^-\pi^0$	0.91×10^{-18}	$(0.3...1.3)\times10^{-18}$

References

[1] V. M. Abazov et al. (D0 Collaboration)Phys. Rev. Lett. **101**, 232002 (2008)
[2] T. AALTONEN et al. (CDF Collaboration) Phys. Rev. D **80**, 072003 (2009)
[3] P. L. Frabetti et al. (E687 Collaboration), Phys. Lett. B **338**, 106 (1994)
[4] D. Cronin-Hennessy et al. (CLEO Collaboration), Phys. Rev. Lett. **86**, 3730 (2001), B. Aubert et al. (BaBar Collaboration), Phys. Rev. Lett. **97**, 232001 (2006) , C. Amsler et al., Phys. Lett. B **667**, 1 (2008)
[5] P C Vinodkumar, J N Pandya, V M Bannur and S B Khadkikar, Euro. J. Phys. A **4**, 83 (1999)
[6] S B Khadkikar and S K Gupta, Phys. Lett. B **124**, 523 (1983)
[7] S B Khadkikar and K B Vijayakumar, Phys. Lett. B **254**, 320 (1991)
[8] S B Khadkikar and K B Vijayakumar, Pramana J. Phys. **36**, 557 (1991), P C Vinodkumar, K B Vijayakumar and S B Khadkikar, Pramana J. Phys. **39**, 47 (1992)
[9] K B Vijayakumar and S B Khadkikar, Nucl. Phys. A **556**, 396 (1993)
[10] Sven Fallera and Thomas Mannela arXiv:1503.06088v2 [hep-ph]
[11] K.A. Olive et al. (Particle Data Group), Chin. Phys. C, **38**, 090001 (2014)

Masses and magnetic moment of doubly heavy baryons

A N Gadaria, N R Soni,* and J N Pandya†
Applied Physics Department, Faculty of Technology and Engineering,
The M S University of Baroda, Vadodara, Gujarat, INDIA.

Introduction

Doubly heavy baryons are composed of two heavy quarks (b and/or c) and one light quark (u, d or s). There have been many theoretical attempts to compute masses of these states [1]. Experimental observation of such heavy resonances are expected from the facilities such as LHCb and Bell II. We employ the extended relativistic harmonic confinement model (ERHM) to compute the masses of doubly heavy baryons. The magnetic moments of heavy flavour baryons are also computed using the spin-flavour wave functions of the constituent quarks and their effective masses within the baryon.

Theoretical framework

In the relativistic harmonic confinement model (RHM) with scalar plus vector potential for the quark confinement, coloured quarks in a hadron are confined through the action of a Lorentz scalar plus a vector harmonic oscillator type of potential. The RHM has been extended to accommodate multiquark states from lighter to heavier flavour sectors with unequal quark masses [2]. The mass of baryon in the N energy eigenstate and J spin state can be computed as [2, 3]

$$M_N^J = \sum_{i=1}^{3} \epsilon_N(q_i)_{conf} + \sum_{i<j=1}^{3} \epsilon(q_i,q_j)_{coul} + \sum_{i<j=1}^{3} \epsilon_N^J(q_i,q_j)_{S.D.} \quad (1)$$

First term is confinement energy of the constituent quarks inside the baryon; second term is the residual colour coulomb interaction between confined quarks and the third term corresponds to the spin-dependent interactions. The colour coulomb interaction energy is computed using the residual coulomb potential $V_{coul}(q_iq_j) = \frac{k\alpha_s(\mu)}{\omega_n r}$. Where ω_n is the state dependent colour dielectric coefficient [2]. It is also the measure of confinement strength through the non- perturbative contributions to the confinement scale at the respective threshold energy of the quark- antiquark excitations.

The wave function for the baryons are constructed through the single particle wave function but with the three particle size parameters [2, 3]. The spin averaged mass of the doubly heavy baryons are obtained using the model parameters $k = 0.37$, confinement parameter $A = 2166$ MeV$^{3/2}$, quark masses $m_u = 240$ MeV, $m_d = 243$ MeV, $m_s = 450$ MeV, $m_c = 1275$ MeV, $m_b = 4660$ MeV. The octet and decuplet masses are computed by considering the residual two body chromomagnetic interaction through the spin dependent term of confined one gluon exchange potential perturbatively.

Magnetic Moment

Considering the mass of bound quark inside the baryon as effective mass, the magnetic moment is computed using [4]

$$m_i^{eff} = m_i\left(1 + \frac{\langle H\rangle}{\sum_i m_i}\right) \quad (2)$$

such that the mass of the bayron is

$$M_B = \sum_i^3 m_i^{eff} \quad (3)$$

*Electronic address: nrsoni-apphy@msubaroda.ac.in
†Electronic address: jnpandya-apphy@msubaroda.ac.in

TABLE I: Masses of doubly heavy baryons in MeV

Baryon	quark content	present	[4]	[5]	[6]	[7]	[8]
Ξ_{cc}^{++}	ccu	3542	3439	3612	3620	3532	
Ξ_{cc}^{*++}	ccu	3677	3516	3706	3727	3623	
Ξ_{cc}^{+}	ccd	3544	3440	3605	3620	3537	3520
Ξ_{cc}^{*+}	ccd	3677	3518	3685	3727	3629	
Ω_{cc}^{+}	ccs	3644	3479	3702	3778	3667	
Ω_{cc}^{*+}	ccs	3717	3559	3783	3872	3758	
Ξ_{bc}^{+}	bcu	6928	6834	6919	6933	6988	
Ξ_{bc}^{*+}	bcu	6990	6865	6986	6980	7083	
Ξ_{bc}^{0}	bcd	6929	6838	6820	6933	–	
Ξ_{bc}^{*0}	bcd	6990	6870	—-	6980	–	
Ω_{bc}^{0}	bcs	7012	6893	6986	7088	7103	
Ω_{bc}^{*0}	bcs	7045	6936	7046	7130	7200	
Ξ_{bb}^{0}	bbu	10257	10114	10197	10202	10344	
Ξ_{bb}^{*0}	bbu	10289	10165	10236	10237	10431	
Ξ_{bb}^{-}	bbd	10257	10117	10197	10202	–	
Ξ_{bb}^{*-}	bbd	10289	10170	10236	10237	–	
Ω_{bb}^{-}	bbs	10333	10164	10260	10359	10397	
Ω_{bb}^{*-}	bbs	10350	10236	10297	10389	10495	

$*$ indicates $J^P = \frac{3}{2}^+$ state

TABLE II: Magnetic moments in μ_N

Baryon	present	[4]	[5]	RQM [11]	NRQM [11]	[9]
Ξ_{cc}^{++}	-0.169	-0.137	-0.208	-0.130	-0.010	
Ξ_{cc}^{*++}	2.72	2.749	2.670	–	–	2.59
Ξ_{cc}^{+}	0.853	0.859	0.785	0.720	0.740	
Ξ_{cc}^{*+}	-0.23	-0.168	-0.311	–	–	-0.20
Ω_{cc}^{+}	0.74	0.783	0.635	0.670	0.670	
Ω_{cc}^{*+}	0.16	0.121	0.139	–	–	0.12
Ξ_{bc}^{+}	-0.52	-0.400	-0.475	-0.120	-0.290	-0.387
Ξ_{bc}^{*+}	2.68	2.052	2.27	–	–	2.011
Ξ_{bc}^{0}	0.63	0.476	0.518	0.420	0.460	0.499
Ξ_{bc}^{*0}	-0.76	-0.567	-0.712	–	–	-0.551
Ω_{bc}^{0}	0.49	0.396	0.368	0.450	0.390	0.399
Ω_{bc}^{*0}	-0.32	-0.316	-0.261	–	–	-0.279
Ξ_{bb}^{0}	-0.89	-0.656	-0.742	-0.530	-0.580	-0.665
Ξ_{bb}^{*0}	2.30	1.576	1.870	–	–	1.596
Ξ_{bb}^{-}	0.32	0.190	0.251	0.180	0.189	0.208
Ξ_{bb}^{*-}	-1.32	-0.951	-1.11	–	–	-0.984
Ω_{bb}^{-}	0.16	0.109	0.101	0.040	0.100	0.111
Ω_{bb}^{*-}	-0.86	-0.711	-0.662	–	–	-0.703

$*$ indicates $J^P = \frac{3}{2}^+$ state

Here the magnetic moment is obtained in terms of its constituent quarks as

$$\mu_B = \sum_i \langle \phi_{sf} | \mu_i \vec{\sigma_i} | \phi_{sf} \rangle \qquad (4)$$

where $\mu_i = e_i/2m_i^{eff}$. e_i and σ_i shows the charge and spin of the quark constituting the baryonic state and $|\phi_{sf}\rangle$ represents the spin flavor wave function of the respective baryonic state. [10].

Results and Discussion

We have employed ERHM to compute masses of baryons double heavy quarks. The computed mass spectra is found to be matching with available results from other theoretical approaches and are listed with them in table I. The magnetic moments are computed without introducing any extra parameters or correction to the wave function and are found in agreement with other theoretical calculations. It is observed that presence of b quark in the baryons raises the magnitude of the magnetic moments by a factor. This suggests that inclusion of some relativistic corrections and use of other suggested approaches for computation of magnetic moments may improve the results.

Acknowledgments

This work is supported by the University Grants Commission of India under Major Research Project F.No.42-775/2013(SR)

References

[1] Y. L. Ma and M. Harada, Phys. Lett. B **754**, 125 (2016) and references there in.
[2] P C Vinodkumar *et al.*, Eur. J. Phys. A **4**, 83 (1999).
[3] J. N. Pandya and P. C. Vinodkumar, Pramana J. Phys. **57**, 821 (2001).
[4] B Patel *et al.*, J. Phys. G:Nucl. Part. Phys **35**, 065001 (2008).
[5] C. Albertus *et al.*, Eur. Phys. J. A. **31**, 691 (2007).
[6] D Ebert *et al.*, Phys. Rev. D **66**, 014008 (2002).
[7] Z. Ghalenovi *et al.*, Mod. Phys. Lett. A, **29**, 1450106 (2014).
[8] K.A. Olive *et al.* (Particle Data Group), Chin. Phys. C, **38**, 090001 (2014).
[9] R. Dhir and R. C. Verma, Eur. Phys. J. A **42**, 243 (2009); R. Dhir *et al.*, Phys. Rev. D **88**, 094002 (2013).
[10] Yu A Simonov *et al.*, Phys. Rev. D **65**, 094013 (2002).
[11] A Faessler *et al.*, Phys. Rev. D **73**, 094013 (2006).

Masses and radiative decay of Ω_{cc}^{+} baryon

N R Soni* and J N Pandya†
Applied Physics Department, Faculty of Technology and Engineering,
The Maharaja Sayajirao University of Baroda, Vadodara 390001, Gujarat, INDIA.

Introduction

The fact that the energy scales of doubly heavy baryons are much larger in comparison to strong interaction scale Λ_{QCD}, makes study of their spectroscopy an important tool for testing quantum chromodynamics [1, 2]. We employ extended relativistic harmonic model for computing the masses of Ω_{cc}^{+} baryon. Though this state is yet to be observed experimentally, many theoretical models have computed their mass spectra and decay modes. We compute masses and radiative decay widths using the model parameters along with spin-flavor wave functions and compare the results with the available theoretical predictions.

Methodology

For computation of bound state masses of baryon, we use the relativistic harmonic confinement model in which the quarks are confined through the Lorentz scalar plus vector potential of the form

$$V_{conf} = \frac{1}{2}(1+\gamma_0)A^2r^2 \qquad (1)$$

Where A is the confinement strength mean field parameter and γ_0 is the Dirac matrix. The non relativistic reduction of the Dirac equation is performed for the potential Eq. (1) and the energy eigen values (ϵ_{conf}) are obtained. We perturbatively add the Columb potential along with state dependent colour dielectric coefficient (ω_n) given by [3]

$$V_{coul} = \frac{k\alpha_s(\mu)}{\omega_n r} \qquad (2)$$

Where $\alpha_s(\mu)$ is the strong runing coupling constant. The mass of baryon in the different $n^{2S+1}L_J$ state acording to different J^{PC} can be written as [3]

$$M_N^J = \sum_{i=1}^{3}\epsilon_N(q_i)_{conf} + \sum_{i<j=1}^{3}\epsilon(q_i,q_j)_{coul} + \sum_{i<j=1}^{3}\epsilon_N^J(q_i,q_j)_{S.D.} \qquad (3)$$

where the last term corresponds to the expectation value of spin dependent part of confined one gluon exchange potential.

The potential parameters used in computation of octet and decuplet masses of Ω_{cc}^{+} are as follows: $k = 0.37$, confinement mean field parameter $A = 2166$ MeV$^{3/2}$, quark masses: $m_c = 1315$ MeV and $m_s = 470$ MeV.

TABLE I: Masses of Ω_{cc}^{+} baryon in MeV

State	Present	[4]	[5]	[6]	[7]	[8]
Ω_{cc}^{+}	3769.91	3770	3747	3713	3738	3650
Ω_{cc}^{*+}	3835.3	3824	3819	3785	3822	3810

$*$ indicates $J^P = \frac{3}{2}^+$ state

Radiative decays

The radiative decay width can be expressed in terms of transition magnetic moment (in nuclear magneton μ_N) as [9]

$$\Gamma_{B^*\to B\gamma} = \frac{\omega^3}{4\pi}\frac{2}{2J+1}\frac{e^2}{m_p^2}\mu^2_{B^*\to B\gamma} \qquad (4)$$

*Electronic address: nrsoni-apphy@msubaroda.ac.in
†Electronic address: jnpandya-apphy@msubaroda.ac.in

TABLE II: Radiative transition magnetic moment in μ_N and radiative decay width in keV

	Present	[10]	[11]	[4]	[12]	[13]
$\mu_{\Omega_{cc}^{*+}\to\Omega_{cc}^{+}\gamma}$	-0.877	1.54	0.789	–	–	-0.89
$\Gamma_{\Omega_{cc}^{*+}\to\Omega_{cc}^{+}\gamma}$	0.89	9.45	0.949	8.61	6.93	–

where, m_p is the mass of proton, μ is the transition magnetic moment that can be written in terms of magnetic moment of constituent quark of final and initial state of baryons as $\mu_{B^*\to B\gamma} = \langle B|\hat{\mu}_{B^*z}|B^*\rangle$.

Result and discussion

We employed the extended relativistic harmonic model (ERHM) for computing the masses of doubly heavy Ω_{cc}^{+} baryon and our results are tabulated in Table I. Since no experimental results are available for these state we compare our results with theoretical predictions such as relativistic quark model [4], hypercentral model [8] as well with lattice QCD [5–7]. Our results deviate by less than 2 % from those obtained using lattice QCD as well as relativistic quark model.

Next we compute the radiative transition width of Ω_{cc}^{+} baryons. The decay rate is expressed in terms of transition magnetic moment. Considering the masses of confined quarks as the effective mass, the magnetic moments are obtained using the spin flavor structure of constituent quarks. The computed results are tabulated in Table II and compared with the other theoretical predictions. Our results for transition magnetic moments are matching well with modified Bag model [11] and chiral constituent quark model [13]. We also compare our result for radiative decay width with modified Bag model [11], chiral constituent quark model [13] along with recent papers on chiral quark model [10] and relativistic quark model [4]. We observe that our results match very well with modified Bag model.

Conclusion

Employing extended relativistic harmonic confinement model, we compute the mass of doubly heavy Ω_{cc}^{+} baryon which are matching well with lattice QCD results. The computed radiative transition magneic moment and decay width are lower than the recent theoretical predictions. However, due to the fact that the results from lattice calculations and experimental results are still awaited, the present results might be of interest as they are in tune with chiral constituent quark model and modified Bag model. Further study on the radiative decay properties of doubly heavy baryons is underway.

Acknowledgments

This work is supported by the University Grants Commission of India under Major Research Project F.No.42-775/2013(SR)

References

[1] H.-X. Chen *et al.*, Rept. Prog. Phys. **80**, 076201 (2017).
[2] E. Klempt and J.-M. Richard, Rev. Mod. Phys. **82**, 1095 (2010).
[3] J. N. Pandya *et al.*, Chin. Phys. C **39**, 123101 (2015), Pramana **57**, 821 (2001), Eur. J. Phys. A **4**, 83 (1999).
[4] Q.-F. Lu, K.-L. Wang, L.-Y. Xiao, and X.-H. Zhong, arXiv:1708.04468 [hep-ph].
[5] K. U. Can, G. Erkol, M. Oka and T. T. Takahashi, Phys. Rev. D **92**, 114515 (2015).
[6] P. Perez-Rubio, S. Collins and G. S. Bali, Phys. Rev. D **92**, 034504 (2015).
[7] Z. S. Brown, W. Detmold, S. Meinel and K. Orginos, Phys. Rev. D **90**, 094507 (2014).
[8] Z. Shah, K. Thakkar and A. K. Rai, Eur. Phys. J. C **76**, 530 (2016).
[9] A. Majethiya, B. Patel, and P. C. Vinodkumar, Eur. Phys. J. A **42**, 213 (2009).
[10] H.-S. Li, L. Meng, Z.-W. Liu, and S.-L. Zhu, arXiv:1708.03620 [hep-ph].
[11] A. Bernotas and V. Šimonis, Phys. Rev. D **87**, 074016 (2013).
[12] L.-Y. Xiao *et al.*, arXiv:1708.04384 [hep-ph].
[13] N. Sharma, H. Dahiya, P. K. Chatley, and M. Gupta, Phys. Rev. D **81**, 073001 (2010).

Chapter 174
Mass and Hadronic Decay Widths of Z States as Di-meson Molecule

N. R. Soni , R. R. Chaturvedi , A. K. Rai and J. N. Pandya

After the discovery of Z_c^+ and Z_b^+ hadronic states by BESIII [1] and BELLE [2] collaborations respectively, there have been many attempts to describe these states either as tetra quark states or as hadronic molecules. The charged states and the masses of these exotic states are nearer to the threshold of $D^+\bar{D}^*$ and $B\bar{B}^*$ and respectively suggesting them to be di-mesonic molecular states. We treat them as hadronic molecules of $D^+\bar{D}^*$ mesons and $B\bar{B}^*$ mesons. We consider the interaction between the constituent mesons of the type modified Woods-Saxon plus Coulomb repulsive terms of the form [3]

$$V(r) = \frac{V_0}{1 + Exp\left[\frac{r-R_0}{a}\right]} + \frac{C\,Exp\left[\frac{r-R_0}{a}\right]}{\left(1 + Exp\left[\frac{r-R_0}{a}\right]\right)^2} - \frac{b}{r} \tag{174.1}$$

where the potential parameters are the strength of the potential $V_0 = 15\ MeV$, $b = 0.08$, size of the hadron $R_0 = 1.75$ fm, diffuseness of the surface of the molecule $a = -0.51$ fm. C determines the depth of the potential ($0 < C < 150$ MeV) [3]. For computation of binding energy, we solve the Schrödinger equation numerically for the interaction potential defined in Eq. 174.1. Binding energy and thus the di-mesonic molecular masses are given in Table 174.1.

N. R. Soni · J. N. Pandya (✉)
Applied Physics Department, Faculty of Technology and Engineering,
The Maharaja Sayajirao University of Baroda,Vadodara, Gujarat 390001, India
e-mail: jnpandya-apphy@msubaroda.ac.in

N. R. Soni
e-mail: nrsoni-apphy@msubaroda.ac.in

R. R. Chaturvedi · A. K. Rai
Applied Physics Department, Sardar Vallabhbhai National Institute of Technology,
Surat, Gujarat 395007, India
e-mail: raghavr.chaturvedi@gmail.com

A. K. Rai
e-mail: raiajayk@gmail.com

Md. Naimuddin (ed.), *XXII DAE High Energy Physics Symposium*, Springer
Proceedings in Physics 203, https://doi.org/10.1007/978-3-319-73171-1_174

Table 174.1 Masses of $Z_c^+(D^+\bar{D}^*)$ and $Z_b^+(B\bar{B}^*)$ molecular states (in MeV) with the variation in potential depth C (in MeV)

C	$D^+\bar{D}^*$		$B\bar{B}^*$	
	Binding energy	Mass	Binding energy	Mass
0	11.82	3864.74	5.58	10598.9
50	11.96	3864.61	7.05	10597.4
100	12.07	3864.5	8.04	10596.4
150	12.15	3864.42	8.72	10595.7
PDG [5]		3883.9±4.5		10607.2±2.0

Table 174.2 Decay widths of Z_c^+ and Z_b^+ molecular states (in MeV)

Decay mode	Decay width					
	C = 0	C = 50	C = 100	C = 50	Exp [6]	[4]
$Z_c^+ \to \psi(1s)+\pi$	11.7202	11.7553	11.7849	11.8064	–	10.43–23.89
$Z_c^+ \to \psi(2s)+\pi$	2.1166	2.1146	2.1127	2.1114	–	1.28–2.94
$Z_b^+ \to \Upsilon(1s)+\pi$	22.8443	22.9280	22.9998	23.0567	22.9±7.3	13.3–30.8
$Z_b^+ \to \Upsilon(2s)+\pi$	26.9257	26.9858	27.0443	27.0930	21.1±4.0	15.4–35.7

We employ the method of Phenomenological Lagrangian mechanism developed by Y. Dong et al. [4] to compute hadronic decay widths. The corresponding two body decay widths for Z_c^+ and Z_b^+ can be written as [4]

$$\Gamma_{Z_c^+\to\Psi(ns)\pi^+} \simeq \frac{g^2_{Z_c\Psi(ns)\pi}}{96\pi M^3_{Z_c}}\lambda^{3/2}(M^2_{Z_c}, M^2_{\psi(ns)}, M^2_{\pi})\left(1+\frac{M^2_{\psi(ns)}}{2M^2_{Z_c}}\right) \quad (174.2)$$

$$\Gamma_{Z_b^+\to\Upsilon(ns)\pi} \simeq \frac{g^2_{Z_b\Upsilon(ns)\pi}}{16\pi M_{Z_b}}\lambda^{1/2}(M^2_{Z_b}, M^2_{\Upsilon(ns)}, M^2_{\pi}) \quad (174.3)$$

where $\lambda(x, y, z) = x^2 + y^2 + z^2 - 2xy - 2yz - 2zx$ is the Källen function, $g's$ are the coupling constant corresponds to the coupling between hadron to its constituent mesons. The computed decay widths are given in Table 174.2.

Result and Conclusion

The masses of Z_c^+ and Z_b^+ considering them as molecular states of $D^+\bar{D}^*$ and $B\bar{B}^*$ respectively are found to be below the mass of their resonance. We have analysed the nature of potential with the parameters such as diffuseness and depth of the potential. We have also computed the hadronic decay widths of these states in formalism of interaction Lagrangian mechanism and compare with the experiments. Our predictions of decay widths are in good agreement with the data from experiments.

Acknowledgements This work is supported by the University Grants Commission of India under Major Research Project F.No.42-775/2013(SR)

References

1. M. Ablikim et al., BESIII collaboration. Phys. Rev. Lett. **110**, 252001 (2013)
2. Z.Q. Liu et al., Belle collaboration. Phys. Rev. Lett. **110**, 252002 (2013)
3. H. Fakhri, J. Sadeghi, Mod. Phys. Lett. A 29, 615 (2004); C. Berkdemir, A. Berkdemir, R. Sever, Phys. Rev. C **72**, 027001 (2005)
4. Y. Dong et al., Phys. Rev. D **88**, 014030 (2013); J. Phys. G **40**, 015002 (2013)
5. C. Patrignani et al., Particle data group. Chin. Phys. C **40**, 100001 (2016)
6. I. Adachi et al., (Belle Collaboration), arXiv:hep-ex/1105.4583

Decay properties of Ξ_{cc}^{++} baryon

A. N. Gadaria[1],* N. R. Soni[1],† Raghav Chaturvedi[2], Ajay Kumar Rai[2], and J. N. Pandya[1‡]
[1] *Applied Physics Department, Faculty of Technology and Engineering, The Maharaja Sayajirao University of Baroda, Vadodara 390001, Gujarat, INDIA. and*
[2] *Department of Applied Physics, Sardar Vallabhbhai National Institute of Technology, Surat 395007, Gujarat, INDIA.*

Introduction

The doubly heavy baryons are among the best tools to understand the quantum chromodynamics and heavy quark effective theory. Using weak decays of doubly heavy baryons, one can determine the elements of CKM matrix that help to understand quark mixing angle. The first doubly heavy baryon Ξ_{cc}^{+} was discovered by SLEX collaboration [1, 2] and recently LHCb have discovered the doubly charmed Ξ_{cc}^{++} in the $\Lambda_c^+ K^- \pi^+ \pi^-$ mass spectrum at $\sqrt{s} = 13$ TeV [3]. There are many theoretical approaches in literature to compute the mass spectra and decay properties. The models based on lattice QCD [7], QCD sum rules [8] relativistic quark model (RQM) [9], hypercentral constituent quark model [10] and many more.

In this article we compute the mass of doubly heavy Ξ_{cc}^{++} in the extended version of relativistic harmonic confinement model (ERHM). The spin dependent part of the confined one gluon exchange interaction is employed to compute the mass of excited state. Using the potential parameters and spin flavor wave-functions, we compute the transition magnetic moments between $3/2^+ \to 1/2^+$ states. We also compare our findings with the available experimental data and other theoretical predictions.

*Electronic address: angadaria-apphy@msubaroda.ac.in
†Electronic address: nrsoni-apphy@msubaroda.ac.in
‡Electronic address: jnpandya-apphy@msubaroda.ac.in

Formulation

We employ the extended relativistic harmonic confinement model (ERHM) to compute the masses of Ξ_{cc}^{++} baryon. In ERHM, the quarks are confined through in the Lorentz scalar with vector harmonic oscillator potential of the form[4, 5].

$$V_{conf} = \frac{1}{2}(1+\gamma_0)A^2 r^2 \qquad (1)$$

We employ the nonrelativistic reduction of Dirac equation to compute the bound state masses of the doubly heavy baryons for the potential Eq. (1). In above equation A is the confinement mean field parameter and γ_0 is the Dirac matrix. Using the wave function, we incorporate the Coulomb potential with color dielectric coefficient perturbatively. The Coulomb potential is given by

$$V_{coul} = \frac{k\alpha_s}{\omega r} \qquad (2)$$

Here, in this equation ω is the state dependent color dielectric coefficient and α_s is the strong running coupling constant. We also include the spin dependent part of confined one gluon exchange potential perturbatively to compute the mass of excited state. We assume here that the light quark interacts with both the heavy quarks separately (three body description) and not with a heavy diquark as proposed by other theoretical approach [6] as that causes increase in the baryon mass as a consequence. The mass of baryonic system in the

TABLE I: Masses of Ξ_{cc}^{++} baryon in MeV

State	Present	[9]	[10]	[7]
Ξ_{cc}^{++}	3620.75	3620	3511	3610 (23) (22)
Ξ_{cc}^{*++}	3752.28	3727	3687	3692 (28) (21)

$*$ indicates $J^P = \frac{3}{2}^+$ state

different $n^{2S+1}L_J$ state can be written as

$$M_N^J = \sum_{i=1}^{3} \epsilon_N(q_i)_{conf} + \sum_{i<j=1}^{3} \epsilon(q_i,q_j)_{coul} + \sum_{i<j=1}^{3} \epsilon_N^J(q_i,q_j)_{S.D.} \quad (3)$$

The potential parameters are: Coulomb interaction strength $k = 0.37$, the mean field parameter $A = 2166$ MeV$^{3/2}$ and quark masses $m_c = 1315$ MeV and $m_u = 240$ MeV. The computed masses of Ξ_{cc}^{++} is tabulated in Tab. I

Transition Magnetic Moment

The radiative transition magnetic moment in terms of nuclear magneton (μ_N) is computed using

$$\mu_{B^* \to B\gamma} = \langle B|\hat{\mu}_{B^* z}|B^*\rangle \quad (4)$$

where B and B' represents the constituent quarks of parent and daughter baryon respectively. We obtain the following result

$$\mu_{\Xi_{cc}^{*++} \to \Xi_{cc}^{++}} = 1.564\ \mu_N$$

Our results are in good agreement with the other theoretical approaches such as χCQM [11] and the model based on effective mass scheme [12].

Conclusion

We have computed the masses of doubly heavy baryons employing the extended version of relativistic harmonic confinement model and the results are tabulated in Tab I in comparison with results from LQCD [7], relativistic quark model [9] and hypercentral quark model [10]. Our results are in good agreement with LQCD and RQM. We have also computed the weak transition magnetic moment and it is in compliance with the other theoretical predictions. We notice that the three body description of the double heavy baryons provide better mass spectra without addition of correction terms. The study on computation of weak decay properties and lifetimes of differently charged states of doubly heavy baryons are underway.

Acknowledgments

J.N.P. acknowledges the support from the University Grants Commission of India under Major Research Project F. No. 42-775/2013 (SR).

References

[1] M. Mattson *et al.* (SELEX Collaboration), Phys. Rev. Lett. **89**, 112001 (2002).
[2] A. Ocherashvili *et al.* (SELEX Collaboration), Phys. Lett. **B628**, 18 (2005).
[3] R. Aaij *et al.* (LHCb Collaboration), Phys. Rev. Lett. **119**, 112001 (2017).
[4] J. N. Pandya *et al.*, Chin. Phys. C **39**, 123101 (2015), Pramana **57**, 821 (2001), Eur. J. Phys. A **4**, 83 (1999).
[5] N. R. Soni and J. N. Pandya, DAE Symp. Nucl. Phys. **62**, 770 (2017), **61**, 698 (2016), **60**, 694 (2015).
[6] C. Albertus, E. Hernandez, J. Nieves and J. Verde-Velasco, Eur. Phys. J. A **31** 691 (2007).
[7] Z. S. Brown *et al.*, Phys. Rev. D **90**, 094507 (2014).
[8] T. M. Aliev, K. Azizi, M. Savci, Nucl. Phys. A **895**, 59 (2012), J. Phys. G **40**, 065003 (2013).
[9] D. Ebert, R. N. Faustov, V. O. Galkin, and A. P. Martynenko, Phys. Rev. D **66**, 014008 (2002).
[10] Z. Shah and A. K. Rai Eur. Phys. J. C **77**, 129 (2017), **76**, 530 (2016).
[11] N. Sharma *et al.*, Phys. Rev. D **81**, 073001 (2010).
[12] R. Dhir and R. C. Verma Eur. Phys. J. A **42**, 243 (2009).

Study of Decay Properties of Heavy Flavor and Exotic Hadrons

Abstract

In this thesis, we study the mass spectra and decay properties of heavy quarkonia, doubly heavy baryons, exotic states and open flavor mesons using different approaches. For heavy quarkonia, we employ Cornell potential and the ground state energy is obtained by solving the Schrödinger equation numerically. Using the potential parameters and numerical solution of wave-function, we study the decay properties of charmonia, bottomonia and B_c mesons. The computation of excited state masses and decay properties are then performed without additional parameters. For doubly heavy baryons, we employ the relativistic harmonic confinement potential and ground state energy is obtained using the non-relativistic reduction of Dirac equation. The exotic states are investigated using the modified Woods-Saxon potential by solving the Schrödinger equation numerically. We also compute the leptonic and semileptonic branching fractions of D and D_s mesons in Covariant Confined Quark Model based on the effective field theory formalism.

Organization of the thesis:

The thesis entitled "Study of Decay Properties of Heavy Flavor and Exotic Hadrons" has been organized in total 6 chapters. A chapter-wise brief description of the work done is as follows.

Chapter 1: Theoretical Developments in Particle Physics

This chapter introduces the field of particle physics and its key aspects. Some major experiments in hadron physics and theoretical approaches are outlined. This chapter provides the motivation and objectives of the present work.

Chapter 2: Heavy Quarkonium Spectroscopy

This chapter corresponds to the spectroscopy of heavy quarkonia that includes charmonia ($c\bar{c}$), bottomonia ($b\bar{b}$) and B_c ($c\bar{b}$) mesons. We have reported a comprehensive study of heavy quarkonia in the framework of nonrelativistic potential model considering the Cornell potential with least possible number of free model parameters such as confinement strength and quark masses. We predict the masses of excited states including spin dependent part of confined one gluon exchange potential perturbatively. The potential parameters and numerical solution of wave-function are then used to study various decay properties. It is observed that the nonrelativistic treatment for heavy quarkonium gives very good agreement

with experimental data and other theoretical approaches.

Chapter 3: Decay Properties of Heavy Baryons

In this chapter, we compute the masses of heavy flavour baryons using confinement scheme based on harmonic approximation with Lorentz scalar plus vector character. The residual two body coulomb interaction is included to compute the spin average masses. The spin hyperfine interaction of confined one gluon exchange potential is added to the confinement energy to get the masses of baryons. The mass spectra of baryons are computed using spin-flavour wave function for constituent quarks. The magnetic moments in all systems are then computed without additional parameters. We also compute the radiative transition ($3/2^+ \to 1/2^+$) widths of these states. The computed masses, magnetic moments and decay widths are compared with the experimental data and results of other theoretical models.

Chapter 4: Study of Exotic States as Dimesonic Molecules

This chapter is dedicated to the study of newly observed states that require consideration of physics beyond the Standard Model, the exotic states. These are multiquark or hybrid states other than familiar mesons and baryons. We study the tetra-quark Z states considering them as dimesonic molecules employing modified Woods-Saxon plus Coulomb potential for interaction between the constituent mesons. We compute the bound state masses of the exotic states by solving the Schrödinger equation numerically. We also compute the hadronic two body decay width using the Phenomenological Lagrangian mechanism.

Chapter 5: Weak Decays of Open Flavor Mesons

In this chapter, the leptonic and semileptonic decays of charmed meson ($D_{(s)} \to \ell^+\nu_\ell$ and $D_{(s)} \to (P,V)\ell^+\nu_\ell$) are computed in the Covariant Confined Quark Model (CCQM) formalism with the built-in infrared confinement within the Standard Model framework. Here P and V correspond to pseudoscalar and vector mesons respectively. The CCQM is an effective quantum field approach for the hadronic interaction based on effective Lagrangian of hadrons interacting with the constituent quarks. The required form factors are computed in the entire range of momentum transfer and used to determine semileptonic branching fractions.

Chapter 6: Conclusion and Future Scopes

This chapter is an accomplishment of the work done in the thesis. Along with that, we also discuss the future prospects of research in the area of weak decays using the covariant quark model.

List of Publications

Papers in peer reviewed Journals

1. J. N. Pandya, N. R. Soni, N. Devlani, A. K. Rai, "Decay rates and electromagnetic transitions of heavy quarkonia", Chin. Phys. C **39**, 123101 (2015).

2. N. R. Soni and J. N. Pandya, "Decay $D \to K^{(*)}\ell^+\nu_\ell$ in covariant quark model", Phys. Rev. D **96**, 016017 (2017).

3. N. R. Soni, B. R. Joshi, R. P. Shah, H. R. Chauhan, J. N. Pandya "$Q\bar{Q}(Q \in \{b, c\})$ spectroscopy using Cornell potential", Eur. Phys. J. C **78**, 592 (2018).

4. N. R. Soni, M. A. Ivanov, J, G, Körner, J. N. Pandya, P. Santorelli, C. T. Tran, "Semileptonic $D_{(s)}$-meson decays in the light of recent data", Phys. Rev. D **98**, 114031 (2018).

Papers in Conference Proceedings

1. N. R. Soni and J. N. Pandya, "Masses and radiative leptonic decay properties of B_c meson", DAE Symp. Nucl. Phys. **58**, 674 (2013).

2. N. R. Soni and J. N. Pandya, "Semileptonic and pionic decays of doubly strange baryons", DAE Symp. Nucl. Phys. **60**, 694 (2015).

3. A. N. Gadaria, N. R. Soni, J. N. Pandya, "Masses and magnetic moment of doubly heavy baryons", DAE Symp. Nucl. Phys. **61**, 698 (2016).

4. N. R. Soni, J. N. Pandya, "Masses and radiative decay of Ω_{cc}^+ baryon", DAE Symp. Nucl. Phys. **62**, 770 (2017).

5. N. R. Soni, R. R. Chaturvedi. A. K. Rai, J. N. Pandya, "Mass and Hadronic Decay Widths of Z States as Di-meson Molecule", Springer Proc. Phys. **203**, 729 (2018).

6. A. N. Gadaria, N. R. Soni, Raghav Chaturvedi, A. K. Rai, J. N. Pandya, "Decay Properties of Ξ_{cc}^{++} baryons", DAE symp. on Nucl. Phys. **63**, 912 (2018).

Study of Decay Properties of Heavy Flavor and Exotic Hadrons

One of the most challenging task in particle physics is to encompass the diversity and the complexity observed in the decay modes and the fractions of particles. For example, there are twenty-two quantitative modes and total forty-nine decays modes of $K^{\pm}$, and ratio of highest to lowest of these fractions amounts to 10^{11}. The spectroscopy and decay rates of various hadronic states are quite important to study due to huge amount of high precession data acquired using large number of experimental facilities viz. BESIII at the Beijing Electron Positron Collider (BEPC), E835 at Fermilab and CLEO at the Cornell Electron Storage Ring (CESR), the B-meson factories, BaBar at PEP-II, Belle at KEKB, the CDF and D0 experiments at Fermilab, the Selex experiment at Fermilab, ZEUS and H1 at DESY, PHENIX and STAR at RHIC, NA60 and LHCb at CERN and new future facility $\overline{\mathsf{P}}$ANDA at FAIR, GSI. The plethora of observations from these facilities offer greater challenges and opportunities in theoretical high energy physics. The hadronic states are not only identified with their masses but also with their various decay rates. All the hadronic states along with experimentally identified decay channels are reported in Particle Data Group (PDG) [1]. Decay properties of these sates are of special interest because they provide the further insight into the dynamics of these states. For example, the semileptonic decays of D and B mesons give the accurate determination of Cabibbo-Kobayashi-Maskawa (CKM) matrix since they involve strong as well as weak interaction. Heavy quarkonium states have very rich spectroscopy with narrow experimentally characterized states and the interaction potential is of prime importance for analysis of underlying physics of strong interaction.

Also, a large number of exotic hadronic states have been observed in the heavy flavor sector that do not fit into the conventional mesonic or baryonic states. Quite a few of these newly observed states are above the $D\bar{D}$ and $B\bar{B}$ threshold. There are variety of theoretical models available in the literature to study the production and decays of these states. The most successful theories are based on the first principle such as lattice quantum chromodynamics (LQCD) [2, 3] and QCD sum rules (QCDSR) [4]. Other attempts are based are QCD, perturbative QCD [5], effective field theory [6], Bethe-Salpeter approach [7, 8], quark models [9, 10]. There are nonrelativistic models such as nonrelativistic QCD (NRQCD) [11, 12], perturbative nonrelativistic QCD (pNRQCD) [13] and models based on phenomenological potential such as relativistic potential model [14] and nonrelativistic potential models [15, 16, 17] to study these hadronic states. Many of these approaches sometimes precisely explain the masses of hadrons but not the decay properties and vice-versa. A comprehensive review of experimental and theoretical status and challenges in study of hadronic decays are found in the literature [18, 19, 20, 21, 22].

In 2003, the Belle Collaboration [23] discovered a new exotic particle named $X(3872)$ in the $B \to K(\pi^+\pi^- J/\psi)$ channel followed by its repeated observations in different channels at other experimental facilities [24]. Later, several other resonances were also discovered near and above the first open flavor threshold region of $c\bar{c}$ and $b\bar{b}$. Several theoretical attempts have been made to understand exotic hadrons and their decay properties. Since they are not the part of standard model and Quark Model also fails to explain these states, these states are claimed to be a cluster of four quarks or multi-quark states, hydrocharmonium states, composition of hadronic molecules such as di-mesonic molecule, diquark-diantiquark molecule or $q\bar{q}g$ hybrid states according to the Quantum Chromodynamics [25, 26, 27].

Organization of the thesis:

The thesis entitled "Study of Decay Properties of Heavy Flavor and Exotic Hadrons has been organized in total 6 chapters. A chapter-wise brief description of the work done is as follows.

Chapter 1: Theoretical Developments in Particle Physics

This chapter introduces the field of particle physics and its key aspects. Some major experiments in hadron physics and theoretical approaches are outlined. This chapter provides the motivation and objectives of the present work.

Chapter 2: Heavy Quarkonium Spectroscopy

This chapter comprises of calculations for the mass spectra of heavy quarkonia in nonrelativistic quark-antiquark Cornell potential model. We have employed the numerical solution of Schrödinger equation to obtain their mass spectra using least number of parameters. The spin hyperfine, spin-orbit and tensor components of the one gluon exchange interaction are computed perturbatively to determine the mass spectra of excited S, P, D and F states.

The mass spectra and numerical solution of wave-function are then used to compute various decay properties such as decay constants, digamma, digluon and dilepton annihilation rates. We also compute the electromagnetic dipole transition rates between the S and P waves. The mass spectra, decay modes and the life time of the B_c^+ meson are also computed without introducing any new parameter and the results are consistent with available experimental data and other theoretical studies. The outcome of this study has been published in [28, 29].

Chapter 3: Decay Properties of Heavy Baryons

We compute the masses of heavy flavour baryons using confinement scheme based on harmonic approximation with Lorentz scalar plus vector character. The residual two body coulomb interaction is included to compute the spin average masses. The spin hyperfine in-

teraction of confined one gluon exchange potential is added to the confinement energy to get the masses of baryons. The mass spectra of baryons are computed using spin-flavour wave function for constituent quarks. The magnetic moments in all systems are then computed without additional parameters. We also compute the radiative transition ($3/2^+ \to 1/2^+$) widths of these states. The computed masses, magnetic moments and decay widths are compared with the experimental data other theoretical models.

Chapter 4: Study of Exotic States as a Dimesonic Molecules

This chapter dedicate to the study of newly observed state which was not explained by the Standard Model, the exotic states. The exotic states are multiquark or hybrid states other than familiar mesons and baryons. In PDG, there are more than 25 exotic states reported by the experimental facilities world wide. We study the tetra quark states (X, Y and Z) considering a them as dimesonic molecules employing modified Woods-Saxon plus Coulomb potential for interaction between the constituent mesons. We compute the bound state masses of the exotic states by solving the Schrödinger equation numerically. We also compute the hadronic two body decay width using the method of Phenomenological Lagrangian mechanism.

Chapter 5: Weak Decays of Open Flavor Mesons

In this chapter we present the leptonic and semileptonic decays of charmed meson ($D_{(s)} \to \ell^+\nu_\ell$ and $D_{(s)} \to (P,V)\ell^+\nu_\ell$) in the Covariant Quark Model (CQM) formalism with the built-in infrared confinement within the Standard Model framework.

Here P and V corresponds to pseudoscalar and vector mesons respectively. The CQM is an effective quantum field approach for the hadronic interaction based on effective Lagrangian of hadrons interacting with the constituent quarks. The required form factors are computed in the entire range of momentum transfer and used to determine semileptonic branching fractions. Our findings have been published in PRD [30] and they are presented here along with the experimental, LQCD and other theoretical data.

Chapter 6: Conclusion and Future Scopes

This chapter is an accomplishment of the work done in the thesis. Along with that, we also discuss the future prospects of research in the area of weak decays using the covariant quark model.

References

[1] M. Tanabashi *et al.* (Particle Data Group), Phys. Rev. D **98**, 030001 (2018).

[2] J. J. Dudek, R. G. Edwards, N. Mathur, D. G. Richards, Phys. Rev.D **77**, 034501 (2008).

[3] Y. Burnier, O. Kaczmarek, A. Rothkopf, JHEP **12**, 101 (2015).

[4] S. Cho, K. Hattori, S. H. Lee, K. Morita, S. Ozaki, Phys. Rev. D **91**, 045025 (2015).

[5] Y. Kiyo, Y. Sumino, Phys. Lett. B **730**, 76 (2014).

[6] W. Y. Wang, Y. L. Wu, and M. Zhong, Phys. Rev. D **67**, 014024 (2003).

[7] V. Sauli, Phys. Rev. D **86**, 096004 (2012)

[8] C. S. Fischer, S. Kubrak, R. Williams, Eur. Phys. J. A **51**, 10 (2015).

[9] T. Palmer and J. O. Eeg, Phys. Rev. D **89**, 034013 (2014).

[10] S. Fajfer and J. F. Kamenik, Phys. Rev. D **71**, 014020 (2005), **72**, 034029 (2005).

[11] T. Liu, A. A. Penin, A. Rayyan, JHEP **02**, 084 (2017).

[12] R. J. Dowdall, C. T. H. Davies, T. Hammant, R. R. Horgan, Phys. Rev. D **89**, 031502 (2014).

[13] Y. Koma, M. Koma, Prog. Theor. Phys. Suppl. **186**, 205 (2010).

[14] S. F. Radford, W. W. Repko, Phys. Rev. D **75**, 074031 (2007), Nucl. Phys. A **865**, 69 (2011).

[15] P. C. Vinodkumar, J. N. Pandya, V. M. Bannur, S. B. Khadkikar, Eur. Phys. J. A **4**, 83 (1999).

[16] J. N. Pandya and P. C. Vinodkumar, Pramana **57**, 821 (2001).

[17] A. K. Rai, J. N. Pandya, P. C. Vinodkumar, Eur. Phys. J. A **38**, 77 (2008).

[18] E. Eichten, S. Godfrey, H. Mahlke, J. L. Rosner, Rev. Mod. Phys. **80**, 1161 (2008).

[19] S. Godfrey, S. L. Olsen, Ann. Rev. Nucl. Part. Sci. **58**, 51 (2008).

[20] T. Barnes, S. L. Olsen, Int. J. Mod. Phys. A **24S1**, 305 (2009).

[21] N. Brambilla *et al.*, Eur. Phys. J. C **74**, 2981 (2014).

[22] A. Ryd and A. A. Petrov, Rev. Mod. Phys. **84**, 65 (2012).

[23] S. K. Choi *et al.* (Belle Collaboration), Phys Rev Lett. **91**, 262001 (2003).

[24] R. Aaij *et al.* (LHCb Collaboration), Phys. Rev. Lett. **110**, 222001 (2013).

[25] R. F. Lebed, R. E. Mitchell and E. S. Swanson, Prog. Part. Nucl. Phys. **93**, 143 (2017).

[26] M. Nielsen, F. S. Navarra and S. H. Lee, Phys. Rept. **497**, 41 (2010).

[27] E. Klempt and A. Zaitsev, Phys. Rept. **454**, 1 (2007).

[28] J. N. Pandya, N. R. Soni, N. Devlani, A. K. Rai, Chin. Phys. C **39**, 123101 (2015).

[29] N. R. Soni, B. R. Joshi, R. P. Shah, H. R. Chauhan, J. N. Pandya, Eur. Phys. J. C **78**, 592 (2018).

[30] N. R. Soni and J. N. Pandya, Phys. Rev. D **96**, 016017 (2017).

* * * * * * * * *

Synopsis submitted by

Mr. Soni Nakul Rajendrakumar

Endorsement of the Supervisor:

Synopsis is approved by me

Dr. Jignesh Narendrakumar Pandya

Head
Dr. B. S. Chakrabarty
Applied Physics Department,
Faculty of Technology and Engineering,
The M. S. University of Baroda, Vadodara.

Dean
Prof. Arun Pratap
Faculty of Technology and Engineering,
The M. S. University of Baroda, Vadodara.

List of Publications

Papers in peer reviewed Journals

1. J. N. Pandya, N. R. Soni, N. Devlani, A. K. Rai, "Decay rates and electromagnetic transitions of heavy quarkonia", Chin. Phys. C **39**, 123101 (2015).

2. N. R. Soni and J. N. Pandya, "Decay $D \to K^{(*)}\ell^+\nu_\ell$ in covariant quark model", Phys. Rev. D **96**, 016017 (2017).

3. N. R. Soni, B. R. Joshi, R. P. Shah, H. R. Chauhan, J. N. Pandya "$Q\bar{Q}(Q \in \{b, c\})$ spectroscopy using Cornell potential", Eur. Phys. J. C **78**, 592 (2018).

4. N. R. Soni, C. T. Tran, M. A. Ivanov, J. N. Pandya, "Semileptonic decays of D and D_s mesons in covariant quark model" (manuscript under preparation).

Papers in Conference Proceedings

1. N. R. Soni and J. N. Pandya, "Masses and radiative leptonic decay properties of B_c meson", DAE Symp. Nucl. Phys. **58**, 674 (2013).

2. N. R. Soni and J. N. Pandya, "Semileptonic and pionic decays of doubly heavy baryons", DAE Symp. Nucl. Phys. **60**, 694 (2015).

3. A. N. Gadaria, N. R. Soni, J. N. Pandya, "Masses and magnetic moment of doubly heavy baryons", DAE Symp. Nucl. Phys. **61**, 698 (2016).

4. N. R. Soni, J. N. Pandya, "Masses and radiative decay of ω_{cc}^+ baryon", DAE Symp. Nucl. Phys. **62**, 770 (2017).

5. N. R. Soni, R. R. Chaturvedi. A. K. Rai, J. N. Pandya, "Mass and Hadronic Decay Widths of Z States as Di-meson Molecule", Springer Proc. Phys. **203**, 729 (2018).